SYNTHESIS AND MORPHOLOGICAL ELUCIDATION OF CYSTEINE BASED SHORT PEPTIDE NANOSTRUCTURES AND THEIR EFFICACY STUDIES

A THESIS SUBMITTED FOR THE DEGREE OF DOCTOR OF PHILOSOPHY IN THE FACULTY OF SCIENCE, JADAVPUR UNIVERSITY

2023

BY

MISS. SASWATI GHOSH

CSIR-INDIAN INSTITUTE OF CHEMICAL BIOLOGY
ORGANIC AND MEDICINAL CHEMISTRY DIVISION
4, RAJA S. C. MULLICK ROAD, JADAVPUR
KOLKATA-700 032, INDIA

INDIAN INSTITUTE OF CHEMICAL BIOLOGY
CSIR-IICB, 4, RAJA S.C.MULLICK ROAD, JADAVPUR,KOLKTA 700032, INDIA
PHONE:+91-33-24730492/3491/3493/6793, FAX: 033-2473 5197/ 2472 3967

Dr. Biswadip Banerji, Senior Principal Scientist
Ph.D (IIT - Kanpur), M.Sc.(Calcutta University)
2009 – Onwards: CSIR-IICB, Kolkata, India
2008: Team Lead, Chembiotek-Kolkata
2006 – 2008: Postdoctoral Research Fellow, (Prof. K.C. Nicolaou); CSL@ICES-A*-STAR
2003 – 2006: Postdoctoral Research Fellow, (Prof. C.J. Schofield); Oxford Centre for Molecular Science (OCMS) & Chemistry-Research Laboratory (CRL), Oxford University, UK.

Office address:
Room No. 17 &12 (Ground Floor)
Phone No. +91-33-24735709
Hand Phone No. 09903752881
Email: biswadip@iicb.res.in
biswadip.banerji@gmail.com

CERTIFICATE FROM THE SUPERVISOR

This is to certify that the thesis entitled "SYNTHESIS AND MORPHOLOGICAL ELUCIDATION OF CYSTEINE BASED SHORT PEPTIDE NANOSTRUCTURES AND THEIR EFFICACY STUDIES" submitted by SASWATI GHOSH, who got her name registered on 09.08.2019 [Registration no. SCHEM1501319, Index no. 13/19/Chem./26] for the award of Ph.D. (Science) degree of Jadavpur University, is absolutely based upon her own work under the supervision of Prof. BISWADIP BANERJI and that neither this thesis nor any part of it has been submitted for either any degree/diploma or any other academic award anywhere before.

Biswadip Banerji..
15.02.2023.

(Prof. BISWADIP BANERJI)
(Signature of the Supervisor & date with official seal)

Prof. Biswadip Banerji
PhD (IIT-Kanpur), M.Sc (Cal)
Senior Principal Scientist
Organic & Medicinal Chemistry Division
CSIR-Indian Institute of Chemical Biology (IICB)
4, Raja S.C. Mullick Road, Kolkata - 700 032

DECLARATION

I, **Saswati Ghosh** hereby declare that the work emphasized in this thesis entitled "**SYNTHESIS AND MORPHOLOGICAL ELUCIDATION OF CYSTEINE BASED SHORT PEPTIDE NANOSTRUCTURES AND THEIR EFFICACY STUDIES**" is my own work and carried under the guidance of Prof. Biswadip Banerji, senior principal scientist, CSIR-Indian Institute of Chemical Biology, Jadavpur, Kolkata, India.

I have duly acknowledged all the sources of information which have been used in this thesis. To the best of my knowledge and belief, this work is original and has not been submitted in part or full, in any degree or diploma of this or any other university.

(**SASWATI GHOSH**)

Organic and Medicinal Chemistry Division

CSIR-Indian Institute of Chemical Biology

Jadavpur, Kolkata-700032, India

DEDICATED TO MY PARENTS, MY BROTHER, AND GOD

Acknowledgment

As this may be my only opportunity to thank these individuals in writing, I may be a bit more verbose in my thanks than necessary.

It gives me a great pleasure to express my gratitude toward all the people who contributed to the completion of this thesis. First and foremost, I want to thank my advisor and mentor Prof. Biswadip Banerji, Senior Principal Scientist, Organic & Medicinal Chemistry Division, Indian Institute of Chemical Biology, Kolkata, whose innovative thinking, high perception of knowledge, practical insight, and experience in the subject have resulted in the success of the entire attempt. I am very lucky to have such a caring, patient, encouraging, and experienced supervisor who ensured all the positive inputs to cross all the toughest of the hurdles during this eventful journey. He provided the combination of necessary freedom and control for fulfilling the desired research objectives. I will always remember his encouraging stories and brainstorming discussions that changed my way of doing science and exploring out of the box ideas.

I sincerely thank CSIR-Indian Institute of Chemical Biology for giving me the platform to carry on my research. I take this opportunity to sincerely acknowledge the Council of Scientific & Industrial Research, Government of India, New Delhi, for providing financial assistance in the form of fellowship which buttressed me to perform my work comfortably. I would like to acknowledge ex-director Prof. Samit Chattopadhyay and present director Prof. Arun Bandyopadhyay of CSIR-IICB for allowing me to be a part of this institute and providing the necessary facilities to carry out my research work.

I would like to thank each and every member and staff of the Central Instrumentation Facility (CIF) Department of CSIR-IICB for helping me with conducting a variety of experiments and processing the data.

I am indebted to my lab seniors. Firstly, thanks to Dr. Moumita Chatterjee and Leena Majumder, for their unconditional help and support throughout my

research work. They helped me out in every possible manner whether it was related to research or any other problem of my life and they treated me like their own younger sister. I would like to thank other senior lab members Dr. Suvankar Bera, Dr. Chandrasekhar Kadaiahgadi, Dr. Kill Sunil Kumar, Dr. Satadru Chatterjee, Dr. Saswati Adhikary, Dr. Ravuri Srinath, Mr. Krishnendu Khamaru and Mr. Sourav Pakrashi for their kind support and help. I would like to especially thank Chandu anna, Sunil anna, Leena di, Moumita di, and Srinath for making my stay in this city easier and more joyful which helped me a lot to release the stress of this hectic life throughout my Ph.D. journey. I would like to thank my lab friend Debabrata Sarkar for his tremendous help whenever I needed it. I would like to thank all my beloved junior lab members Abhudyay Guin, Vijay Babu Pathi, Arindam Manna, Suvankar Shee, Kaushik Seal, Asikul SK, and Arpan Adhikari for maintaining a positive environment in the lab and immense support on workbench, without your support it would not be possible to complete this journey in such a smooth manner. The friendship between all the lab members was flourished with scientific and non-scientific talks giving us memorable days and endless bonding. These people will always have a special room in my heart and I will always cherish those golden days in my memory.

Although there are so many people who directly or indirectly helped me throughout my Ph.D. journey I would like to mention some of my beloved friends from IICB who helped me a lot Dr. Rajiv Maity, Himadri Nath, Deeti Jyothi, Sukanya De, Debosmita Das.

I am grateful to our collaborators Dr. Krishna Das Saha, Dr. Sayoni Nag, Dr. Nayim Sepay for their enormous support during the progression of my thesis work.

Last on the list and first in my mind, I pay my deep sense of admiration to my parents Mr. Alo Baran Ghosh and Mrs. Sarama Ghosh for bringing me up to this academic field and believing in me. I would like to thank my most loved younger brother Mr. Arka Prabha Ghosh who always had belief in me when no one other

had and supported me in each of my decision in life. I am also grateful to my other family members whose silent blessings, constant support, love, and encouragement enabled me to reach my destiny.

Above all, I thank my Lord, for giving me the intelligence to understand and resolve the problem arising during the experiment and giving me the strength to complete this research.

Thank you.

Saswati Ghosh

Organic and Medicinal Chemistry Division

CSIR-Indian Institute of Chemical Biology, Kolkata, India

CONTENTS

Page No.

List of Abbreviations……. **3-4**

General Remarks…… **5-7**

Prelude…… **8-11**

Chapter 1: General Introduction and Scope of the Present Work…… **12-30**

1.1 Nanotechnology

1.2 Self-assembly

1.3 Scope of this thesis

Chapter 2: Cysteine Derived Cyclic Dipeptide Super Hydrogelator: Enhancing Efficacy of an Anticancer Drug via Sustainable Release……. **31-67**

2.1 Aim of the present work

2.2 Introduction

2.3 Results and Discussion

2.4 Conclusion

2.5 Future Scope

2.6 Spectral Characterization and Additional Results

Chapter 3: Hydrophobicity Controlled Self-Assembly of Non-Symmetrical Cyclic Dipeptides: Exploring Application in Waste Water Management by Toxic Dye Removal …….. **68-131**

3.1 Aim of the present work

3.2 Introduction

3.3 Results and Discussion

3.4 Conclusion

3.5 Future Scope

3.6 Experimental Procedures and Spectral Data

Chapter 4: Controlling Self-Assembly of Small Peptides into Different Nanostructures by Quinazolinone Capping …….... **132-178**

4.1 Aim of the present work

4.2 Introduction

4.3 Results and Discussion

4.4 Conclusion

4.5 Future Scope

4.6 Experimental Procedures and Spectral Data

References…….. **179-206**

List of Publication…… **207**

LIST OF ABBREVIATIONS

AFM:	Atomic Force Microscopy
FE-SEM:	Field Emission Scanning Electron Microscopy
FT-IR:	Fourier Transform Infrared
UV-vis:	Ultraviolet visible
NMR:	Nuclear Magnetic Resonance
ESI:	Electron Spray Ionization
DFT:	Density Functional Theory
CD:	Circular Dichroism
TLC:	Thin Layer Chromatography
BOC:	Tertiary butoxy carbonyl
EDC.HCl:	1-Ethyl-3-(3-dimethylaminopropyl) carbodiimide hydrochloride
HOBt:	Hydroxybenzotriazole
Th-T	Thioflavin-T
^{o}C:	Temperature in degrees centigrade
K:	Temperature in Kelvin
G′:	Storage modulus
G″:	Loss modulus
ml:	Milli liter
ppm:	Parts per million
HS:	Hirshfield Surface
DFT:	Density Function Theory
h:	Hour
min:	Minute

g:	Gram
mg:	Milligram
mM:	Millimolar
μM:	Micromolar
CDP:	Cyclic Dipeptide
DCM:	Dichloromethane
DMF:	Dimethyl formamide
DMSO:	Dimethyl sulfoxide
TEA:	Triethyl amine
TMOF:	Trimethyl orthoformate
*p*TSA:	*p*-toluenesulfonic acid
rt:	Room temperature
5FU	5-Fluorouracil
IC_{50}:	Concentration of the tested compound able to cause the death of 50 % of the cells
MTT:	3-(4,5-dimethylthiazolyl-2-yl)-2,5-diphenyltetrazolium Bromide
MGC:	Minimum Gelation Concentration
T_g:	Gel melting temperature

GENERAL REMARKS

- ^{1}H NMR and ^{13}C NMR were measured on a Bruker DPX 300 MHz and Bruker DRX 600 MHz NMR instrument. Generally, DMSO-d_6 and D_2O have been used for NMR sample solution preparation. Chemical shifts (δ) were reported in parts per million (ppm) and tetramethylsilane (δ = 0.00) was used as the internal standard. The standard abbreviations s, d, t, q, m, and J refers to singlet, doublet, triplet, quartet, multiplet, and the coupling constant respectively.

- Analytical thin layer chromatography (TLC) was obtained via standard Merck TLC silica gel 60 F254 aluminium sheets. Visualization of the spots on TLC plate was achieved through exposure to UV light, iodine vapour, etc. Progress of the reaction was monitored via TLC checking. Moisture sensitive reactions were carried out using standard syringe-septum techniques. Column chromatography was carried out with silica gel 60-120 and 100-200 mesh. Ethylacetate:petroleum ether and methanol:dichloromethane solvent partners were used as eluent for column chromatography.

- Unless otherwise mentioned, petroleum ether refers to fraction boiling in the range of 60-80 ^{o}C. All reagents and solvents were purified and dried by conventional protocol.

- All evaporation of solvents was carried out under reduced pressure in Heidolph Rotary Evaporator of Cat. No: P/N Hei-VAP Value/G3: 560-01300-001.

- CD spectra (190-250 nm) were recorded at 200 nm/min scan speed, with 1 nm bandwidth on a Jasco J-810 spectrometer using a 10 mm quartz cell. CD measurements were carried out at 25°C.

- AFM images were obtained on Pico Plus 5500 AFM (Agilent Technologies, Inc., Santa Clara, CA, USA) with the piezo scanner range of 9 μm. The images (256 × 256 pixels) were captured with a scan size between 0.5 and 5 μm at the scan speed rate of 0.5 rpm. The images were processed through flattening via Pico view software (Molecular Imaging Inc., Ann Arbor, MI, USA). For this purpose, sample solutions were incubated at room temperature for required time, drop cast on a mica foil. After drying the sample solution placed on the mica foil, the specimen was observed through atomic force microscopy.

- UV−Vis absorption spectra of the samples were acquired using a JASCO V-630 spectrophotometer (JASCO International Co. Ltd., Japan) within the wavelength range of 200−700 nm. A high-quality quartz cuvette having path length 1 cm was used for spectral measurement.

- Fluorescence spectra were measured with the PTI QM-400 spectrophotometer.

- The rheological measurement of the gel obtained from the peptides was performed using Modular Compact Rheometer (Anton Parr, MCR 102, Austria). The instrument was equipped with an air compressor unit which maintained the air pressure at 7 kg/cm2. Standard cone-plate geometry (CP-40, 40 mm outer diameter, angle 1◦) was employed in the study. Frequency sweep (G, G versus angular sweep) was measured in oscillation mode. The data was analyzed using Rheoplus software (US 200, version 3.62).

- Single crystal XRD analyses were performed either with a Bruker APEX-II diffractometer, equipped with MoKα radiation and a CCD detector, or with a Bruker D8 Venture diffractometer, equipped with CuKα radiation, microfocus optics, and Photon-III detector. The crystals were analyzed under polarized

optical microscope. Suitable single crystals were isolated and covered with paratone oil and mounted using MiteGen loops. Diffraction data were collected and processed with the Bruker Apex III software suite incorporated with multiple tools such as cell_now and RLATT for the determination of the unit cell, SAINT-plus for data reduction, and SADABS for absorption correction. The structure solutions were performed with SHELXT and the full-matrix least-squares refinements were performed with SHELXL suite of programs incorporated in Apex III suite and Olex 2.

- The Fourier transform infrared (FT-IR) spectra of the samples were recorded on a Bruker TENSOR27 spectrometer. FT-IR spectra of the samples in solid and gel states were recorded using the attenuated total reflection (ATR) technique. Bruker software was used for data processing. Experimental data obtained were analyzed using Origin Pro 8.0 SRO software (OriginLab Corporation).

- The fluorescence measurement during Th-T experiments was done using PTI QM-400 spectrophotometer in a quartz cuvette of 1 cm path length. The excitation and emission slit widths were fixed at 5 nm each and the emission range was 420-600 nm. The chosen excitation wavelength was 410 nm.

PRELUDE

Many studies on peptide-based self-assembling systems were conducted during the last few decades. Especially among these, self-assembling short peptides, their bio-physical characteristics, and their applications are fascinating areas to study. Peptides provide the platform for biomaterial inspired nanomaterials development for their application in nano-devices, drug delivery agents, biosensors, tissue engineering, waste water management, therapeutics, etc. Due to this wide range of applicationsof peptide-based nanomaterials, short yet functional self-assembled peptides are the subject of study in this thesis. The simplicity of their design and synthesis serves as the fundamental benefit of choosing short peptides for the above mentioned applications. Simple laboratory techniques may provide high yield products and peptides are regarded as excellent model systems for understanding biological self-assembly. Self-assembly is a phenomenon of non-covalent interaction-based arrangement of separate units of small monomeric molecules into well-ordered coherent structures. Such self-assembly often led to further extent of self-assembly into a complex 3D network of nanostructures which can immobilize the solvent molecules inside the cavity of the network and in turn give rise to gelation. Several research teams have carefully explored self-assembled short peptide-based hydrogels, organogels as well as the nanostructures associated with them. Short peptide based gels, especially hydrogels have gained special attention for their biomaterial and biomedical applications due to their biocompatibility, high water content, and low toxicity. Thus, in this thesis entitled "Synthesis and Morphological Elucidation of Cysteine Based Short Peptide Nanostructures and Their Efficacy Studies," efforts were made to design and synthesize cysteine based short peptides and their self-assembly process was studied in detail. All the peptides were synthesized in simple organic reaction steps and their characterization was thoroughly done by NMR (^{1}H, ^{13}C), FT-IR, ESI-mass

spectroscopy, etc. The morphology of the nano-structures obtained from the self-assembled peptides was thoroughly elucidated by AFM and FE-SEM spectroscopy and several spectroscopic techniques like NMR, FT-IR, CD, UV, and fluorescence spectroscopy, powder XRD, single crystal X-ray, and finally DFT studies were employed to gain insight about the self-assembly pattern involved in the formation of those nano-structures. Focus has also been made on the application of the self-assembled nanomaterials formed by synthesized short peptides in drug delivery, dye adsorption, and α-synuclein aggregation Inhibition. This thesis is divided into four chapters. A brief description of the work of each chapter is discussed below.

Chapter 1

Chapter 1, contains brief background of nanotechnology, nanoscience, and short peptide based self-assembled nano-structures as well as organogel, hydrogels like soft nano-materials, and their potential applications in several fields. Previous literatures on short peptide-based self-assembly were thoroughly explored and the basic logic of this thesis work was discussed in detail. Self-assembly requires low-energy non-covalent interactions such as hydrogen bonding, van der Waals interactions, hydrophobic interaction, π-π interactions, etc. which come together to create stable and well defined supramolecular structures. Because of the chemical adaptability of the amino acid motif combined with the simplicity and chemical accessibility of peptides, the utilization of short and simple peptide-based derivatives is currently thought of as a flexible building block which offers a suitable platform for various applications. Studies using amphiphilic peptides, cyclic peptides, amyloid-inspired peptides, and aromatic or heterocyclic capped peptides that can self-assemble into a variety of nano to micro supramolecular structures have already been conducted. Therefore, self-assembly of peptide molecules and their applications in modern nanotechnology owing to their specific molecular recognition patterns and the feasibility to tune their physicochemical properties

by small changes in their constituting amino acids for specific applications was discussed here.

Chapter 2

The majority of anticancer medications suffered several drawbacks, including a very short half-life and significant cytotoxicity when administered in high concentrations. Therefore, it is crucial to design a potent, affordable method of drug administration in order to maintain the correct dosage. This chapter deals with the designing and synthesis of a cyclic dipeptide based super hydrogelator as sustainable drug delivery vehicle containing *S*-benzyl-L-cysteine and L-leucine as constituting amino acids. This cyclic dipeptide spontaneously self-assembled itself in 1% DMSO-PBS buffer at physiological conditions (at 37 ^{o}C and pH = 7.46) and formed self-supported stable hydrogel. FE-SEM, AFM, FT-IR, NMR, and rheological experiments were used to characterize the structural, morphological, and mechanical insights of this hydrogel. In vitro measurements were made for the encapsulation and release of anticancer drug 5-Fluorouracil from the hydrogel matrix. This chapter also includes information on the cyclic dipeptide's cytotoxicity as well as the anticancer properties of the hydrogel-drug co-assembly when applied to the human cancer cell line HCT116.

Chapter 3

In this chapter, efforts were made to synthesize a series of six cyclic dipeptides (CDPs) having *S*-benzyl-L-cysteine as common partner to set up a structure-morphology or structure-gelation relationship as a factor of hydrophobicity of other constituting amino acid partner. Small variations of the constituting amino acids in the peptide moieties caused significant differences in their morphology as well as in gelation properties. The physical properties of all six CDPs were studied in methanol-water solvent system where the CDPs formed self-assembled materials like fine crystals, loose gels, and hydrogels depending upon their chemical structure. AFM, NMR, FT-IR, CD, and single crystal X-ray crystallography experiments were used to characterize the morphological and

structural insights of these peptides. Rheological studies were used to look into the mechanical durability of the gels. Hirshfeld surface analysis and DFT study of all six CDPs came to the same conclusion as the single crystal X-ray, AFM, and CD analyses. Additionally, the hydrogel obtained from one of the cyclic dipeptides was used in waste water management by eliminating harmful organic dyes from contaminated water. Cytotoxicity of all CDPs were checked via MTT assay against human cervical canvcer cell line HeLa.

Chapter 4

While the amino acid sequence greatly influences the physical and chemical characteristics of the self-assembly as well as the gelation property, short peptides frequently require an aromatic or heterocyclic capping group at their N-terminus to facilitate self-assembly or gel formation. In these systems, self-assembly is triggered by the hydrophobic contacts of this capping group in conjunction with hydrogen bonds formed by the peptide backbone. This chapter contains the design and synthesis of four cysteine based hybrid peptides capped with medicinally important aromatic heterocyclic moiety, quinazolinone. Four different as such peptides were synthesized where two contained quinazolinone moiety at the N-terminus and the other two at C-terminus. Morphological analysis of these hybrid peptides revealed peptides with C-terminus capping produced spherical assembly while peptides with N-terminus capping produced fibrillary assembly. Morphological and structural insights into the self-assembly pattern of these peptides were elaborately discussed in this chapter with the help of AFM, FESEM, and crystallographic study. The influence of the capping group and reversal of amide bond sequence on hydrogelation property of theses peptides at physiological conditions were also shown in this chapter.

CHAPTER-1

General Introduction and Scope of the Present Work

1.1 NANOTECHNOLOGY

1.1.1 History of Nanotechnology

Innovations in science and technology frequently start with human dreams and imagination. Nanotechnology, a 21st-century frontier, was born out of such aspirations. The term nanotechnology has been derived from the Greek word “nanos” which means “dwarf”.[1]Itis commonly defined as the understanding, control, and restructuring of matter on the order of nanometers (i.e., less than 100 nm) to produce materials with fundamental new properties and functions.[2] However, the definition of "nanotechnology" varies from field to field and country to country and is frequently used as a "catch-all" description for anything very small. Nanotechnology involves design, characterization, synthesis, and application of materials, structures, devices, and systems by controlling shape and size at nanometre scale.[3]Nanotechnology is not a new field, scientists have been studying nanoscience for many years in a variety of scientific and medical fields. For example, the identification and study of carbon fullerenes in the 1980s and Watson and Crick's discovery of the structure of DNA in 1953 can both be regarded as nanoscience.[4,5]Since the beginning of the cosmos, there have been nanoparticles in the atmosphere with at least one dimension on the nanoscale (1–100 nm). Richard Zsigmondy, a chemistry Nobel Prize winner from 1925, was the one who first coined the term "nanometer." He was the first to measure the size of particles like gold colloids using a microscope and he is credited with inventing the term "nanometer" specifically to describe particle size.[6]Although human exposure to nanoparticles has occurred throughout human civilization, it dramatically increased during the industrial revolution. The concept of nanotechnology was first discussed by

Caltech physicist Richard Feynman in a lecture titled "There's Plenty of Room at the Bottom" during the American Physical Society meeting in 1959.[7] Dr. Feynman's presentation was the first academic talk to address one of the fundamentals of nanotechnology- the direct manipulation of individual atoms or molecular manufacturing. With this innovative concept, new methods of thinking were demonstrated, and Feynman's theories were later found to be true. For these reasons, he is regarded as the originator of contemporary nanotechnology. Over 15 years after Feynman's talk, in 1974, a Japanese scientist named Norio Taniguchi was the first to adopt the term "nanotechnology" in a publication to describe semiconductor operations that took place on the order of a nanometer. In that article, he stated that "Nano-technology mainly consists of the processing of, separation, consolidation, and deformation of materials by one atom or one molecule".[8]However, it wasn't until the 1980s that nanotechnology began to take off as a field.The golden era of nanotechnology began in the 1980s with the discovery of fullerenes by Kroto, Smalley, and Curl. Feynman's idea of molecular manufacturing was elaborated upon by Eric Drexler, a scientist at MIT in 1979 using the most recent research on the function of proteins. Many people think that this was the beginning of the field of nanotechnology. Drexler first wrote about the topic in 1981 and published it in the Proceedings of the National Academy of Sciences journal under the title "Molecular engineering: An approach to the creation of broad capabilities for molecular manipulation". Drexler highlighted the potential for molecular manufacturing in this essay, which would include employing specially created protein molecules to create products with precise atomic specifications. In his book "Engines of Creation: The Coming Era of Nanotechnology," Drexler developed the potential of these ideas.Drexler offered the concept of a nanoscale "assembler" with the ability to duplicate itself and other objects of any complexity. Drexler's vision of nanotechnology is often called as ''molecular nanotechnology.'[9]The science of nanotechnology

moved much farther When another second Japanese scientist named Iijima developed carbon nanotubes.[10]Nanotechnology has been fuelled by the improvement of instrumentation and the availability of tools that allow scientists to see things that they were not able to perceive in the past, just like Watson and Crick's discovery of the structure of DNA led to a biotechnology revolution.In the 1990s and 2000s, the use of nanomaterials in a wide range of consumer products significantly increased the popularity of nanotechnology and the production of various nanomaterials.

1.1.2 Approaches of Nanotechnology

Following Feynman's discovery of this new area of study that attracted the attention of numerous scientists, two approaches have been developed that describe the various options for the synthesis of nanostructures. A wide range of experimental approaches that are beyond the scope of a brief introduction can be used in the synthesis of nanoengineered materials and devices, which can use precursors from the solid, liquid, or gas phases. However, the majority of synthetic methods can be divided into "top-down" and "bottom-up" approaches and as well as combinations of these two approaches.

i) the "top-down" method, in which larger structures are scaled down to the nanoscale while retaining their original properties without atomic-level control. The best-known illustration of a "top-down" strategy is the photolithography method used by the semiconductor industry to make integrated circuits by etching patterns in silicon wafers. To examine neuron-astrocyte communication, a similar strategy was employed to create microscale linked wells in agar using poly(dimethylsiloxane) moulds. This is an illustration of lithographic technology being used in cell biology. True nanoscale features can be created in a variety of materials using other types of nanolithographic techniques, such as dip-pen nanolithography and electrostatic atomic force microscope

nanolithography, which deposit or move individual molecules into desired configurations, respectively.[11]

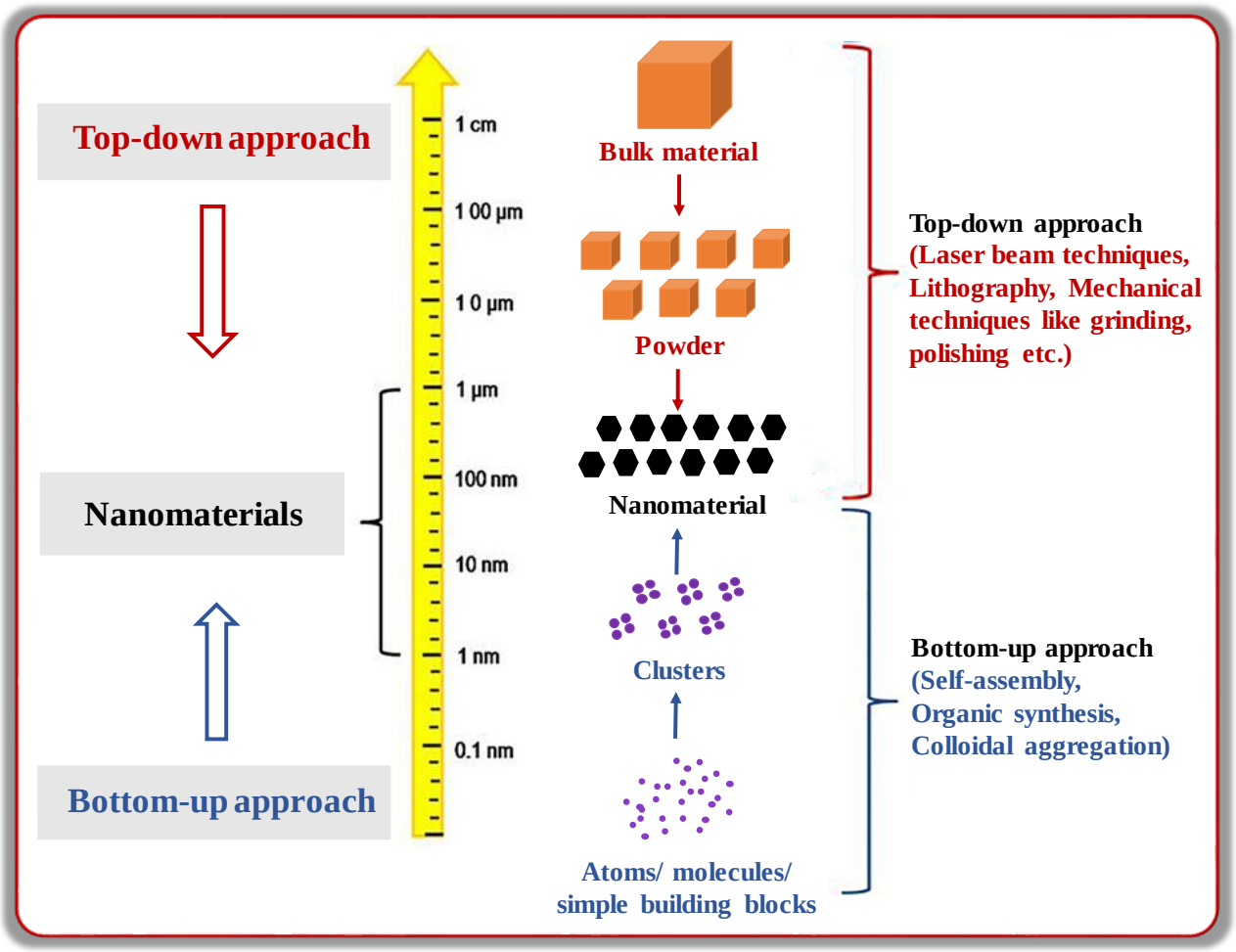

Figure 1. *The schematic representation of the concept of top-down and bottom-up technology: different methods for nanoparticle synthesis.*

ii) Conversely, the "bottom-up" method, also known as "molecular nanotechnology" or "molecular manufacturing," was first proposed by Drexler et al started by creating and synthesizing unique molecules with the capacity to self-assemble or self-organize into higher order mesoscale and macroscale structures. Synthesizing molecules that spontaneously self-assemble in response to a controlled change in a particular chemical or physical trigger, such as a change in pH, the concentration of a particular solute, or application of an

electric field, is a difficult task. Thermodynamics and competing molecular interactions, such as hydrophobic/hydrophilic forces, hydrogen bonds, and van der Waals interactions, are the physical mechanisms that produce self-assembly, or the driving forces that push these molecules to self-assemble into organized structures. The trick is to design systems that self-assemble into macroscopic higher order structures with desirable chemical and/or physical properties that the individual constituent molecules do not exhibit. While most contemporary technologies use a "top-down" approach, the "bottom-up" approach has significant potential for advancements in the fields of materials and manufacturing, electronics, medicine and healthcare, energy, biotechnology, information technology, and national security.[11,12]

1.1.3 Impact and Future of Nanotechnology

Nanotechnology has developed rapidly with exponential growth over the past 50 years and now serves as the basis for many impressive industrial applications. Nanotechnology, for instance, had a significant influence on medical equipment like imaging probes, medication delivery systems, and diagnostic biosensors in the pharmaceutical industry. Nanomaterials are now widely used in the food and cosmetics industries to enhance manufacturing, packaging, shelf life, and bioavailability.[13–15] Nanotechnology now has an everyday impact on human life. There are numerous and diverse possible advantages. However, there is a great deal of worry about the potential health and environmental hazards due to the vast human exposure to nanoparticles. These worries sparked the development of new scientific fields including nanotoxicology and nanomedicine. The study of nanoparticles' possible negative health impacts is known as nanotoxicology.[16] To investigate the advantages and risks of using nanomaterials in medicine and medical devices, the field of nanomedicine was formed. It encompasses subfields including tissue engineering, biomaterials, biosensors, and bioimaging. Improved medication

delivery, antimicrobial coatings for medical equipment, less inflammation, better surgical tissue repair, and the identification of circulating cancer cells are just a few of the potential advantages of medical nanomaterials.[16–18] However, the potential to have an impact on human health continues to be a serious worry regarding the toxicological qualities of inorganic, metallic, semiconductor, and polymer based nanoparticles as their uses have become more diversified in contemporary nanotechnology. For example, carbon nanoparticles, have some biological restrictions. It has been demonstrated to cause pulmonary inflammation in rats and lipid peroxidation in fish brain cells.[19,20] As a result, several people began considering an alternate strategy that would produce nanoparticles using more biocompatible peptides and proteins as the basic building blocks. This gave rise to the new field of bionanotechnology. Additionally, peptide and protein based self-assembled nanostructures have drawn a lot of interest because of their potential use in nanomedicine, drug delivery, tissue engineering, oil spill recovery, and adsorbents for eliminating environmental pollutants.[22-36]One of the important subfields of nanoscience and nanotechnology is self-assembly. Additionally, peptide and protein based self-assembled nanostructures have drawn a lot of interest because of their potential use in nanomedicine, drug delivery, tissue engineering, oil spill recovery, and adsorbents for eliminating environmental pollutants and thus making ‘peptide self-assembly’ as one of the important subfields of nanoscience and nanotechnology.

1.2 SELF-ASSEMBLY

1.2.1 Introduction

Self-assembly has proven to be one of the most potent and effective ways to create nanostructures at the atomic and molecular levels. The weak intermolecular forces that are present when two molecules interact have been

characterized and analyzed during many years of research in physical organic chemistry. Every bimolecular reaction starts with a recognition event, whether it takes place in the gas phase, diluted solution, or the inner of an enzyme. When given the right instructions, molecules can spontaneously assemble themselves into multi-component, complex structures. The molecular shape, chemical surfaces, and how well a molecule fills a space during the assembly phase are all examples of the ways in which the molecular structure provides instructions. During the molecule's synthesis, these directives are encoded. The dynamic and reversible nature of each phase in the assembly process allows for the rectification of faults as the assembly goes along.[36] Self-assembly is a crucial phenomenon to many biological systems because it either carries out its biological function or participates in pathogenic processes. For instance, the formation of DNA double helix through particular hydrogen bonding interactions, the development of biological membranes upon phospholipid self-assembly, the formation of amyloid fibrils applicable to a variety of generic neurodegenerative disorders, as well as the formation of protein microtubules and microfilaments as functional units of intracellular interaction, are a few examples. Through the previously mentioned "Bottom-up" approach known as molecular self-assembly, a range of biological and biomimetic materials have been created that are inspired by these biological processes.[37–43]The traditional definition of self-assembly is the spontaneous and reversible arrangement of molecular building blocks into ordered structures through non-covalent interactions.[44,45] This definition argues that the spontaneity of the self-assembly process is the first characteristic of a self-assembled system. The nanostructure builds itself that is the interactions that lead to the production of self-assembled systems take place strictly locally.[46–48]Numerous non-covalent interactions, such as hydrogen bonds, -stacking interactions, hydrophobic interactions, electrostatic interactions, non-specific Van der Waals forces, and dipole-dipole interactions, help the self-assembly process. Although these interactions are

modest on their own, when combined they have the power to control the self-assembly process.[49–51]

1.2.2 Characteristic Properties of Self-assembly

One could contend that any chemical reaction that causes atoms and molecules to assemble together to form larger structures, could be considered a form of self-assembly. However, self-assembly is a separate idea that should have at least these distinguishing characteristics-

i) First, whether it be a shape or a specific duty that the self-assembled entity may execute, the self-assembled structure must be of a higher order than the isolated components. In chemical reactions, this is typically not the case since, depending on the thermodynamic factors, an ordered state may move towards a disordered state.

ii)The second significant characteristic of self-assembly is the predominance of weak interactions (e.g., Van der Waals, π-π stacking, hydrophobic interactions, electrostatic interactions, hydrogen bonds, etc.) over more "conventional" covalent, ionic, or metallic bonds.[52]

iii) The third distinguishable characteristic of self-assembly is that the building blocks are a variety of nano- and mesoscopic structures with various chemical compositions, functionalities, and forms rather than just atoms and molecules.[53,54]

iv) Fourthly, the thermodynamic stability of almost all self-assembled systems is another feature in common. Self-assembled structures are thermodynamically more stable than single, unassembled components because the process must result in reduced Gibbs free energy for self-assembly to occur without the assistance of outside forces.[55,56]

1.2.3 Advantages of Peptides as Molecular Building Blocks in Self-Assembly

The fabrication of nanostructures using biomolecules is a popular research subject worldwide. Peptides have emerged as one of the most promising biomolecules due to their unrivaled biocompatibility, biodiversity, chemical variety, and most notably, their striking resemblance to proteins. Several self-assembled structures made of various amino acid sequences were designed, inspired by protein self-assembly in living organisms.[24,57–59]There are 20 natural amino acids that in numerous combinations make up the peptide that gave rise to the self-assembling nanostructures. The quantity, variety, order, and side chain of amino acid residues can all be used to influence or optimize the formation of nanostructures. In order to tailor the peptide design and give it better self-assembling properties, modified amino acids can also be incorporated into the peptide design in addition to natural amino acids. This bottom-up strategy was largely influenced by the wonders of nature operating at the nanoscale, which can produce several biological nanostructures, such as proteins, DNA/RNA, and others. Top-down science aids in the discovery of new peptide sequences based on the precise binding site on biological macromolecules based on those molecules' structural characteristics. These particular benefits of peptides persuaded researchers to explore these macromolecules and find novel molecular self-assemblies. Additionally, peptide synthesis is a straightforward and affordable chemical synthetic process using traditional techniques, in solution or solid phase. Peptides are beneficial for numerous medicinal and biological applications due to their inherent biological characteristics.[60–62] They can also replicate the behaviors and functionalities of proteins, offering an alternate model for understanding how proteins self-assemble and function in biological systems. Again, the distinct self-assembling abilities of synthesized or isolated peptide building blocks allow them to

develop into precise nanostructures with a variety of applications. Significant advancements in this area have arisen during the last few decades. In order to build functional supramolecular architectures and investigate their potential uses in biology, nanotechnology, and supramolecular chemistry, a variety of peptide-derived building blocks, including amphiphilic peptides, cyclic peptides, dendritic peptides, co-polypeptides, and aromatic or heterocyclic capped hybrid peptides have been designed and developed.[63–65]

1.2.4 Different Nanostructures Formed by the Self-assembly of Short Peptides

Nano-sized materials are the most influential players in the field of nanotechnology and offer a wide range of applications for contemporary civilization. The direction towards the development of improved materials and well-ordered nano-architectures was set in motion by molecular assembly. Peptides, out of all organic compounds, offer the main framework for creating bioinspired nanomaterials. For the purpose of creating diverse supramolecular assemblies, a variety of peptide-based building blocks have been created, including cyclic peptides, amphiphilic peptides, co-polypeptides, surfactant-like oligopeptides, dendritic peptides, aromatic dipeptides.[59,66–70] These different classes of peptides adopt versatile structures including fibers, tubes, spheres, vesicles, rods, coils, ribbons, etc. at nano dimension depending on their type, sequence, and self-assembling conditions. Zhang and co-workers demonstrated that 7-8 residue long peptides with distinct hydrophilic and hydrophobic residues could self-assemble in water to create well-ordered nanotubes and nanovesicles.[71] Hydrophilic head groups of these peptides were made of aspartic acids, and their hydrophobic tails were composed of amino acids like alanine, valine, or leucine as the primary regulating factor for the self-assembly of these peptides was self-association by hydrophobic interactions.[71]The majority of amphiphilic peptides have a hydrophilic peptide headgroup and a hydrophobic

alkyl tail, with the tail helping to align the head group into different secondary, super-secondary, and tertiary conformations.[72–74] These peptides self-assembled to create a range of nanoscale morphological forms, including micelles, vesicles, and tubules.[66,71,75,76]A family of amphiphilic compounds known as bola-amphiphiles consists of two hydrophilic groups that are flanked by hydrocarbon chains.[77] Their peptide segment engages in β-sheet hydrogen bonding to create different supramolecular nanostructures like fibers, rods, tubes, ribbons, and spheres, etc.[78–81]Lately, it was demonstrated that very small peptides can self-assemble into a variety of nanomorphologies, reducing the complexity and expense of their manufacturing while also boosting their stability. The majority of these short peptide fragments were found during research to establish the bare minimum sequence necessary for amyloid formation.NFGAIL, a hexapeptide fragment of the islet amyloid polypeptide (IAPP), and FGAIL a pentapeptide fragment of IAPP form well-ordered amyloid fibrils similar to that formed by the full length polypeptide.[82]Similarly, NFLVH and NFGSVQ were identified by Westermark et al. as the Aortic Medial Amyloid's minimal active amyloidogenic peptide fragments.[83,84]Even tetrapeptides can generate amyloid fibrils by Johansson et al.[85] They proposed that there are additional factors along with hydrophobic interactions that favor peptides self-assembling into fibers. Working with smaller peptides, Banerjee et al. showed, that tripeptide like Boc-AUV-OMe, Boc-AUI-OMe, and Boc-AGV-OMe, where U is γ-amino isobutyric acid, self-associated to produce super-molecular -sheet structures, which then organized into fibrils that resembled amyloid fibrils.[86] A tripeptide, TUA underwent a pH-responsive nanostructural change from nanotubes to nanovesicles in another study by Banerjee et al.[87]Researchers tried to investigate the self-assembly of peptides as tiny as dipeptides as they continued in this approach. The first study on dipeptide self-assembly was made by Gazit's team, who looked into how the dipeptide, FF, a key motif of the amyloid β (Aβ) polypeptide segment, self-assembles. This

dipeptide was self-assembled into nanotubes, microtubes, nanowires, and nano forests with a high degree of order.[88–93] A unique quality required in any biologically inspired material was discovered to be present in FF nanotubes: thermal stability.[94]Ihee and his team showed how diphenylalanine-based nanowires and nanotubes can undergo an intriguing morphological change. While nanotubes were created by dissolving the peptide in water using sonication and heating, nanowires were obtained in water at high ionic strength, and these two morphologies are interconvertible.[95] Hydrophobic dipeptides like LL, LF, FL, and IL self-assembled into nanotubes, as demonstrated by Görbitz et al., by generating head-to-tail (NH3+ OOC) hydrogen bonds.[96–100]Additionally, these researchers demonstrated the formation of water-filled nanotubes by dipeptide WG[101,102] and nanoporous structures by dipeptides VA and FF[96,99,103,104]. Additionally, Gazit et al. showed how the addition of a thiol group to FF caused it to assemble into spherical structures rather than tubular ones.[105] They further demonstrated the assembly of other aromatic homo-dipeptides into nanospheres, nanoplates, nanofibrils, and hydrogel.[106]These peptide nanostructures can be utilized as a casting mold for the production of coaxial nanocables and metallic nanowires.[88,107]Sozzani and his colleagues have demonstrated that crystalline dipeptides like AV, VA, IV, and VI can self-assemble into nanoporous materials with the ability to adsorb, segregate, and store a variety of gases, including methane, carbon dioxide, and hydrogen.[108] A dipeptide, IF, at pH 5.8 self-associated into a network of nanofibrous structures in water, according to Ventura and his coworkers.[109] Modified dipeptides have also been investigated as templates for creating biologically useful self-assembled nano or microstructures due to their improved proteolytic stability. Both in the solid state and aqueous solution, two modified dipeptides (β-AA,δ-Ava-F) with an N-terminally located β-amino acid residue self-associated to create a uniform and well-ordered hollow nanotubular structures with varying dimensions.[110]BPhg-A (Phg: phenylglycine) and Phg-β-A, two water-soluble

synthetic dipeptides, were seen to create dipeptide-based nanoporous materials that have demonstrated the ability to adsorb N_2 gas.[111]Gazit et al demonstrated that in an aqueous solution, Fmoc-FF generated nanofibrillar shape[112] whereas uncharged peptide analogue Ac-FF-NH_2, self-assembled into tubular forms.[113]

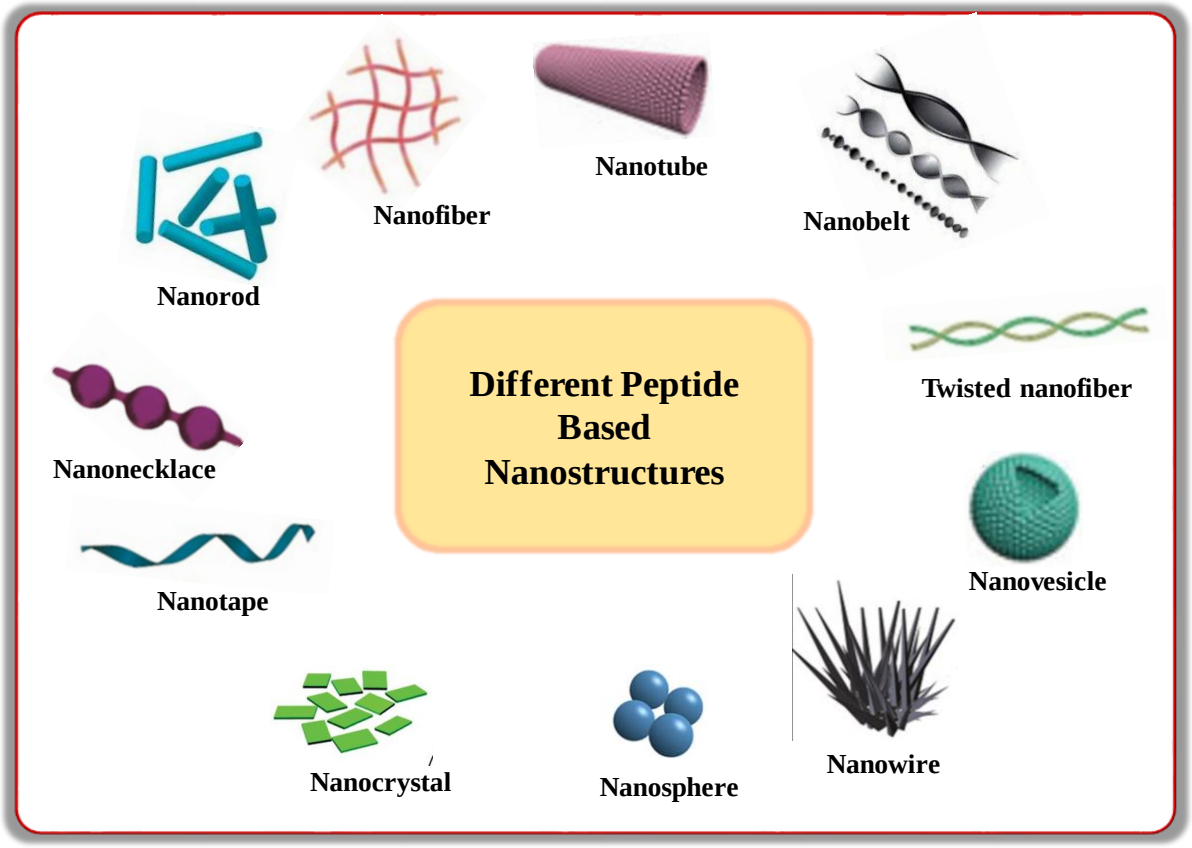

Figure 2. *Different nanostructures produced by the self-assembly of short peptides.*

Other diphenylalanine peptide analogues with amine and carboxyl modifications were subsequently investigated by Gazit et al., and it was discovered that these dipeptides produced organized tubular structures at the nanometric scale.[113] Ulijn and colleagues demonstrated that Fmoc dipeptides, which were created by combining four different amino acids (glycine, alanine, leucine, and phenylalanine), produced hydrogels with a variety of structural and physical characteristics.[30] It has been demonstrated that peptides with different aromatic moieties, such as Fmoc, naphthalene, and pyrene, make excellent

templates for nanofibrillar hydrogel networks.[114–120]Ordered fibrillar nanostructures were also produced by dipeptides such as di-D-1-Nal (Nal: naphthalene)and di-D-2-Nal, which were created by replacing phenyl groups with naphthyl groups.Naphthalene-derived di-D-1-Nal produced fibers with a 10 nm diameter. In contrast, di-D-2-Nal peptide generated more coiled, broader tubular structures.[106]Another intriguing example was the concentration-dependent transformation of a nanovesicle into a nanotube by the peptide Acp-YE (Acp, ε-amino caproic acid). Acp-YE created vesicles at a concentration of 6.9 mg ml-1, while 2.3 mg ml-1 of the peptide produced nanotubular structures, and an intermediate dose of 3.4 mg ml-1 of the peptide produced a variety of fused vesicular structures that, upon dilution, fused to form nanotubular structures.[121] Research has been carried out with dipeptides containing an unnatural amino acid α,β-dehydrophenylalanine (ΔPhe; ΔF) in the peptide backbone and it was reported that the dipeptide FΔF, can self-assembled into distinct tubular structures similar to FF.[122]EΔF and KΔF, two dipeptides with amphiphilic ΔF residues, self-assembled into anionic and cationic vesicular structures, respectively.[123]The ability of single amino acids to form self-assembling structures have also been studied with various chemical modifications.Ryan et al. demonstrated formation of fibrillar nanostructures by self-assembly of single amino acid based molecule Fmoc-F and its fluorinated derivatives like penta-fluorophenylalanine (5-Fl-Phe) and tri-fluorophenylalanine (3-Fl-Phe).[124]Enzyme-triggered dephosphorylation of Fmoc phosphotyrosine into Fmoc protected tyrosine (Fmoc-Y) also results in self-assembled hydrogels.[125–127]In a relatively recent work, the self-assembly of just one amino acid, phenylalanine, into organized fibrils at pathogenic concentration found in the mental disease, phenylketonuria was also demonstrated by Gazitet al.[128]Another interesting type of peptides that has become an interesting area of research is cyclic peptides. For example, the self-assembly of cyclic peptides cyclo(Gly–Gly), cyclo(l-Trp–l-Trp), and cyclo(l-

Phe–l-Phe) resulted in the formation of distinct morphologies such as mesh like nanoporous structures, nanofiber, nano-tape respectively depending on the composition of amino acids in their molecular structures.[129–132] So, by altering the type, and sequence, or by using external triggers like temperature, pH, concentration, medium, solvent, ionic strength, etc., the self-assembled nanostructures can be adjusted or altered. One peptide self-assembled nanostructures can serve a variety of purposes, such as adsorbing pollutants from the environment, medication delivery, tissue engineering, cell penetration, etc.

1.2.5 Peptide-Based Organogels and Hydrogels: An outcome of Peptide Self-assembly

Self-assembly of short peptides, which is the spontaneous arrangement of individual molecules into ordered structures through non-covalent weak interactions often leads to the formation of soft nanomaterials called gel. Gel may be classified as a solid, in the sense that it has its own shape and stands its own weight, and is easily identified by the simple ‘‘inversion test’’ (turn a pot of gel upside down and it can support its own weight without falling out), but actually it is made of about 99% of a liquid and of 1% of a solid (called ‘‘gelator’’). The definition that was put forth by Flory in 1974 is the one that is most commonly used: "a gel has a continuous structure that is permanent on the analytical time scale and is solid-like in its rheological behavior."[133] The ability of peptide-based scaffolds to self-assemble through a variety of noncovalent interactions, such as hydrogen bonding, electrostatic interactions, or π-π interactions, makes them intriguing candidates for hydrogelation and organogelation. These interactions result in the creation of well-organized supramolecular structures that, given the right circumstances, can trap and immobilize a large number of solvent molecules which in turn results in the formation of gel. They can also be easily manipulated chemically and

biologically, and they are simple to produce in vast quantities. The hierarchical self-assembly process that underlies the method through which LMWGs function includes the following steps: (i) The molecular-scale building blocks can self-assemble into supramolecular polymers known as fibrils; (ii) the fibrils frequently then assemble into nanoscale bundles, known as fibers; and (iii) the fibers tangle and interact with one another to form a self-supporting, "solidlike" network, which underpins the macroscopic gel.[134]Gel-phase materials are commonly prepared by heating and cooling a gelator-solvent mixture, then solubilizing the gelator and gel fibers using heat or ultrasound irradiation. Short peptide based LMWGs can give rise to two types of gels namely hydrogel or organogel or both. Hydrogels are made up of peptides and water whereas organogels are made up of peptides and any kind of organic solvents.[134]Supramolecular hydrogels, in contrast to polymeric hydrogels, have the ability to change their pore sizes during the shrinkage and swelling processes. This ability to self-adjust pore sizes may make supramolecular hydrogels "smart" matrices for controlled drug release.[135]

1.3 SCOPE OF THIS THESIS

Peptide self-assembly resembles many biological functions and also the nanostructures and nano-materials produced via self-assembly of short peptides have many applications in biomedical and biomaterial fields. Thus, it is very important to get information about the mechanism involved in peptide self-assembly formation. For example, it is evident that the formation of amyloid fibrils is associated with several serious human diseases, such as Alzheimer's disease, Parkinson's disease prion disorders, type II diabetes, etc.[136–143]For figuring out the pathway directing fibrilar construction, a lot of research was done on short peptide-based model systems that can generate fibril structures. According to Ehud Gazit and other groups, aromatic π-π stacking interactions may instead of other hydrophobic interactions supply the activation energy and

directionality necessary for the production of amyloid fibril assemblies. This hypothesis led to the identification of diphenylalanine as the core recognition motif of Alzheimer's β-amyloid polypeptide.[88,144]In recent times, many studies were carried out using phenylalanine based self-assembly systems but little is known about other amino acids which can form amyloid fibrils as well as other various nanostructures. In this thesis, we mainly focused on the self-assembled nanostructures obtained from cysteine based small peptide moieties. Cysteine is one of 20 naturally occurring amino acids and like the other amino acids, cysteine is abundant as L-form. It is necessary for the synthesis of protein as well as other metabolic processes. Cysteine is the major component of hair, skin, and nails. It is required for collagen production and is also found in beta-keratin. There are examples of long and short peptides containing one or more cysteine amino acid residues that can form self-assembled nanostructures but the examples are fewer and there are very less examples of self-assembling short peptides having benzyl protected cysteine. Moreover, in several other previous works from our lab, it was observed that benzyl protected cysteine based peptides possessed a tendency to form various unique self-assembled nanostructures including nano-sphere, nano-tube, nanofibril, protofibril, etc.[145–148] Here, in the second chapter of this thesis a cyclic dipeptide was synthesized containing L-leucine and S-benzyl-L-cysteine which can form hydrogel at physiological conditions. It was intended to synthesize a hydrogelator which could be used as a template for sustainable drug release. In vitro drug release study from the hydrogel was performed using anticancer drug 5-Fluorouracil (5FU). This hydrogelator was found to encapsulate anticancer drug 5FU and lowered the IC_{50} dosage of the drug via sustainable release. The structural insight of the hydrogelator and the non-covalent interactions involved in the self-assembly process were analyzed by AFM, FE-SEM, FT-IR, NMR, and CD experiments. In the next chapter, studies were aimed to know how small variations of constituting amino acids in the peptide moieties caused a

significant difference in their morphology as well as in gelation properties. Thus a series of six cyclic dipeptides were synthesized and thoroughly characterized by NMR FT-IR etc. The morphology of these peptides was thoroughly studied by AFM microscopy and the formation of fibrillar nano-structures due to presence of different hydrophobic interactions between the cyclic peptides was explained with help of crystallographic study. DFT and Hirshfield surface experiemnts were employed to get information about how hydrophobicity of different side chains in the above mentioned CDPs controlled the self-assembly pattern of the respective CDPs. In the last chapter, we have designed and synthesized two sets of a total of four heterocyclic capped peptide scaffolds having quinazolinone and S-benzyl-L-cysteine as common residues with some structural twists. Interestingly, one set of the peptides self-assembled in fibrillar nano-structure while another set of peptides produced spherical assembly. So, this chapter gives an idea about small variation in the molecular structure of the peptides can alter the self-assembly pattern as well as the morphology produced by them. The heterocyclic capping also induced hydrogelation in two of the molecules. Crystallograpic evidences showed diiferent types of hydrophobic interations present in the self-assembled structure of the peptides in the solid state.

CHAPTER-2

Cysteine Derived Cyclic Dipeptide Super Hydrogelator: Enhancing Efficacy of an Anticancer Drug via Sustainable Release

2.1 AIM OF THE PRESENT WORK

Study of low molecular weight gelators derived from self-assembling short peptides is a fast-growing area of research due to their numerous uses in the fields ranging from biomedicals to biomaterials. Short peptide based hydrogels are gaining special attention because of their biocompatibility and less toxicity compared to other available synthetic polymeric or bio-polymeric gels. More to it, the reversible nature of peptide-based hydrogels makes them superior as they are formed by weak non-covalent interactions, unlike synthetic polymeric gels which involve chemical interactions. Thus in this work, efforts were made to synthesize a short peptide that could form hydrogel with high water content under physiological conditions. The main motive behind this hydrogel formation was to examine the applicability of the hydrogel as a drug delivery template. In this regard, a cyclic dipeptide containing S-benzyl-L-cysteine and L-leucine was synthesized which formed hydrogel at physiological conditions. Cyclic dipeptide was chosen over its linear counterpart as cyclic peptides possess high structural rigidity and less enzymatic degradation which enabled them to sustain extreme physical conditions. Then the capability of this hydrogel to act as a drug-delivery vehicle was examined by in-vitro studies using 5FU as a template anticancer drug. Cytotoxicity assay of the hydrogel and comparative anticancer activity of the drug loaded in hydrogel and its bare form was performed. All these experiments and results as a whole were aimed to develop a suitable hydrogelator as a drug-delivery vehicle.

2.2 INTRODUCTION

Hydrogels are a new class of soft materials which are in high demand these days due to their wide range of potential uses in industries like biomaterials, biosensors, drug delivery, tissue engineering, wound healing, removing toxins from water, and several bio-nanotechnology-based electronic and photonic

energy storage.[149–154]Small monomeric units self-assemble into supramolecular hydrogels using weak yet potent non-covalent interactions such as hydrogen bonds, van der Waals contacts, π-π stacking, electrostatic interactions, and others.[155–157]Together, these factors create a three-dimensional cross-linked network that can cage water molecules and render them immobile.[158–160] Supramolecular hydrogels are more adaptable than traditional polymeric and biopolymer gels because they have reversible properties and possess facile sol-gel-sol transition due to the presence of non-covalent interactions.[161,162]The physicochemical characteristics of peptide-based hydrogels can be easily modified to attain specific properties suitable for a desired application due to the availability of a variety of self-assembling domains.[163] Additionally, peptide hydrogels are strong candidates for material and biomedical applications due to their straightforward large-scale production, thermal stability, tuneable rheological characteristics, aqueous processability, and biocompatibility.[33,164] However, hydrogels obtained from the self-assembly of linear peptides suffer from instability and rapid enzymatic degradation because they lack molecular stiffness and have a low environmental tolerance at physiological conditions.[165–167]Therefore, it is imperative to develop new kinds of modified peptide hydrogels to bypass the drawbacks of linear peptide-based hydrogels and improve their practical applicability.

The lowest and most basic type of cyclic peptides is cyclic dipeptides (CDPs) or 2,5-diketopiperazines which contain a six-membered heterocyclic lactam ring core. The majority of naturally occurring CDPs are secondary metabolites that are present in species ranging from bacteria to people.[168] Synthetic molecules, metabolites, or organic compounds with CDP core displayed a wide range of biological activities, including anticancer, antimalarial, antimicrobial, hypoglycaemic agents, quorum sensing, blood-brain barrier (BBB) transporters, drug delivery vehicles, tissue engineering, and more.[169–175] When compared to their linear equivalents, CDPs show high structural rigidity, high physiological

stability, low enzymatic degradation, and superior biological activity.[165,176]The lack of conformational mobility and the presence of two cis amide groups with four hydrogen-bonding sites (two donors and two acceptors) in CDPs favour the formation of gels.[177,178] Furthermore, by selecting desirable amino acid composition or altering the side chains of constituent amino acids in the CDP scaffold, additional noncovalent interactions that are important in promoting molecular self-assembly can be easily incorporated into the CDP moiety.[171] However, there are limited examples of CDP-based gelators that can produce hydrogel at physiological conditions,[179–182] necessitating the urgent need for the creation of new CDP based gelators that can produce diverse hydrogels for a wider variety of biomedical applications.

Our study is primarily focused on the synthesis of peptide-based small molecules that produce various nanostructures via self-assembly and in turn results in gels. For use in biomaterial applications like drug delivery, in this chapter work, focus was made on synthesizing small peptides that could form hydrogel under physiological conditions. In previous research works our team has reported that benzyl protected tyrosine-based dipeptides formed organogels through nanofibrillar self-assembly in several mixed organic solvents.[183]From earlier research conducted on benzyl protected cysteine, it was evident that di- and tripeptides formed from benzyl protected cysteine had produced a variety of self-assembled nanostructures, such as nanofibrils, protofibrils, nanospheres, and so on.[145,148,184] In each case, participation of the benzyl protecting group in π-π stacking interactions was crucial in creating the self-assembly structure in those di- and tripeptides. Considering these details, the cyclic dipeptide cyclo-(Leu-S-Bzl-Cys) (**S1**) was designed and synthesized which has the amino acids L-leucine and S-benzyl-L-cysteine as its constituents. In presence of a very little amount of polar organic solvents(DMSO, DMF, methanol, acetonitrile, etc.), the cyclic dipeptide was found to form a hydrogel both in water and in the PBS buffer of pH 7.46. The addition of the benzyl group to the cysteine moiety was

planned ahead of time to introduce π-π stacking, which when combined with the hydrogen bonding interaction of two amide groups and the hydrophobic backbone of the leucine side chain, promoted the self-assembly of the cyclic dipeptide **S1** into a highly entangled fibrillar nanostructure. The hydrogel thus obtained from cyclic dipeptide **S1** exhibited excellent resistance to environmental factors including pH and temperature and remained stable for more than a year without any deformation. The hydrogel was thermoreversible and its stability in different pH was also investigated. By using rheology experiments, the mechanical strength of **S1** hydrogel was determined. Morphological insight of **S1** was visualized by Atomic force microscopy (AFM) and field emission scanning electron microscopy (FE-SEM). Circular dichroism(CD), Fwier transform infrared (FT-IR) and NMR investigations were also performed to gain information about the non-covalent interactions involved in the self-assembly. **S1** falls under the "super gelator" category because to its extremely low minimum gelation concentration (MGC) of 0.05% (w/v)qualifies it as a "super gelator".[180,185] High water content and great stability under physiological conditions of **S1** hydrogel further motivated research into its use in drug delivery.

A promising chemotherapeutic medication called 5-Fluorouracil (5FU) was selected as a test candidate for a slow and sustained drug delivery trial.[186] 5FU is a potent anticancer drug mostly used to treat colorectal cancer as well as other cancers like breast cancer and gastrointestinal cancer, bladder cancer, neuroendocrine tumors, cervical cancer, and many more.[187–189]However, 5FU chemotherapy is also associated with several limitations, including a very short half-life and significant cytotoxicity when used at high concentrations.[187,190–192]Therefore, it is crucial to create a potent drug delivery system that is both affordable and effective in order to maintain a consistent dosage of 5FU over an extended length of time. Encapsulation and slow release of the anticancer drug 5FU from the hydrogel **S1** was discussed in this chapter. The cytotoxicity of **S1**

hydrogelator was examined in the human colorectal cancer cell line HCT116, and a comparison of the anticancer activity of 5FU in both its bare and hydrogel-encapsulated state was conducted.

2.3 RESULTS AND DISCUSSION

2.3.1 Synthesis of Cyclic Dipeptide S1

All chemicals were purchased from Sigma-Aldrich and used without further purification unless otherwise stated. Solvents were freshly distilled by the standard procedures before use. Column chromatography was performed on silica gel (Merck, 60–120 mesh) with the required eluent. Finally, compounds were characterized by ^{1}H-NMR, ^{13}C-NMR, and mass spectrometry**.** The cyclic dipeptide **S1** was synthesized by conventional solution phase methodology. The N-terminus was protected through BOC (tert-butoxycarbonyl) group and the C-terminus was protected through methyl ester. The coupling reaction was mediated using 1-ethyl-3,3-(dimethylamino)propylcarbodiimide hydrochloride (EDC.HCl) and hydroxybenzotriazole (HOBt). The synthetic route to **S1** is shown in Scheme 1.

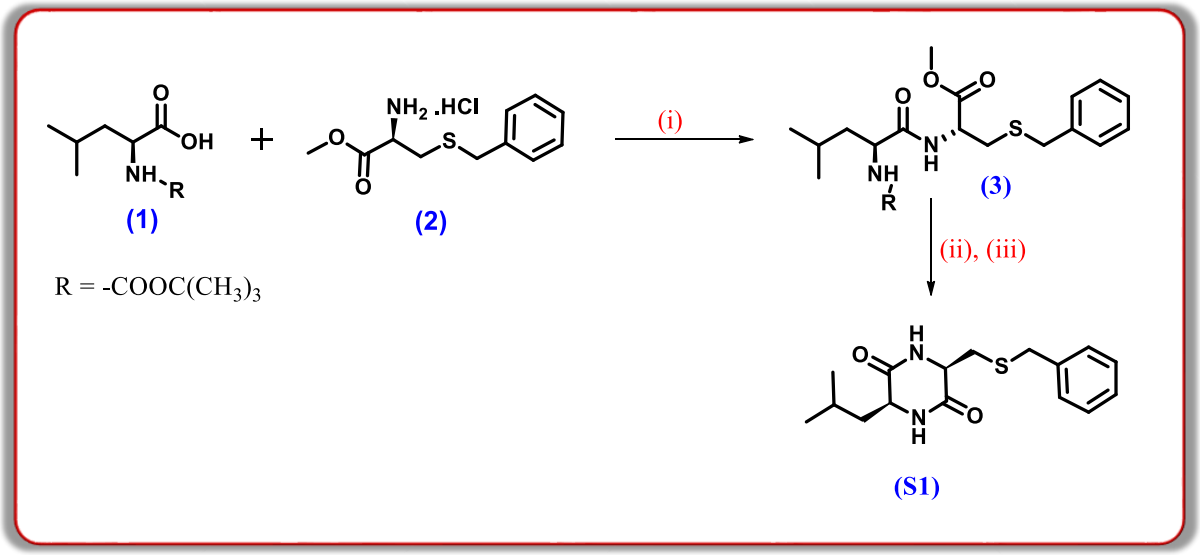

Scheme 1. *Schematic presentation of the synthesis of the dipeptide.* ***[a]Reagents and Condition:*** *(i) EDC·HCl, HOBt, TEA, 0°C to r.t, 8 h, (ii) TFA, DCM, 0°C to r.t, 4 h, (iii) $NaHCO_3$, H_2O, pH=8-9.*

Synthetic procedure: To a well-stirred solution of *N*-(*tert*-Butoxycarbonyl)-L-leucine (**1**; 500 mg, 2.16 mmol) dissolved in *N,N*-dimethylformamide (10 ml), was added anhydrous hydroxybenzotriazole (HOBT; 350 mg, 2.59 mmol) slowly followed by 1-ethyl-3,3-(dimethylamino) propyl carbodiimide hydrochloride (EDC·HCl; 622 g, 3.24 mmol) at 0 ^{o}C under nitrogen atmosphere. Then stirring was continued for 10 mins at ice-cooled condition and after that to this mixture, triethylamine (TEA; 1.5 ml, 10.8 mmol) was added followed by S-benzyl-L-cysteine methyl ester hydrochloride (**2**; 679 mg, 2.59 mmol). The reaction was further continued for 8 h at room temperature (monitoring via TLC). The reaction mixture was then concentrated under reduced pressure and extracted with ethyl acetate (3 × 20 ml). Evaporation of solvent left a crude residue, which was purified by column chromatography over 60-120 mesh silica gel (hexane/ethyl acetate 70:30) to afford the intermediate compound '**3**' as white solid (yield = 74%). In the next step, intermediate '**3**' (700 mg, 1.59 mmol) was treated with trifluoroacetic acid (TFA; 732 µl, 9.58 mmol) in dichloromethane solvent (12 ml) at 0 ^{o}C. The reaction mixture was slowly brought to room temperature and stirring continued. After 6 h, the completion of the reaction was confirmed via TLC and the reaction mixture was then concentrated under reduced pressure. The crude mixture was then treated with 1 (N) sodium bicarbonate solution until the pH reached 8-9 and extracted with dichloromethane (3 x 20 ml) from the aqueous layer.[173,193] After evaporation of the solvent, the product was purified by column chromatography over 60-120 silica gel using dichloromethane/methanol 95:5 as eluent to afford the final product '**S1**' (yield=50%) as white solid (Scheme 1). The purity of compound '**S1**' was checked by analytical HPLC (**Figure S4**) using acetonitrile/water as eluent and '**S1**' was characterized by ESI-MS (**Figure S3**) and ^{1}H, ^{13}C NMR (600 MHz) spectroscopy (**Figure S1, S2**).

2.3.2 Gelation Study of Cyclic Dipeptide S1

The ability of cyclic dipeptide **S1** to gel at various solvents and concentrations in neutral and physiological pH was investigated. First, 1 mg of the hydrogelator (**S1**) was weighed in a tiny screw-capped glass vial for the hydrogel preparation and dissolved in 10 µl of HPLC grade DMSO. The addition of water or PBS buffer (990 µl) resulted in the appearance of a white, non-homogeneous, loose gel that, when heated vigorously, disintegrated and produced a clear solution. As the heated solution cooled to ambient temperature a homogenous transparent hydrogel with a slight white tint was developed within a few mins which did not show any gravitational flow upon inversion of the vial (**Figure 1A, 1B**). The minimal gelation concentration (MGC) for **S1** hydrogel was found to be 0.05% (w/v) in both water and PBS buffer after hydrogels of various concentrations were prepared using lesser quantities of hydrogelator. **S1** failed to produce a robust, self-supported gel that can defy gravity below this concentration rather formed only a loose gel. Due to its extremely high water content and low MGC value, **S1** hydrogel fits well within the range of 'super hydrogel'. It was also seen that hydrogel formation was also attained by diluting the CDP with water after being dissolved in very little amount of polar organic solvents such as DMF or methanol, (**Figure S5**). This indicates that water is crucial for promoting hydrogelation through the creation of hydrogen bonds, which is further supported by the observation that when the proportion of water to the other co-solvent was reduced, the degree of hydrogelation subsequently dropped. In addition, the gelation study was carried out in pure organic solvents, and it was discovered that this **S1** can also form an organogel in solvents like dichloromethane and ethyl acetate. However, in contrast to hydrogels, the gelation in pure organic solvents required a relatively high concentration of the **S1** hydrogelator (MGC = 4% w/v in dichloromethane

and (MGC = 2% w/v in ethyl acetate) and much longer time to form a stable gel.

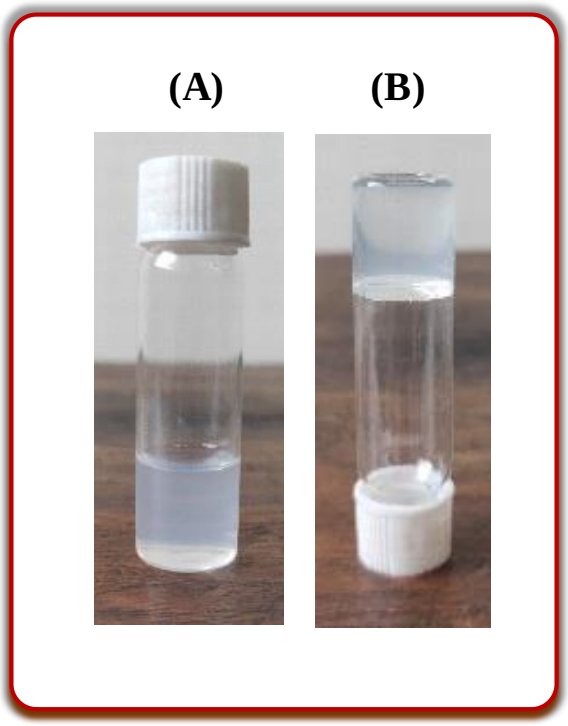

Figure 1. *(A) Photographic image of S1 hydrogel obtained from 1% DMSO in PBS buffer (pH=7.46), (B) vial inversion test performed with S1 hydrogel.*

2.3.3 Thermal and pH Stability of S1 Hydrogel

Since pH and temperature are strongly related to the intermolecular interactions in nanomaterials, they can have an impact on the stability of hydrogels. **S1** hydrogel is thermoreversible by nature because it exhibits a gel-to-sol transition following heating and returns to its gel state upon cooling. The gel-to-sol transition temperature (T_{gel}) was determined by placing the gel-containing screw-capped glass vial into an oil bath and raising the temperature at a rate of 2 $^{o}C\ min^{-1}$. The temperature was monitored using a thermometer and T_{gel} was defined as the temperature (+0.5 ^{o}C) at which the gel melted and showed gravitational flow. The T_{gel} of the **S1** hydrogel was determined to be 75 ^{o}C at its

MGC, and it further rises with increasing gel concentration. This hydrogel demonstrates good thermal stability since it can withstand high temperatures. The hydrogel was then left in place for testing its stability under ambient settings, and even after a year, no physical deformation of the hydrogel was found. In addition, the gel-forming potential of **S1** was tested at pH levels ranging from 4 to 12. It was observed that **S1** can form a stable hydrogel between pH 6 and pH 12, however below pH 6 in aqueous solvent systems, it creates a whitish suspension.

2.3.4 Mechanical Stability Measurement of S1 Hydrogel

Rheological testing was done on the hydrogel made from the cyclic dipeptide **S1** to determine its stiffness and mechanical strength. The rheological measurement of the gel obtained from cyclic dipeptide **S1** in aqueous solvent (1% DMSO in PBS) was performed using Modular Compact Rheometer (Anton Parr, MCR 102, Austria). The instrument was equipped with an air compressor unit which maintained the air pressure at 7 kg/cm2. Standard cone-plate geometry (CP-40, 40 mm outer diameter, angle 1o) was employed in the study. Strain sweep (G′, G″ versus strain) and Frequency sweep (G′, G″ versus angular sweep) were measured in oscillation mode. The data was analyzed using Rheoplus software (US 200, version 3.62).

Rheological experiments are crucial for determining the viscoelastic properties of gel materials.194 The terms "storage modulus" and "loss modulus" refer to two characteristics that relate to a substance's viscoelasticity. The storage modulus G′ denotes a material's capacity to return to its original shape after being deformed, while the loss modulus G″ denotes how the material flows when under stress. When a viscoelastic material is in its gel form, the storage modulus is always greater than the loss modulus, and the opposite is true when it is in its sol state.

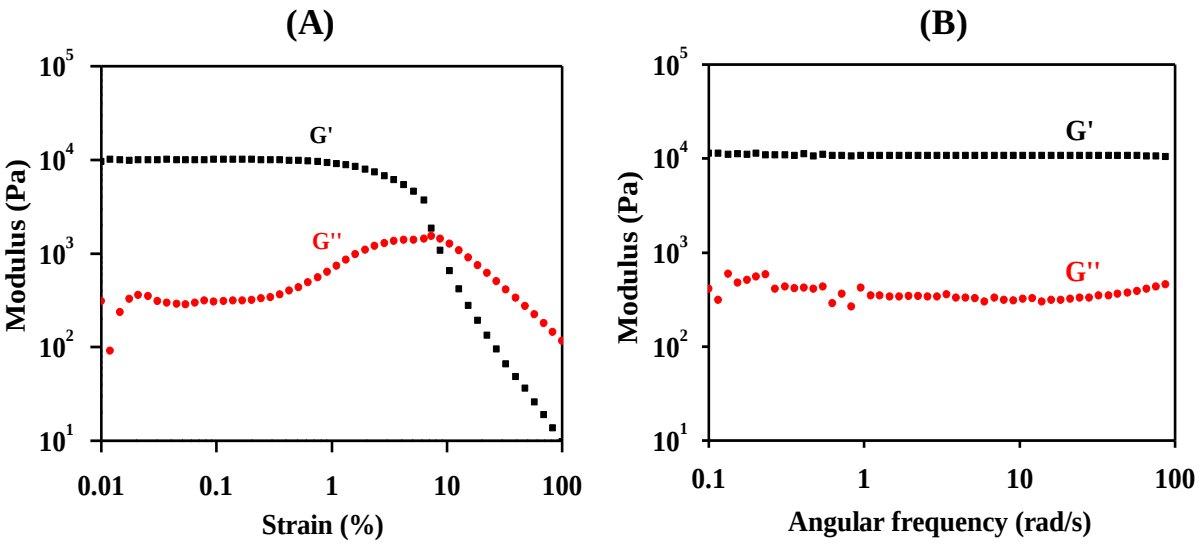

Figure 2. *(A) Strain sweep experiment, and (B) Frequency sweep experiment at 0.1% of constant strain, performed on S1 hydrogel obtained from 1% DMSO in PBS (pH=7.46).*

The results of a typical strain sweep experiment on S1 hydrogel revealed that G′ and G″ are virtually completely unaffected by the applied strain up to a strain value of 10%, demonstrating the gel state of the hydrogelator. The gel began to disrupt at the crossover point, where G′ = G″, and continued to behave like a fluid after this point (**Figure 2A**). The hydrogel made from S1 was then used in a frequency sweep experiment with constant (0.1%) strain, where G′ and G″ were measured as functions of angular frequency. The experiment revealed that the hydrogel behaves linearly and that the lines (G′ and G″) never cross over during the whole frequency range under investigation (**Figure 2B**). It was discovered that G′ was 20 times bigger than G″, which suggested the formation of a solid-like stable gel material.195The high value of storage modulus (104 pa) indicates excellent mechanical resistance of the nanomaterial towards external forces which attributes to the formation of an extremely dense nanofibrillar network within the hydrogel.

2.3.5 Morphological Study

2.3.5.1 Field Emission Scanning Electron Microscopy (FE-SEM) Study

Morphologies of the gel materials were investigated using field emission scanning electron microscopy (FE-SEM). For the FE-SEM study, dilute solutions of gel materials were dried and platinum coating was carried out. Then the micrographs were taken in an FE-SEM apparatus (ZEISS-SIGMA, Carl ZEISS Microscopy, Germany). Field emission scanning electron microscopy (FE-SEM) was used to visualize the microstructure that the hydrogel had adopted using the xerogel made from **S1** in DMSO-PBS solvent (pH 7.46). The FE-SEM pictures (**Figure 3A**) showed that the xerogel developed a highly entangled web-like architecture made up of multiple long nanofibers. This nanofibrous network's ability to trap numerous water molecules inside its cages encouraged the formation of the self-supporting hydrogel. A porous nanostructure with a large surface area is indicated by the nanofibres' average width, which is in the 25–200 nm range, and their length, which is several microns. The nanofibres' average width, which is in the 25–200 nm range, and their length, which is several microns, indicated a porous nanostructure with a high surface area. The multiple branching in the fibrillary network was beneficial in improving the mechanical stability of the hydrogels in extreme conditions. The network is observed to become more densely packed at higher **S1** hydrogelator concentrations as a result of the bundle-up of the thinner nanofibers into thicker, wider structures (**Figure 3B**) with a diameter of up to 400 nm. These networks may be able to accommodate different drugs and other organic molecules and by releasing these molecules into the nearby solvent, these highly cross-linked dense three-dimensional networks may establish a platform for a variety of medicinal and nanotechnological applications.

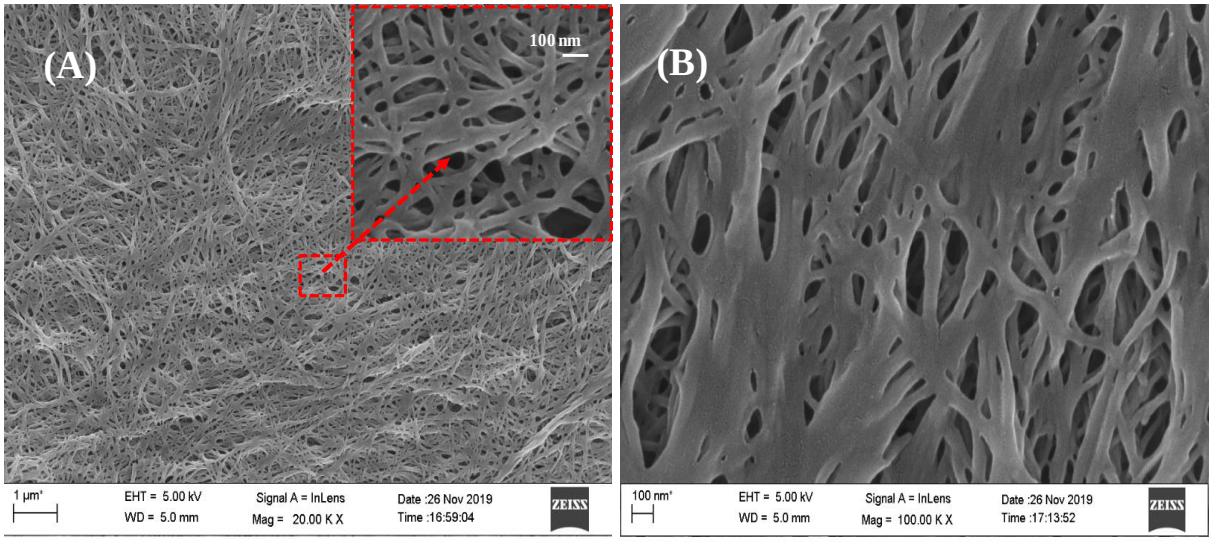

Figure 3. *FE-SEM image of S1 hydrogel obtained from DMSO-PBS at pH=7.46 (A) at 0.5 mg/ml concentration showing the nano-fibrillar self-assembly (the inset picture depicted the enlarged view of the nano-fibrillar network) and, (B) at a concentration of 1 mg/ml depicting bundling up of thin nanofibers into thicker nanofibers.*

2.3.5.2 Atomic Force Microscopy (AFM) Study

To get additional information about the surface morphology and size of the nanofibers, atomic force microscopy experiments were carried out with the dilute solution of the hydrogelator (**S1**). For this purpose, a dilute solution of **S1** was incubated at room temperature for 24 h, and then the solution was drop cast on a freshly cleaved mica sheet. After drying the sample solution placed on the mica sheet, the specimen was observed through Pico Plus 5500 AFM (Agilent Technologies, Inc., Santa Clara, CA, USA) with the piezo scanner range of 9 µm. The images (256 × 256 pixels) were captured with a scan size between 0.5 and 5 µm at the scan speed rate of 0.5 rpm. The images were processed through flattening via Pico view software (Molecular Imaging Inc., Ann Arbor, MI, USA). The AFM pictures revealed highly cross-linked self-assembly of nanofibers with widths between 55 and 120 nm and lengths of several micrometers (**Figure 4C**). It is noteworthy that the cross-linked fibrillar nanostructure appeared similarly when AFM images of **S1** were acquired

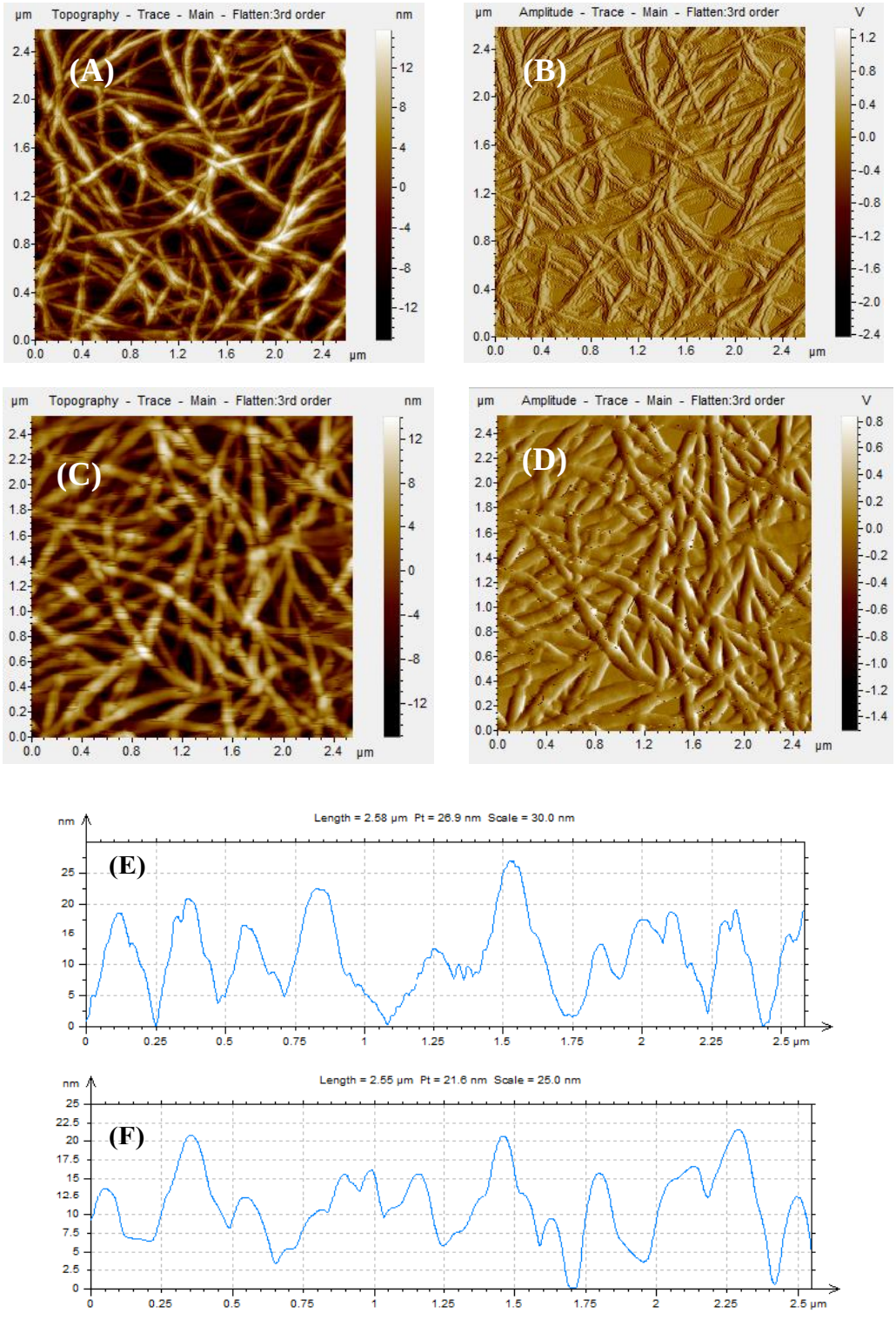

Figure 4. *Atomic force microscopy (AFM) images of S1 in 1% DMSO-PBS (pH = 7.46) solvent system (A) topography of fibrillar assembly having fiber diameter 25–75 nm produced without incubation, and (B) corresponding amplitude image of A. (C) topography of fibrillar assembly having fiber diameter 55–120 nm produced after 24 h of incubation, and (D) corresponding amplitude image OF C. (E) Heightprofile of AFM image A (Length=2.58 µm Pt = 26.9 nm Scale = 30.0 nm), and (F) height profile of AFM image C (Length=2.55 µm Pt = 21.6 nmScale = 25.0 nm).*

immediately after the solution preparation and without allowing it to incubate (**Figure 4A**). This finding demonstrates that the hydrogelator aggregates instantly in aqueous solution, which is supported by the fact that the cyclic dipeptide **S1** turned into hydrogel immediately (within a few mins) once aqueous solvents were added to the solution of **S1** in polar organic solvents. The diameter of the nanofibers obtained from **S1** solution without incubation ranged between 25-75 nm which was smaller than those obtained after 24 h of incubation. As a result, it can be concluded that the degree of self-assembly and the hydrogelation of **S1** in aqueous solution both strengthened over time and generated thicker, rod-like fibrils. Other solvents such as DMF-water, methanol-water, ethyl acetate, dichloromethane, etc. were also used to study the morphology of **S1**, and it was observed that **S1** can also form fibrils from diluted solution in each of these solvent systems (**Figure S7**).

2.3.6 Spectroscopic Study

The structural information of the hydrogelator **S1** as well as the forces involved in the process of self-assembly of the same were accessed using a variety of spectroscopic techniques. One of the most significant weak forces in the development of molecule self-assembly is hydrogen bonding. As a result, various hydrogen-bonding patterns play a significant role in controlling the secondary structure of peptide self-assembly. Since cyclic dipeptides contain two cis amide bonds, there is a strong likelihood that those two amide groups will participate in the self-assembly process by forming hydrogen bonds. The determination of the involvement of those amide groups in the self-assembly may be done very effectively with the help of NMR and FT-IR spectroscopy.

2.3.6.1 NMR Study

H/D exchange NMR experiments and temperature-dependent 1H NMR experiments were carried out to gain a brief understanding of the hydrogen bonding pattern of the amide protons of **S1**.[194] In the proton NMR spectra of **S1** in DMSO-d_6 solvent, the two peaks that appeared at 8.10 ppm and 8.35 ppm arose due to the two lactam amide proton of **S1** molecule (**Figure 5A**). The intensity of both amide proton peaks rapidly dropped within a few mins after adding 10 µl of D_2O to a 10 mM solution of **S1** in DMSO-d_6 (**Figure 5B**), and it nearly disappeared after an hour (**Figure 5C**).

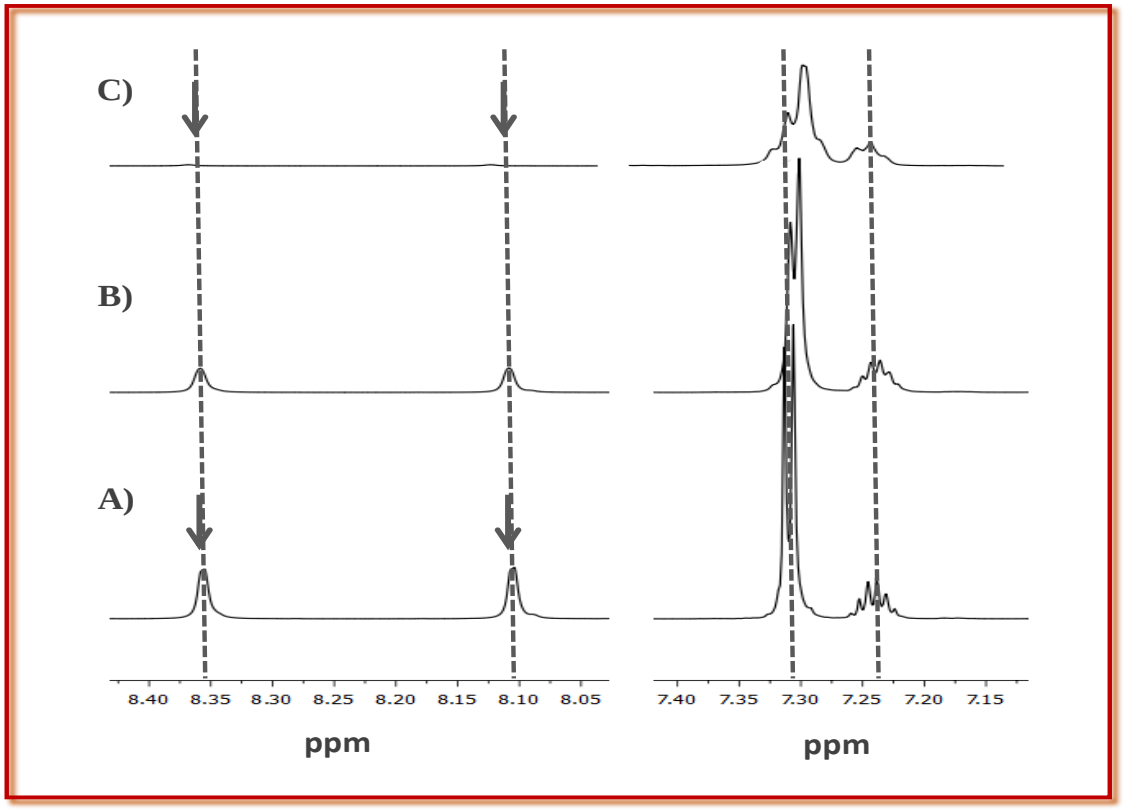

Figure 5. *H/D exchange experiment performed with the cyclic dipeptide S1 (10 mM) in DMSO-d_6: (A) ^{1}H NMR spectra of S1 in absence of D_2O, (B) ^{1}H NMR spectra 5 mins after addition of 10 µl D_2O into the DMSO-d_6 solution of S1, (C) ^{1}H NMR spectra of S1 1 hr after addition of D_2O.*

This finding suggested that those amide protons were deuterium-exchangeable and thus solvent-exposed. Since the H/D exchange rates are a function of two parameters: solvent accessibility and hydrogen bonding, the exchange rate of these two amide protons can be used to infer that **S1** was involved in intermolecular hydrogen bonding with other **S1** molecules as well as with water molecules in its extended structure. As a result, it can be said that intermolecular H-bonding in **S1** produced an ordered secondary structure, and the high affinity of the amide backbone (-CONH-) for the water molecules allowed for the development of a self-assembling porous three-dimensional structure that ultimately resulted in the formation of the hydrogel.

The presence of intermolecular hydrogen bonding within the solution of **S1** was further validated by temperature-dependent ^{1}H NMR study. This was accomplished by obtaining the proton NMR spectra of **S1** at three different elevated temperatures: 313 K, 323 K, and 333 K including ambient temperature (**Figure 6**). The two amide protons appeared at 8.10 ppm and 8.35 ppm, respectively (**Figure 6A**) at ambient temperature (298 K), exhibited a shielding effect as the temperature increased gradually from 298 K to 333 K. At the highest temperature (333 K), both the amide proton peaks at 8.10 ppm and 8.35 ppm (at room temperature) finally relocated to the up-field region by a value of 0.2 ppm each and appeared at 7.90 ppm and 8.14 ppm, respectively (**Figure 6D**). This finding demonstrated that amide protons are involved in intermolecular hydrogen bonding and that the shifting of the amide protons towards the upfield area at higher temperatures is related to the breakdown of intermolecular hydrogen bonding between the cyclic dipeptide molecules. In addition to the intermolecular hydrogen bonding pattern, the thermoreversible character of the hydrogel made from cyclic dipeptide **S1** may also be explained by the temperature-dependent proton NMR investigation. The gel-to-sol transition on heating may be attributed to the disruption of the intermolecular

hydrogen bonding leading to a lower degree of self-assembly of the cyclic dipeptide molecules.

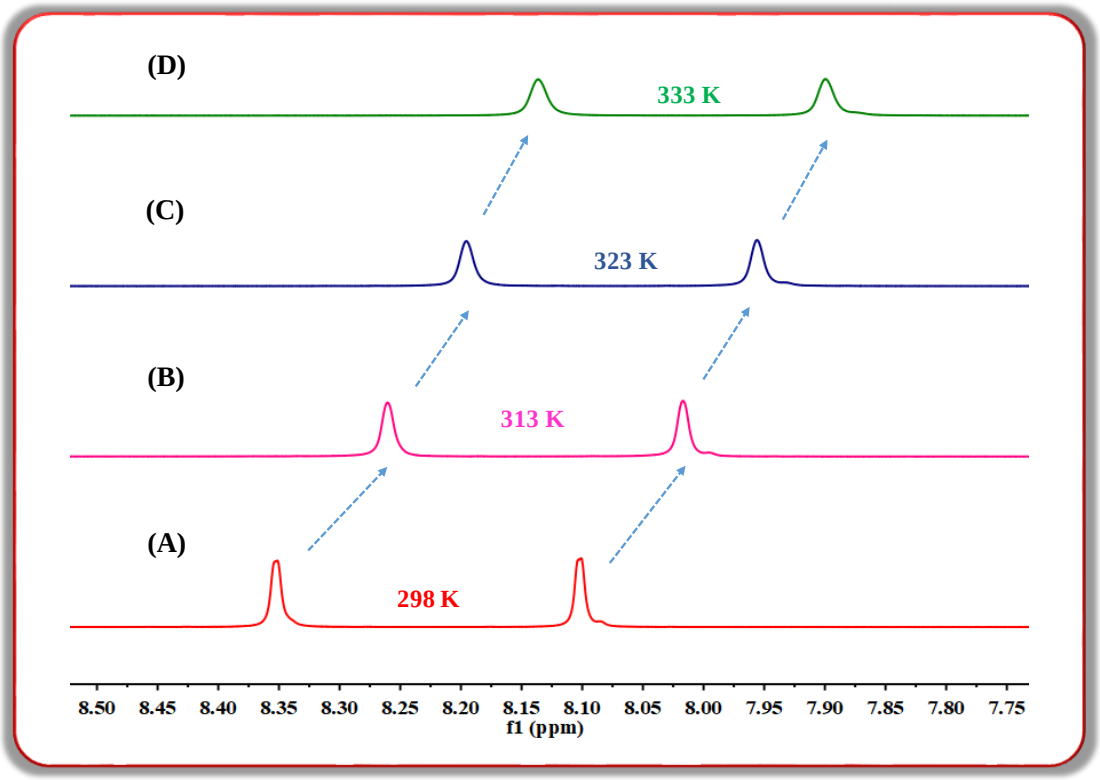

Figure 6. *Temperature-dependent ^{1}H NMR experiment performed with the cyclic dipeptide S1 in DMSO-d6 solvent: ^{1}H NMR of S1 (A) at 298 K, (B) at 313 K, (C) at 323 K, and (D) at 333 K.*

2.3.6.2 FT-IR Study

FT-IR experiments were carried out on **S1** in both its solid and wet-gel states to learn more about the backbone conformation and hydrogen-bonding pattern that caused the cyclic dipeptide to self-assemble. The Fourier transform infrared (FT-IR) spectra of the samples in solid and gel states were recorded on a Bruker TENSOR 27 spectrometer using the attenuated total reflection (ATR) technique. For recording the FT-IR in the wet-gel state, the gel was prepared in 1% DMSO-PBS buffer at its MGC. The spectra were scanned from 600 to 4000 cm^{-1}. Bruker software was used for data processing. Experimental data obtained

were analyzed using Origin Pro 8.0 SRO software (Origin Lab Corporation). In the spectra (**Figure S6**), the significant band locations of **S1** in the solid state were indicated, and the assignments of those marked positions were tabulated (Table S1) in the spectral characterization and additional results section. The amide backbone structure, which is primarily defined by the amide-I, amide-II, amide-III, and amide-A infra-red absorption peaks, has a significant impact on self-assembling interactions.[195,196]While amide-I is primarily related to the >C=O stretching vibration (70-85%), amide-II is mostly caused by the N-H bending vibration (40-60%) and the C-N stretching vibration (18-40%). The FT-IR spectra of **S1** in the solid state revealed three bands in the amide-I region, including two bands at 1658 cm^{-1}, 1666 cm^{-1}, and another weaker transition at 1681 cm^{-1}. These bands were mostly caused by the two amide groups' >C=O stretching (**Figure 7B**). The anti-parallel -sheet conformation of the **S1** in its solid state may have stretched to form an extended structure that is the cause of the vibrational band at 1681 cm-1.[197–199]The appearance of the vibrational band at 1681 cm^{-1}perhaps due to an extended structure of anti-parallel β-sheet conformation of the **S1** in its solid state. In the solid state, the amide-II band for **S1** emerged at 1454 cm^{-1} and had a hump at 1461 cm^{-1} (**Figure 7A**). In the wet gel state, the amide carbonyl stretching band of **S1** appeared at 1662 cm^{-1} associated with a hump at 1633 cm^{-1} (**Figure 7C**) and the intensity of the >C=O stretching band was also seen to increase.[179] This shift in carbonyl stretching frequency was due to the weakening of the >C=O bond which denotes the existence of significant hydrogen bonding in the gel state. However, the amide >C=O stretching band's enlargement caused the weaker band at 1681 cm^{-1} to disappear in the gel state. The water molecules involved in the hydrogen bonding with the amide groups (-CONH-) caused solvation of the amide group and in turn, contributed to the broadening of the band. Participation of **S1** in hydrogen bonding in the gel state was further corroborated by the amide-II

band's shift from 1454 cm^{-1}in the solid state to 1459 cm^{-1}in the wet gel state coupled with the broadening of the band.[179]

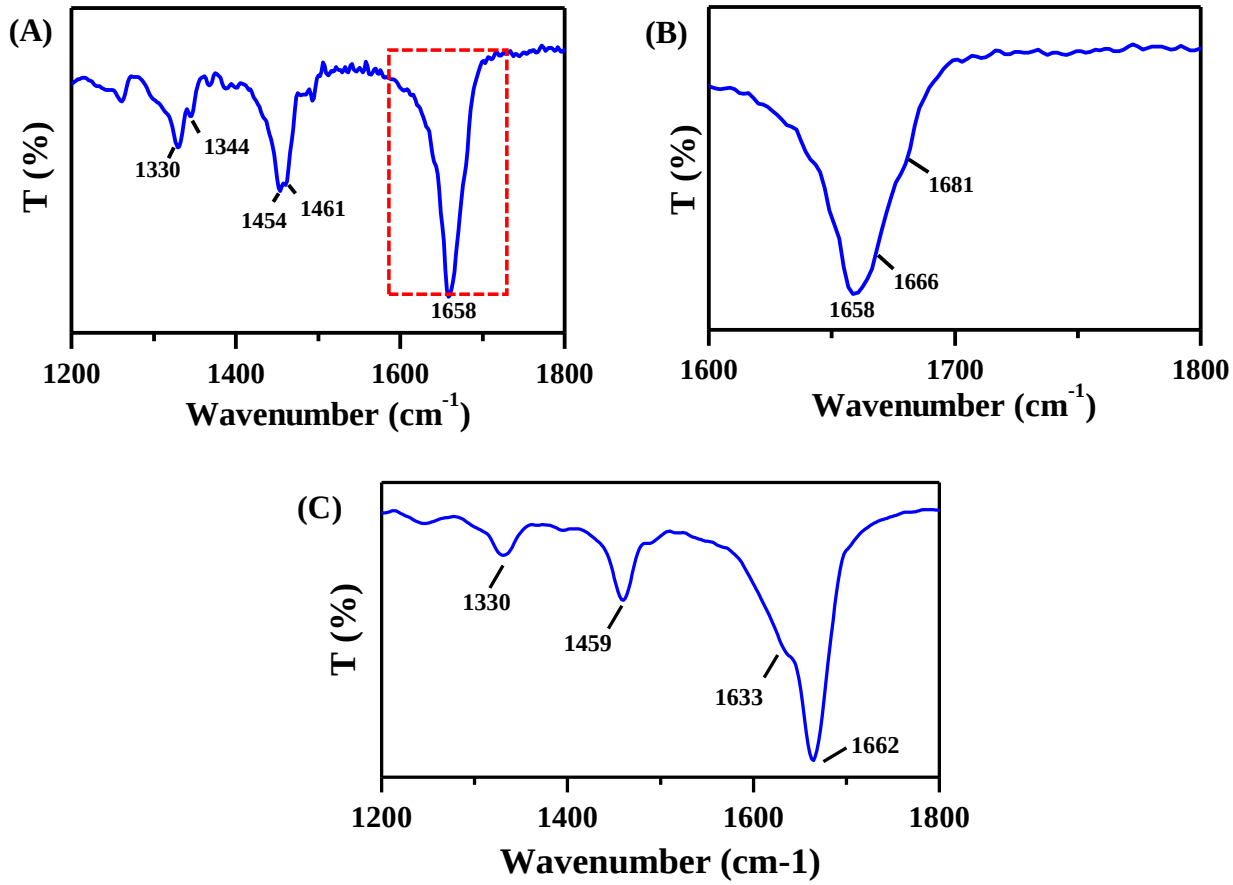

Figure 7. *(A) FT-IR spectra of the cyclic dipeptide S1 in the solid state, (B) shows the enlarged portion of the area enclosed by red dotted line in figure A, and (C) FT-IR spectra of S1 in the wet gel state.*

2.3.6.3 Circular Dichroism Study

Circular dichroism (CD) experiments were conducted to get structural insight into the preferred secondary structure that the hydrogelator **S1** acquired both in the solution and in the gel state. The CD spectrum of the cyclic dipeptide **S1** was measured on a JASCO-810 spectropolarimeter under constant nitrogen flow conditions. 100 μM of concentration of **S1** in 1 mm path length quartz cuvette was used for the CD spectra measurements, and CD measurements were carried out at 25°C with an accuracy of ±0.1. The far-UV region was scanned

between 190 to 250 nm using a bandwidth of 1 nm. The represented spectrum was the average of three individual scans. The CD measurement of **S1** dissolved in 1% DMSO-PBS solvent system and incubated after 24 h showed a broad negative peak with minima at 212 nm and a positive peak at 197 nm (**Figure 8**). This type of CD pattern is characteristic of an antiparallel β-sheet secondary structure.[158,200,201] This result suggested that a significant number of gelator molecules organized in an antiparallel β-sheet fashion, produced fibrillar self-assembled nano-structure having enough empty space for the trapping of water molecules that further encouraged the formation of hydrogel.

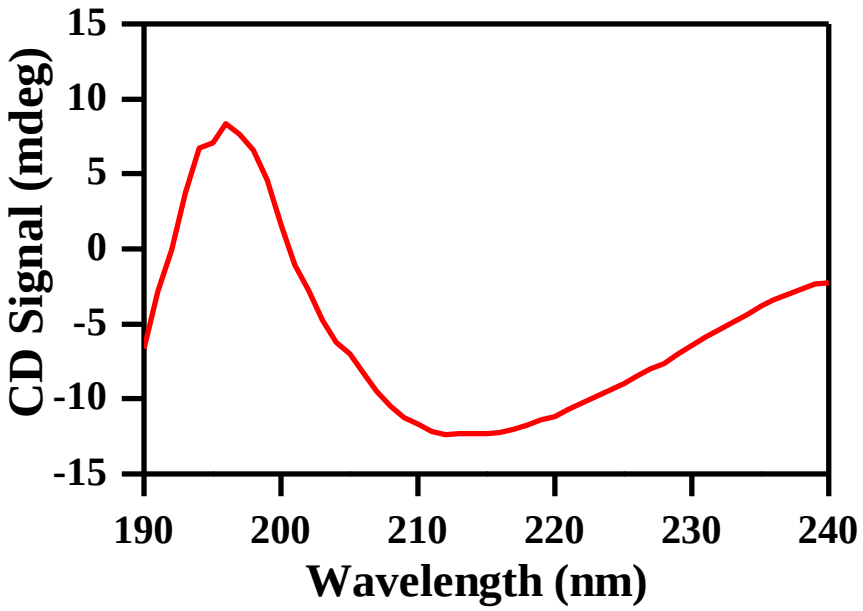

Figure 8. *CD spectra of S1 in 1% DMSO-PBS solvent system (pH=7.46).*

2.3.6.4 Thioflavin-T (Th-T) Binding Study

After NMR, FT-IR, and CD results showed evidence of intermolecular hydrogen bonding and an anti-parallel -sheet-like secondary structure in **S1**, thioflavin-T (Th-T) binding experiment was carried out to further confirm these findings. Th-T is a fluorescent dye that enhances its fluorescence intensity after binding to amyloid assemblies that contain amino acid subunits that are rich in

β-sheet secondary structure.[202–204] For the assay, a stock solution of thioflavin-T (Th-T) was freshly prepared by dissolving 1 mg of Th-T in 1 mL of Milli-Q water and filtered through a 0.2 µm syringe filter. 20 µl of stock solution was diluted with 2ml of Milli-Q water and the fluorescence spectrum of blank Th-T was acquired using a Fluoromax-4 spectrofluorometer using an excitation wavelength of 450 nm and emission range from 460 to 600 nm. 20 µl of ThT stock solution was then mixed with 2 ml of 100 µM cyclic dipeptide (**S1**) solution and the emission spectrum was recorded after incubation of 10 mins at room temperature. An enhancement in the Th-T fluorescence intensity (**Figure 9**) by several folds was observed after binding with **S1** which further confirmed the formation of amyloid-like fibrils and β-sheet secondary structure during self-assembly as well as hydrogelation process of **S1** in aqueous solvents.

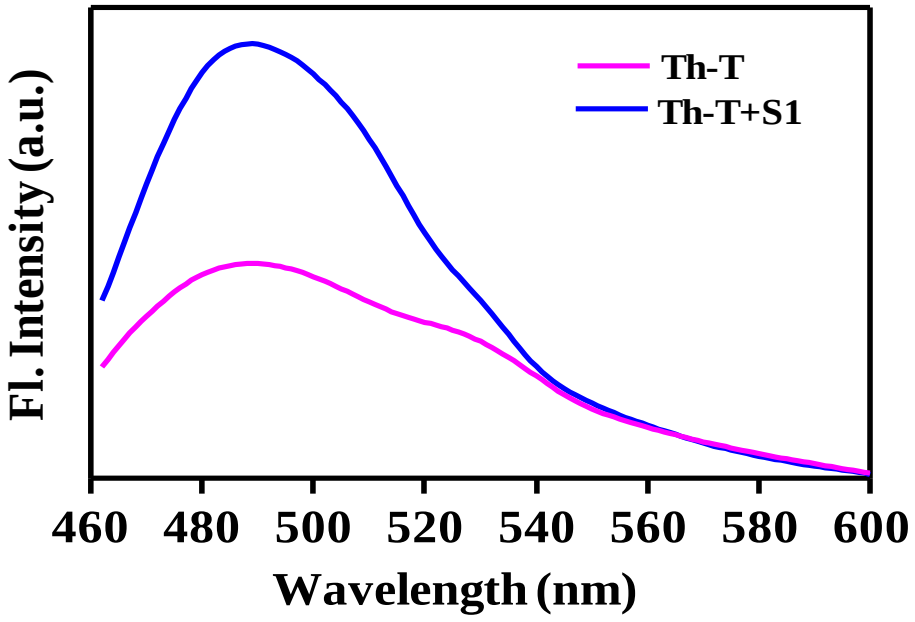

Figure 9. *Thioflavin-T (Th-T) binding assay for amyloid fibril formation from S1 in 1% DMSO-PBS solvent system.*

2.3.7 Encapsulation of 5-Fluorouracil by S1 Hydrogel

At physiological pH (7.46) and temperature, the self-assembly of **S1** molecules within the hydrogel produced an interwoven highly cross-linked nanofibillar network. From FE-SEM and AFM images, it was clear that this network had a lot of cage-like void spaces, and this could serve as a model for the capture and subsequent release of drug molecules under physiological circumstances. To explore the capability of **S1** hydrogelator as a drug delivery vehicle, it was allowed to form hydrogel in an aqueous solution containing the anticancer drug 5FU. For encapsulation, **S1** was dissolved in 10 µl DMSO and, into it, 300 µl of 1 mM 5-Fluorouracil solution and PBS buffer of pH 7.46 was added to attain a final drug concentration of 150 µM for 5FU. The solution was then heated until the dipeptide gets completely dissolved and was then left for cooling at room temperature to get the 5FU incorporated hydrogel. The gel was then allowed to stand for further 10 mins and was washed twice with 1ml of fresh solvents to remove any unconjugated drug. The initial drug used for encapsulation and unbound drugs were estimated by measuring their absorbance (λmax 266 nm) using a JASCO V-630 spectrophotometer (JASCO International Co. Ltd, Japan) and calculating the concentration from a standard curve of 5FU. The standard curve for 5-Fluorouracil was obtained by plotting its concentration against the respective absorbance from 25 µM to 200 µM.

The loaded drug in the hydrogel and the encapsulation efficiency were then calculated as follows:

Drug loaded = initial concentration of the drug – concentration of free non-entrapped drug

$$\text{Encapsulation efficiency} = \frac{\text{Initial concentration of the drug}}{\text{Loaded concentration of the drug}} \text{ x } 100$$

It was noted that at physiological pH, **S1** formed a stable gel and effectively encapsulated the drug 5FU, with an encapsulation efficiency of 94.46±1.04%. Encapsulation of 5-Fluorouracil was evident from the FT-IR spectra of 5FU-loaded hydrogel (**Figure 10C**). In the FT-IR spectra of the hydrogel loaded with 5FU (**Figure 10C**), the vibrational bands at 1240 cm^{-1} and 1723 cm^{-1} matched the vibrational band that appeared for free 5FU. Moreover, incorporation of 5FU did not significantly alter the FT-IR peaks of **S1** hydrogel afterward, indicating that drug encapsulation did not perturb the secondary structure of the self-assembled **S1**. AFM pictures of 5FU-loaded hydrogel (**Figure 10D**) revealed a fibrillar nanostructure that was similar to that of the native hydrogel, which is consistent with the finding that the incorporation of the drug 5FU did not interfere with the process of self-assembly. These findings revealed that the morphology of **S1** and the way it self-assembled in aqueous solution were unaffected by the entrapment of 5FU.

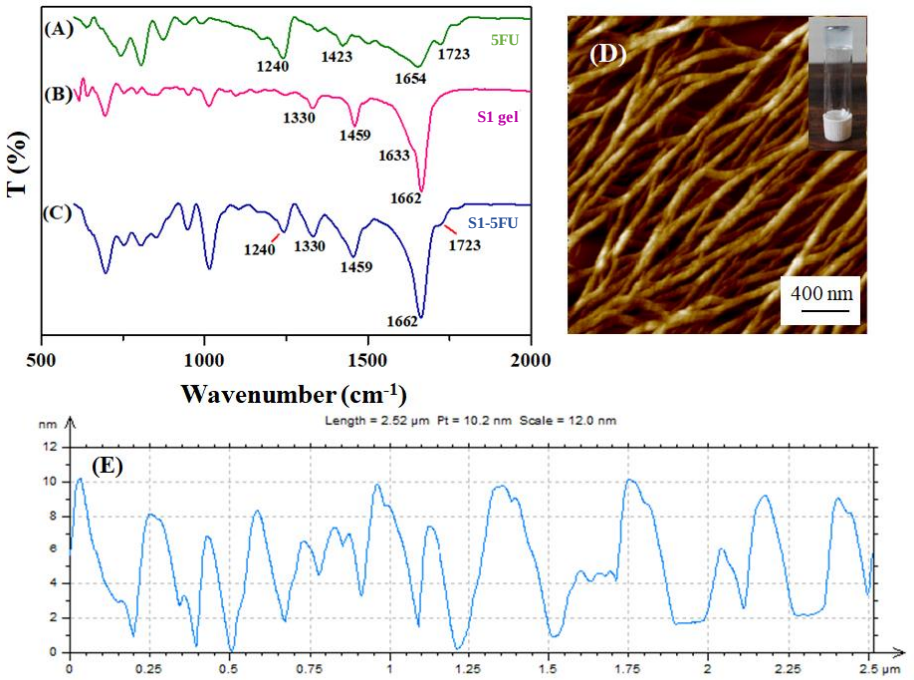

Figure 10. *FT-IR spectra of (A) 5-Fluorouracil, (B) S1 hydrogel, and (C) S1 hydrogel loaded with 5-Fluorouracil. (D) AFM image of xerogel obtained from 5FU loaded S1 hydrogel and the inset picture depicted the tube inversion test of the 5FU loaded S1 hydrogel. (E) Height profile scale of the AFM image D.*

2.3.8 In-vitro Drug Release Study

After the drug was successfully incorporated, the capability of the hydrogel was tested if it could also release the drug effectively and gradually in order to fulfill its intended role as a drug delivery vehicle. For the release study, 5FU incorporated hydrogel was formed as mentioned previously. A blank gel of **S1** was also prepared in absence of 5FU following the same procedure. PBS buffer (pH=7.46) was used as the release medium and each gel was covered with 2ml of PBS buffer. At different time intervals, the respective solutions were removed and UV/vis absorption (λmax 266 nm) of the solution containing 5FU was recorded using the blank solution as a reference medium. The release studies were monitored for 72 h. This approach allows quantifying the amount of 5FU released from the gel. The following equation was used to determine the percentage of the drug released:

$$\% \text{ of drug released } = \frac{C_t}{C_i} \text{ x } 100$$

where C_i and C_t represent the initial concentration of drug-loaded and the concentration of drug released at time t, respectively. The whole process was repeated thrice to get an average drug release profile. According to the drug release profile (**Figure 11**), the drug 5FU was released slowly over the course of 72 hours. The rate was initially somewhat faster for the first 24 h before slowing down as the time got closer to 72 h. Almost 90% of 5FU that had been encapsulated was shown to be released from the gel matrix throughout 72 h, after which the hydrogel began to rupture and started to diffuse into the releasing media.The diffusion coefficient of the drug molecule was also determined with the help of a non-steady-state diffusion model equation:

$$M_t/M_\infty = 4(Dt/\ \pi\lambda^2)^{1/2}$$

where M_t is the total amount of drug released during the measurement, M_∞ is the total amount of drug that was kept within the gel matrix, λ is the hydrogel thickness, t is the time of measurement, and D is the diffusion constant of the drug molecule.[158,205,206]The calculated diffusion coefficient for the hydrogel was found to be 6.45 × 10−11 m^2s^{-1}.[34]This delayed and sustained release of drug molecules from the hydrogel at physiological pH bears interesting future characteristics for **S1** hydrogel as a drug delivery vehicle.

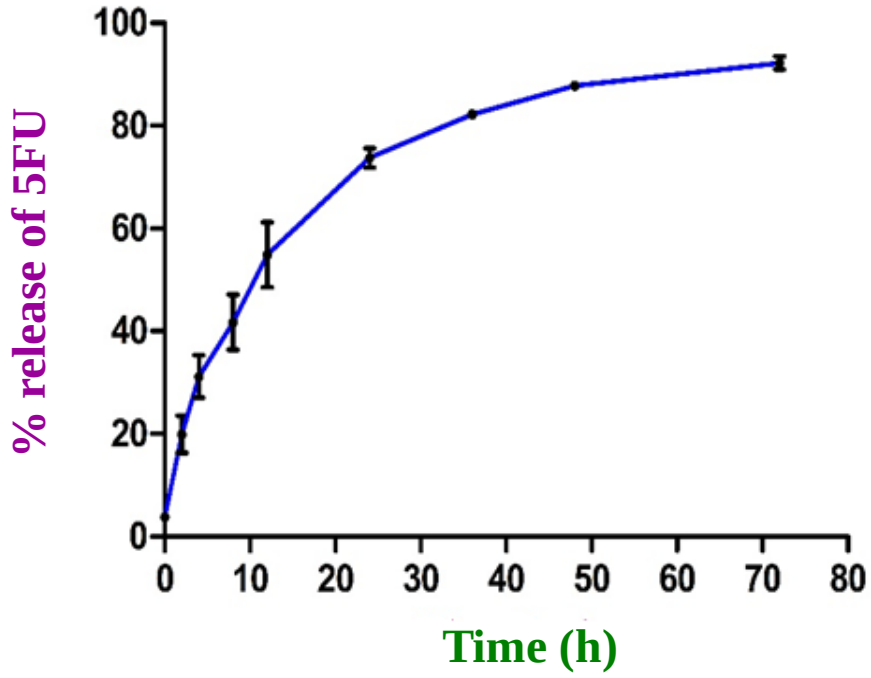

Figure 11. *Release profile of 5-Fluorouracil with error bars from 5FU-loaded S1 hydrogel over a span of 72 h.*

2.3.9 Cytotoxicity Study of S1

To check the practical applicability of this peptide hydrogel as a drug delivery vehicle, the cytotoxicity of **S1** was first checked via MTT assay on HCT116 cancer cell line.[207]For this HCT116 (human colorectal cancer) cells were grown in a culture medium of DMEM with 10% fetal bovine serum (FBS) and 1% penicillin-streptomycin at 37°C in a humidified atmosphere with 5% CO2. After

developing 60–80 % confluency, cells were planted at the required density to allow them to develop well for a day before the experiment. Cells were harvested using 0.05 percent trypsin and 0.50 mM EDTA in phosphate-buffered saline (PBS, pH= 7.46). For the MTT assay, HCT116 cells in the concentration of (1 x 10^5 per well) were seeded in 96 well plates. Cells were then treated with 0, 50, 100, 200, 300, 400, 500, 600, 700, 800, 900, and 1000 µM concentrations of **S1** for 24 hours. In all the experimental batches of cells, four hours after adding MTT, purple-colored formazan crystals were generated. These crystals were solubilized in DMSO, and the absorbance was measured at 595 nm using an ELISA (enzyme-linked immune sorbent assay) reader. Treatment of the HCT116 cancer cells with a range of **S1** concentrations 0, 50, 100, 200, 300, 400, 500, 600, 700, 800, 900, and 1000 µM for 24 h revealed no significant cancer cell death, even at high concentrations.

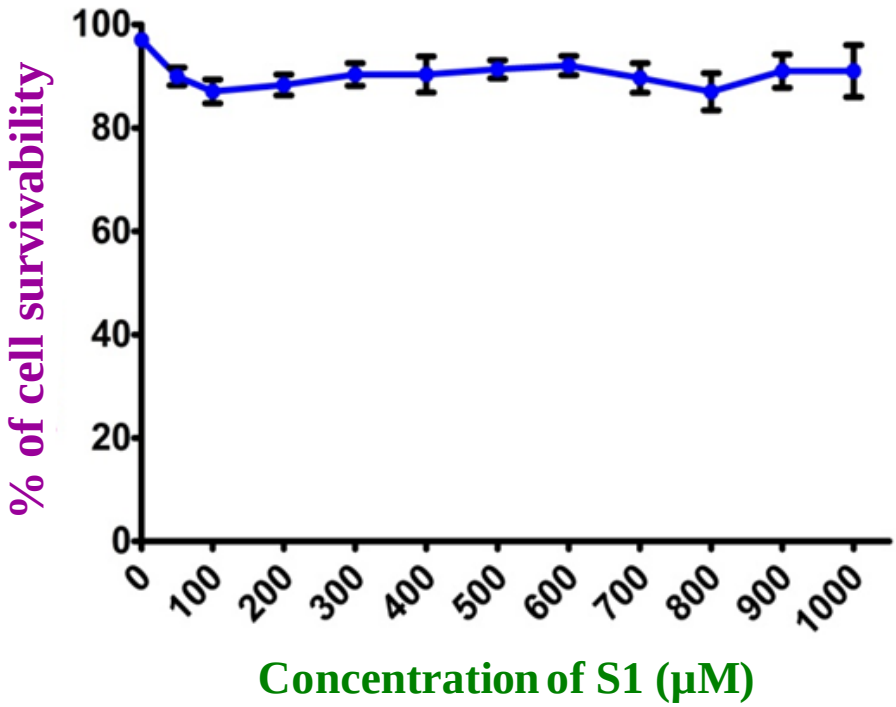

Figure 12. *Growth inhibitory effect of S1 on HCT116 cells, at concentrations ranging between (0-1000) µM. The result is the mean ± SD from triplicate independent experiments.*

At all **S1** concentrations tested, the percentage of cell survivability ranged between 85% and 90%. After being treated with **S1**, the cellular pictures of the HCT116 cells under a light and fluorescence microscope (**Figure 12**) demonstrated healthy cell morphology. Therefore, it was determined that the cyclic dipeptide **S1** had a negligible part in the mortality of HCT116 cells. As a result, additional research employing the HCT116 cell line and a 500 M dosage of **S1** was carried out. Therefore, it was concluded that the cyclic dipeptide **S1** had no significant role in the mortality of HCT116 cells. Hence, further studies were conducted with the HCT116 cell line using a 500 µM dose of **S1**.

2.3.10 Effect of 5FU Loaded Hydrogel on Growth of Cancer Cells and Apoptosis

A comparative anticancer activity study between 5FU-loaded hydrogel (**S1**-5FU) and free 5-Fluorouracil was performed on HCT116 cell line. For this, MTT assay was performed where one batch of cells was treated with concentrations 0, 2, 5, 10, 20, 30, 40, and 50 µM of 5 fluorouracil, and another batch of cells was treated with concentrations 0, 2, 5, 10, 20, 30, 40, 50 µM of 5-Fluorouracil loaded in 500 µM of **S1** hydrogel. This comparative anticancer activity study revealed that co-treatment of 5-Fluorouracil with **S1** hydrogel (**S1**-5FU) promoted enhanced cell death of HCT116 cells as compared to 5-Fluorouracil alone**.** The IC_{50} dose of 5-Fluorouracil was calculated to be 32.23±3.4 µM[208]in **Figure 13A** when cells were treated with only 5FU and in **Figure 13B**, when cells were treated with 5FU loaded hydrogel the IC_{50} value of 5FU was calculated to be 6.7±1.2 µM. Therefore, administration of 5FU-loaded hydrogel (**S1**-5FU) caused a 5-fold reduction in the IC_{50} value 5FU. Thus it is anticipated here that at the same dose of 5-Fluorouracil, the **S1**-5FU co-assembly killed more cancer cells than 5FU alone because of the improved (slow and over a longer period) drug release by **S1** hydrogel.

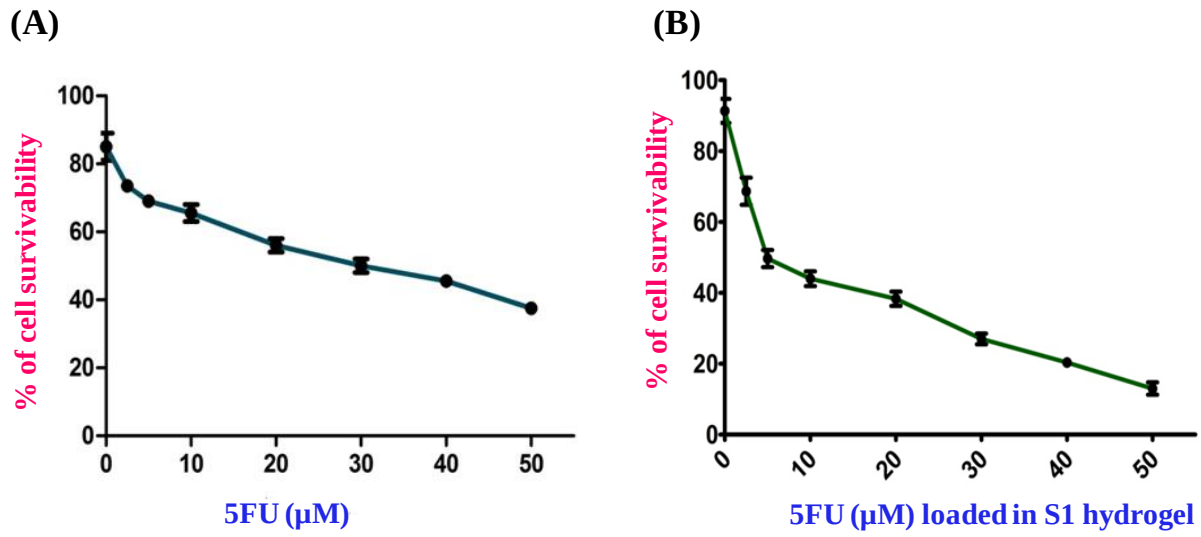

Figure 13. *(A) Changes in the percentage of cellular survivability of HCT116 cells upon treatment with 0, 2, 5, 10, 20, 30, 40, and 50 µM of 5-Fluorouracil. The result is the mean ± SD from triplicate independent experiments, (B) Alterations in the percentage of cellular survivability of HCT116 cells upon treatment with 0, 2, 5, 10, 20, 30, 40, and 50 µM of 5-Fluorouracil loaded in 500 µM of S1 hydrogel. The result is the mean ± SD from triplicate independent experiments.*

2.3.11 Apoptosis Induced by The Co-assembly of Drug and Hydrogel (S1-5FU)

5FU and 5FU-loaded hydrogel treated HCT116 cells were studied to determine programmed cell death (apoptosis) using light and fluorescence microscopy.[209] Under the light microscope, HCT116 control cells looked healthy and were evenly spread out. Cells, treated with 5FU and **S1**-5FU co-assembly at their IC_{50} levels for 24 h, displayed characteristic features of apoptosis like rounding and shrinking under a light microscope (**Figure 14**). Fluorescence microscopy was also employed to examine apoptosis in treated HCT116 cells using acridine orange/ethidium bromide staining. Images were obtained from the fluorescence microscope (Olympus, Tokyo, Japan) at excitation and emission wavelengths of 488 and 550 nm.

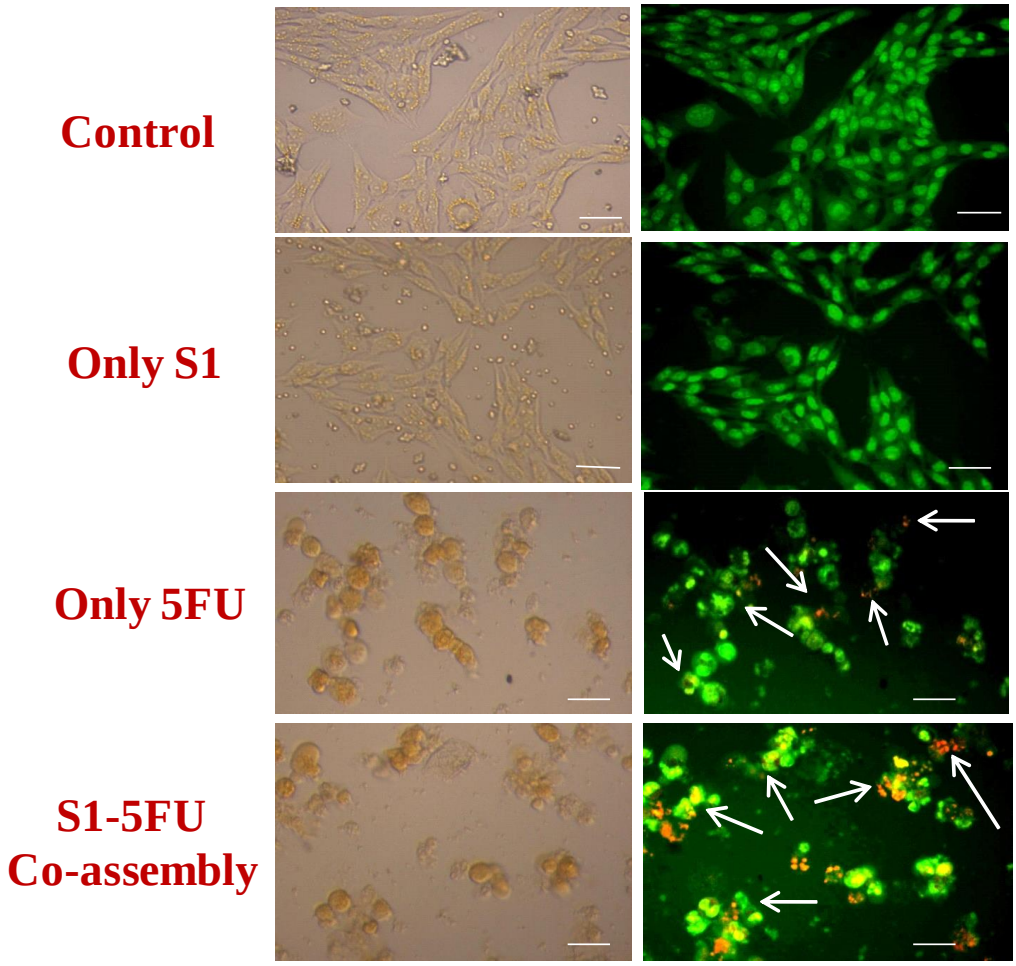

Figure 14. *Morphological and nuclear changes in HCT116 cells after treatment with S1 (500 µM), 5FU, and S1-5FU co-assembly for 24h.* ***Left column:*** *morphological changes seen under a light microscope.* ***Right column:*** *nuclear changes seen under a fluorescence microscope after AO/EtBr staining, respectively. Apoptosis is demarcated using arrows (yellow and orange spots), Scale bar = 40 µm.*

The fluorescence microscopy results showed that whereas the control group's cells had intact green nuclei, the 5FU, and **S1**-5FU-treated cells had greenish yellow, orange, and reddish fragmented nuclei. When cells were treated with **S1**-5FU rather than only 5FU, as was shown by microscopy, apoptosis was more severe (**Figure 14**). As confirmed by microscopy, apoptosis was more profound when cells were treated with **S1**-5FU rather than with only 5FU (**Figure 14).** In light of the fact that conjugation of **S1** hydrogel with 5FU reduced the IC_{50} dose of 5FU,[210] it can be said that hydrogel 5FU drug

conjugate was a superior choice for inducing cell death in HCT116 cells. Additionally, 5-Fluorouracil is known to have a number of side effects, including leukocyte loss, anaemia, shortness of breath, diarrhoea, and hair loss.[211] Therefore, it was anticipated that decreasing the effective dose of 5FU upon conjugation with **S1** hydrogel would reduce the adverse effects of 5FU.

2.4 CONCLUSION

In summary, this work illustrated the design and synthesis of a new cyclic dipeptide **S1** constituting L-leucine and S-benzyl-L-cysteine successfully formed a thermoreversible 'super hydrogel' at physiological conditions (at 37^{o}C and pH=7.46). The extremely low MGC value (0.05% w/v) suggested high water content of the hydrogel which makes it a good candidate for cellular applications like drug delivery. The hydrogel obtained from cyclic dipeptide **S1** showed excellent resistance to environmental parameters including pH and temperature. Morphological investigations by AFM and FESEM showed a highly cross-linked, interwoven nano-fibrillar network both in the gel state and in the solution state of **S1**. NMR, FT-IR, and CD analysis results revealed that intermolecular hydrogen bonding interaction is one of the key driving forces behind the self-assembly of **S1** in aqueous solution and the **S1** molecules are arranged in a β-sheet fashion in its extended self-assembled structure. Furthermore, Th-T binding assay revealed that the nanofibrills that have been produced by the self-assembly of **S1** are amyloid type of fibrils that are rich in β-sheet secondary structure. The ability of **S1** hydrogel to act as a drug delivery template was also investigated by several in-vitro studies. **S1** was found to successfully encapsulate and effectively release an anticancer drug 5-Fluorouracil at physiological conditions. **S1** hydrogel itself was found to be almost nontoxic towards HCT116 cancer cells but was seen to kill more number of HCT116 cells when cells were treated with 5FU-loaded hydrogel than cells treated with bare 5FU. Together, these findings could indicate positive future

developments of this novel hydrogelator to serve as a potential drug delivery system.

2.5 FUTURE SCOPE

Although there are several examples of peptides hydrogels which can function as a template for sustainable drug delivery agents, the search for new biocompatible hydrogelator which is non-toxic up to high concentrations, is short in length i.e. easy to synthesize on large scale, can hold a large volume of water and above all can produce hydrogel at physiological conditions is still on demand. The **S1** hydrogel is mechanically strong enough and is very stable at room temperature for months which makes it easy to handle for any application. **S1** produced hydrogels and organogels in several other aqueous and organic solvents. So, by further optimizing, the solvent systems used for gel production, a wide range of applications can be covered by each of the gels produced by **S1** from different solvent systems depending upon their physicochemical properties. **S1** hydrogel produced from 1% DMSO-PBS in particular can be used for in-vivo treatments for various targeted diseases to improve its ability to perform as sustainable drug delivery vehicle.

2.6 SPECTRAL CHARACTERIZATION AND ADDITIONAL RESULTS

Characterization of the cyclic dipeptide S1

^{1}H NMR of S1 (600 MHz, DMSO-d_6): δ (in ppm) 8.34 (1H, s, NH), 8,09 (1H, s, NH), 7.30 (4H, d, J = 6Hz, Ar-H), 7.25-7.21 (1H, m, Ar-H), 4.41 (1H, s, C_αH), 3.80-3.72 (3H, m, C_αH and -CH_2-Ph), 2.86 (1H, dd, J = 12Hz, J = 6Hz, -CH_2-S), 2.72 (1H, dd, J = 12Hz, J = 6Hz, -CH_2-S), 1.91-1.84 (1H, m, -CH), 1.69-1.59 (2H, m, -CH_2), 0.85 (6H, q, J = 6Hz, -CH_3).

^{13}C NMR of S1 (150 MHz, DMSO-d_6): δ (in ppm) 168.36, 166.52, 138.78, 129.33, 128.78, 127.31, 55.04, 53.03, 44.55, 36.53, 35.12, 23.86, 23.54, 22.19.

ESI-MS: m/z calculated for C16H22N2O2S $[M+H]^+$ = 307.1480; found m/z = 307.1479.

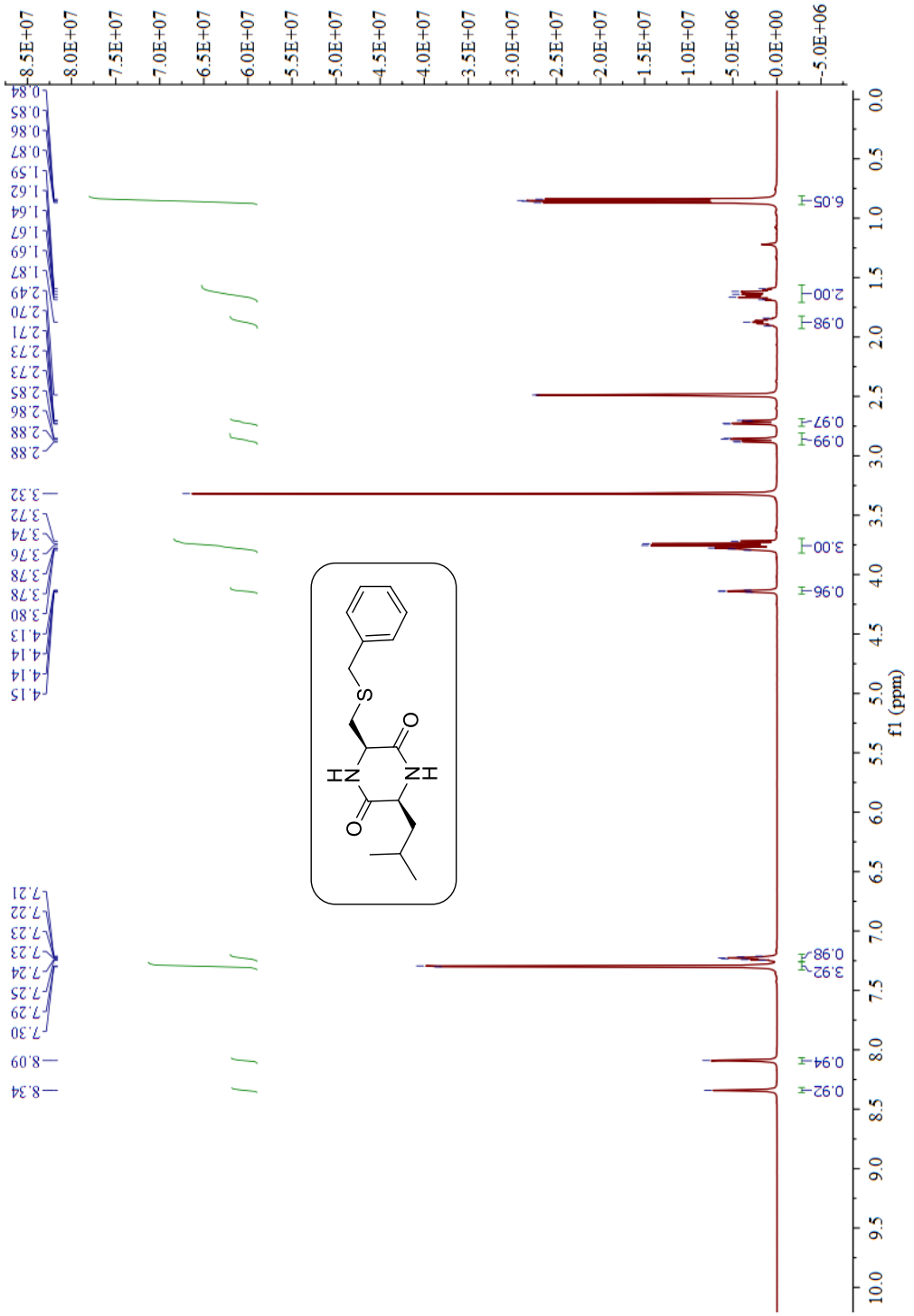

Figure S1. *^{1}H NMR spectra of the cyclic dipeptide S1 dissolved in DMSO-d_6.*

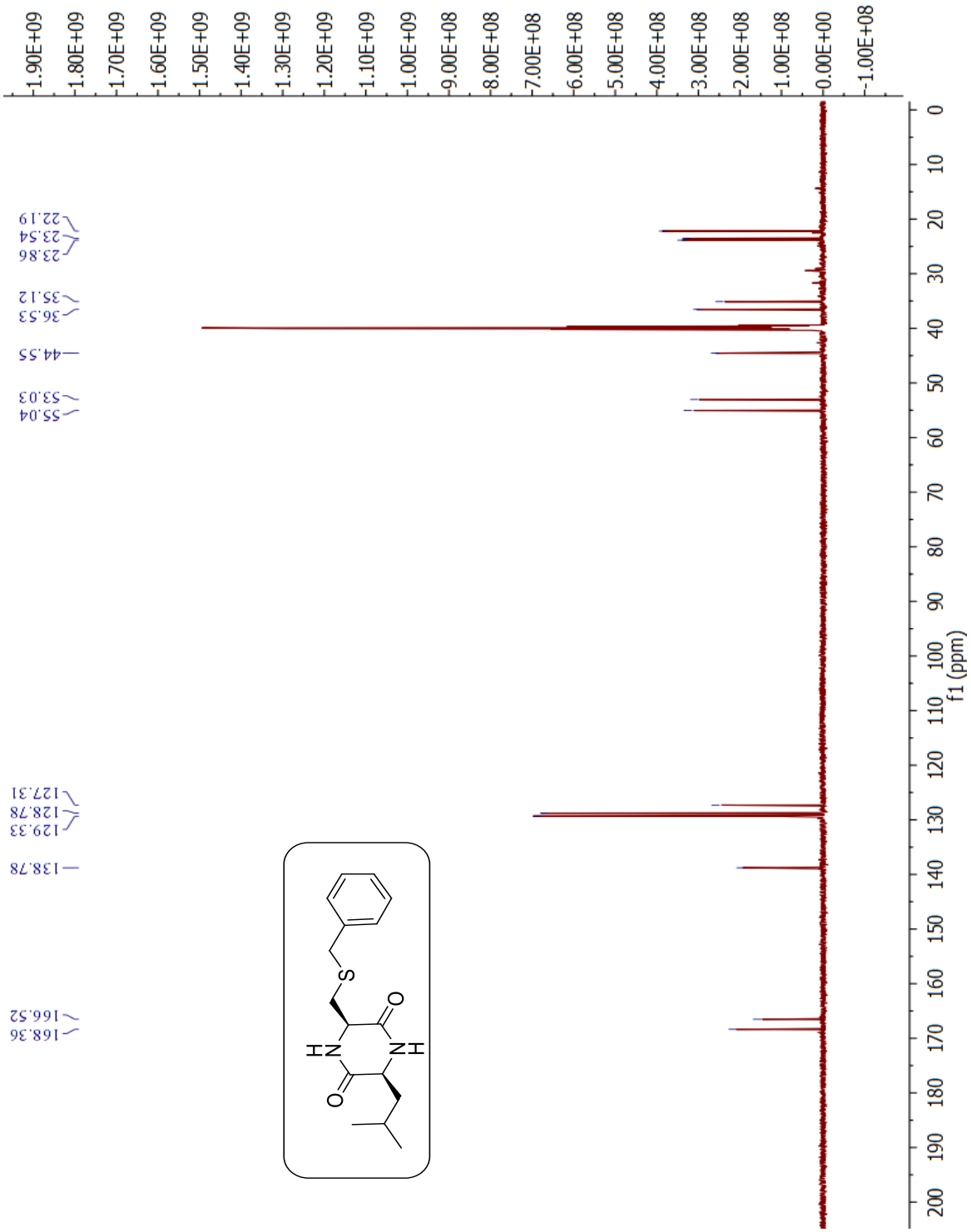

Figure S2. *^{13}C NMR spectra of cyclic dipeptide S1 dissolved in DMSO-d_6.*

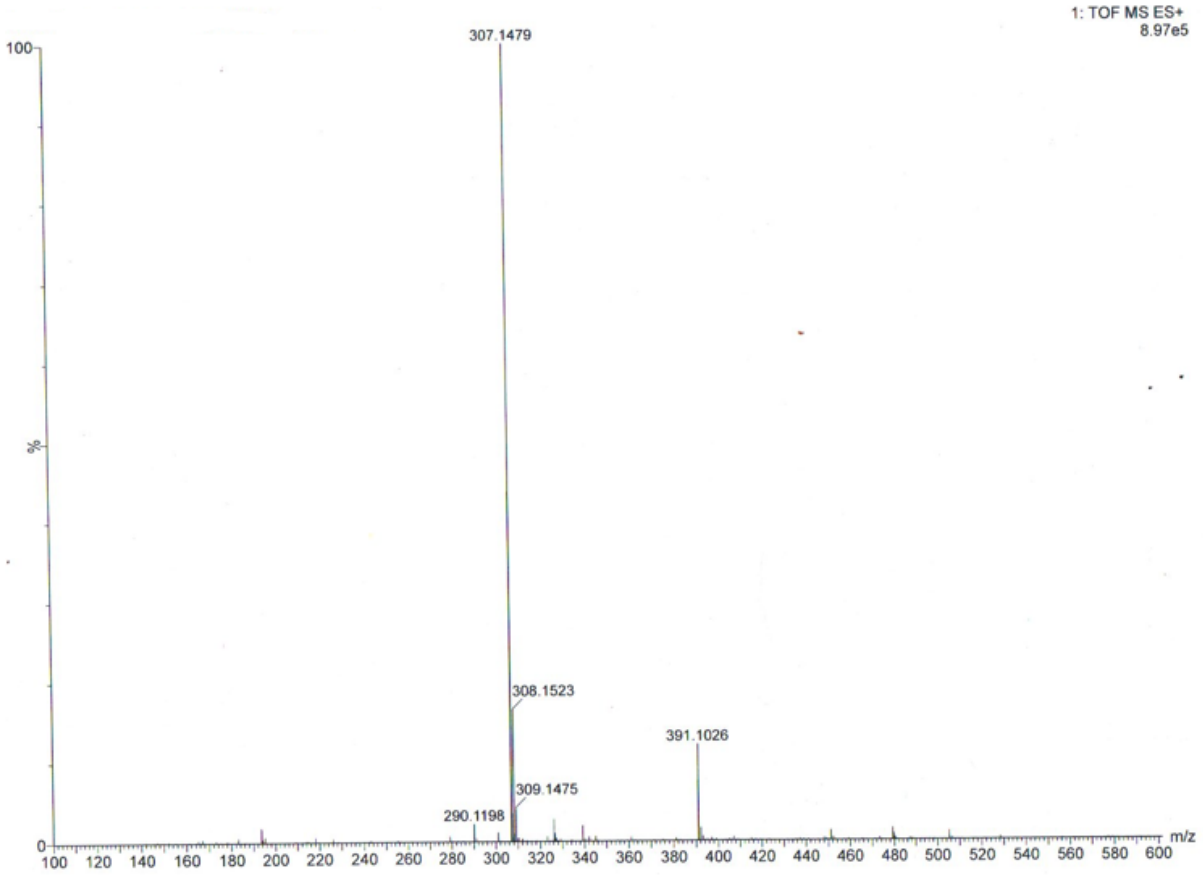

Figure S3: *ESI-mass spectra of the cyclic dipeptide S1.*

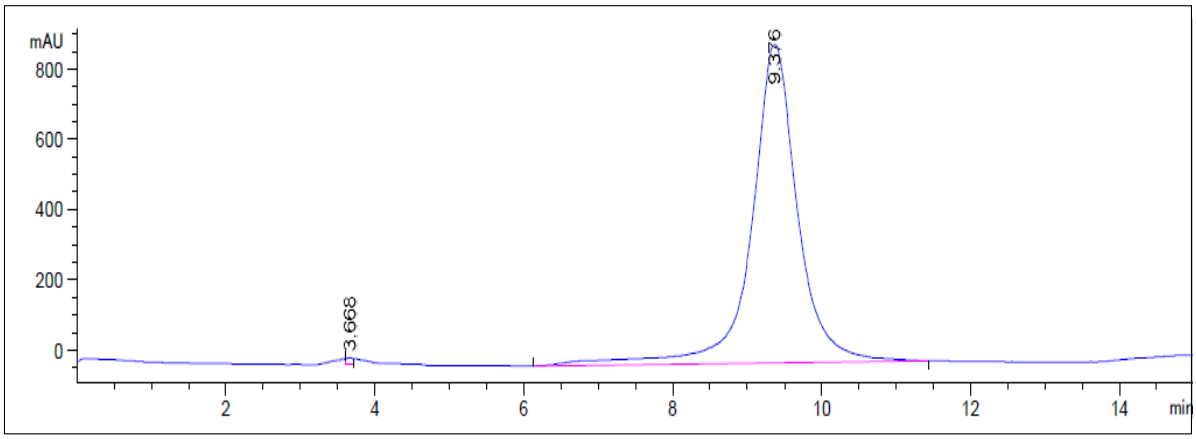

Figure S4. *Analytical HPLC trace of the cyclic dipeptide S1.*

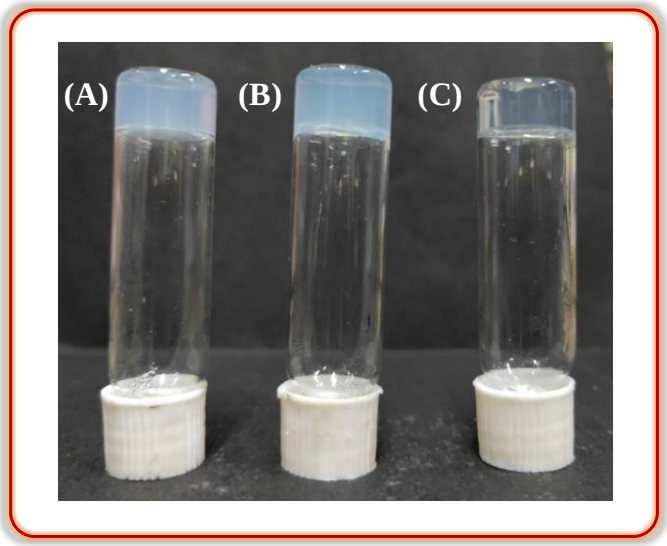

Figure S5. *Images of gels obtained from cyclic dipeptide S1 in (A) DMF-water mixture, (B) methanol-water mixture, and (C) ethyl acetate.*

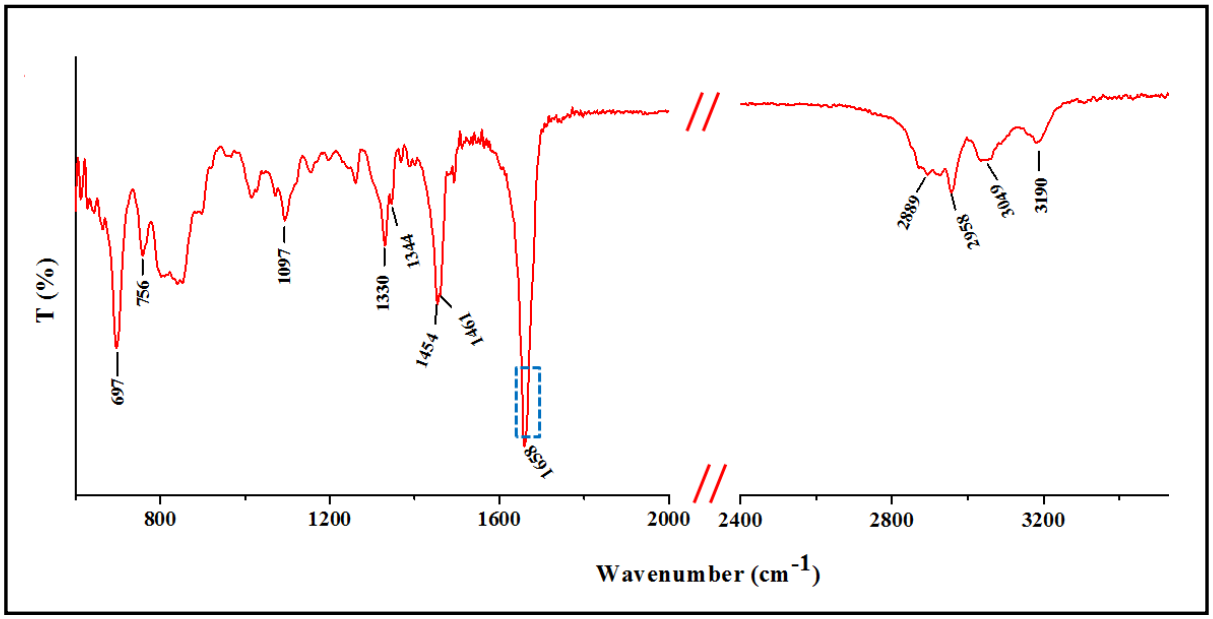

Figure S6. *FT-IR spectra of the cyclic dipeptide S1 in the solid state.*

Table S1. *Assignments of the FT-IR bands of the cyclic dipeptide S1 in solid state.*

IR Frequency (cm^{-1})	Modes of assignments	IR Frequency (cm^{-1})	Modes of assignments
3190	NH Symmetric stretching	1454	Amide II (N–H bend in-plane and C–N stretch)
3049	Aromatic C-H Stretching	1461	Amide II (N–H bend in-plane and C–N stretch)
2958	CH_2 anti-symmetric stretching	1344	C-H methyl rocking
2889	CH_2 symmetric stretching	1330	CH3 symmetric bending
1681	Amide I (amide C=O stretching)	1097	Out of plane CH bending
1666	Amide I (amide C=O stretching)	756	amide IV (mainly O=C-N deformation)
1658	Amide I (amide C=O stretching)	697	Out of plane N-H bending

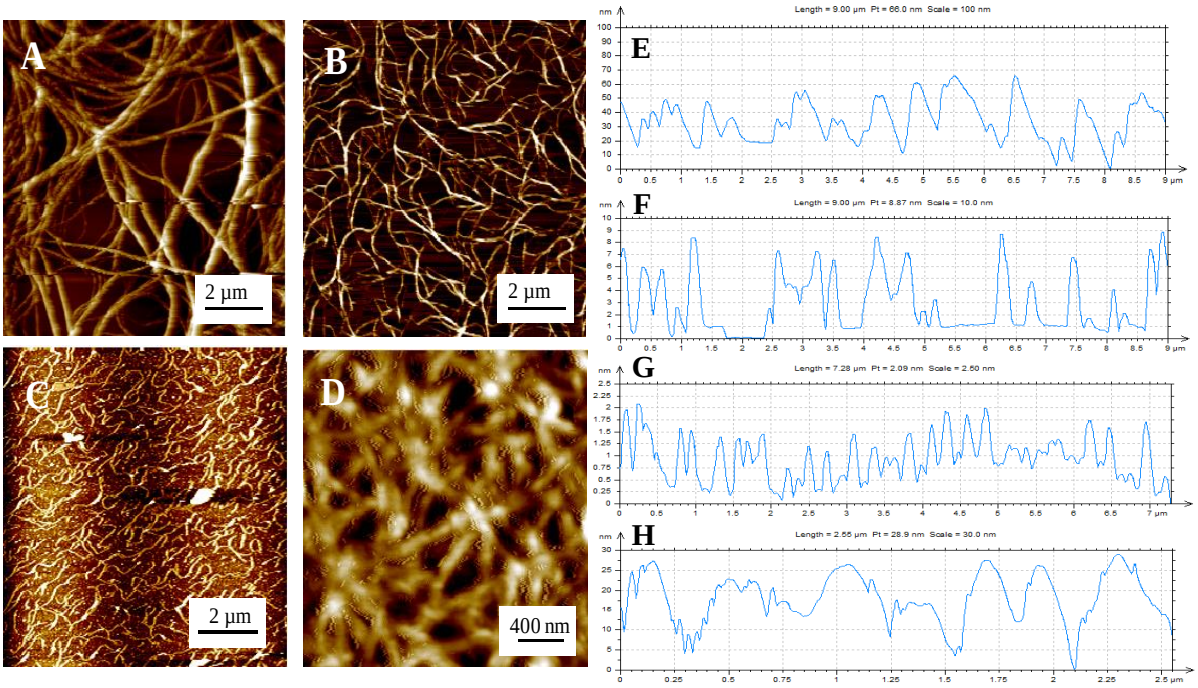

Figure S7. *Atomic Force microscopic images of various fibrillar networks generated from the cyclic dipeptide S1 in (A) DMF-water, (B) methanol-water, (C) ethyl acetate, and (D) dichloromethane; E, F, G, H represent the height profile scale of A, B, C, D respectively.*

CHAPTER-3

Hydrophobicity Controlled Self-Assembly of Cyclic Dipeptides: Exploring its Application in Wastewater Management via Toxic Dye Removal

3.1 AIM OF THE PRESENT WORK

Once considered as undesirable byproducts of peptide synthesis and hydrolysis of functional peptides and protein, cyclic dipeptides (CDPs) have drawn enormous attention from the research community in recent years because of their distinct physical, chemical, and functional properties. In contrast to linear peptides, cyclic peptides are considered as promising building blocks for the generation of self-assembled nanostructures and nanomaterials for various applications from biomedical to biotechnology due to their molecular rigidity, biocompatibility, ease of synthesis, etc. The nature of amino acid side chain of CDPs to form self-assembly is very crucial. Thus, judicious selection or modification of amino acids side chains for the fabrication of self-assembled nanomaterials is very important. In this chapter, six (6) cyclic dipeptides (**P1-P6**) were synthesized keeping the design of the CDPs very minimal to investigate the influence of hydrophobicity of the side chain variations in forming different self-assembled nanostructures. Establishment of a structure-gelation relationship for the synthesized CDPs was also aimed in this work. Cytotoxicity of the CDPs were examined via MTT assay. The hydrogel produced from one of the CDPs was used to remove toxic dyes from contaminated water in order to explore its application in the field of wastewater treatment.

3.2 INTRODUCTION

Nanometer-sized structures nowadays have widespread applications in fields like nanotechnology to biotechnology. Construction of nanomaterials which are susceptible to molecular design from bottom-up approach is necessary for nanoscience and nanotechnology.[212,213] Proteins, DNA, cellular organelles, and microbes are submicron-sized components of biological systems.[214,215] In comparison to synthetic nanostructures, they can be referred to as “biological

nanostructures". Self-assembly is regarded as a bottom-up method for creating nanomaterials and is almost always occurring in nature and in living things from microbes to humans. It is a natural process that results from intramolecular and intermolecular interactions that spontaneously arrange disordered molecular units into ordered structures.[44] The equilibrium of the attracting and repulsive forces within and between molecules governs assembly. The self-assembly process is regulated by noncovalent interactions, such as van der Waals, electrostatic, hydrogen bonding, and stacking interactions.[216,217] Fabrication of new nanomaterials from natural building blocks including phospholipids, oligosaccharides, oligonucleotides, proteins, and peptides has sparked a lot of interest in the field. Amongst them, peptides have received a lot of interest because of their simple structure, relative chemical and physical stability, variety of sequences and shapes, and ease of mass production. Furthermore, due to their inherent biocompatibility and biodegradability, peptides have emerged as incredibly important building blocks for constructing self-assembled nanostructures in medical applications. Molecular building blocks, also known as molecular synthons or scaffolds, contain information that determines the nature and outcome of the self-assembly process. Therefore, with judicious design of molecular synthons, the self-assembly process and applications of the resulting structural or functional systems and materials may be controlled.[218] The versatility of the peptides, in conjunction with their ability to form certain secondary structures offer a special framework for the construction of nanomaterials with tunable structural characteristics. According to reports, peptides can self-assemble into shape specific nanostructures, including fibers, micelles, vesicles, nanotubes, and nanospheres.[219–222] The different shapes of nanostructures adapted by peptides result from a variety of factors including hydrophobic interactions, hydrogen bonds, electrostatic interaction, aromatic stacking, crystallization, and steric effects.[223,224] The development of nano and microstructures as well as molecular gels from their molecular building parts is

an exquisite example of molecular self-assembly. The molecular building blocks' ability to self-assemble into either soft molecular gels or solid nano- and microstructures depends on the minute differences in their interactions with one another and with solvent molecules. Low molecular weight gels (LMWGs), also known as molecular gels, are soft materials created by the self-assembly of small molecules in organic, aqueous, and ionic solvents through attractive noncovalent interactions.[225–227] The increasing popularity of peptides and their derivatives for the development of gel material over other biomolecules and organic molecules is attributed to their inherent biological relevance to normal physiological and pathological conditions.[228–231]

Despite the fact that proteinogenic peptides and their derivatives are intriguing candidates for molecular self-assembly applications, they suffer from fast enzymatic degradation under physiological conditions and lack the molecular stiffness necessary for advantageous self-assembly. To get around the problems of natural peptides being degraded by enzymes, peptide derivatives including either D- or unnatural amino acids, cyclic peptides, and peptoids have been used.[232–234] In comparison to their linear counterparts, cyclic peptides offer molecular stiffness as well as enzymatic stability; however, the main drawbacks of bigger macrocyclic peptides are their high cost and rigidity. In this context, cyclic dipeptides get around limitations such as rapid enzymatic breakdown under physiological conditions in contrast to linear peptides, non-biocompatibility of synthetic peptides, rigidity, and high production costs of macrocyclic peptides. Cyclic dipeptides (CDPs), sometimes called 2,5-diketopiperazines (DKPs), are the smallest cyclic peptides and have a 6-membered core heterocyclic lactam ring as their primary structural component. Due to its cyclic structure and superior hydrogen bonding ability with four hydrogen bonding sites (two donor and two acceptor) from two amide bonds the CDP scaffold is endowed with molecular rigidity, as opposed to the two

hydrogen bonding sites (an acceptor and a donor) in equivalent linear dipeptides with one amide bond.[177,178] The selection of amino acid composition in the CDP scaffold makes it simple to add noncovalent interactions that are important in promoting molecular self-assembly, such as aromatic π-π interactions, van der Waals forces, electrostatic and ionic interactions. Overall, the molecular self-assembly of CDPs would inspire the formation of CDP-based functional and smart materials, such as injectable or in situ forming gels for controlled and on-demand drug delivery, 3D printing, and tissue engineering, hierarchical higher order oligomeric CDPs that mimic synthetic and natural materials, and the hybrid peptoid analogues for a variety of material and biological applications. Hanabusa and co-workers have reported the preparation of physical gels and hardened organic fluids (oils and solvents) using CDPs. In this study, a group of mostly nonsymmetric and symmetric CDPs was synthesized and their propensity to gel in organic fluids was examined. The study revealed that symmetric CDPs failed to induce gelation in organic solvent however asymmetric CDPs exhibited amino side chain substitution-dependent gelation properties with organic solvent and oils.[131] Depending on how different amino acid compositions and side chain substitution affect the propensity of organic liquids to gel, Hanabusa and colleagues later published a library of constructed CDPs. Hanabusa and co-workers later reported a library of designed CDPs and studied the effect of varying amino acid compositions and side chain substitution upon gelation propensity in organic liquids. These experiments on gelation have shown susceptibility of CDPs for composition-dependent gelation.[235] An asymmetric CDP-based hydrogelator [cyclo(L-Tyr-L-Lys)] and its ε-amino derivatives by anhydride condensation or peptide coupling of the corresponding aliphatic anhydrides and free acids has been reported by Feng and colleagues.[235] They then looked into how side chain substitution affected the likelihood of CDP derivatives to form gel. Suzuki and coworkers reported cyclo(L-Phe-L-Asp) tethered with poly(dimethylsiloxane) (PDMS), and they

investigated its propensity to gel in a variety of organic solvents. The idea behind adding PDMS to the CDP structure is to increase the amount of van der Waals contacts. Additionally, the long side chain substitution will stabilise the amorphous self-assembly structure and prevent crystallisation.[236] Hoshizawa and colleagues replaced the alkyl chain with aliphatic diols added through an aspartic acid side chain, extending the thixotropic gelation behavior of cyclo(L-Phe-L-Asp) derivatives from conventional organic solvents to alcohols, water, salt water, and other aqueous solvents. By adding aliphatic diols to the aspartic acid side chain cyclo(L-Phe-L-Asp) was made more soluble in polar solvent and easier to gel in alcohols and aqueous solvents.[237] Hanabusa and coworkers synthesized CDP ionogels employing branched alkyl chains substituted cyclo(L-Phe-L-Asp) derivatives.[238] Feng and colleagues investigated several bi-functional cyclo(L-Lys-L-Glu) derivatives with variable Boc- and Fmoc- modification of glutamic acid and lysine side chains, respectively to further understand the structure-gelation property of CDPs.[239] Verma and coworkers have explored how substituents, particularly aromatic groups, affect CDPs' ability to self-assemble into nanostructures.[132] There are many such reports depicting the modification of side chain amino acids of cyclic dipeptides by various means to produce functional self-assembled nanostructures and nanomaterials. Even though CDPs are promising synthons for engineering molecular self-assembly into a variety of molecular architectures, extreme caution must be taken when changing the amino acid composition, core substitution, and amino acid side-chains to induce self-assembly and to prevent undesirable effects like precipitation instead of the desired molecular gelation. The balance between hydrophobicity and hydrophilicity offered by the side chain of constituting amino acid of CDP is on eof the key factor which decides the fate of the CDP in forming self-assembly and nanomaterials. Taking everything into consideration here in this chapter a series of five non-symmtrical (**P1-P5**) and one symmetrical (**P6**) cyclic dipeptide were

synthesized containing S-benzyl-L-cysteine as common constituting partner. To avoid complexity in modification of the amino acid side chian and to reduce the production cost the hydrophobicity of the CDPs were controlled just by employing natuarlly occurring neutral amino acid partners using glycine, alanine, valine, isoleucine, phenylalanine, and S-benzyl-L-cysteine. The design of these CDPs were kept very simple. In this chapter efforts were made to analyse the effect of hydrophobicity of the neutral amino acid side chains (aliphatic and aromatic) on the self-assembly and hydrogelation to built a structure-gelation relationship of the CDPs under investigation.

3.3 RESULTS AND DISCUSSION

In this chapter total of six cyclic dipeptides were synthesized keeping S-benzyl-L-cysteine as common constituting amino acid in all of them. The second amino acid partner was chosen as a factor of increasing side chain or bulkiness in order to examine the participation of these side chain residues in the self-assembly pattern of the respective CDPs. Formation of different nano-structures due to different self-assembly patterns of the CDPs as well as the hydrogelation properties of these cyclic dipeptides were thoroughly studied in this chapter.

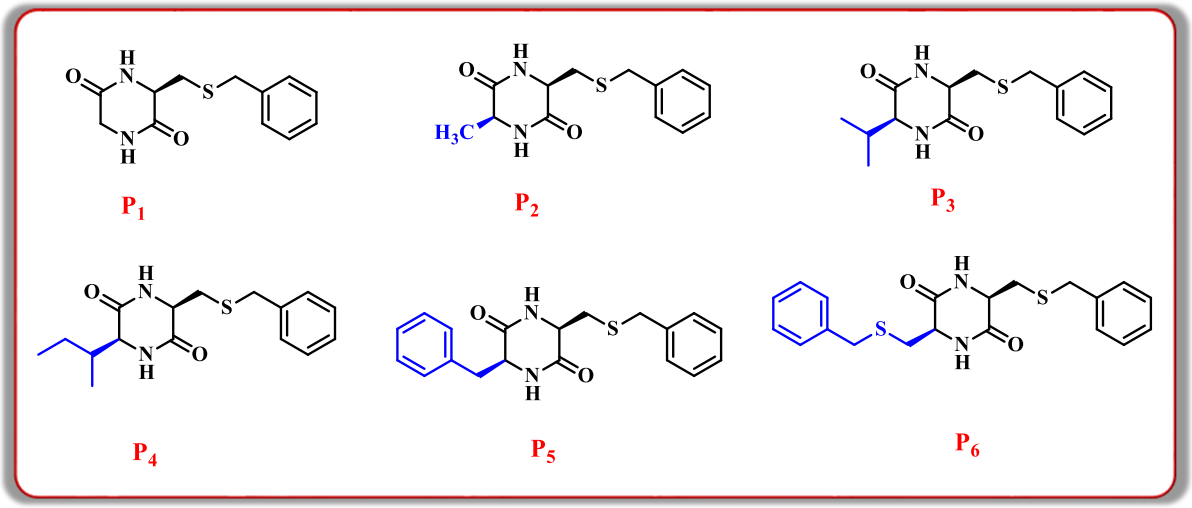

Figure 1. *Chemical structure of synthesized cyclic dipeptides (P1-P6).*

3.3.1 General Synthetic Procedure 'A' for Synthesis of P1 to P6

To a well-stirred solution of *N*-(*tert*-Butoxycarbonyl)-L-amino acids (**1**; 1 eq.) dissolved in *N*,*N*-dimethylformamide (10 ml), was added anhydrous hydroxybenzotriazole (HOBT; 1.2 eq.) slowly followed by 1-ethyl-3,3-(dimethylamino) propyl carbodiimide hydrochloride (EDC·HCl; 1.5 eq.) at 0 ^{o}C under nitrogen atmosphere. Then stirring was continued for 10 mins at ice-cooled condition and after that to this mixture, triethylamine (TEA; 5 eq.) was added followed by S-benzyl-L-cysteine methyl ester hydrochloride (**2**; 1.2 eq.). The reaction was further continued for 8 h at room temperature (monitoring via TLC). The reaction mixture was then concentrated under reduced pressure and extracted with ethyl acetate (3 × 20 ml). Evaporation of the solvent left a crude residue, which was purified by column chromatography over 60-120 mesh silica gel (hexane/ethyl acetate) to afford the intermediate compound '**3**' as a white solid. In the next step, intermediate '**3**' (1eq.) was treated with trifluoroacetic acid (TFA; 6 eq.) in dichloromethane solvent (10 ml) at 0 ^{o}C. The reaction mixture was slowly brought to room temperature and stirring was continued. Completion of the reaction was confirmed after 6 h via TLC and the reaction mixture was then concentrated under reduced pressure. The crude mixture was then treated with 1 (N) sodium bicarbonate solution until the pH reached 8-9 and extracted with dichloromethane (3 x 20 ml) from the aqueous layer.[193,240] After evaporation of the solvent, the product was purified by column chromatography over 60-120 silica gel using methanol/dichloromethane as eluent to afford the final product '**4**' as white solid (Scheme 1). All the final products were characterized by HRMS (EI or ESI mass) and ^{1}H, ^{13}C NMR (600 MHz) spectroscopy (**Figure S1-S12**).

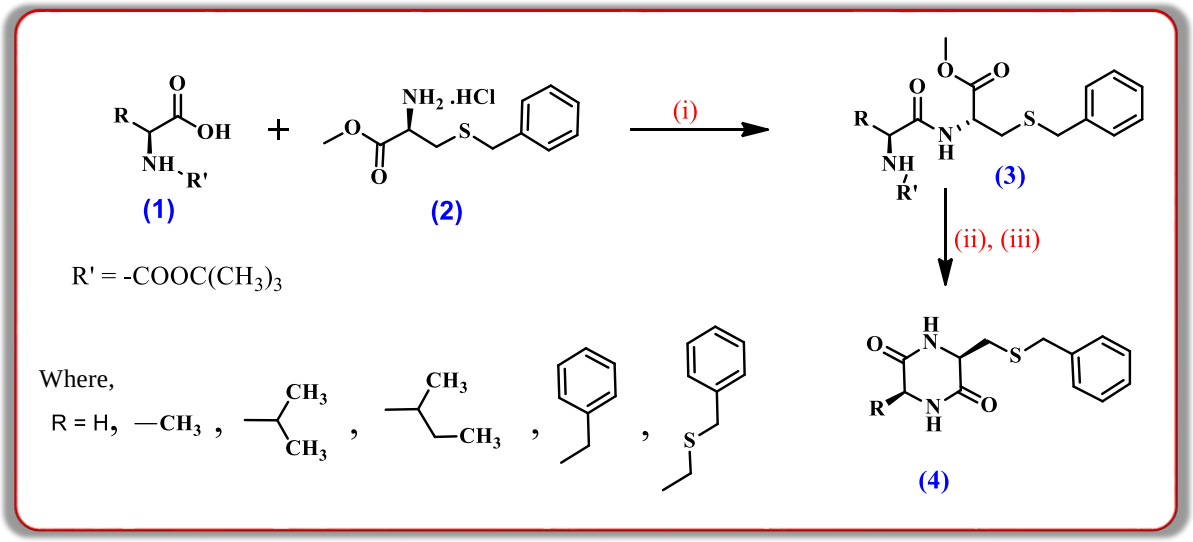

Scheme 1. *General synthetic scheme for synthesis of cyclic peptides P1, P2, P3, P4, P5, and P6.* ***[a]Reagents and Conditions:*** *(i) EDC·HCl, HOBt, TEA, 0°C to r.t, 8 h, (ii) TFA, DCM, 0°C to r.t, 4 h, (iii) $NaHCO_3$, H_2O, pH=8-9.*

3.3.2 Self-assembly Study of CDPs (P1-P6)

The self-assembly and gelation properties of synthesized CDPs were examined in different organic and aqueous solvents. Our primary aim was to examine the significance of the constituting amino acid partners having different chain lengths, branching, and aromatic rings in driving the self-assembly as well as the gelation process and establish a structure-self-assembly relationship of these CDPs. Gelation is one such phenomenon that makes us able to visualize the self-assembly behavior of nanomaterials through our naked eyes. Thus we investigated the gelation ability of these synthesized CDPs in different organic and aqueous solvents. These CDPs were found to be insoluble in pure water as well as in buffers and thus required a polar organic co-solvent like methanol, DMF, DMSO, ethanol, acetonitrile, etc. in order to self-assemble in aqueous solvents. For hydrogelation study, a certain amount of each CDP was weighed out in a screw capped glass vial and dissolved in minimum amount of HPLC grade methanol by heating (if required) after which distilled water or PBS buffer (pH=7.4) was added to that solution and the vials were kept undisturbed.

Hydrogel formation was observed at different time intervals for different CDPs and the formation of self-supporting gel materials was confirmed when no gravitational flow of the gel material was observed on the inversion of the glass vials (**Figure 2**). **P5** and **P6** formed hydrogels instantly after the addition of water whereas in case of **P3** and **P4** complete hydrogelation was observed at 5-7 mins after addition of water or PBS buffer (**Figure 2**). A very interesting observation was experienced in case of **P1**. It did not form hydrogel instead of that within 8-10 mins after addition of water/PBS very fine and tiny needle-shaped crystals were seen to form in the solution of **P1** and with increasing time more numbers of tiny crystals of **P1** got deposited at the bottom of the glass vial (**Figure 2B**). In case of **P2**, after almost 10 mins, dispersed loose gel was seen to be floating in the solution along with some tiny needle shaped crystals on the walls of the glass vial. So, in the same solvent condition and the same amount of peptides one of the six CDPs exhibited quick crystallization, another one showed both crystal and loose gel formation and others offered hydrogelation depending upon their molecular structure. From these observations altogether it can be said that with increasing hydrophobicity of one of the constituting amino acids of these CDPs from glycine to S-benzyl-L-cysteine the extent of self-assembly also increased resulting in formation of hydrogels. **P3** and **P6** formed opaque hydrogels whereas **P4** and **P5** formed translucent hydrogels. The phenyl ring of phenylalanine and s-benzyl-l cysteine in **P5** and **P6** respectively indulge themselves in π-π stacking inducing self-assembly in aqueous solvents giving instant gelation whereas **P3** and **P4** containing valine and isoleucine respectively have only aliphatic side chain which induced slow aggregation and formed gels after 5-7 mins. On the other hand, **P1** having glycine with no side chain residue self-assembled itself in such a way that it formed needle-shaped crystals at a very fast rate.

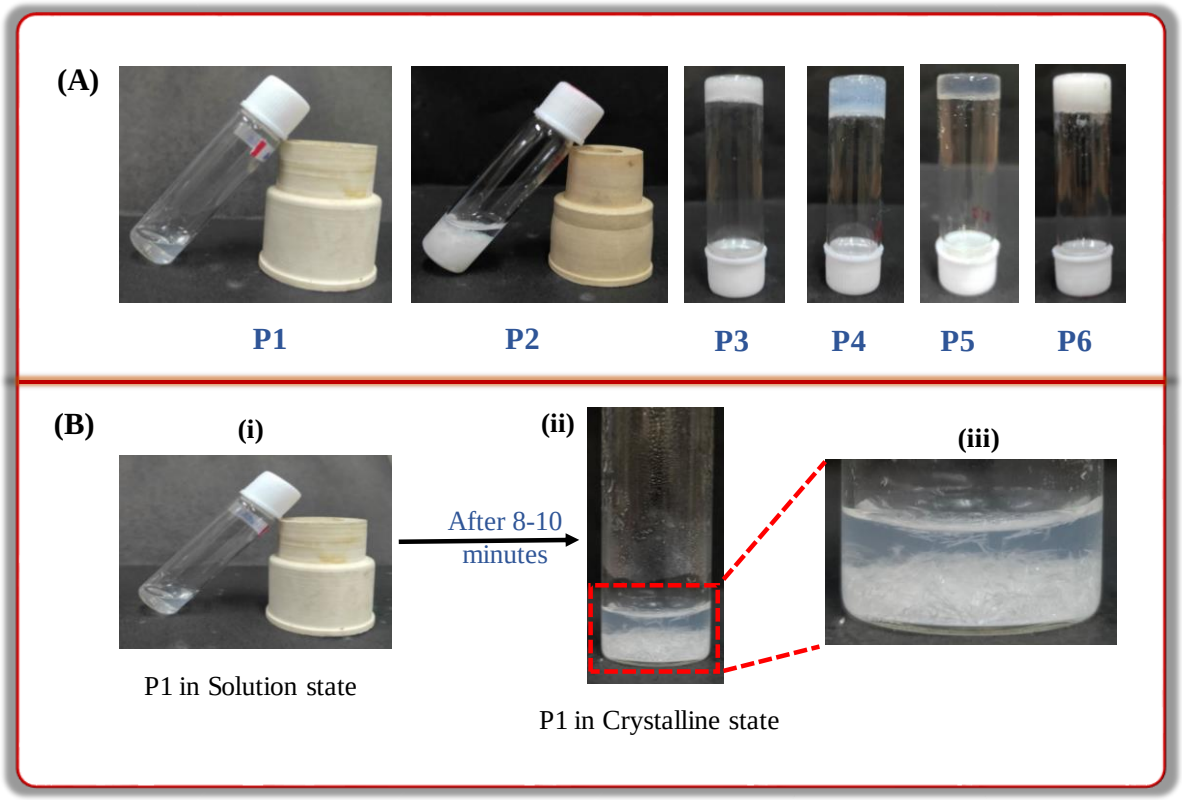

Figure 2. *(A) Images depicting formation of clear solution by P1, loose gel by P2, and tube inversion images of formation of hydrogel by P3, P4, P5, and P6 in methanol-water solvent system. (B) Images of formation of tiny crystals by P1 in methanol-water: (i) clear solution after addition of water, (ii) deposition of tiny crystals 8-10 mins after addition of water to the methanol solution of P1, and (iii) enlarged view of the glass vial enclosed by the red box in image (ii).*

The above described phenomenon was also observed when other polar organic solvents like DMF, DMSO, Acetonitrile were used as co-solvents instead of methanol, but in methanol-water, the CDP molecules might orient themselves in such a way that the rate of crystallization is fastest when methanol was used as co-solvent and also the crystals thus formed were well defined than those formed in other co-solvents. That is why methanol-water mixture was selected as the solvent of choice and all the experiments were carried out in the same solvent system. The minimum gelation concentration (MGC) of hydrogels obtained from **P3**, **P4**, **P5**, and **P6** cyclic dipeptides was found to be 0.5 %, 0.36 %, 0.25 %, 0.42 % (w/v) respectively in methanol-water/PBS buffer solvent

system. The ability to form oraganogel by these CDPs was also examined in different organic solvents like dichloromethane, ethylacetate, xylene, toluene, ethanol, isopropanol, etc. The propensity of gel formation was examined in organic as well as in aqueous solvents only up to a minimum gelation concentration of 1% (w/v). Thus all the hydrogels and organogels mentioned in this discussion fit well in the range of 'Supergels' in respective solvents.

3.3.3 Thermal and pH Stability of CDP Hydrogels (P3-P6)

All the hydrogels as well as the organogels formed by the CDPs are thermos-reversible in nature that means on heating they showed gel-to-sol and on cooling to room temperature showed sol-to-gel transition. Hydrogels obtained from **P3**, **P4**, and **P5** in methanol-water solvent system were found to be stable for several weeks under physiological conditions except for **P6** hydrogel (in methanol-water) which underwent deformation after 24 hours of formation by releasing solvent from the gel network and formed a loose gel. The gel melting temperature or gelation temperatures (T_{gel}) of **P3**, **P4**, **P5**, and **P6** hydrogels in methanol-water solvent were measured by placing the gel-containing screw-capped glass vial into an oil bath and raising the temperature at a rate of 2 ^{o}C min^{-1}. The temperature was monitored using a thermometer and T_{gel} was defined as the temperature (+0.5 ^{o}C) at which the gel melted and showed gravitational flow. T_{gel} for **P3**, **P4**, **P5**, and **P6** hydrogels in methanol-water solvent system were found to be 65^{o}C, 70^{o}C, 77^{o}C, and 72^{o}C respectively at their respective MGCs. These gels can survive a wide range of pH from basic to acidic. For most of the hydrogels, it was observed that they could maintain their gel state in the basic range up to a pH value of 12, above that they formed opaque white suspension. In the acidic region, these hydrogels were found to be stable up to a pH value of 4.5 below which they did not form any gel.

3.3.4 Rheological Properties Study

To investigate the strength of **P3**, **P4**, **P5**, and **P6** hydrogels and other viscoelastic properties, detailed rheological experiments were performed using an Antor Paar Compact Modular Rheometer (MCR 102). PP25 was used as the measuring system and a well-controlled system inside the instrument assured a constant temperature of 25℃ during all the rheological experiments.

Apart from 'inversion of vial' test, a semisolid material must attain some basic requirements in terms of viscoelasticity to be considered as gel. Its storage modulus G′ must be greater than the loss modulus G″ at all frequencies and must also be independent of the oscillatory frequency. Amplitude sweep experiment was performed at a constant 10 rad/s angular frequency (ω) and within the range of 0.01% to 100% shear strain for the gel samples. The crossover of G′ and G″ takes place upon application of 7.7% for **P3**, 15.21% for **P4**, 22.88% for **P5**, and 1.48% of shear strain for **P6** (**Figure 3A-3D**).

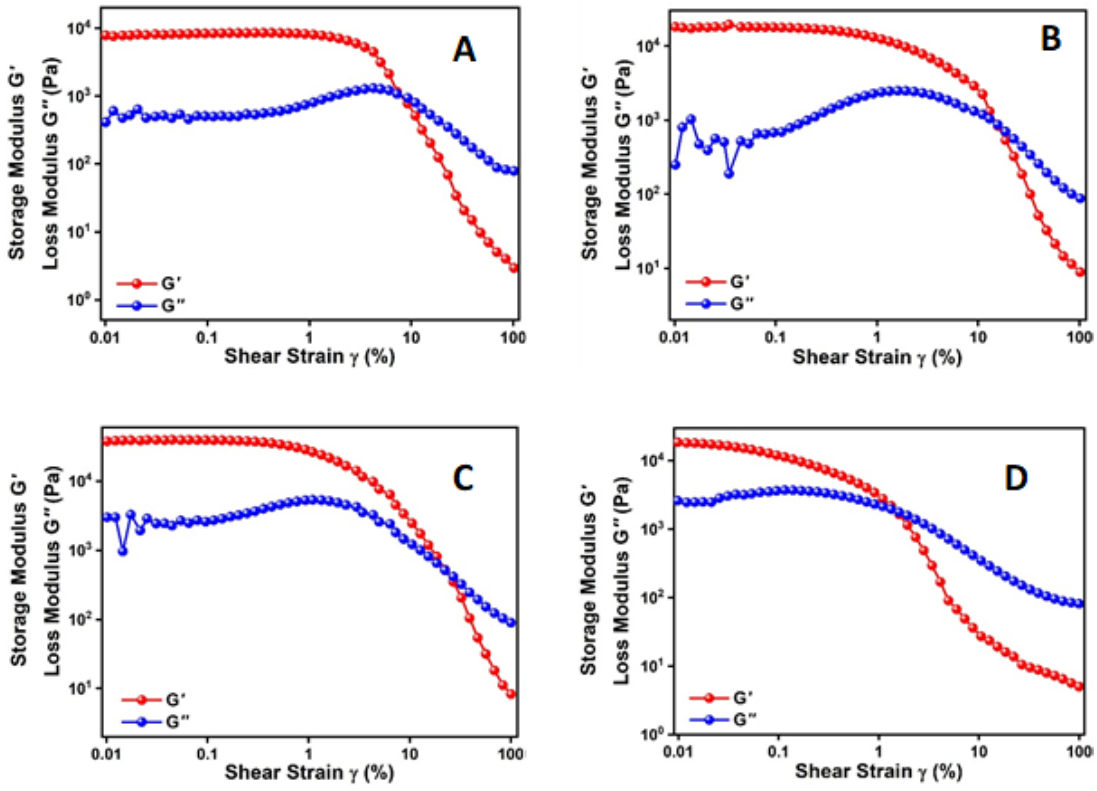

Figure 3. *Strain sweep test of (A) P3, (B) P4, (C) P5, and (D) P6.*

Frequency sweep experiments (**Figure 4A-4D**) were done to investigate the viscoelastic nature of the gel materials and to determine the frequency dependence of G′ and G″ moduli. The experiment was carried out within the range of 100 rad/s to 0.1 rad/s of angular frequency and at a constant 0.05% shear strain for all except 0.01% for **P6** (having insight from the respective strain sweep experiments). There was no entanglement effect in this range and the storage and loss moduli ran in parallel. It is quite evident that the results are associated with all the aforementioned criteria to be considered as perfect gel systems.

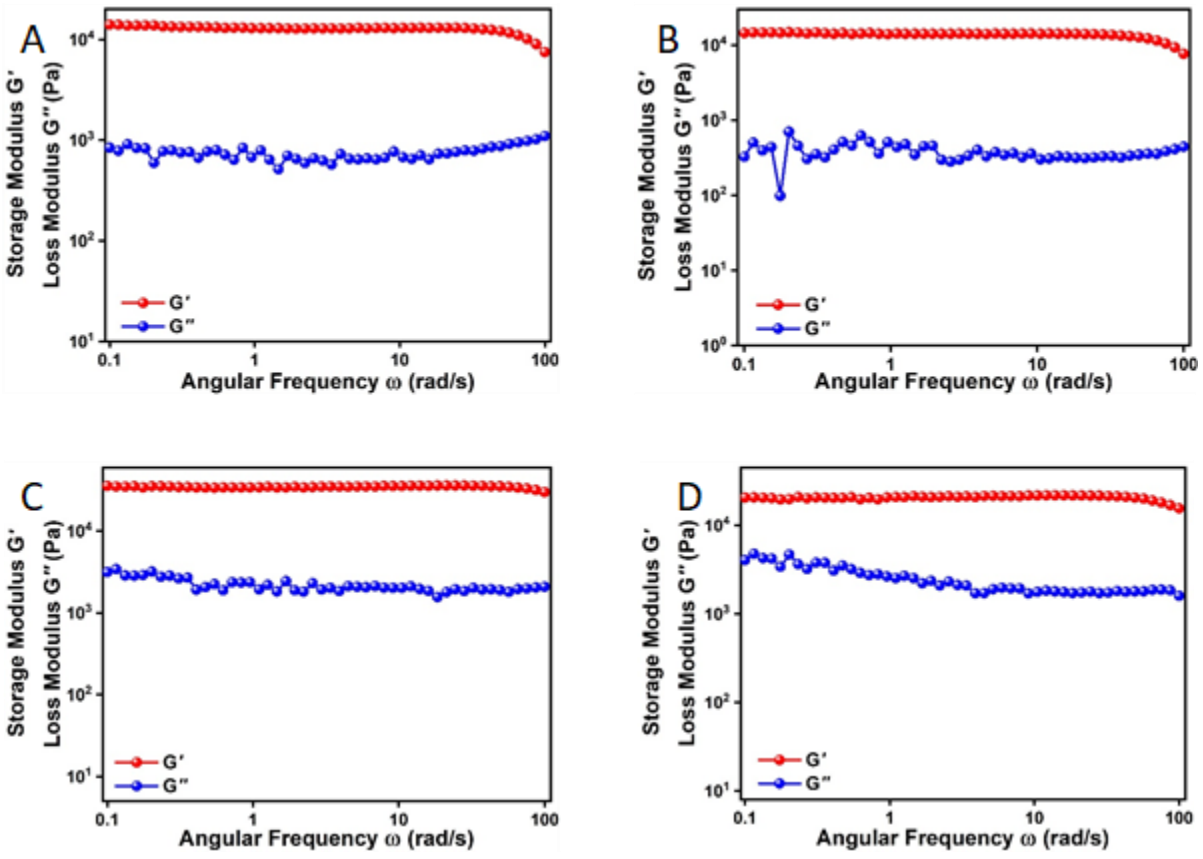

Figure 4. *Frequency sweep test of (A) P3, (B) P4, (C) P5, and (D) P6.*

The gel systems showed an intriguing viscoelastic property, thixotropy.[241] Thixotropy is a significant mechanotropic property of viscoelasticity for some of the non-newtonian pseudoplastic fluids (e.g; gels) which exhibit time-

dependent viscosity. For gel system, it refers to an isothermal gel-to-sol and sol-to-gel reversible transition in which the gel state undergoes conversion to sol state upon the application of certain external stimuli such as mechanical shaking, agitating, etc., and returns to the gel state on resting.

The thixotropic nature of the gel samples was proved by performing time sweep experiments (**Figure 5**) i.e. sequential application of low and high strains, separated by enough time to ensure the complete gel-to-sol ($G' > G''$) and sol-to-gel ($G'' > G'$) conversions. This sol-gel interconversion was performed repeatedly for seven consecutive steps.

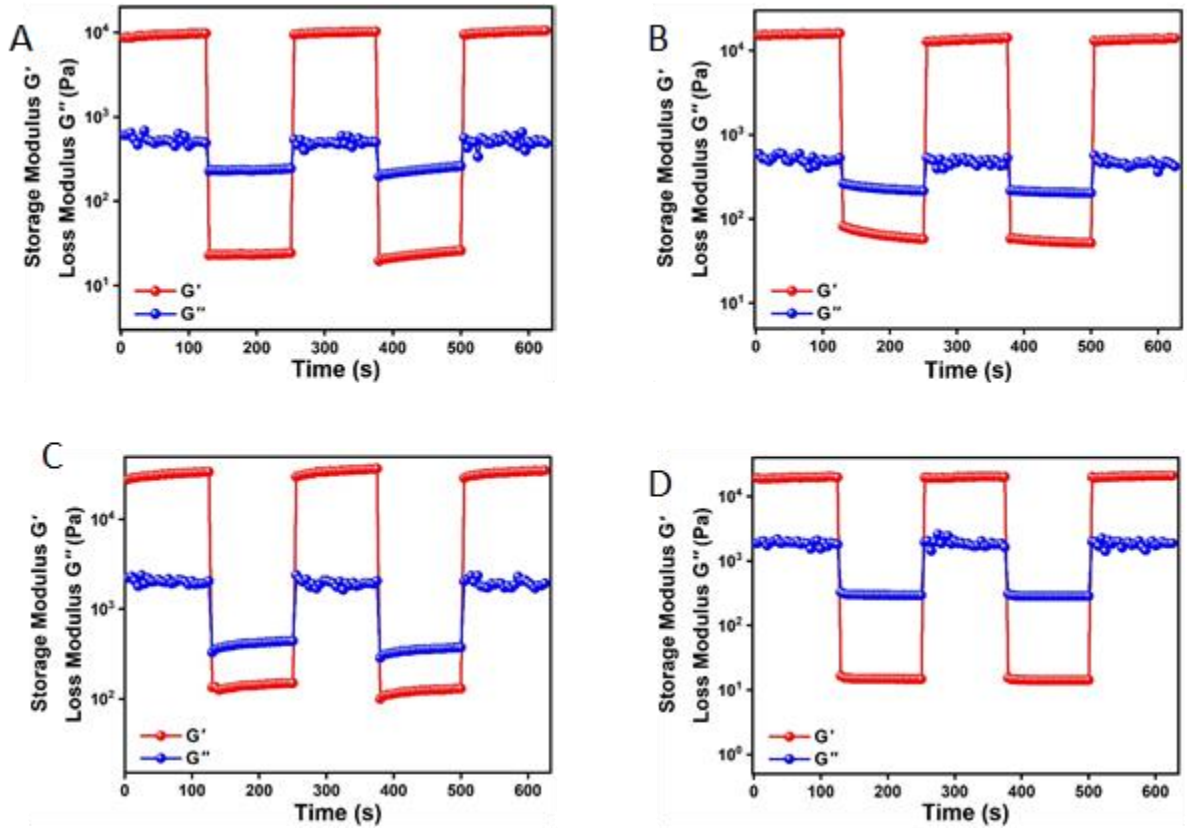

Figure 5. *Time sweep test of (A) P3, (B) P4, (C) P5, and (D) P6.*

The first step of time sweep experiment was started off with low shear strain. In the second step, the gel was completely destroyed and transformed into a quasi-liquid state (sol) by the application of high strain which is evident from the

modulus values (G′ < G″). In the third step, recovery of the gel was monitored with a time sweep experiment under the application of same strain value as that of step 1, and the modulus values which give support to the reformation of the gel (G′ > G″). In the fourth step, the gel was again ruptured with high strain and was recovered in the fifth step with the application of low strain. The experiments for all the gel systems were performed at a particular 10 rad/s angular frequency. All these observations proved that the gel materials are thixotropic as well as self-healing in nature. The values of low and high strains which were applied sequentially are summarised in Table 1.

Table 1. *Table containing applied strain values during frequency sweep and strain sweep experiments performed on the hydrogels*

CDP	% Strain value during frequency sweep test	% Strain value during time sweep test	
		Gel step	Sol step
P3	0.05	0.05	30
P4	0.05	0.05	30
P5	0.05	0.05	30
P6	0.02	0.02	10

3.3.5 Morphological Study of The CDPs: AFM Study

Atomic Force Microscopy technique is one of the most useful tools to visualize the surface morphology of nanomaterials formed by the self-assembly of constituting monomeric units. Thus all the peptide samples were subjected to AFM study to establish a structure-morphology relationship by determining the morphology of the nano-structures formed by them in methanol-water solution. For this, solutions of all the peptides of equal concentrations were prepared by dissolving them in methanol and diluting them with water to get a final concentration of 50 μM for each peptide. Those peptide solutions were then individually dropped cast on freshly cleaved mica sheets after 12 h of

incubation and the samples were then scanned under AMF laser after evaporating the solvents from the samples. From the AFM images, we have observed that different peptides produced different patterns of self-assembled nanostructures. Such as, **P1** formed unbranched thin fibers with an average diameter of 10-35 nm. The nanostructure thus formed by **P1** showed lesser well-defined fibrillar properties rather exhibited crystallinity in their morphology, thus looking like microcrystals (**Figure 6A-6C**). **P2** formed slightly branched nano-fibers along with some flat nano-sheet like morphology, initially thought to be formed by the stacking of thinner nanofibers (**Figure 6D-6F**). The diameter of the nanofibers formed by **P2** ranged between 70-160 nm and the average diameter of the nano-sheet was found to be 480-530 nm and the length of both the nano-fiber and

.

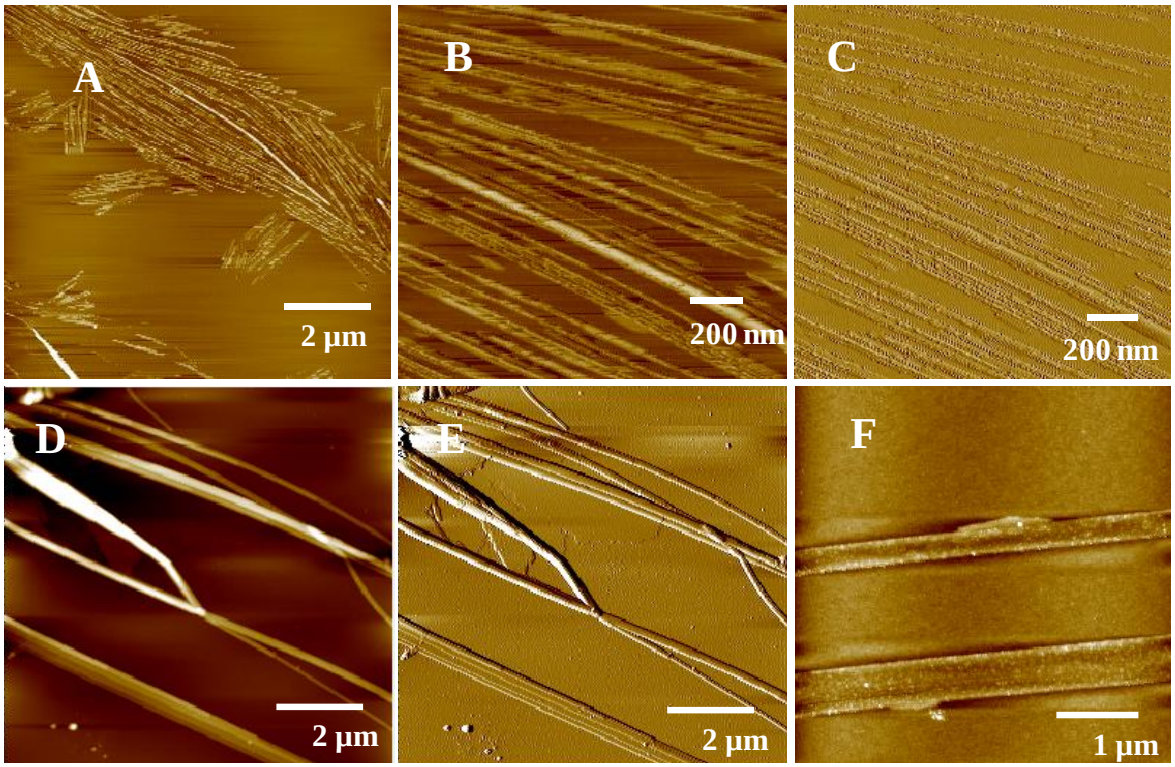

Figure 6. *Atomic Force microscopy images of P1 and P2 obtained from methanol-water solvent system. (A) Aggregates obtained from P1, (B) higher magnification view of A and (C) amplitude image of B. (D Aggregates obtained from P2, (E) amplitude image of D and (F) formation of nano-sheet after 24 h of incubation by P2.*

nano-sheet were several microns. The presence of sheet like structure further encouraged us to examine the morphology of **P2** at higher incubation time. Thus **P2** solution was allowed to incubate for another 12 h and after total incubation of 24 h, the AFM images showed only nano-sheets of average diameter of 300-560 nm. So, with increasing incubation time tendency to form nano-sheet by **P2** also increased.

In methanol-water solvent system, **P3** produced a unique network of entangled nanofibers interwoven in such a way leaving circular void spaces in-between them (**Figure 7A-7C**). A close look at the fibrillar network revealed this unique network was constructed by intersecting nano-fibers having average width of 20-75 nm and each nano-fiber twisted itself around other nano-fibers before and after intersecting each other to give a highly cross-linked helical network. This cross-linking may be aroused due to higher extent of self-assembly of **P3** cyclic dipeptide due to presence of hydrophobic valine side chain residue which in turn induces the gelation ability of **P3**. The isoleucine side chain in **P4** brought out an interesting fibrillar nano-structure in methanol-water solvent where some of the nanofibers were seen to be covered up with unsymmetrical annular assemblies. We further increased the incubation time and after 24 h all the fibers were seen to be covered up by those annular assemblies producing 'beads-on-a-thread' type rare morphology (**Figure 7G-7I**). The average width of the nano-fibers was 60 nm-130 nm and the spherical assembly had an average diameter of 125-200 nm.

As we further increased the hydrophobicity of the CDP by incorporation of aromatic ring bearing phenylalanine (**P5**), a highly cross-linked and super twisted dense nano-fibrillar network was observed (**Figure 8A-8C)**. As the incubation time increased the fibers became even more twisted giving rise to extensive cross-linking in the network. If each nanofiber can be assumed as a strand of hair, then this whole network can be compared to an arrangement of

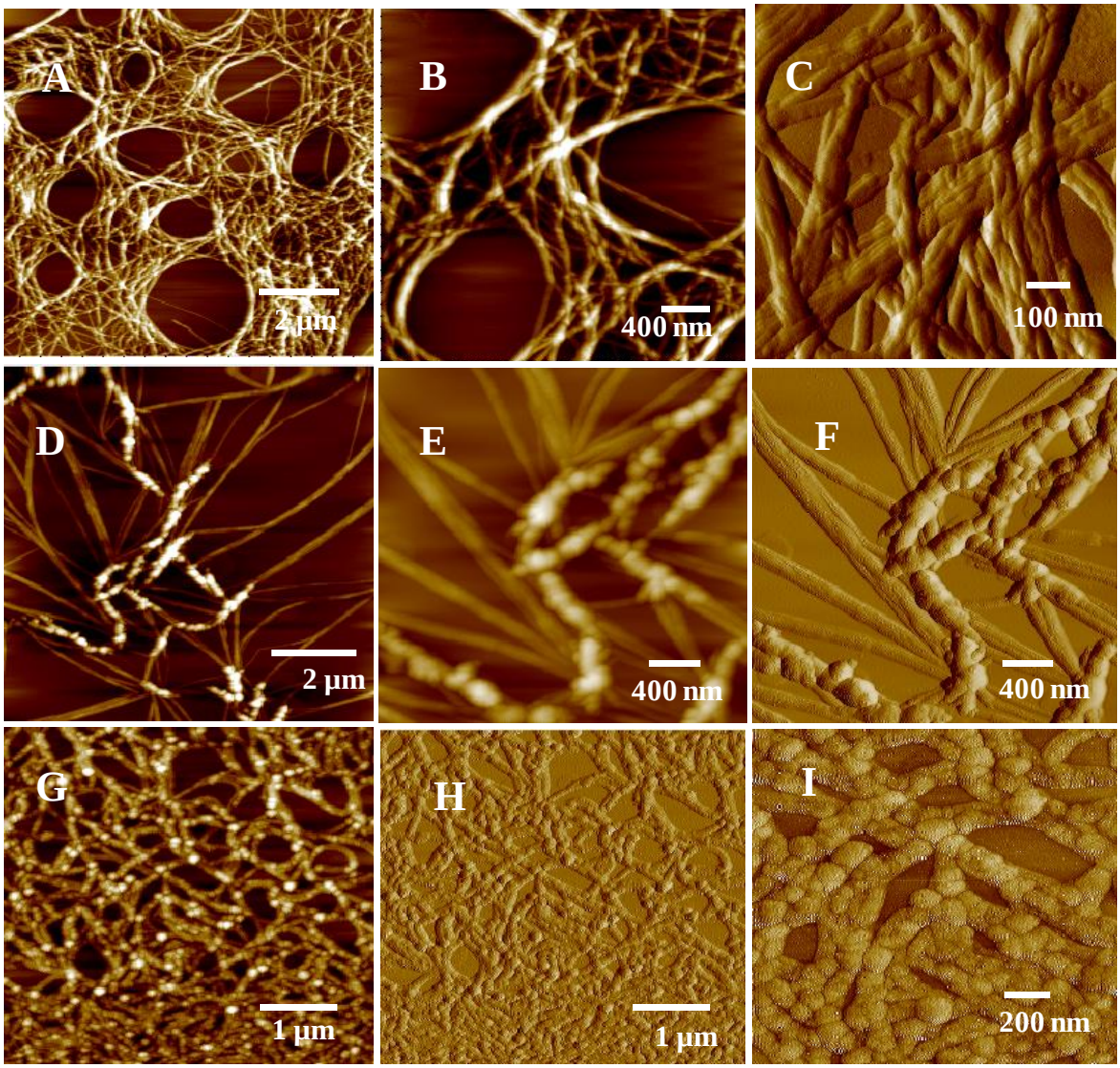

Figure 7. *Atomic Force microscopy images of P3, and P4 obtained from methanol-water solvent system. (A) Nano-fibrillar network formed by P3, (B), and (C) higher magnification view of A depicted twisting of nano-fibers. (D unique morphology obtained from P4, (E), and (F) higher magnification view of D and corresponding amplitude image. (G) Beads-on-a-thread architecture formed by P4 after 24 h of incubation, (H) and (I) are amplitude images of G at different magnifications.*

thousands of hair braids entangled with each other (**Figure 8D-8F**). Phenyl alanine residue in **P5** cyclic dipeptide introduced extra π-π interaction between the molecules which further reinforce the molecules to self-assemble into such a highly cross-linked dense nano-architecture which in turn induced the hydrogelation process.

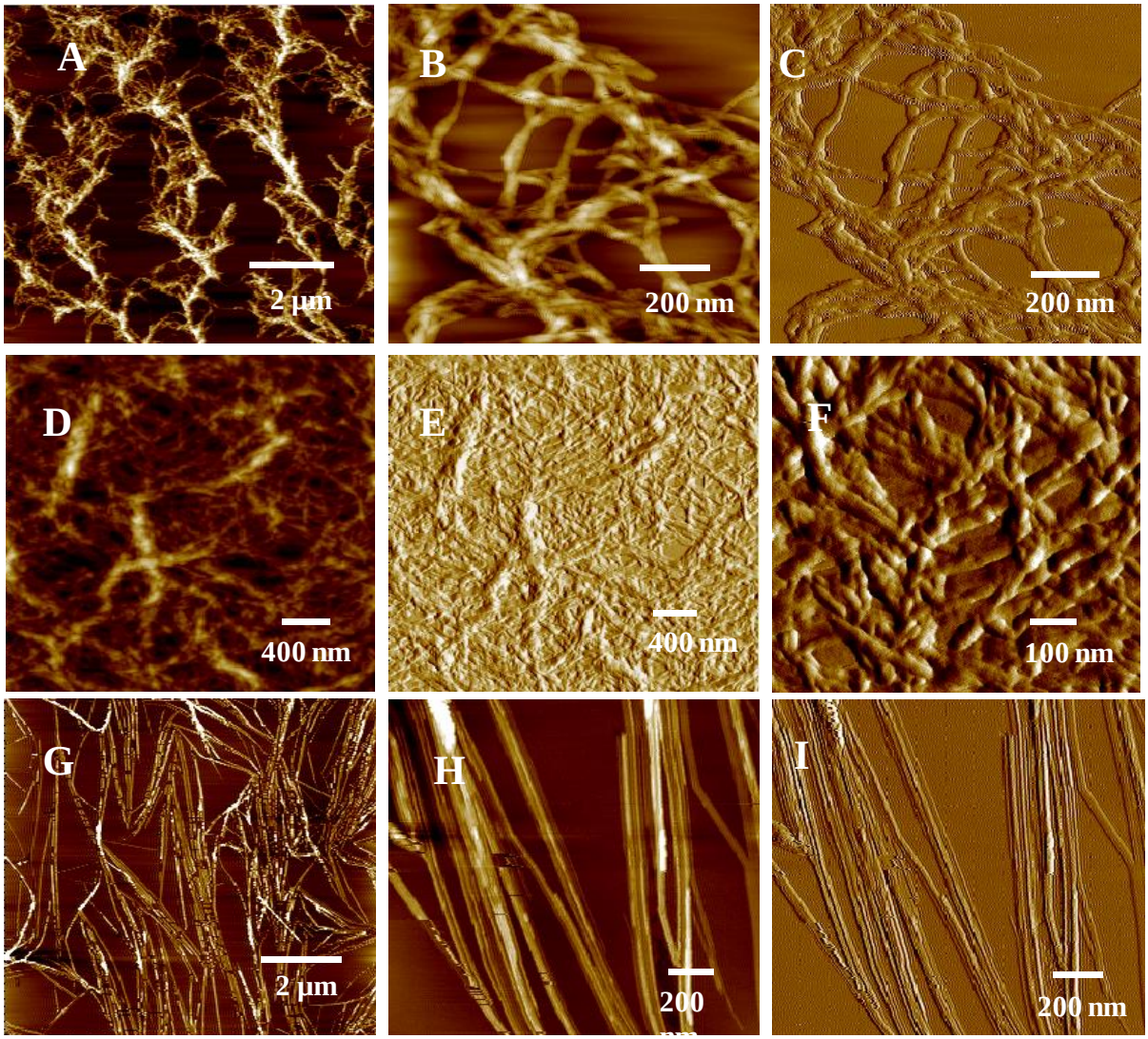

Figure 8. *Atomic Force microscopy images of P5, and P6 obtained from methanol-water solvent system. (A) Unique pattern of nanofibrillar assembly formed by P5, (B), and (C) topography and amplitude image of A at higher magnification. (D) and (E) topography and amplitude image of dense fibrillary network by P5 at higher concentration, (F) amplitude image AT higher magnification showing interconnected hair braid-like morphology formed by P5. (G) Self-assembly formed by P6, (H), and (I) topography and amplitude image of G at higher magnification respectively.*

On the other hand, **P6** bearing S-benzyl cysteine group and having a symmetrical structure resulted in a unique morphology of straight nanofibers with very few branching (**Figure 8G-8I**). These fibers have average width of 25-70 nm, had stripe like texture along the length of the fibers, and looked like thin wooden sticks or dried branches of small trees. From the AFM study, it can be concluded that all the cyclic dipeptides exhibited different nano-architectures

in methanol-water solvent system. Although most of them have shown nano-fibrillar self-assembly but the shape, size, and appearance of the nano-fibers formed by each CDP were very much distinct from each other. The complexity of the self-assembled structure was seen to differ with different hydrophobicity of the CDPs. Thus it can also be concluded that hydrophobicity of the amino acid side chain residue played a very important role in the self-assembly pattern and production of different nano-architectures.

3.3.6 Circular Dichroism (CD) Study

Circular dichroism is one of the most useful tools for identification of preferable secondary structures such as α-helix, β-sheet, β-turn, random coil, etc. acquired by the self-assembling peptide molecules in solution state. Solutions of all the six CDPs having same concentrations in methanol-water solvent system were prepared and after incubating those solutions for 24 h, CD spectra were collected for each peptide solution. It was quite surprising to see that despite having different macroscopic behavior, all six cyclic dipeptides majorly resulted in β-sheet rich secondary conformation in aqueous solution which are evident from the CD spectra. **P1** produced an intense negative peak at 219 nm in the CD spectra which is indicative of β-sheet rich arrangement of the peptide in aqueous solution (**Figure 9A**). Likewise, the characteristic β-sheet peak for **P2** appeared at 214 nm along with a positive peak at 197 nm. This pattern is characteristic of a well-defined antiparallel β-sheet structure (**Figure 9B**). Notably, this positive peak is absent in **P1** which may be due to the presence of some random secondary structure which cancelled out the positive peak around 195-200 of **P1**. On the other hand, both **P3** and **P5** produced strong negative bands at 229 nm in their respective CD spectra (**Figure 9C and 9E**) which is a characteristic signature peak for twisted antiparallel β-sheet secondary structure[242] that corroborated well with the twisted fibrillar morphology of **P3** and **P5** obtained

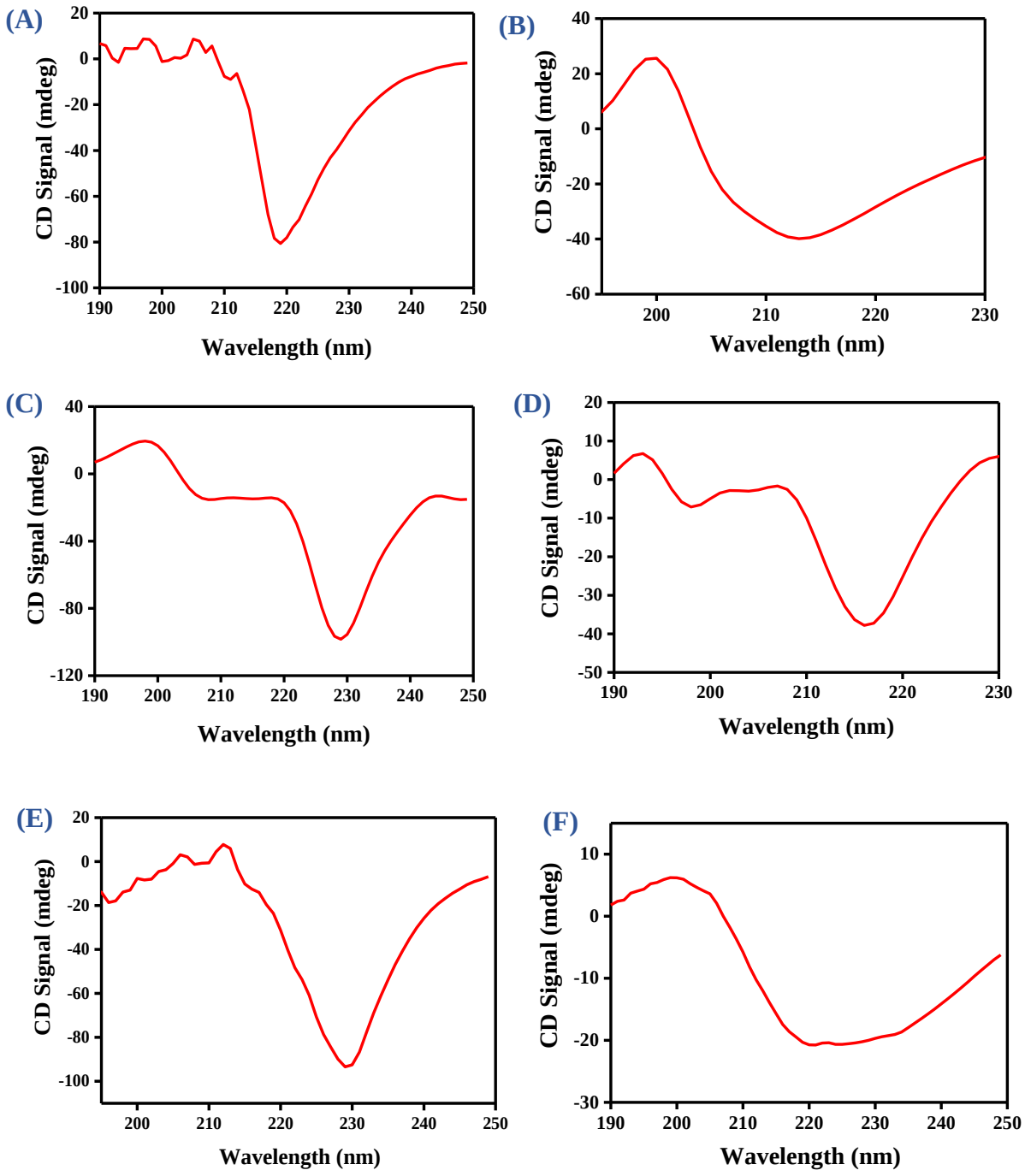

Figure 9. *CD spectra of (A) P1, (B) P2, (C) P3, (D) P4, (E) P5, and (F) P6 obtained from their methanol-water solution.*

from AFM experiments. **P3** also contains a negative band around 207 nm which may be attributed to the helical nature of the nanofibers. **P4** and **P6** also acquired well defined antiparallel β-sheet structures and displayed broad

negative peaks with minima at 216 nm and 220 nm and positive peaks with maxima at 192 nm and 199 nm respectively in their CD spectra (**Figure 9D and 9F**). The negative peak at around 198 nm in the CD spectra of **P4** indicated the presence of some random coil in the secondary structure which may be attributed to the formation of annular assemblies along with fibrillar assemblies in its aqueous solution.

3.3.7 Thioflavin-T (Th-T) and Congo Red (CR) Binding Study

The ability of the cyclic dipeptides to acquire β-sheet enriched secondary structure in aqueous solution was further investigated by Thioflavin-T and Congo Red binding assay. Thioflavin-T is an amyloid specific fluorescent dye which particularly binds to the β-sheet rich amyloid fibrils and exhibits visible changes in its fluorescence spectra. Th-T shows low fluorescence emission with maxima around 478 nm when excited at 410 nm which is known to be enhanced when it binds to β-sheet enriched amyloid fibrils. Thus emission spectra of free Th-T and Th-T with six CDPs (**P1**, **P2**, **P3**, **P4**, **P5**, **P6**), pre-incubated for 24 h in methanol-water solvent were recorded individually. An enhancement in the Th-T fluorescence intensity by several fold was observed in all cases after binding with CDP which indeed confirms the formation of β-sheet rich amyloid like fibrils by the CDPs in methanol-water solvent system (**Figure 10A**). This result was further supported by Congo Red binding assay which too is an amyloid specific dye. CR after binding with amyloid fibrils exhibits red shift of absorption maxima along with slight increase in the absorbance intensity. Pre-incubated solutions of CDPs in methanol-water were individually mixed with CR solution of certain concentration and then optical absorption spectra of CR were recorded in the wavelength range 400-600 nm before and after mixing with CDPs. The excitation maxima of free CR was obtained at 490 nm which was seen to red shifted to 492 nm after binding with **P1**, 493 nm after binding with **P2**, **P3**, **P4**, and **P5** individually, and 494 nm after binding with **P6** along

with an increase in the CR absorption intensity in all cases (**Figure 10B**). This observation reconfirmed the presence of β-sheet rich self-assembled fibrils in the aqueous methanol solution of CDPs which are similar to the short fragments derived from amyloid β peptides.

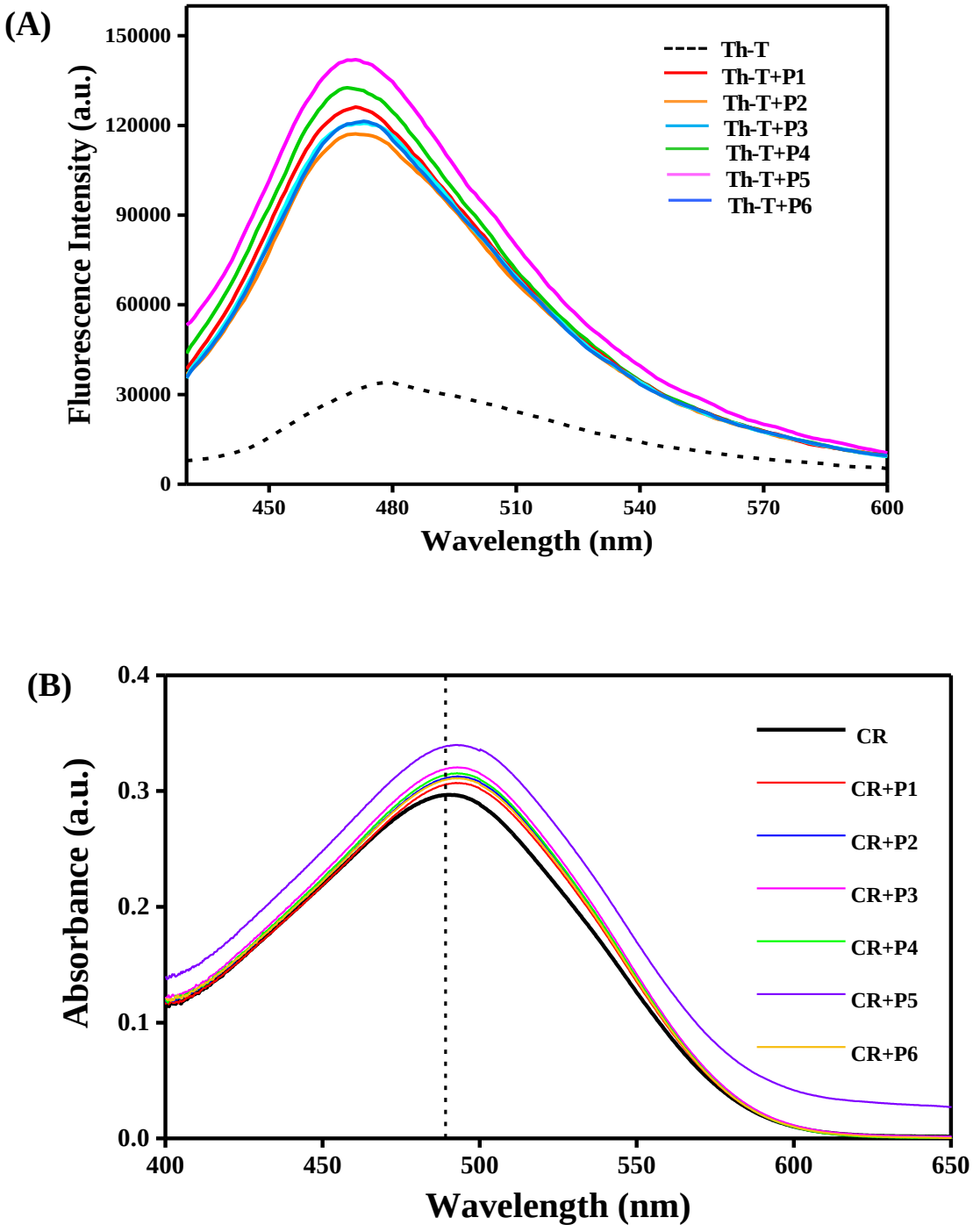

Figure 10. *(A) Thioflavin-T (Th-T) binding study and (B) Congo red (CR) binding study of the CDPs in methanol-water solvent system.*

3.3.8 NMR Study

Hydrogen bonding interaction is one of the major driving force to induce self-assembly as well as gelation in CDPs as they contain two cis amide groups with two H-donor and two H-acceptor sites in their rigid rings. Deuterium exchange ^{1}H NMR and temperature-dependent ^{1}H NMR experiments were performed to get important insight into hydrogen bonding pattern and nature of the hydrogen bonding involved in the self-assembly process. For D/H exchange experiment, first, ^{1}H NMR of all the CDPs was recorded in DMSO-d_6 solvent and then D_2O was added to the same solution of each CDP, and ^{1}H NMR was recorded at different time intervals.^{1}H NMR peak for two amide protons of **P1** and **P6** appeared as one singlet peak at 8.19 and 8.27 ppm respectively and that of **P2**, **P3**, **P4**, and **P5** appeared as two singlet peaks at δ value 8.32, 8.07 ppm; 8.12, 8.09 ppm; 8.11, 8.08 ppm; and 8.22, 8.03 ppm respectively in DMSO-d_6 solvent. On addition of D_2O to the CDP solutions in DMSO-d_6, the intensity of amide proton peaks of each CDP was seen to decrease rapidly and tend to vanish as time passed (**Figure 8**). This rapid D/H exchange rate indicates the amide protons in CDPs are solvent exposed and were involved in strong inter-molecular hydrogen bonding with other nearby CDP molecules and solvent molecules.

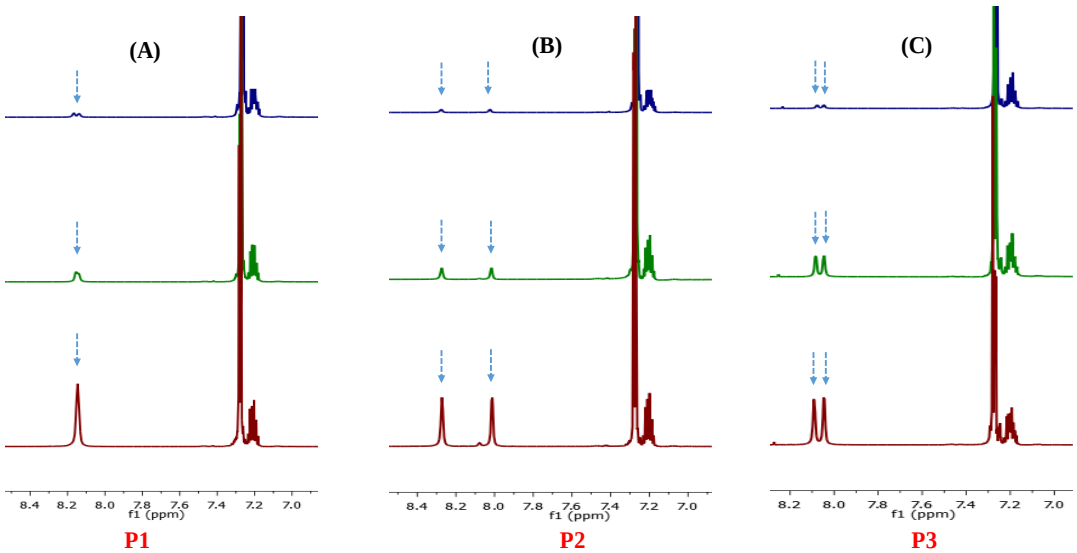

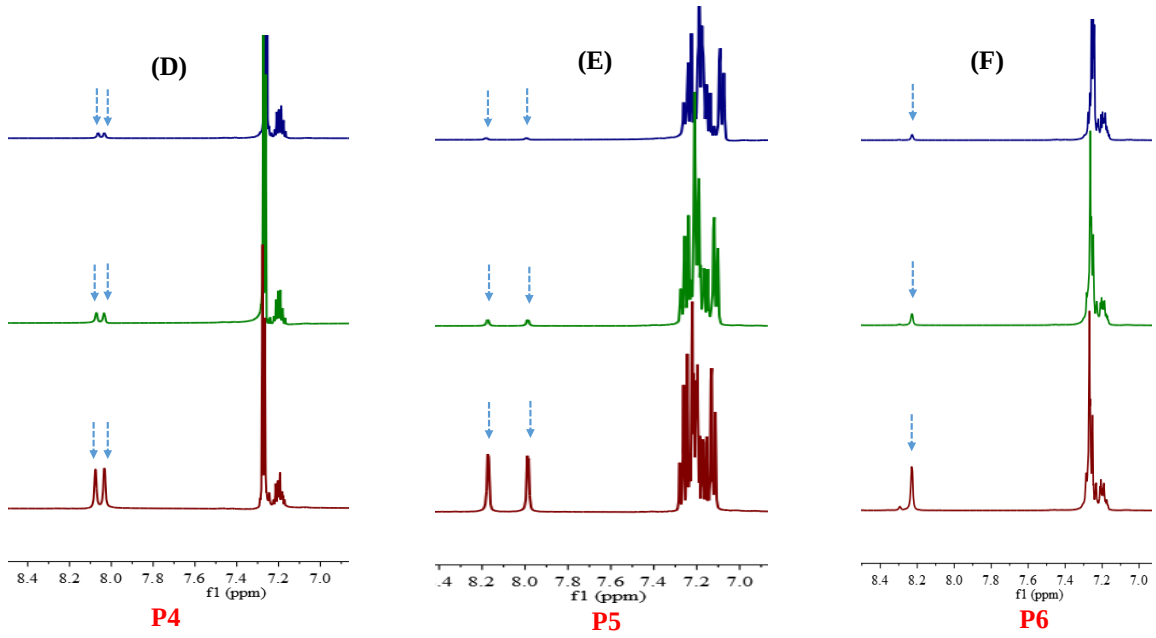

Figure 11. *H/D exchange ^{1}H NMR study of (A) P1, (B) P2, (C) P3, (D) P4, (E) P5, and (F) P6 in DMSO-d_6 solvent.*

The presence of strong intermolecular hydrogen bonding interaction was further evaluated by temperature-dependent ^{1}H NMR experiments, recorded at four different elevated temperatures such as 313 K, 323 K, 333 K, and 343 K starting from 298 K in DMSO-d6 solvent. At 298 K the amide protons of **P1** at 8.19 ppm and that of **P6** at 8.27 ppm showed upfield shift to 7.94 ppm ($\Delta\delta$ = 0.25 ppm) and 7.98 ppm ($\Delta\delta$ = 0.29 ppm) respectively as the temperature was increased to 343 K confirming the presence of strong intermolecular hydrogen bonding interactions (**Figure 9A, 9F**). Similarly, amide protons at 8.32, 8.07 ppm of **P2** shifted to 8.07 ($\Delta\delta$ = 0.25 ppm) and 7.80 ppm ($\Delta\delta$ = 0.27 ppm); that of **P3** at 8.12, 8.09 ppm shifted to 7.86 ($\Delta\delta$ = 0.26 ppm), 7.80 ($\Delta\delta$ = 0.29 ppm); amide proton peaks of **P4** at 8.11, 8.08 ppm shifted to 7.86 ($\Delta\delta$ = 0.25 ppm), 7.79 ppm ($\Delta\delta$ = 0.29 ppm), and amide protons of **P5** at 8.22, 8.03 ppm shifted to 7.92 ($\Delta\delta$ = 0.30 ppm), 7.76 ($\Delta\delta$ = 0.27 ppm) as a function of temperature from 298 K to 343 K (**Figure 9B-9E**). Shifting of these amide protons towards more shielded up field region with increasing temperature indicates disruption of intermolecular hydrogen bonding offered by the amide protons of CDPs on

heating. This fact can also be used to explain the thermoreversibility of the hydrogels obtained from these CDPs. The deformation of intermolecular hydrogen bonding by the heat energy enabled the gel-to-sol transition in these CDPs. Therefore, temperature-dependent ^{1}H NMR spectroscopy analysis reassured the presence of strong intermolecular hydrogen bonding in these CDPs which plays a key role in self-assembly to form nano-structures and in turn, induces hydrogelation.

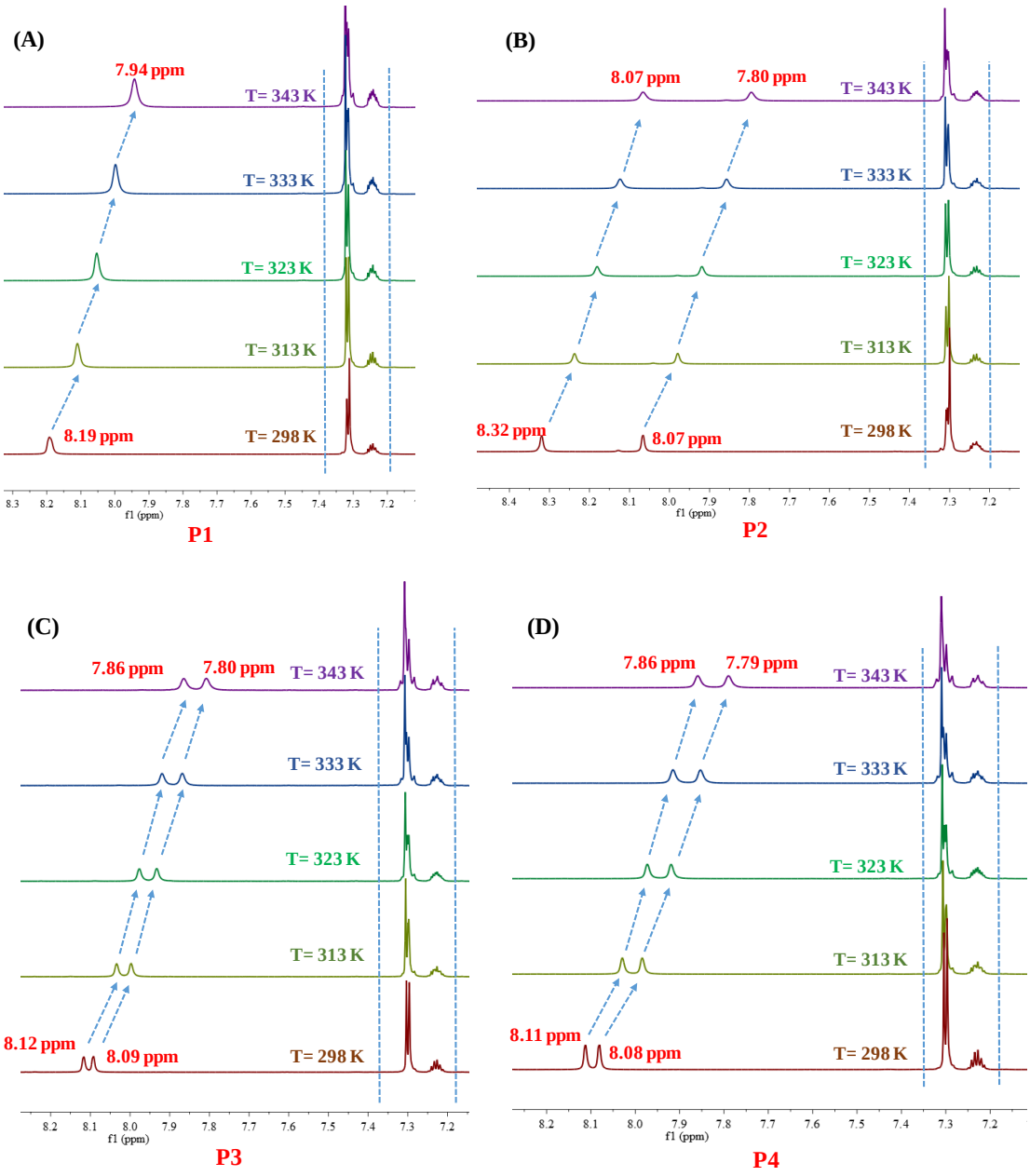

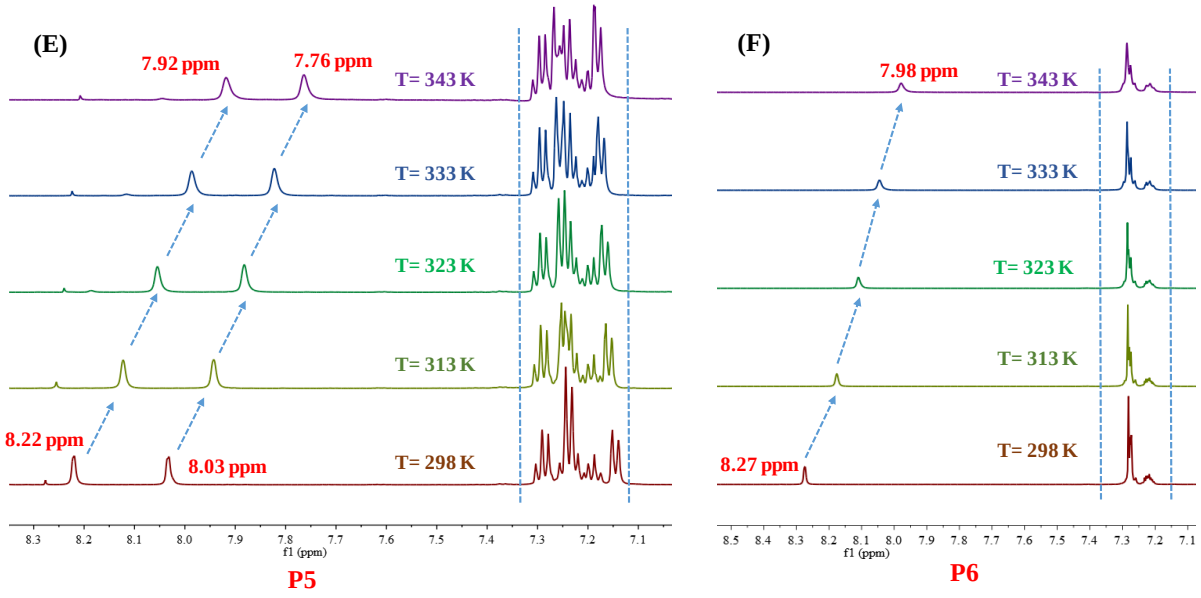

Figure 12. *Temperature dependent ^{1}H NMR study of (A) P1, (B) P2, (C) P3, (D) P4, (E) P5, and (F) P6 in DMSO-d_6 solvent.*

3.3.9 FTIR Study

Infrared spectroscopy (IR) is the most significant tool for elucidating the structural aspect of self-assembled peptides as well as protein molecules. The Fourier transform infrared (FT-IR) spectra of the samples were recorded on a Bruker TENSOR 27 spectrometer using the attenuated total reflection (ATR) technique. The spectra were scanned from 600 to 4000 cm^{-1}. Bruker software was used for data processing. Experimental data obtained were analyzed using Origin Pro 8.0 SRO software (Origin Lab Corporation).

Molecular arrangement of the peptide backbone can be analyzed by analyzing the most sensitive bands like amide I, amide II, and amide III which depend highly on the geometry and hydrogen bonding pattern offered by the amide groups. Herein, FTIR spectra investigate the structural orientation of these CDPs in solid state (for **P1-P6**), as well as in gel (for **P3**, **P4**, **P5,** and **P6** in methanol-water) state. The important FTIR band positions of all the CDPs in solid state are marked in their respective spectra (**Figure S13-S18**). In most

cases, the amide-I band appeared at 1600–1690 cm^{-1} mainly originating due to the >C=O stretching vibration mode while amide-II generally appeared at 1440–1580 cm^{-1} and amide-III at 1230– 1300 cm^{-1} results from the coupling of N-H bending vibration and C-N stretching vibration. The amide-I band for all six CDPs was obtained at 1656-1668 cm^{-1} and the amide-II band appeared in the range 1441-1457 cm^{-1} in its solid state which indicated presence of strong hydrogen bonding between the CDPs in their extended structure in solid state.

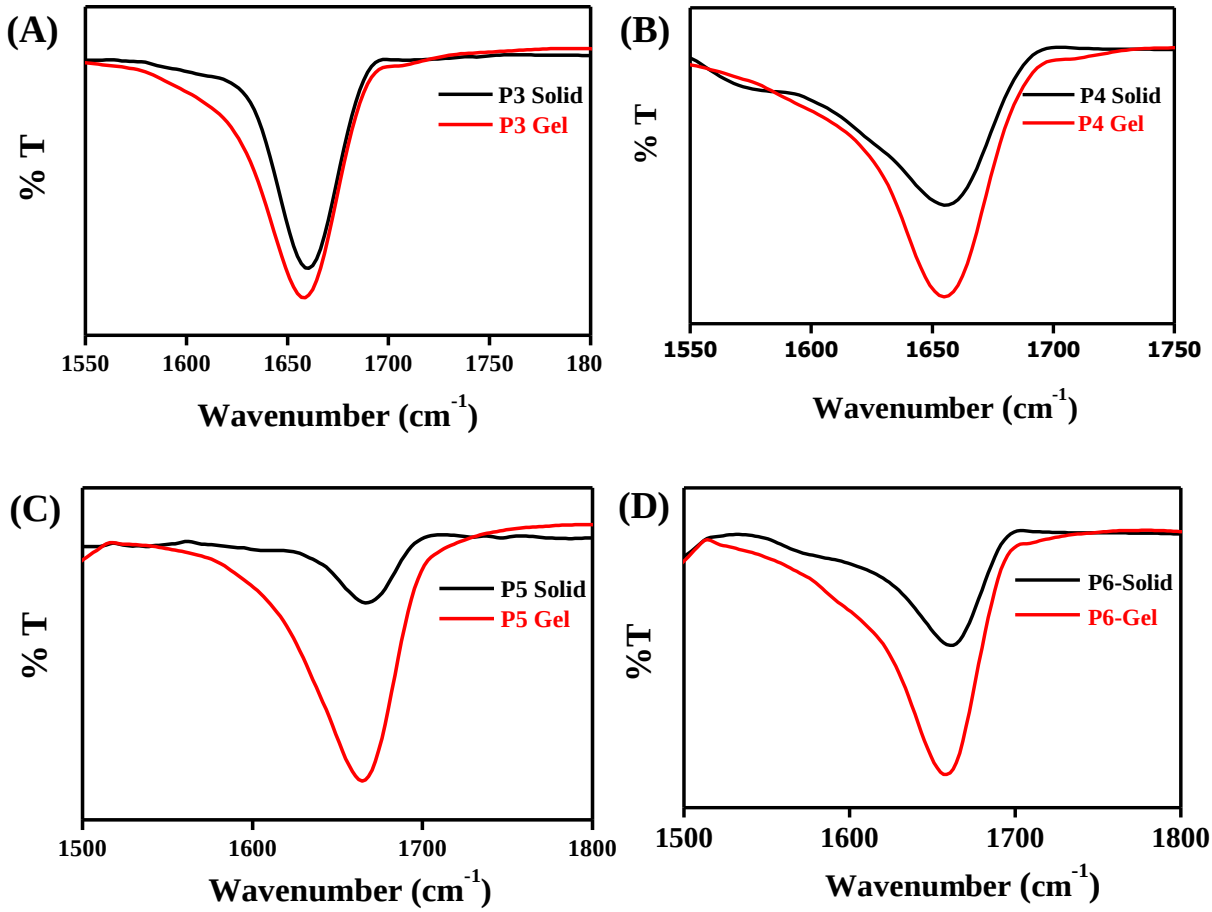

Figure 13. *FT-IR spectra in the solid and gel state of (A) P3, (B) P4, (C) P5, and (D) P6.*

The carbonyl stretching frequency of solid **P1** appeared at 1666 cm^{-1} and the amide-II band appeared at 1458 cm^{-1}. The amide-I band of **P3**, **P4**, **P5**, and **P6** appeared at 1660 cm^{-1}, 1656 cm^{-1}, 1668 cm^{-1}, and 1662 cm^{-1} in their respective solid states shifted to the lower frequency values and appeared at 1656 cm^{-1},

1654 cm^{-1}, 1661 cm^{-1}, 1659 cm^{-1} in their hydrogel state obtained from methanol-water solvent mixture (**Figure 13**). This shifting of amide carbonyl stretching frequency indicates weakening of those carbonyl bonds by greater extent of inter-molecular hydrogen bonding in the gel state. Moreover, for all six CDPs, appearance of the amide NH stretching band at around 2961 cm^{-1} to 3175 cm^{-1} in the solid as well as in the gel state indicated that the CDPs may exist as an inter-molecularly hydrogen-bonded extended structure in both the states.

3.3.10 Crystallographic study

The self-assembly mechanism of compounds **P1**-**P6** can be understood using their X-ray crystal structure. X-ray crystallography is one of the trustable methods which can provide information about the non-covalent interactions involved in constructing the self-assembly of any molecule. Due to lack of proper solvent system for these compounds, quality crystal did not obtain for the compounds **P3**-**P5**. However, compounds **P1** and **P2** were crystallized from methanol-water and **P6** was crystallized from acetonitrile-water solvent system. Compound **P1** crystallized in triclinic unit cell with **P1** space group whereas **P2** having one extra methyl group to **P1** crystallized in orthorhombic unit cell with $P2_12_12_1$ space group. Again, **P6** forms triclinic unit cell with P-1 space group.

Desiraju *et al*. showed that supramolecular synthons can form molecular self-assembly through various non-covalent interactions. Here, hydrogen bonding between amide groups of two adjacent molecules is the said supramolecular synthons (Figure 14a). Such hydrogen bonding and π…S interactions were responsible for the one-dimensional β-sheet chain like structure (**Figure 14b**). It is interesting to note that such interactions and one-dimensional β-sheet chain geometry are common in remaining both crystal structures (**Figure 14c** and **14d**). It is also evident from the CD spectra. In the case of **P2** and **P6**, in addition to the aforesaid interactions, C-H….O=C and π….π interactions also

played important roles in the molecular self-assembly of these peptides. Therefore, such interactions strengthen the self-assembly structure which was also evident from AFM studies.

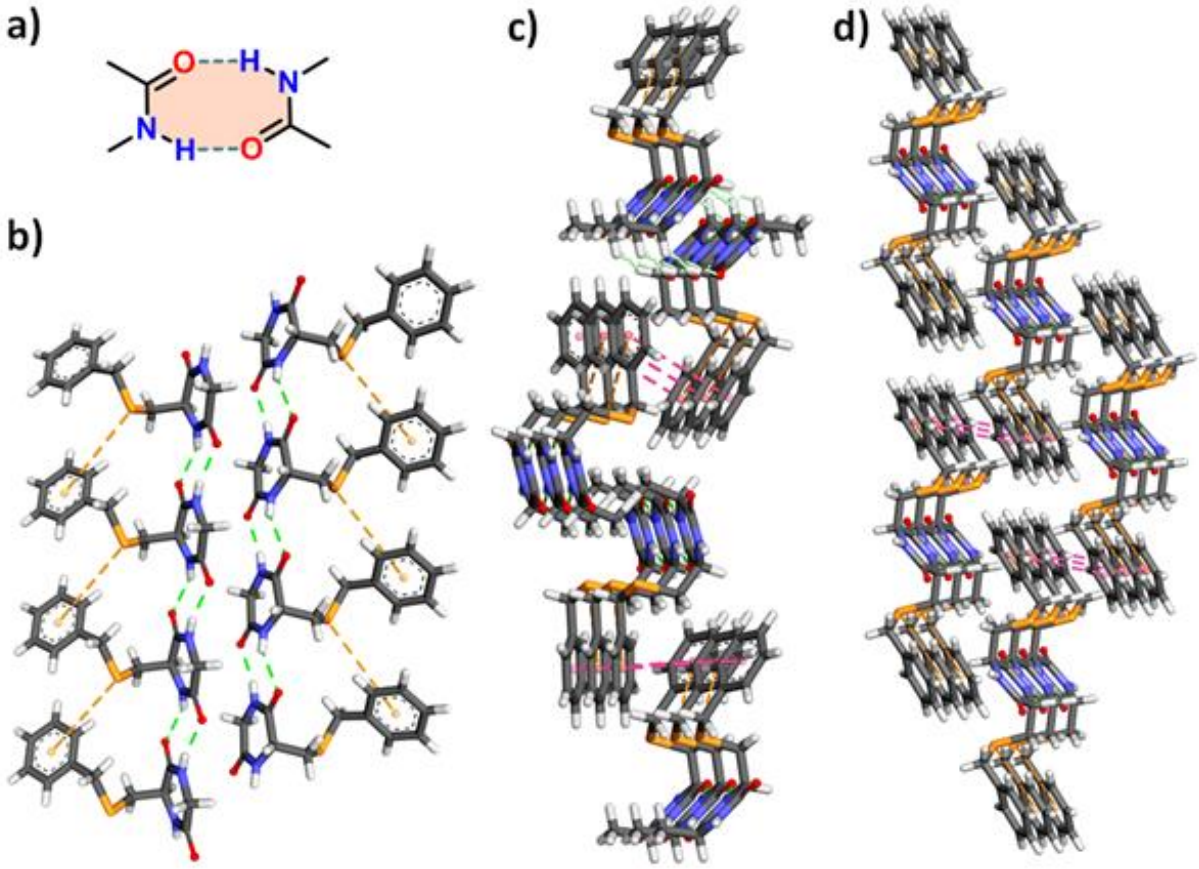

Figure 14. *a) Supramolecular synthon found in the crystal structure of P1. Network of noncovalent interactions in the β-sheet structure of b) P1, c) P2, and d) P6.*

3.3.11 Theoretical Studies

To understand the effect of side chains in the molecular self-assembly of **P1-P6**, theoretical studies can provide very important insight in this case. The non-covalent interactions involved in the crystal formation can be better understood using Hirshfeld surface analysis.

3.3.11.1 Hirshfeld Surface (HS) Aalysis

Hirshfeld surface is the surface of a molecule having electron density half or more at a point of it. There is a relationship between the distances from Hirshfield Surface to the closest nucleus internal (d_i) and external (d_e) to it, which depends on the normalized contact distance (d_{norm}). Hirshfield Surface ($d_{norm)}$ are colored as indicated by blue, white, and red regions, which indicate the maximum, closest, and the shortest distance between two neighboring atoms, relative to their van der Waals radii, respectively.

The bright red spots on the d_{norm} surface of **P1**, **P2**, and **P6** indicated that the above-mentioned hydrogen bonding (as shown by the crystallographic study) is common in all the cases and it is the driving interactions for their self-assembly. In the case of d_i surface, the bright red spots appeared at the same position as d_{norm} surface. It indicated that strong hydrogen bonding is one of the essential criteria for the self-assembly process. The triangular shaped red and blue patches are present adjacent to each other at the amino acid side chain region of all three molecules which indicated this aromatic region was capable of forming π…π staking interactions. The shape index HS of all three crystal structures showed sharp edges which indicated they were able to interact with adjacent molecules through various non-covalent interactions.

The interactions can be identified quantitatively using d_e versus d_i fingerprint plots. In all the three crystal structures of the molecules, C...H, H…H, O...H, and S…H interactions played a key role in the formation of self-assembly. Among these interactions, H…H contacts contributed the maximum in all the molecules and it is almost 60% of all the interactions. Therefore, hydrophobic interactions played a primary role in the construction of the crystal structures. In **P2**, this interaction is the highest in all the cases. The next highest interaction among all the interactions is O…H contacts. In the case of **P1**, O…H contacts are the highest. The C…H interactions are the third highest interactions in the

crystals. The S…H interactions are another important interaction and **P6** is having the maximum of such kinds of interactions. Therefore, with the help of the analogy of non-covalent interactions obtained from the crystal structure of **P1**, **P2**, and **P6** it can be said that such interactions may be analogous in the rest of the compounds **P3**, **P4**, and **P5** because all the investigating compounds showed mostly β-sheet self-aggregation patterns which are evident from the CD studies.

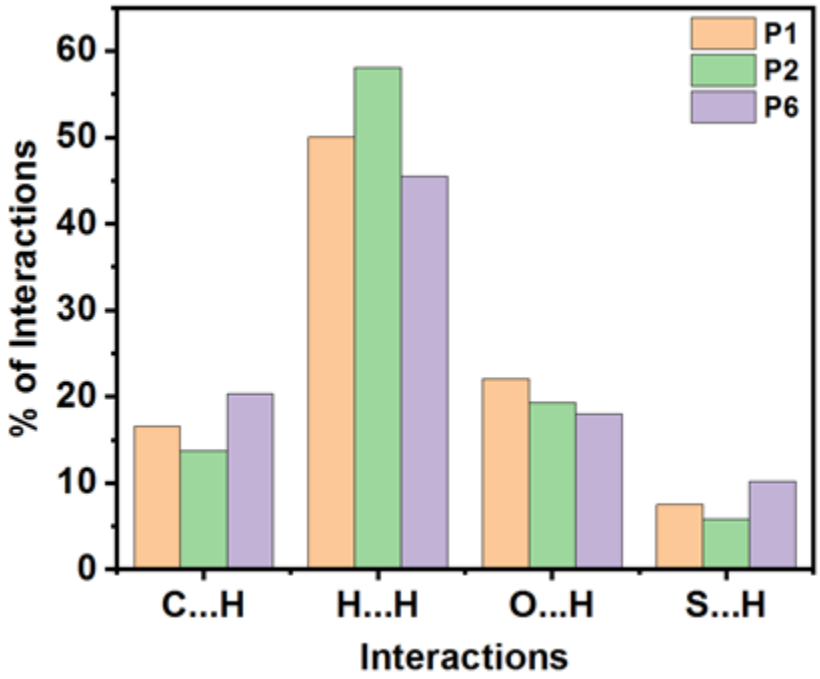

Figure 15*. Percentage of different non-covalent interactions found in P1, P2, and P6.*

3.3.11.2 Density Functional Theory

Density functional theory (DFT) is one of the most important tools to predict the molecular properties. Molecular electrostatic potential (MEP) is one of the DFT methods which can be used to find the electronic environment around the molecules. In this MEP surface, red, blue, and green regions indicate the electron-rich, electron-poor, and neutral regions, respectively (Figure 16). In the case of **P1**, it has two red regions which can act as hydrogen-bond acceptors.

The CH_2 region of the glycine part of **P1** is slightly acidic due to the presence of blue colour. This part becomes green in **P2** for the presence of methyl group. This region becomes larger and greener on moving from **P2** to **P6**. These results revealed that the said region has hydrophobic effects. It is clear from the experimental findings that moving from **P1** to **P6** the ability of formation and stability of self-assembly increases. Therefore, increasing hydrophobicity of the said part of the molecule is a key factor for stable self-assembly formation.

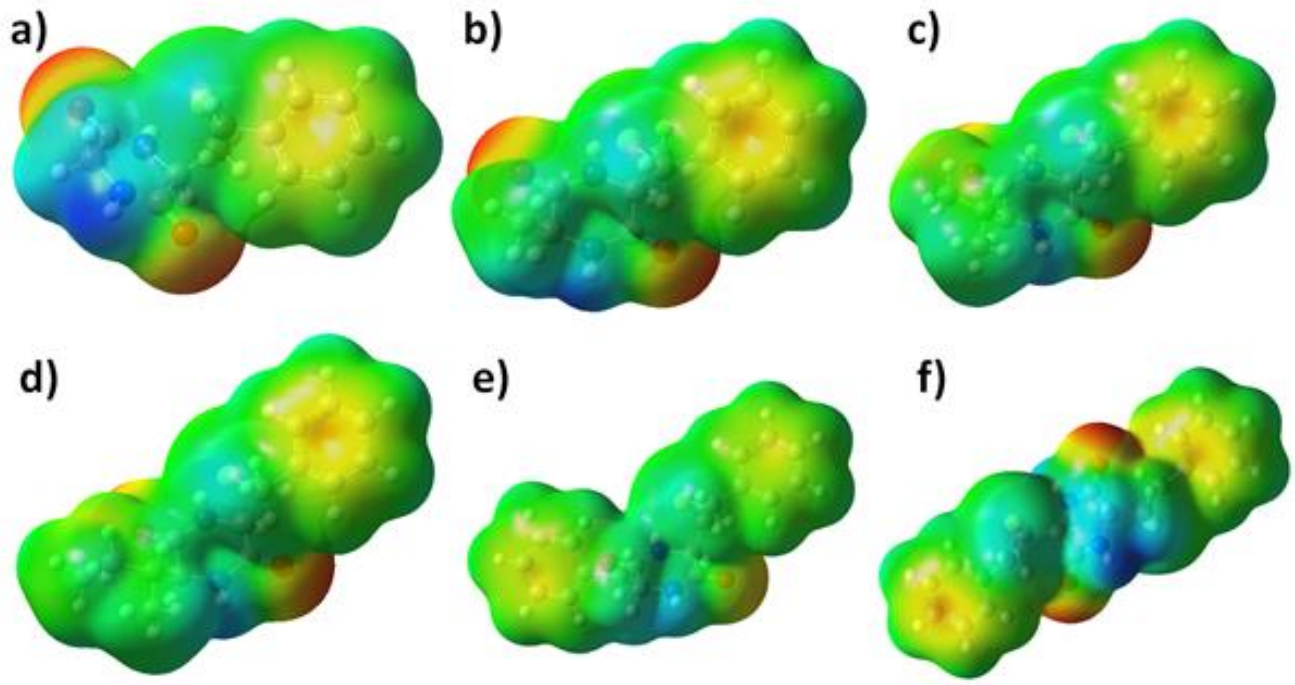

Figure 16. *Molecular electrostatic potential of P1, P2, and P6.*

3.3.12 Dye Adsorption Study

Dyes are frequently produced as a by-product in textile, printing, and other chemical manufacturing industries and they are a major contributor to the toxicity of contaminated water. Numerous organic dyes have a carcinogenic character, which poses a serious risk to both the environment and human life. Even low concentrations of their presence in water can be detrimental to humans and other living organisms because these toxic dyes are typically nondegradable in nature. As a result, the necessity for an effective method of dye removal from wastewater is growing in importance. Membrane separation, flocculation, ion exchange, electrochemical treatment, and so forth are examples of classic methods for managing wastewater. But these methods have limitations in terms of their expense, effectiveness, and complexity. Adsorption is considered as one of the best technologies out of all the different methods because of its effectiveness, recycling potential, and affordability. Self-assembled gelators are highly effective for adsorption because of their high porosity and larger surface area. Thus, peptide based low molecular weight porous gel materials has recently been employed in the field of adsorption and separation of toxic dyes from contaminated water. For example, in one of the earliest reports from 2007, Banerjee and co-workers described the adsorption of dyes like crystal violet, naphthol blue black, and pyrene by phenylalanine based metallated xerogels. Das and colleagues developed a series of dipeptide organogelators containing phenylalanine and tryptophan moieties which were used to adsorb crystal violet and rhodamine 6G dyes without any metal co-ordination. Banerjee and colleagues reported a library of tripeptide-based hydrogelators, and the capacity of their wet hydrogels to extract rhodamine B, reactive blue 4, and direct red 80 from water was investigated. Ju and co-workers reported adsorption of positively charged rhodamine 6G and acriflavine

and negatively charged fluorescein and cresol red by organogels based on triterpenoid–tripeptide conjugates.

Preliminarily, dye adsorption experiment was performed with all four hydrogels (**P3**, **P4**, **P5**, and **P6**) formed in methanol-water solvent mixture and it was found that the hydrogel obtained from **P5** is the most efficient one amongst them in removing the dyes from contaminated water and further experiments were performed only with **P5** hydrogel. For the experiment, first **P5** hydrogels (5 mg/ml) were prepared in methanol-water as described previously in glass vials. Then the gels were scooped out and added to the glass vials containing 1 ml of different dye solutions. Three different dyes rhodamine B, bromocresol green, and eriochrome Black T were used for the study. Instead of adding dye solution onto the hydrogel for adsorption, hydrogels were scooped out and added into the dye solution to increase the available surface area of the porous material for dye adsorption. A better adsorption of dyes was observed in the later process using the same amount of hydrogelator. The dye solutions along with the hydrogel were then left undisturbed at room temperature to adsorb the dye and in different time intervals the amount of dye adsorbed was determined by UV/Vis spectroscopy.

UV−vis absorption spectra were recorded using a JASCO V-630 spectrophotometer(JASCO International Co. Ltd, Japan). A high-quality quartz cuvette was used for measuring the absorbance. The initial dye concentrations used for the adsorption study were estimated by measuring their absorbance (rhodamine B: λmax 553 nm, bromocresol green: λmax 558 nm, eriochrome black T: λmax 531 nm) using a JASCO V-630 spectrophotometer and calculating the concentration from their respective standard curves.

The concentration of the dyes used for this investigation was, 0.01 mM rhodamine B, 0.02 mM of bromocresol green, and 0.04 mMof eriochrome black

T. Within 2 h a great reduction in the absorbance intensity of the initial dye solutions was observed in UV/Vis spectra (Figure 18) of the respective dyes. It was found that 60.64 % of rhodamine B, 54.35 % of bromocresol green, and 37 % of eriochrome black T dye was adsorbed by P5 within only 2 h of time span. Dye adsorption study was further investigated and it was observed that after 6 h the colour of the dye solutions was almost get adsorbed by the hydrogel leaving behind clear water (**Figure 17**). From UV-Vis spectroscopy study it was calculated that almost 95.08 % of initial rhodamine B, 97.47 % of initial bromocresol green, and 90.77 % of initial eriochrome black T was get adsorbed by the hydrogel after 6 h (**Figure 18**).

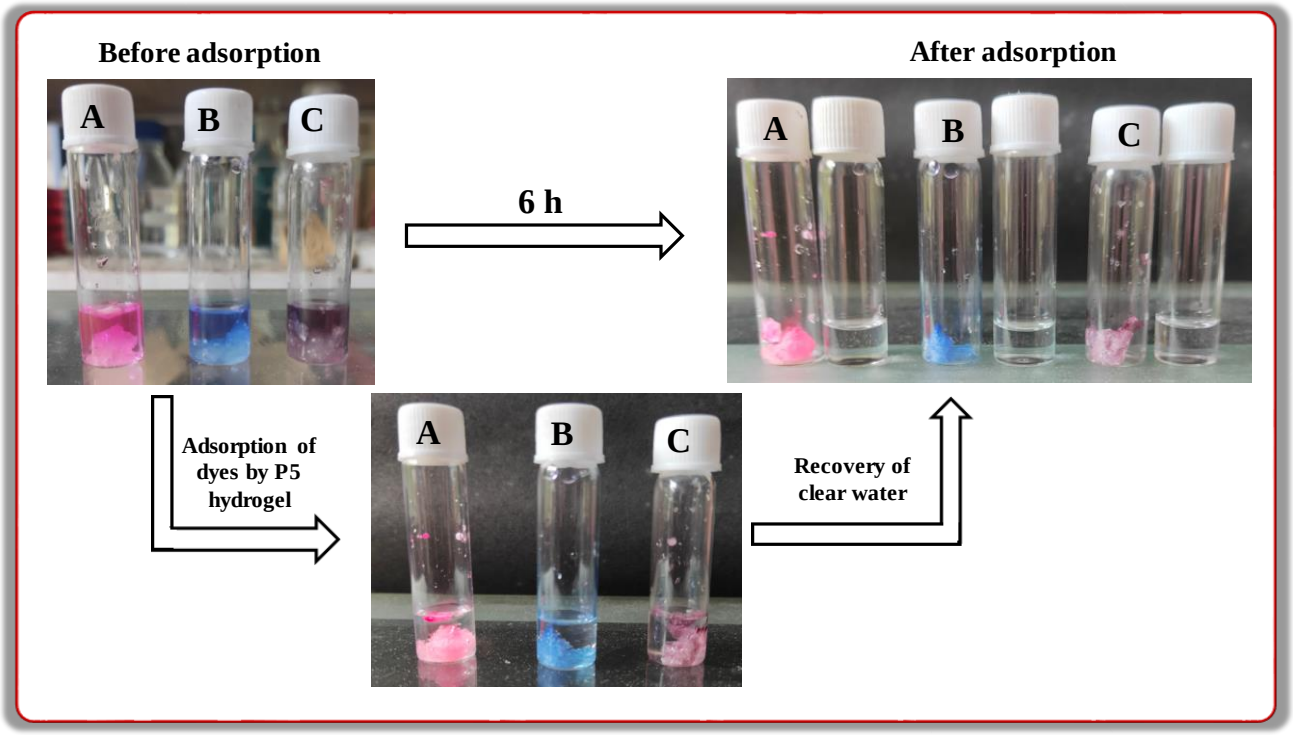

Figure 17. *Photographic images of solutions containing dyes (A) Rhodamine B, (B) Bromocresol green, (C) Eriochrome black T before adsorption and after adsorption by P5 hydrogel.*

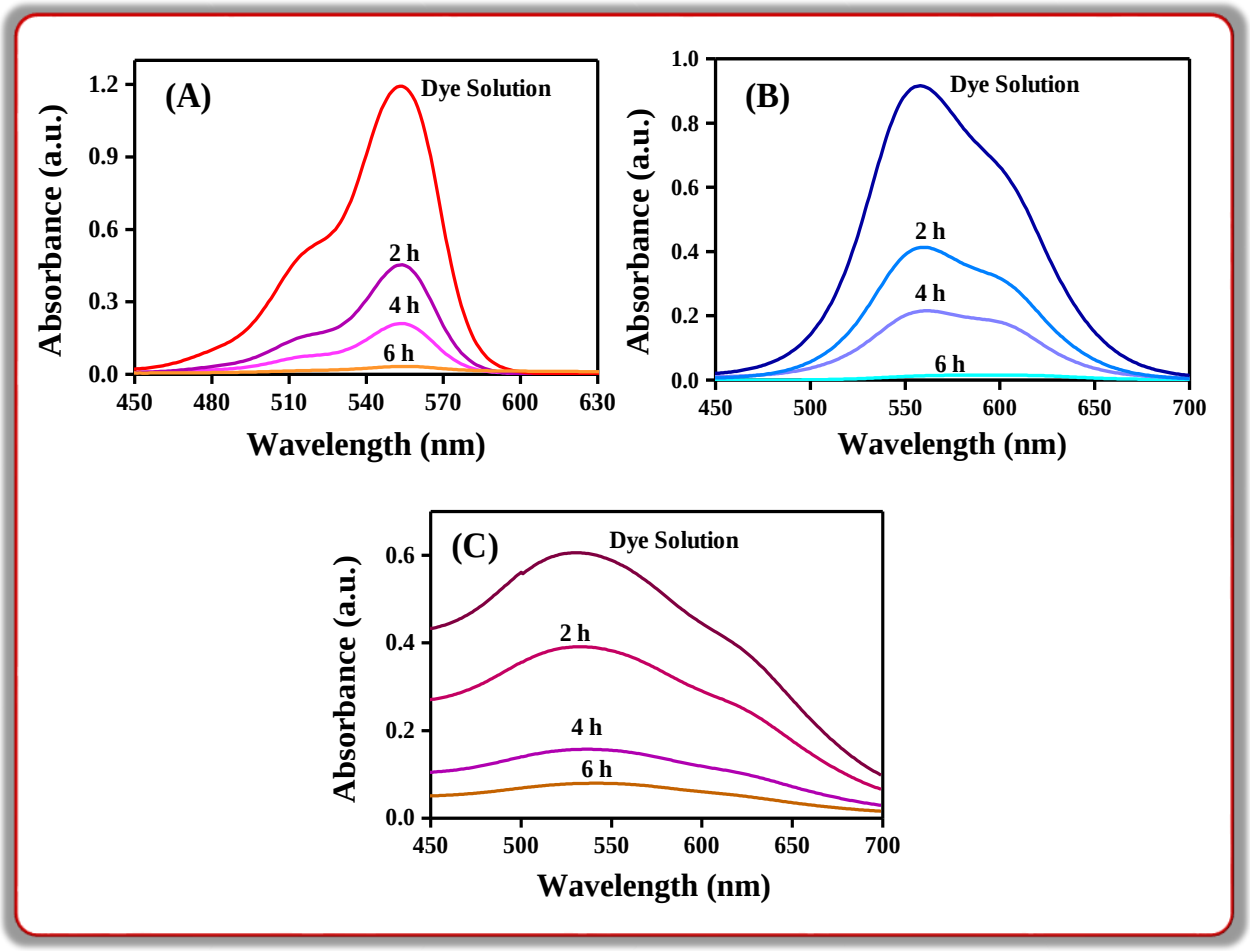

Figure 18. *UV data for time dependant adsorption of (A) Rhodamine B, (B) Bromocresol green, and (C) Eriochrome black T dyes from their aqueous solutions by P5 hydrogel.*

3.3.13 Cytotoxicity Study

To address whether the CDPs (**P1-P6**) have any toxic effect or not cellular toxicity from the CDPs was determined by performing MTT assay. Cervical cancer cells HeLa (1× 10^4 cells/well) were seeded in 96-well plates. Te synthesized compounds were added to the wells to various final concentrations (0, 10, 25, 50, and 100 μM). Cells were incubated in presence of these molecules for 24 h at 37 °C. Following treatment, 3-(4,5-dimethylthiazol-2-yl)-2,5-diphenyl tetrazolium bromide(MTT) solution (100 μg/well, dissolved in medium) was added to each well of the 96-well plate, and further incubated at

37 °C for 3 h for formazan crystal formation. The supernatant was removed. Dimethyl sulfoxide (200 µL/well) was added to dissolve the formazan crystals produced by the viable cells and the absorbance of the purple color was recorded on a microplate reader (Thermo Scientific, USA) at a wavelength of 550 nm. The intensity of color indicates the number of viable cells. Experiments were performed in triplicate and the relative cell viability (%) was expressed as a percentage relative to the untreated control cell.

Treatment of HeLa cells with each CDP revealed that almost 70-90% of the cells survived even up to 50 µM concentrations as determined by the MTT assay (**Figure 19**). These results showed that the synthesized CDPs do not induce any acute cytotoxic effects in HeLa cells. **P1**, **P3**, and **P5** attained half-maximal inhibitory concentration (IC_{50}) at almost 80-85 µM of concentrations whereas **P2**, **P4,** and **P6** could not attain their IC_{50} value even after 100 µM of concentration. Therefore, it was determined that the cyclic dipeptides (**P1-P6**) had a negligible part in the mortality of HeLa cells.

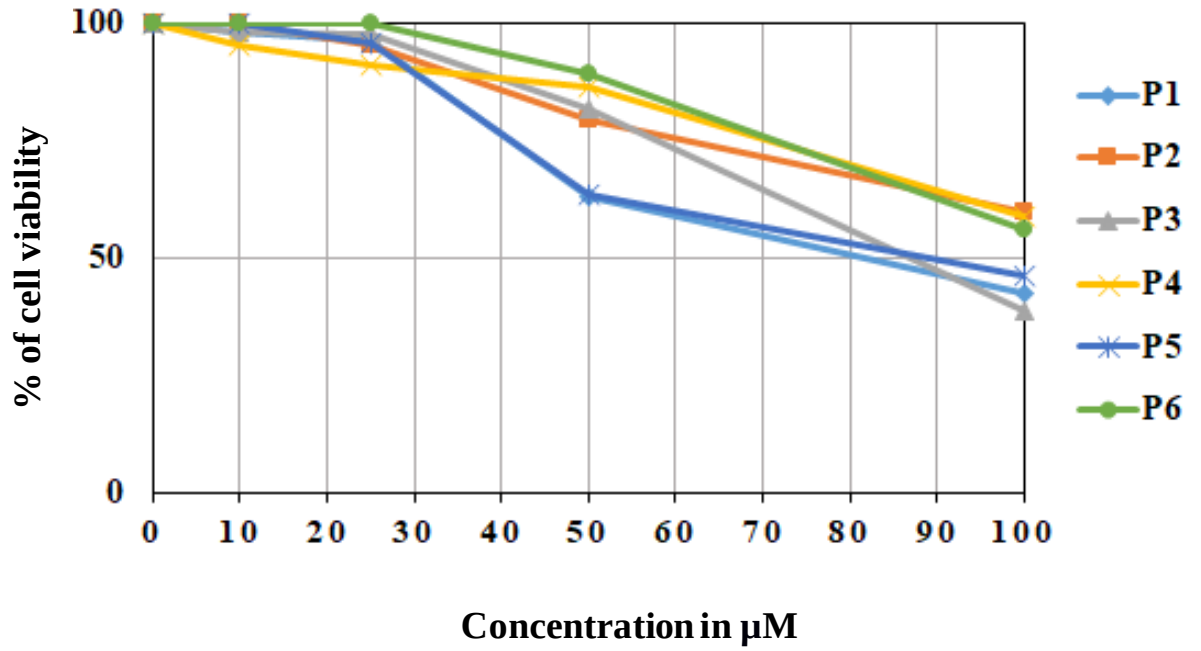

Figure 19. *Growth inhibitory effect of the synthesized CDPs (P1-P6) on HeLa cells, at concentrations ranging between (0-100) µM.*

3.4 CONCLUSION

In summary, this work demonstrated the design and synthesis of a series of *S*-benzyl-L-cysteine based six cyclic dipeptides (**P1-P6**) containing various lengths of hydrophobic side chain partners. Side chain variation of the constituting amino acids in the CDPs caused significant differences in their morphology as well as in gelation properties. Due to the increased hydrophobicity offered by the amino acid side chains from **P1** to **P6**, the complexity of the fibrillar network formed by the self-assembly of the CDPs also increased following almost a linear relationship which is evident by the AFM experiments. The effect of side chain variation of the CDPs was also reflected in their macrostructure; **P1** produced crystals, **P2** produced crystals with loose gel type structures, and **P4-P6** formed hydrogels in methanol-water solvent system. Morphological analysis of these CDPs by atomic force microscopy although revealed nano-fibrillar self-assembly for almost all the CDPs under same solvent condition but there were distinct morphological variations in their respective nano structures. Different spectroscopic techniques like NMR, FT-IR, CD, Thioflavin-T, Congo Red study revealed that CDP molecules were interlinked by intermolecular hydrogen bonding giving rise to β-sheet secondary structure which is responsible for the formation of nanostructures. Single crystal X-ray crystallographic study of the crystal obtained from **P1**, **P2**, and **P6** showed that along with intermolecular hydrogen bonding C-H….O=C and π….π, and π…S interactions were also very important for the formation of one dimensional β-sheet selfassembled structure. In addition to that, theoretical studies like Hirshfield surface analysis and DFT analysis revealed that the hydrophobicity of the amino acid side chain region is the key reason for the self-assembly formation. This whole study helped to construct a structure-morphology as well as structure-gelation relationship between the CDPs. Finally, the hydrogels obtained from CDPs were tested for dye adsorption from contaminated water and it was found that **P5** hydrogel

efficiently adsorbed toxic dyes like rhodamine B, eriochrome black T, and bromocresol green leaving behind clear water. This kind of hydrogel may further be modified to use in wastewater management on large scale.

3.5 FUTURE SCOPE

Cyclic dipeptides are the smallest class of cyclic peptides which can efficiently form hydrogels if designed properly as they possess structural rigidity. The effect of various side chain functionalities play important role in inducing hydrogelation in these molecules. Thus, it is important to understand the the effect of different side chain variations in order to understand the self-assembly mechanism. In this work, a series of CDPs with varying hydrophobic side chains were synthesized and their self-assembly pattern was elaborately discussed which may contribute to a better understanding of such trends in other molecules having similar side chain variations. Moreover, keeping these results in mind, synthesis of more new CDPs having different polar, nonpolar, and charged amino acid partners are also included in future plan to set a structure-gelation relationship. Modification of these hydrogels as well as the organogels are going on to increase their ability to adsorb toxic dyes and other toxic elements from water.

3.6 EXPERIMENTAL PROCEDURES AND SPECTRAL DATA

3.6.1 Synthesis of Cyclic Dipeptide P1

The same general procedure **A** was followed starting with 500 mg (2.85 mmol, 1.0 equiv.) of N-BOC-glycine. Final column chromatography (SiO_2, eluting with 5% methanol/dichloromethane) afforded the desired product as white solid (yield = 63%).

^{1}H NMR of P1 (600 MHz, DMSO-d_6): δ (in ppm) 8.20 (d, *J* = 6.0 Hz, 2H, -NH), 7.31 (d, *J* = 4.0 Hz, 4H, Ar-H), 7.24 (m, 1H, Ar-H), 4.09 (s, 1H), 3.89 (d,

J = 18.0 Hz, 1H), 3.80 – 3.70 (m, 3H, $C_{\alpha}H$ and –CH_2Ph), 2.94 (dd, *J* = 15.0, Hz, 1H, -CH_2S), 2.73 (dd, *J* = 15.0 Hz, 1H, -CH_2S).

13C NMR of P1 (151 MHz, DMSO-d6): δ (in ppm) 166.58, 165.73, 138.34, 128.94, 128.43, 126.94, 54.53, 44.44, 36.09, 35.41.

HRMS (**EI-MS):** m/z calculated for $C_{12}H_{14}N_2O_2S$ = 250.0776; found m/z = 250.0773.

3.6.2 Synthesis of Cyclic Dipeptide P2

The same general procedure **A** was followed starting with 500 mg (2.64 mmol, 1.0 equiv.) of N-BOC-L-alanine. Final column chromatography (SiO_2, eluting with 5% methanol/dichloromethane) afforded the desired product as white solid (yield = 62%).

^{1}H NMR of P2 (600 MHz, DMSO-d_6): δ (in ppm) 8.31 (s, 1H), 8.06 (s, 1H), 7.31 (d, *J* = 6.0 Hz, 4H), 7.24 (h, *J* = 4.0 Hz, 1H), 4.18 (m, 1H), 3.95 – 3.87 (m, 1H), 3.78 – 3.71 (m, 2H), 2.91 (dd, *J* = 15.0 Hz, 1H), 2.72 (dd, *J* = 15.0 Hz, 1H), 1.37 (d, *J* = 6.0 Hz, 3H).

^{13}C NMR of P2 (150 MHz, DMSO-d_6): δ (in ppm) 168.18, 165.79, 138.47, 128.92, 128.40, 126.91, 54.65, 50.00, 36.20, 34.57, 20.39.

HRMS (ESI-MS): m/z calculated for $C_{13}H_{16}N_2O_2S$ $[M+H]^+$ = 265.1011; found m/z = 265.1006.

3.6.3 Synthesis of Cyclic Dipeptide P3

The same general procedure **A** was followed starting with 600 mg (2.76 mmol, 1.0 equiv.) of N-BOC-L-valline. Final column chromatography (SiO_2, eluting with 5% methanol/dichloromethane) afforded the desired product as white solid (yield = 64%).

^{1}H NMR of P3 (600 MHz, DMSO-d_6): δ (in ppm) 8.14 (s, 1H), 8.09 (s, 1H), 7.33 – 7.29 (m, 4H), 7.23 (m, 1H), 4.17 (s, 1H), 3.80 – 3.69 (m, 3H), 2.86 (dd, *J*

= 12.0 Hz, 1H), 2.77 (dd, *J* = 15.0 Hz, 1H), 2.21 (m, 1H), 0.98 (d, *J* = 6.0 Hz, 3H), 0.88 (d, *J* = 6.0 Hz, 3H).

^{13}C NMR of P3 (151 MHz, DMSO-*d*$_6$): δ (in ppm) 166.85, 166.53, 138.58, 128.88, 128.37, 126.85, 59.40, 54.18, 36.08, 34.53, 31.20, 18.62, 17.31.

HRMS (EI-MS): m/z calculated for $C_{15}H_{20}N_2O_2S$ = 292.1245; found m/z = 292.1240.

3.6.4 Synthesis of Cyclic Dipeptide P4

The same general procedure **A** was followed starting with 650 mg (2.82 mmol, 1.0 equiv.) of N-BOC-L-isoleucine. Final column chromatography (SiO_2, eluting with 5% methanol/dichloromethane) afforded the desired product as white solid (yield = 68%).

^{1}H NMR of P4 (600 MHz, DMSO-*d*$_6$): δ (in ppm) 8.11 (s, 1H), 8.07 (s, 1H), 7.32 – 7.27 (m, 4H), 7.23 (m, 1H), 4.17 (m, 1H), 3.80 – 3.71 (m, 3H), 2.87 (dd, *J* = 15.0 Hz, 1H), 2.77 (dd, *J* = 15.0 Hz, 1H), 1.93 – 1.87 (m, 1H), 1.48 (m, 1H), 1.26 – 1.17 (m, 1H), 0.95 (d, *J* = 6.0 Hz, 3H), 0.83 (t, *J* = 6.0 Hz, 3H).

^{13}C NMR of P4 (151 MHz, DMSO-*d*$_6$): δ (in ppm) 166.93, 166.44, 138.57, 128.87, 128.36, 126.84, 58.81, 54.21, 38.02, 36.19, 34.46, 24.38, 15.09, 11.95.

HRMS (ESI-MS): m/z calculated for $C_{16}H_{22}N_2O_2S$ $[M+H]^+$ = 307.1480; found m/z = 307.1475

3.6.5 Synthesis of Cyclic Dipeptide P5

The same general procedure **A** was followed starting with 800 mg (3.01 mmol, 1.0 equiv.) of N-BOC-L-phenylalanine. Final column chromatography (SiO_2, eluting with 5% methanol/dichloromethane) afforded the desired product as white solid (yield = 62%).

^{1}H NMR of P5 (600 MHz, DMSO-*d*$_6$): δ (in ppm) 8.23 (s, 1H), 8.04 (s, 1H), 7.30 (t, *J* = 7.4 Hz, 2H), 7.27 – 7.22 (m, 5H), 7.20 (m, 1H), 7.15 (d, *J* = 7.0 Hz,

2H), 4.19 (s, 1H), 3.87 – 3.80 (m, 1H), 3.55 (s, 2H), 3.14 (dd, *J* = 12.0 Hz, 1H), 2.93 (dd, *J* = 12.0 Hz, 1H), 2.31 (dd, *J* = 12.0 Hz, 1H), 1.50 (q, *J* = 6 Hz, 1H).

^{13}C NMR of P5 (150 MHz, DMSO-d_6): δ (in ppm) 166.69, 166.32, 138.79, 136.70, 130.68, 129.36, 128.79, 128.62, 127.28, 127.13, 55.86, 54.07, 35.70.

HRMS (**EI-MS):** m/z calculated for $C_{19}H_{20}N_2O_2S$ = 340.1245; found m/z = 340.1242.

3.6.6 Synthesis of Cyclic Dipeptide P6

The same general procedure **A** was followed starting with 750 mg (2.24 mmol, 1.0 equiv.) of N-BOC-S-benzyl-L-cysteine. Final column chromatography (SiO_2, eluting with 5% methanol/dichloromethane) afforded the desired product as white solid (yield = 62%).

^{1}H NMR of P6 (600 MHz, DMSO-d_6): δ (in ppm) 8.23 (s, 1H), 8.04 (s, 1H), 7.30 (t, *J* = 7.4 Hz, 2H), 7.27 – 7.22 (m, 5H), 7.20 (q, *J* = 7.3, 6.0 Hz, 1H), 7.15 (d, *J* = 7.0 Hz, 2H), 4.19 (s, 1H), 3.87 – 3.80 (m, 1H), 3.55 (s, 2H), 3.14 (dd, *J* = 13.6, 4.6 Hz, 1H), 2.93 (dd, *J* = 13.6, 5.0 Hz, 1H), 2.31 (dd, *J* = 13.7, 4.0 Hz, 1H), 1.50 (dd, *J* = 13.7, 7.4 Hz, 1H).

^{13}C NMR of P6 (151 MHz, DMSO-d_6): δ (in ppm) 166.69, 138.79, 136.70, 130.68, 129.36, 128.79, 128.62, 127.28, 127.13, 55.86, 54.07, 35.70.

HRMS (ESI-MS): m/z calculated for $C_{20}H_{22}N_2O_2S_2$ $[M+H]^+$ = 387.1201; found m/z = 387.1207.

^{1}H and ^{13}C NMR Spectra of Synthesized CDPs:

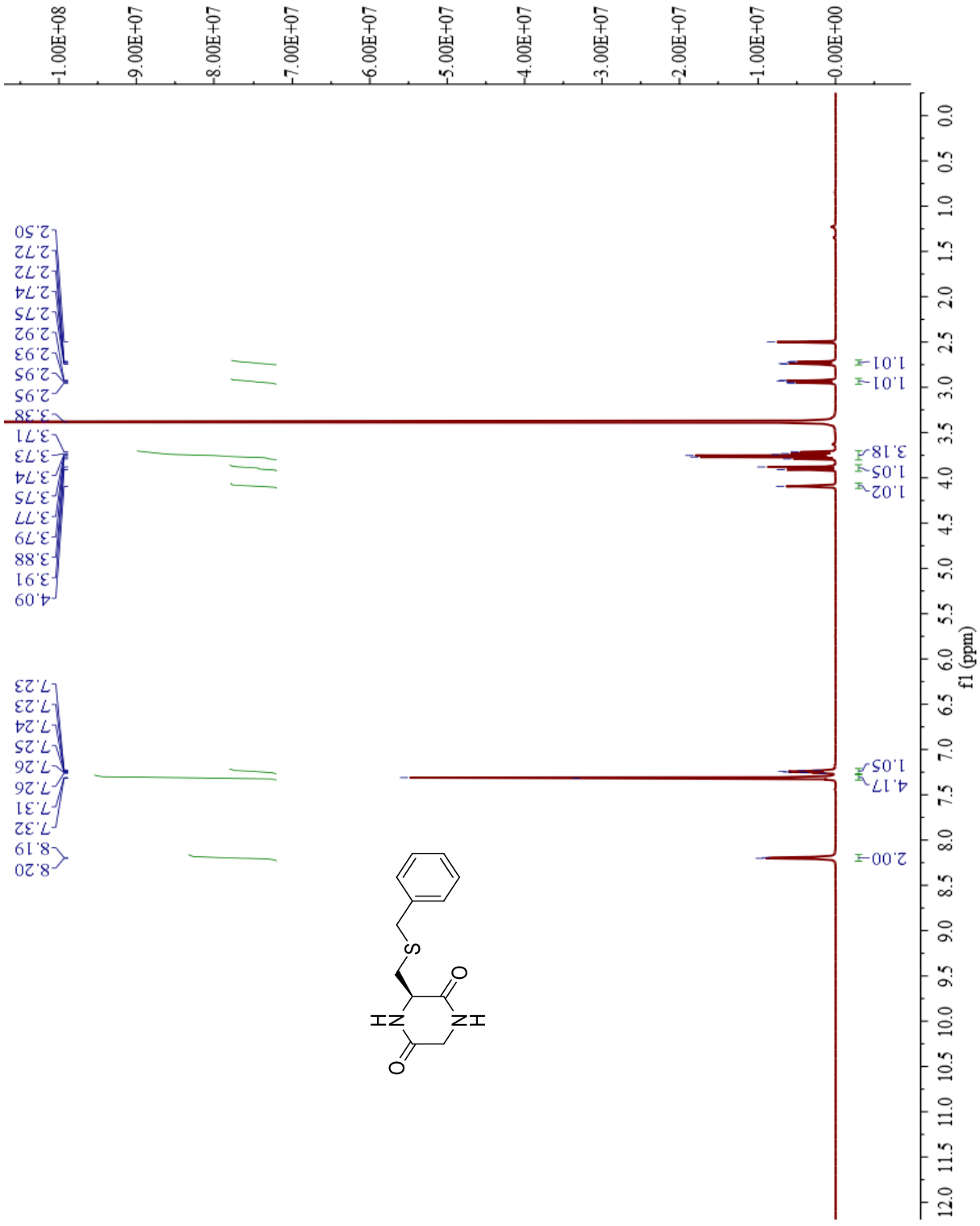

Figure S1. *^{1}H-NMR spectra of P1 dissolved in DMSO-d_6 solvent.*

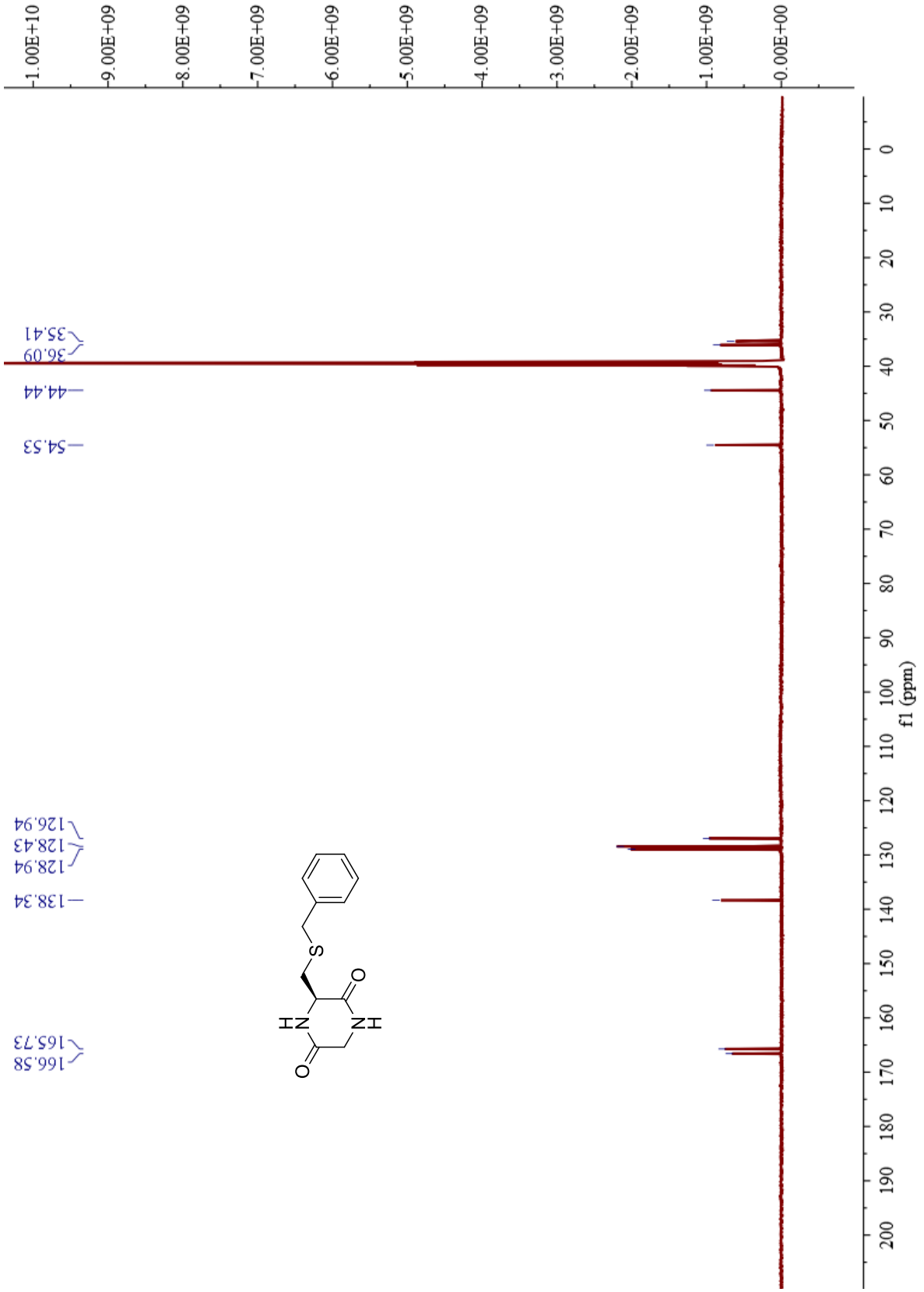

Figure S2. *^{13}C-NMR spectra of P1 dissolved in DMSO-d_6 solvent.*

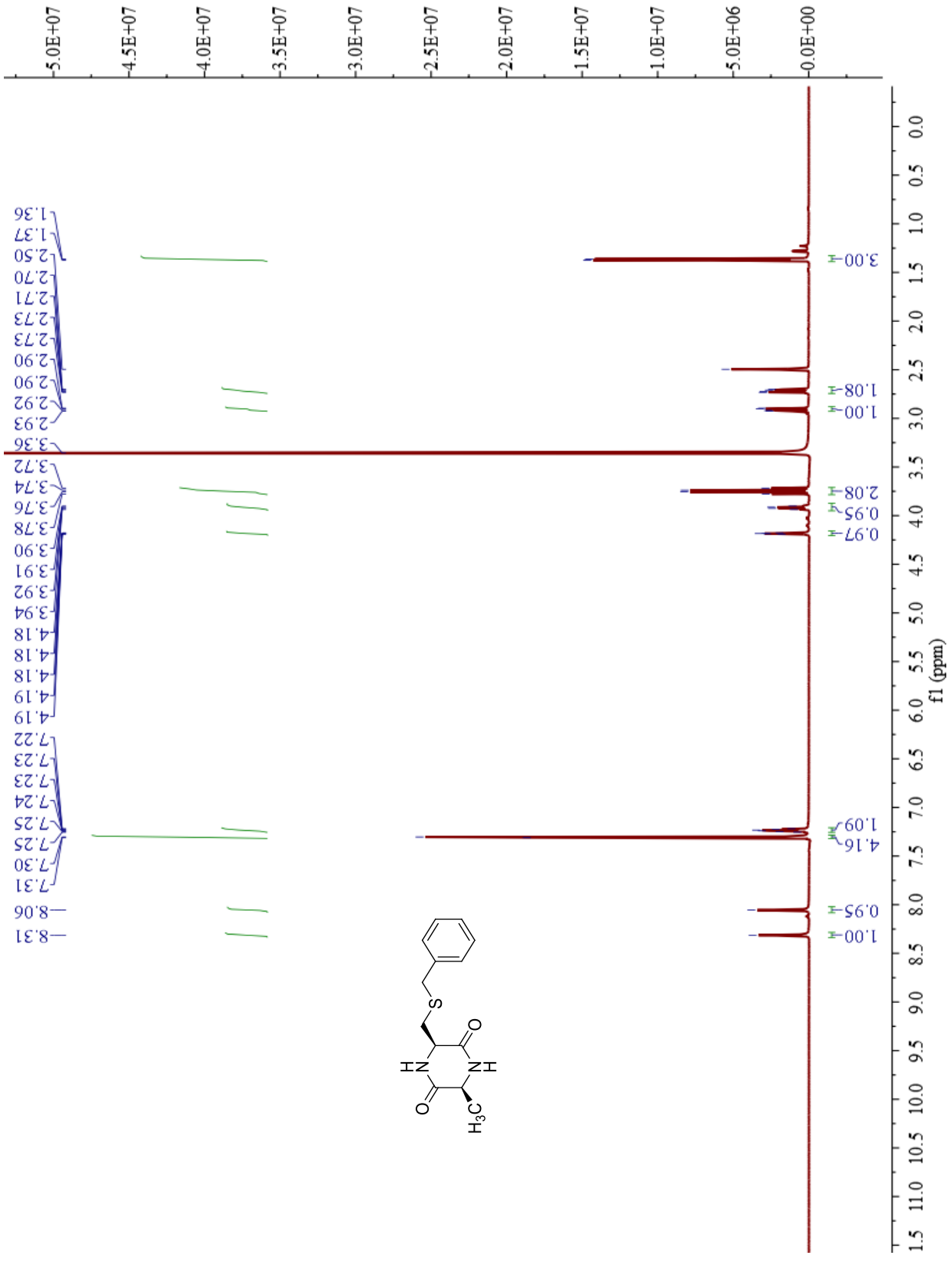

Figure S3. *^{1}H-NMR spectra of P2 dissolved in DMSO-d_6 solvent.*

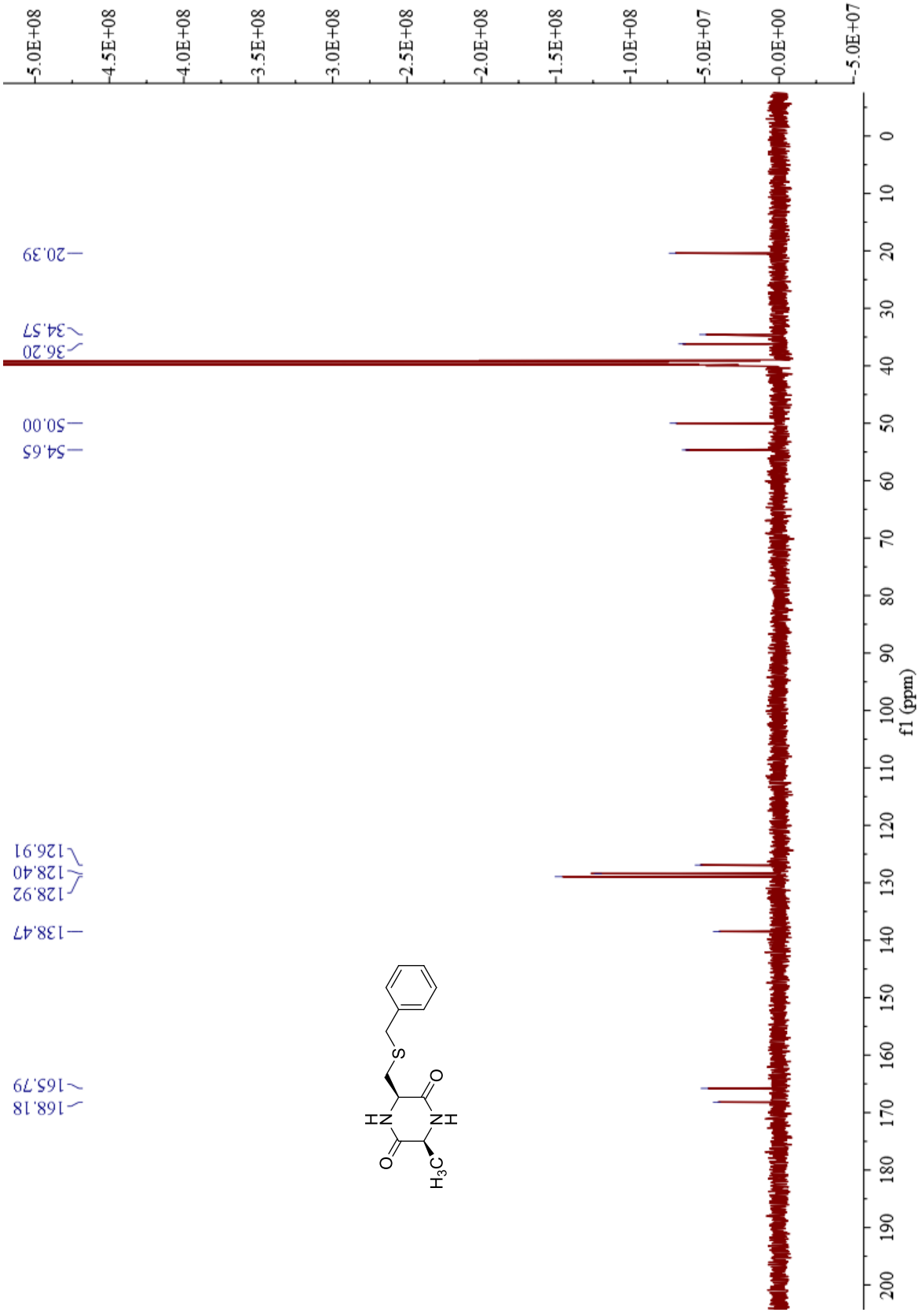

Figure S4. *^{13}C-NMR spectra of P2 dissolved in DMSO-d_6 solvent.*

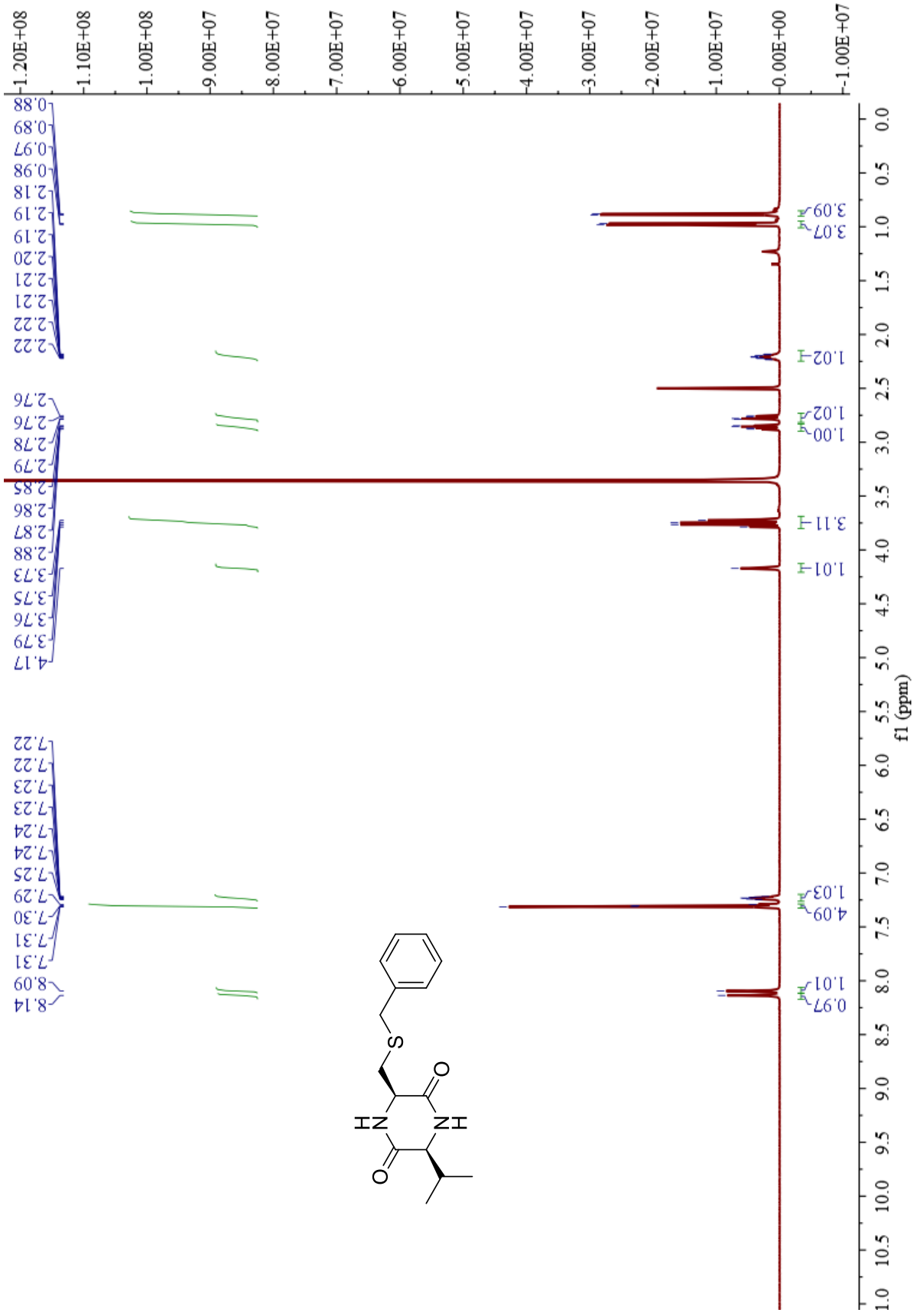

Figure S5. *^{1}H-NMR spectra of P3 dissolved in DMSO-d_6 solvent.*

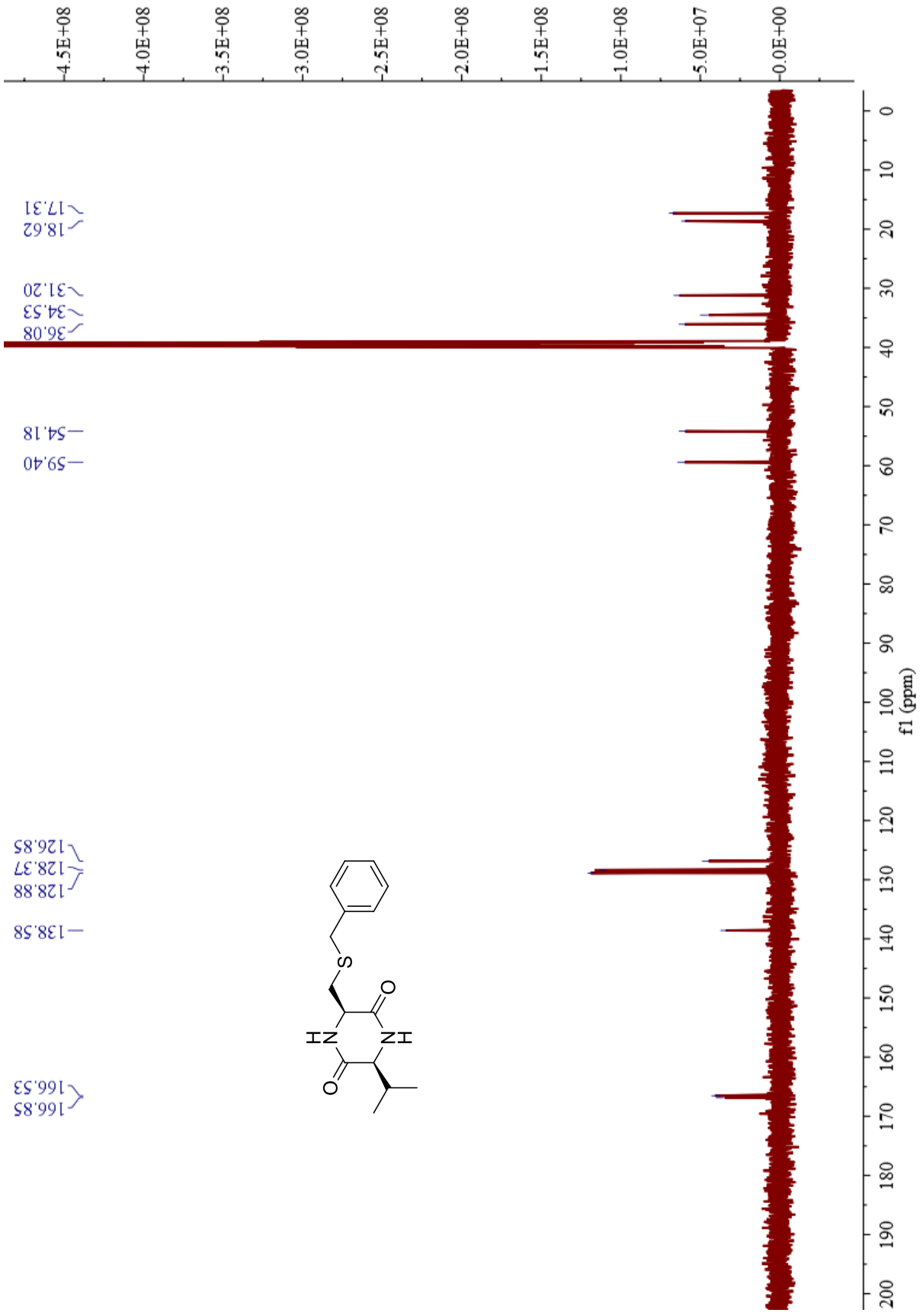

Figure S6. *^{13}C-NMR spectra of P3 dissolved in DMSO-d_6 solvent.*

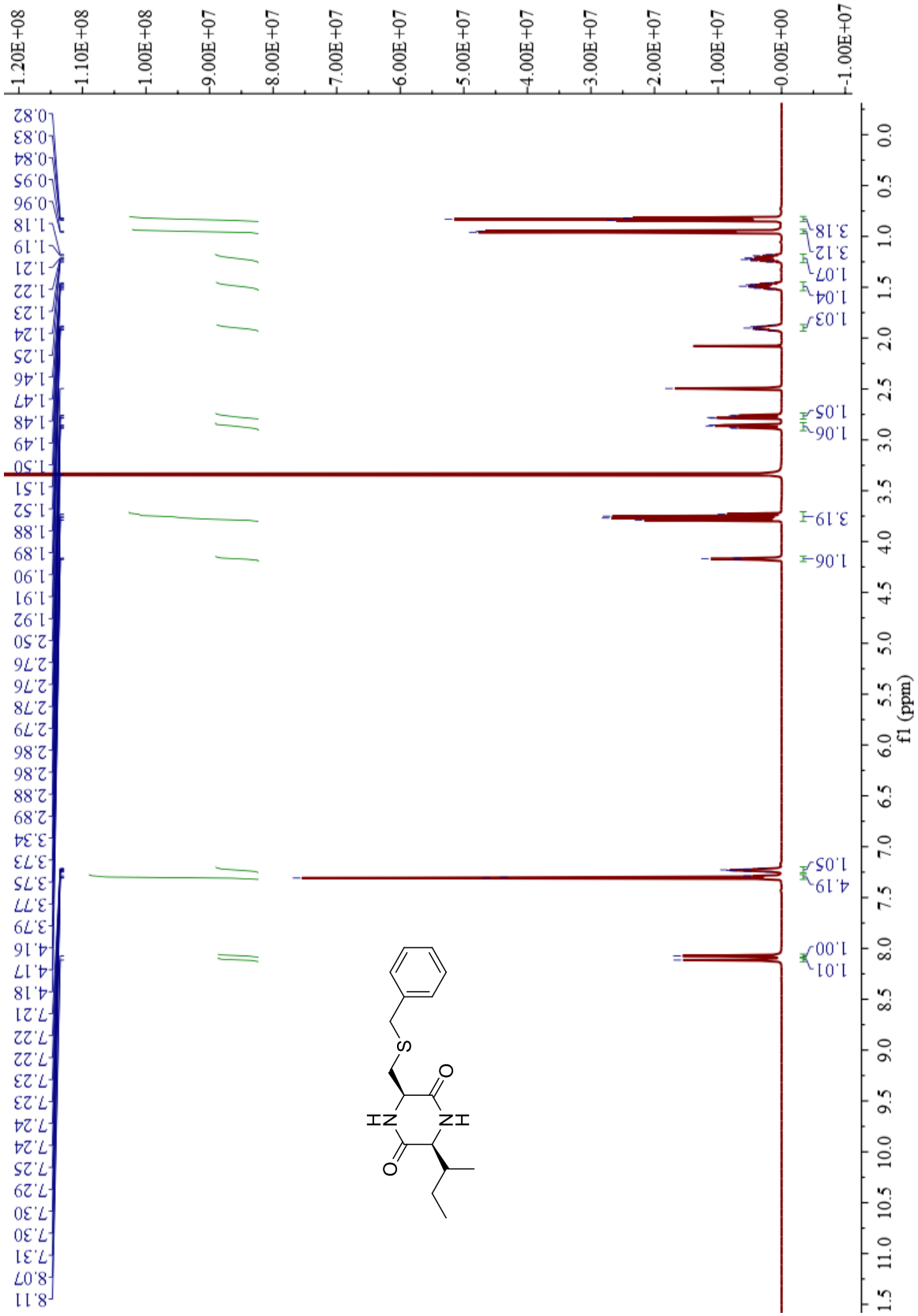

Figure S7. *^{1}H-NMR spectra of P4 dissolved in DMSO-d_6 solvent.*

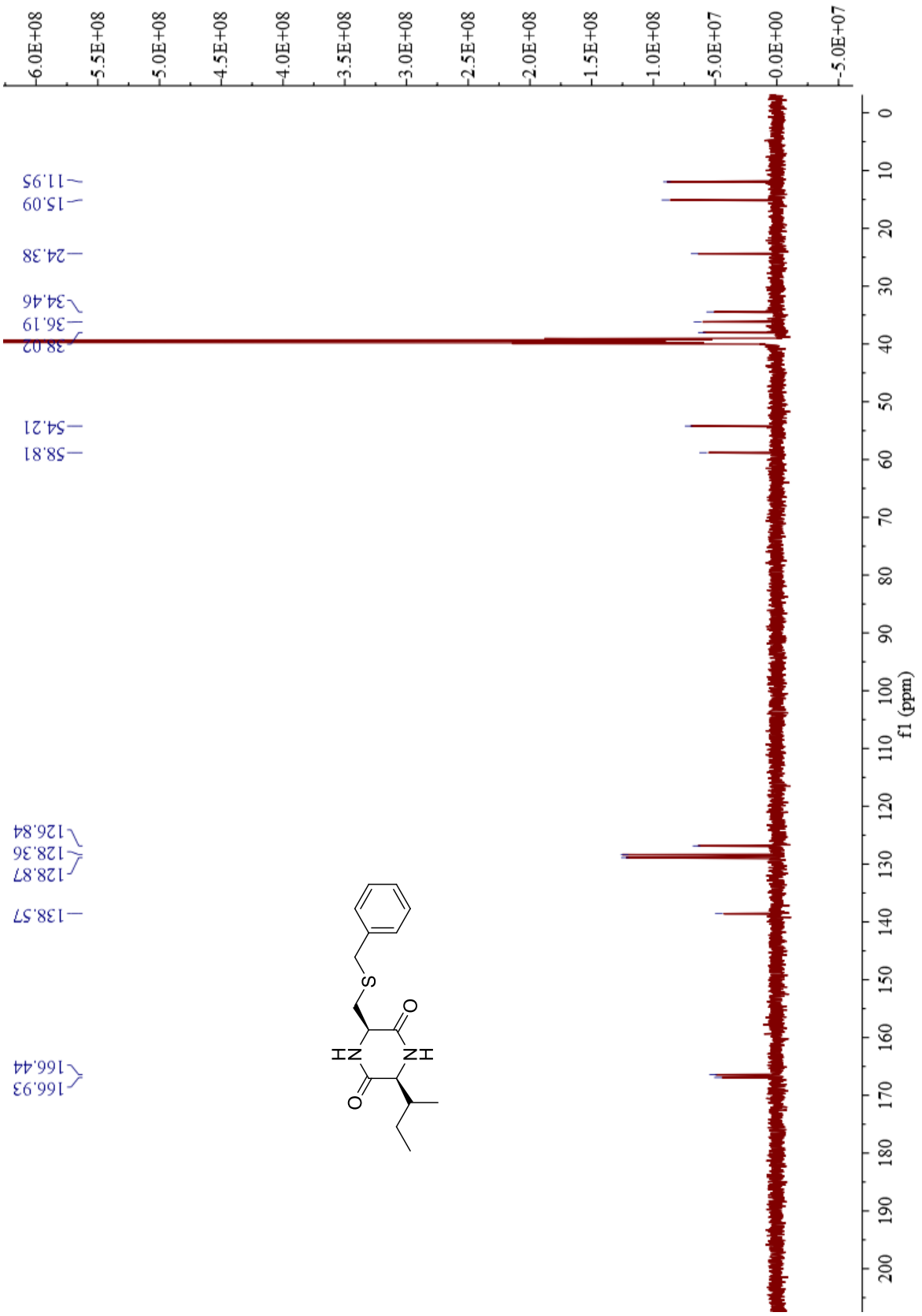

Figure S8. *^{13}C-NMR spectra of P4 dissolved in DMSO-d_6 solvent.*

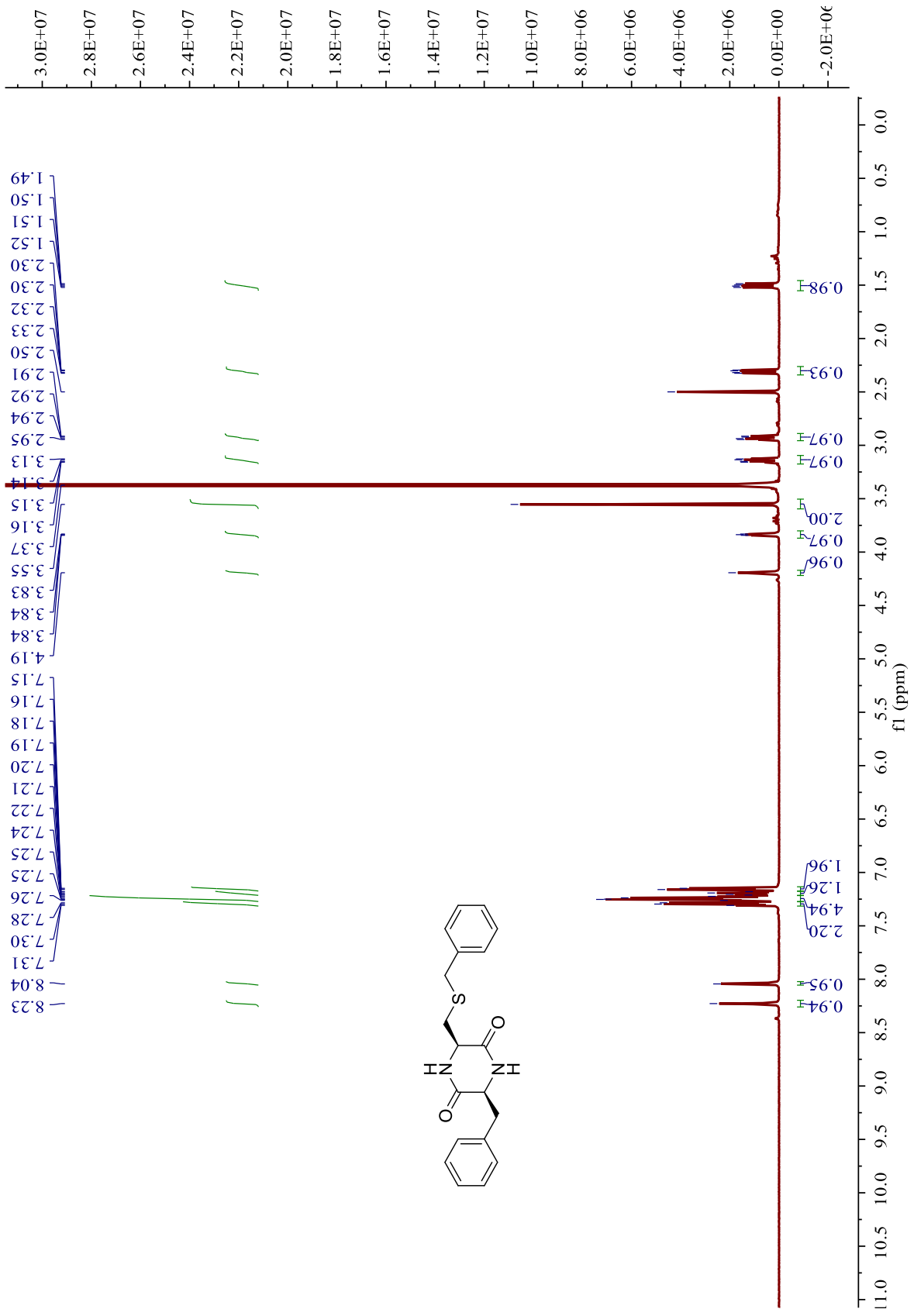

Figure S9. *^{1}H-NMR spectra of P5 dissolved in DMSO-d_6 solvent.*

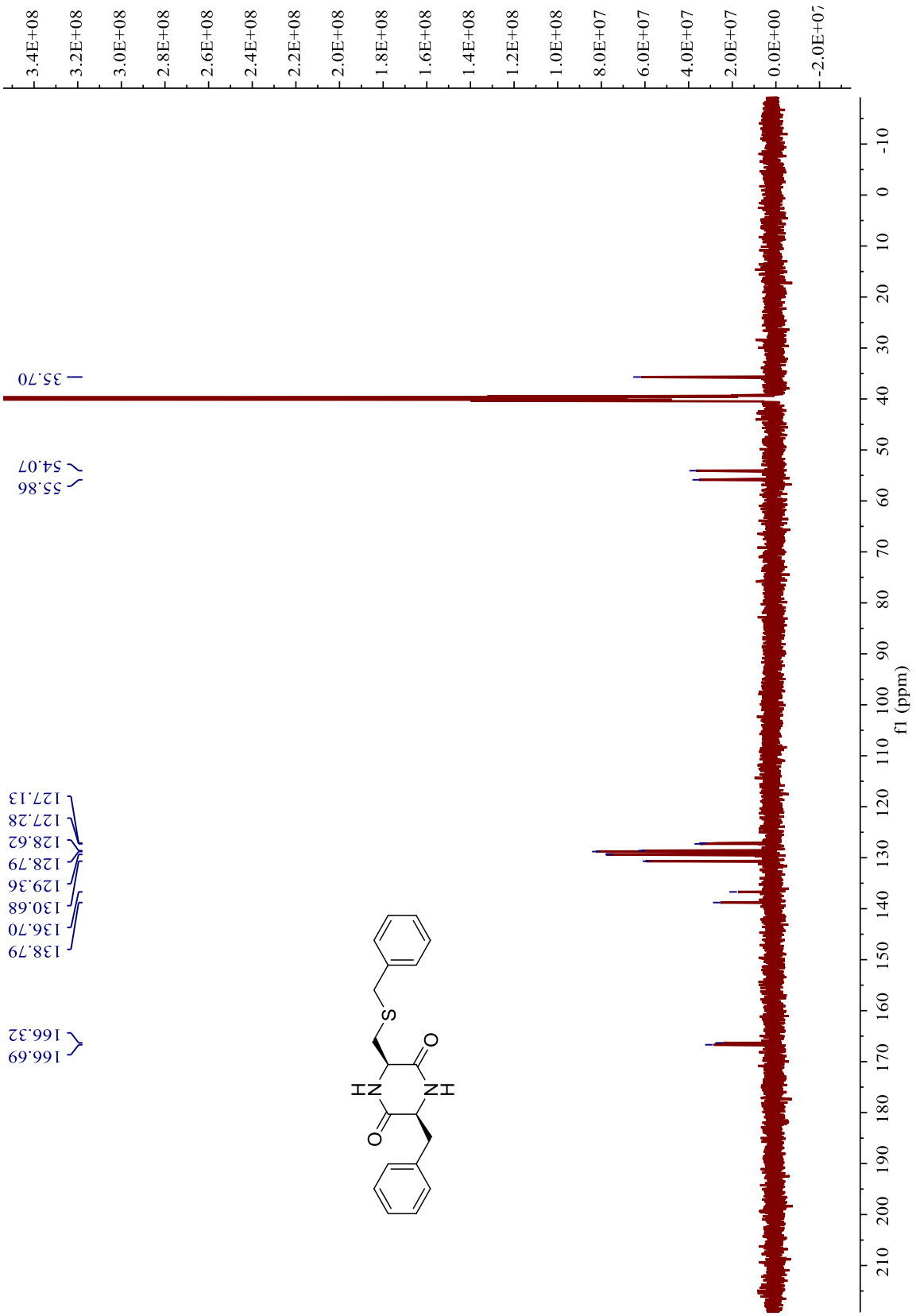

Figure S10. *^{13}C-NMR spectra of P5 dissolved in DMSO-d_6 solvent.*

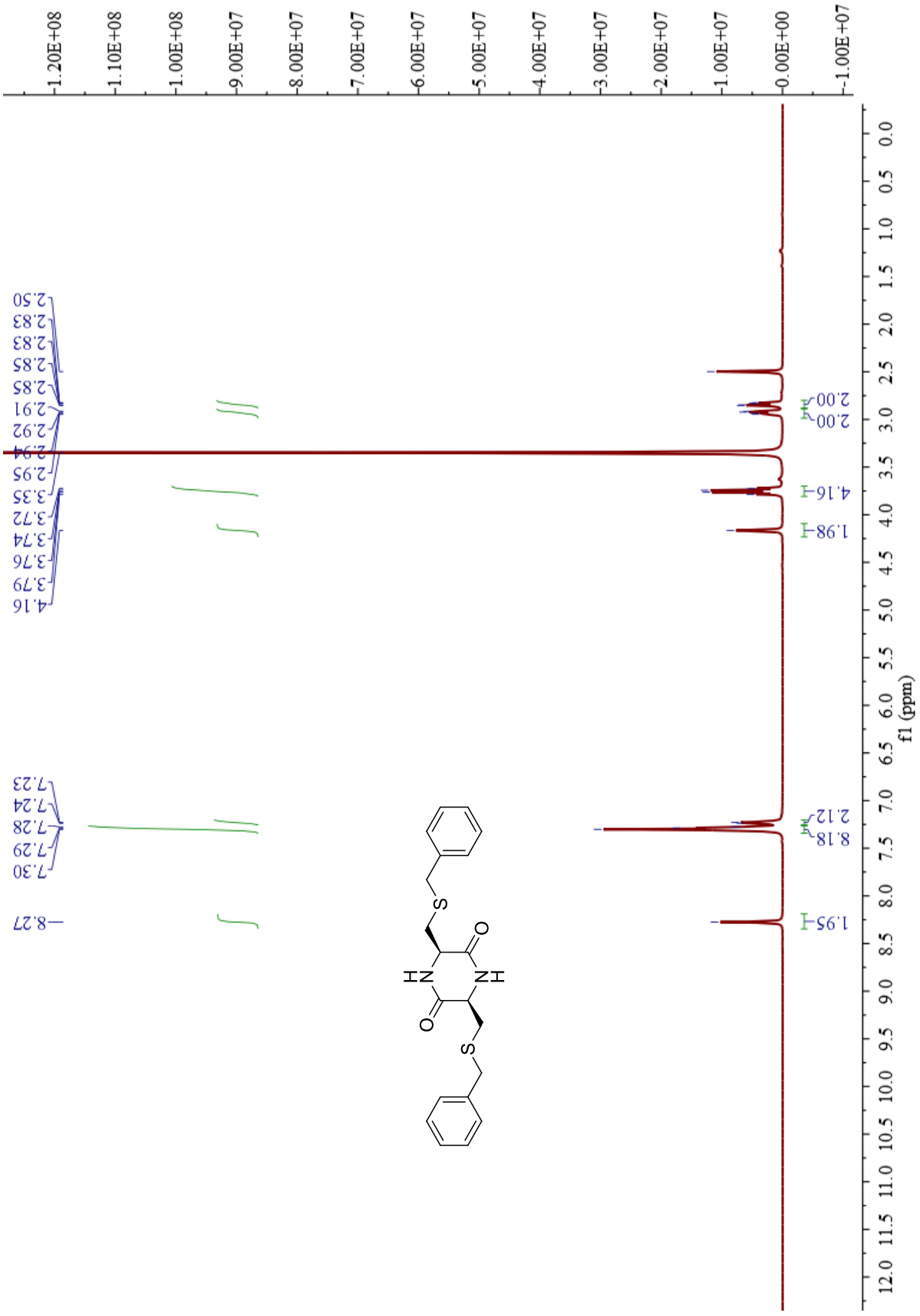

Figure S11. *^{1}H-NMR spectra of P6 dissolved in DMSO-d_6 solvent.*

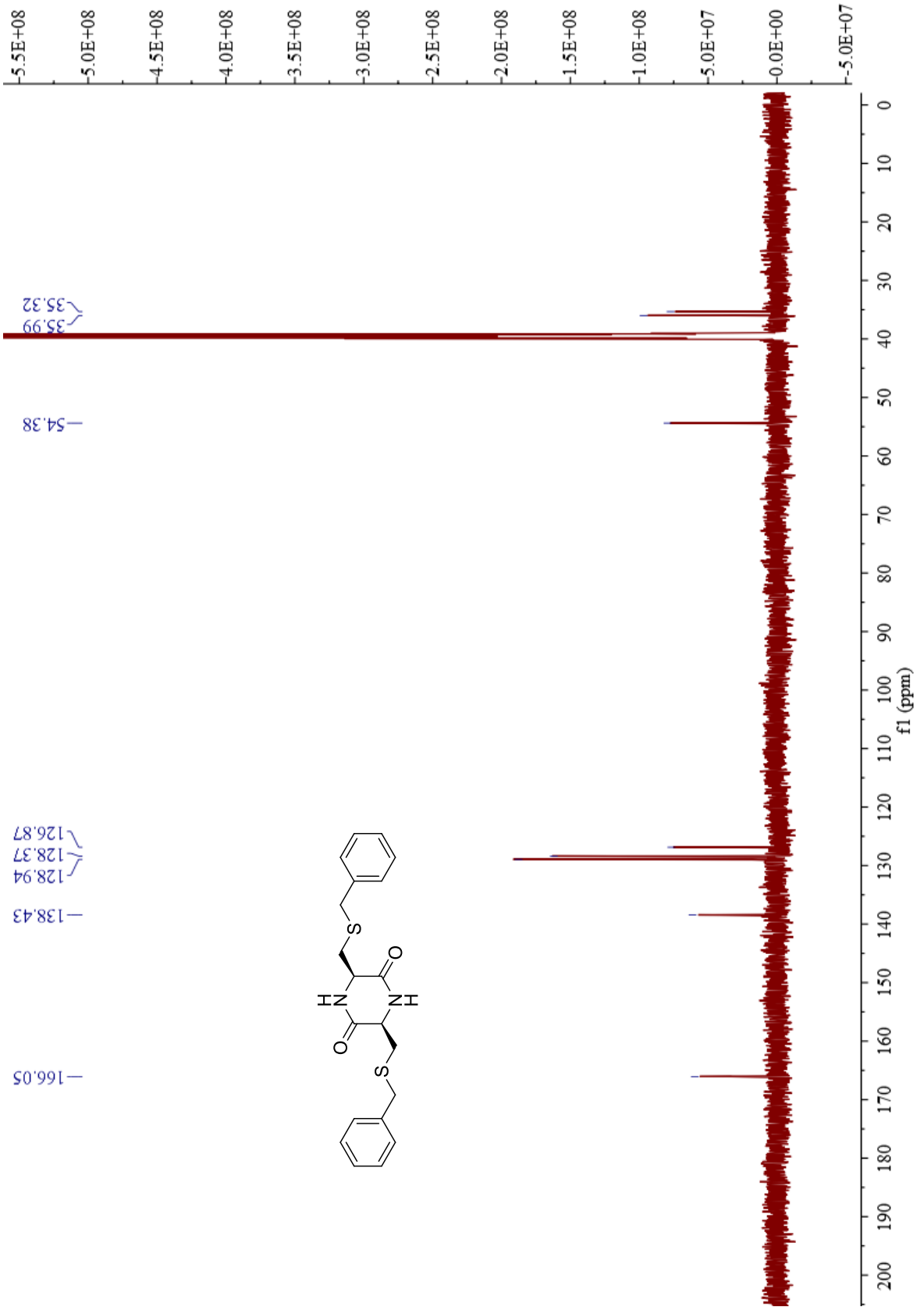

Figure S12. *^{13}C-NMR spectra of P6 dissolved in DMSO-d_6 solvent.*

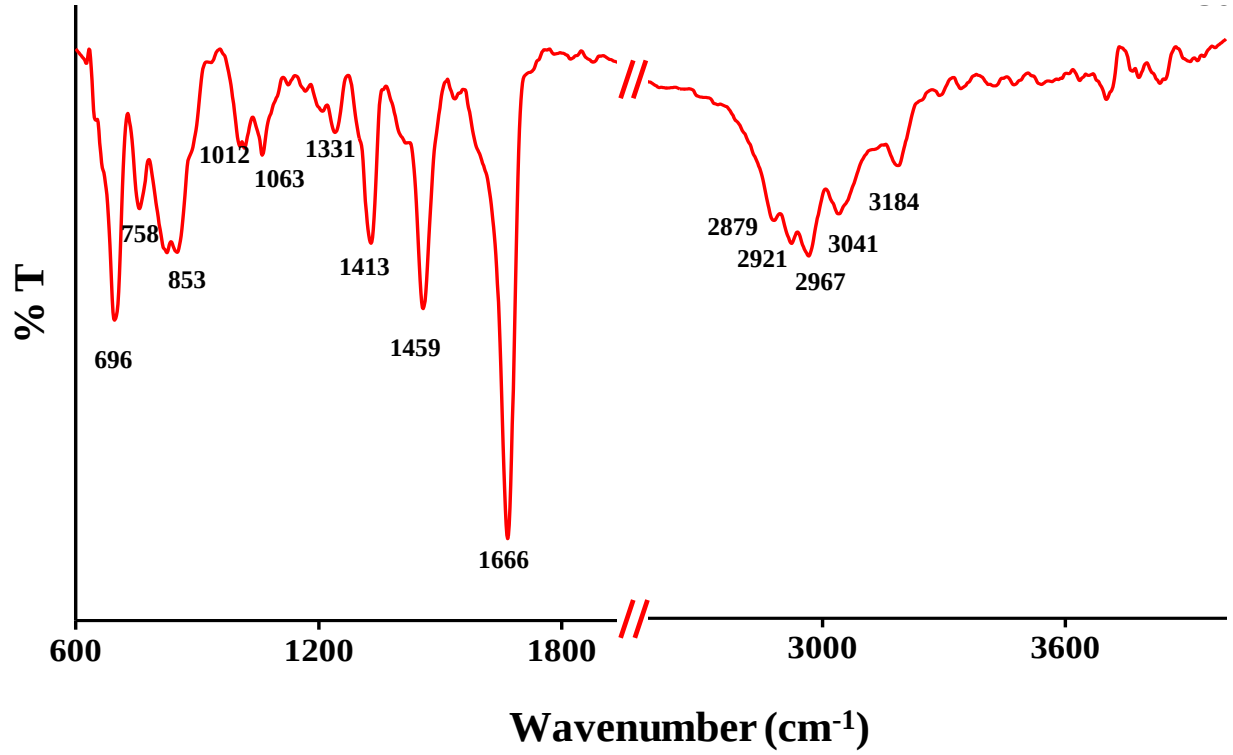

Figure S13. *FTIR spectra of cyclic dipeptide P1 in solid state.*

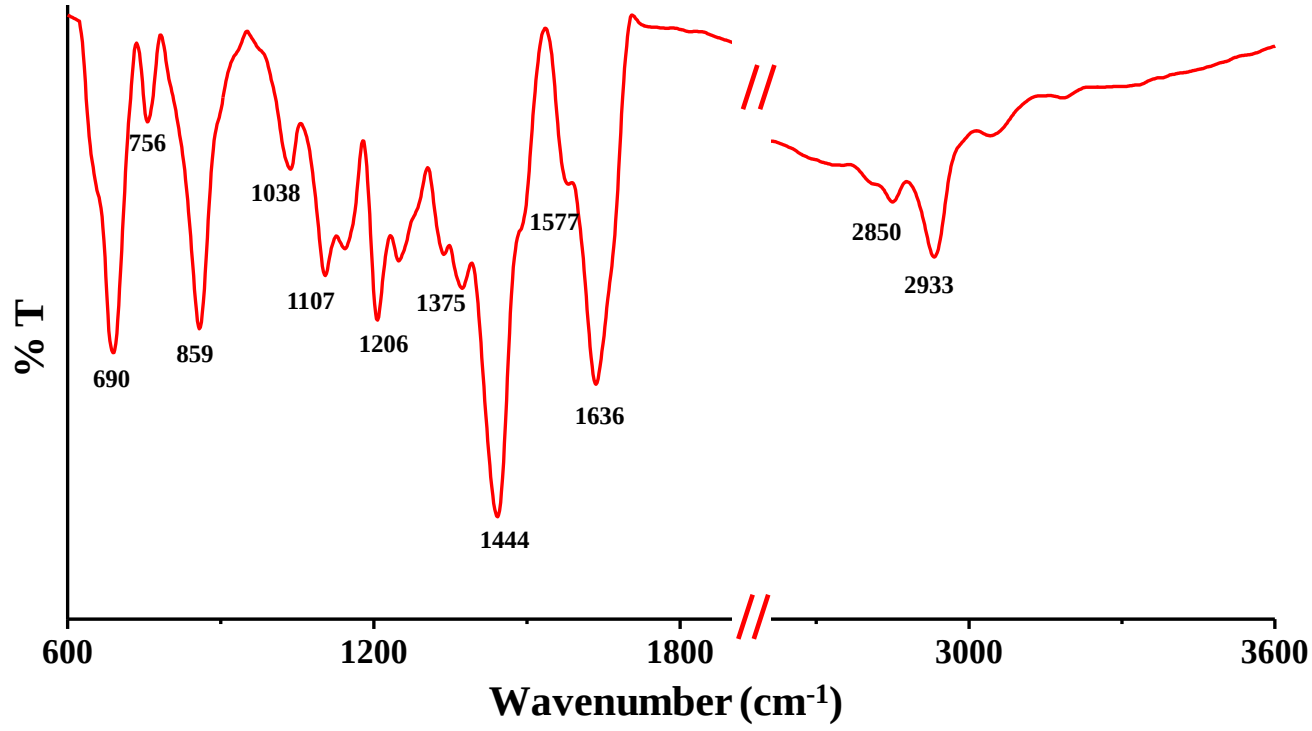

Figure S14. *FTIR spectra of cyclic dipeptide P2 in solid state.*

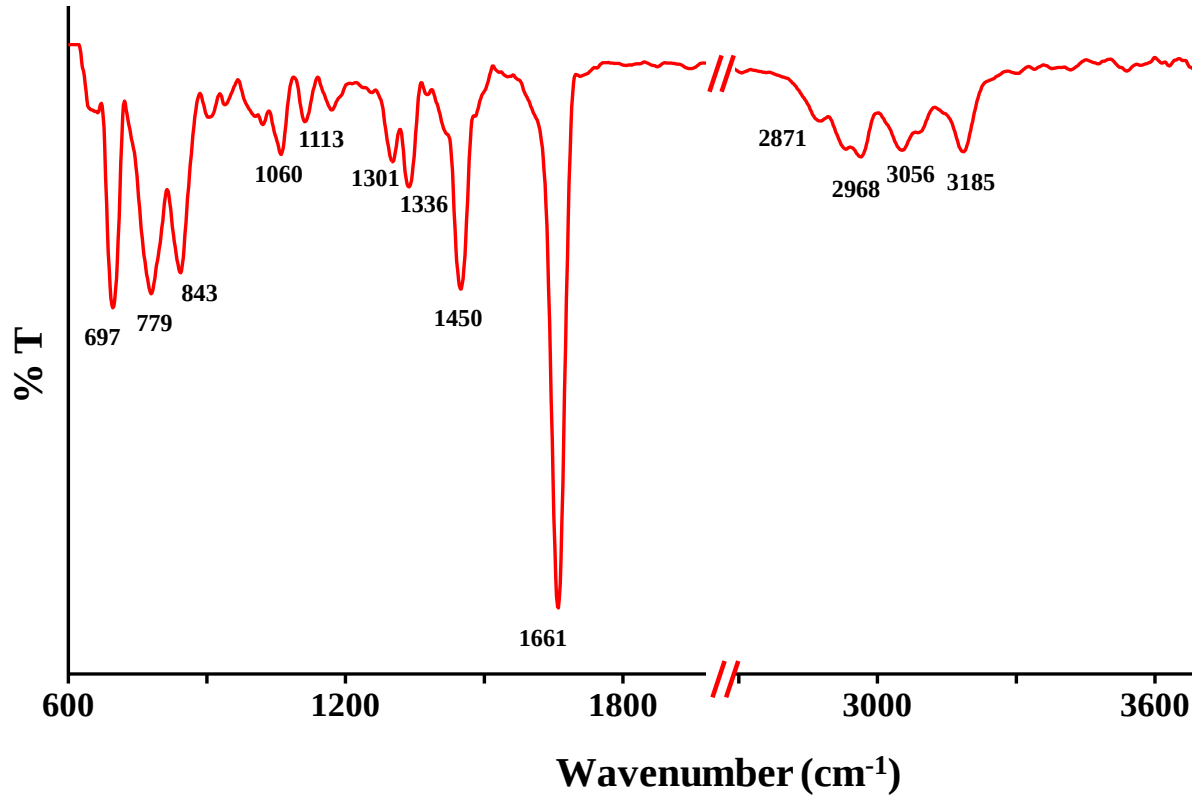

Figure S15. *FTIR spectra of cyclic dipeptide P3 in solid state.*

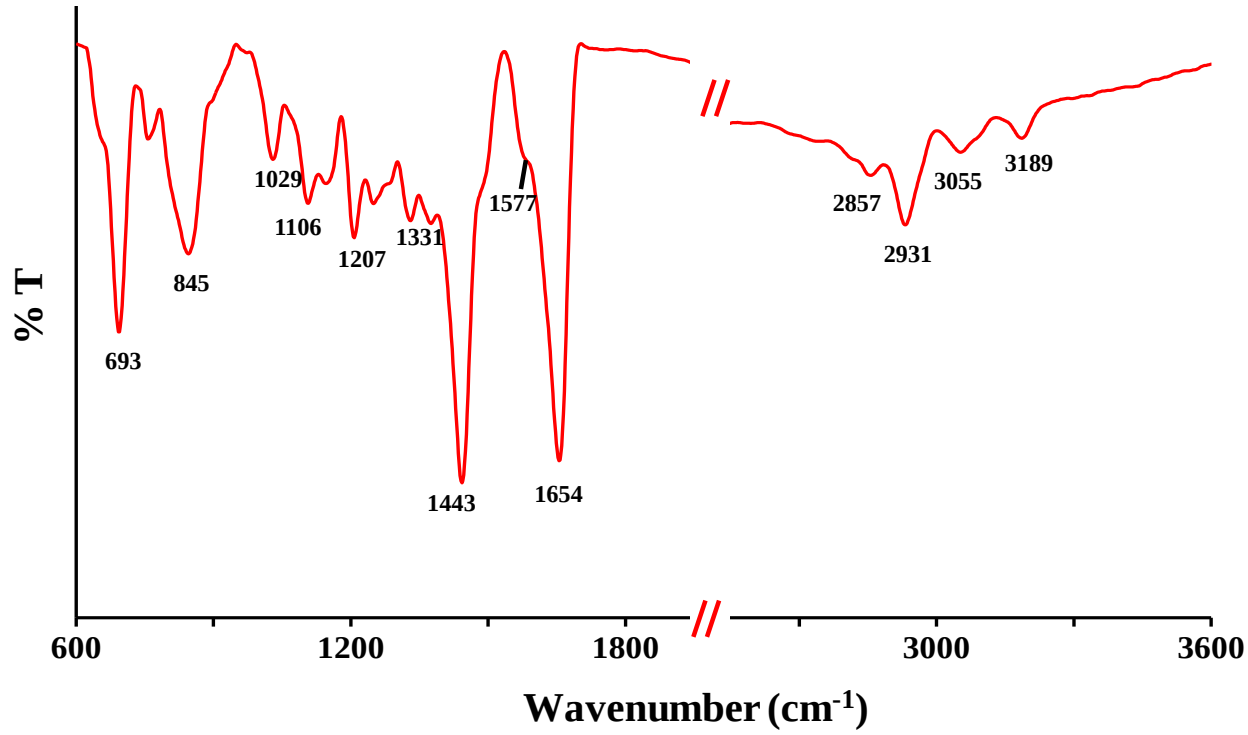

Figure S16. *FTIR spectra of cyclic dipeptide P4 in solid state*

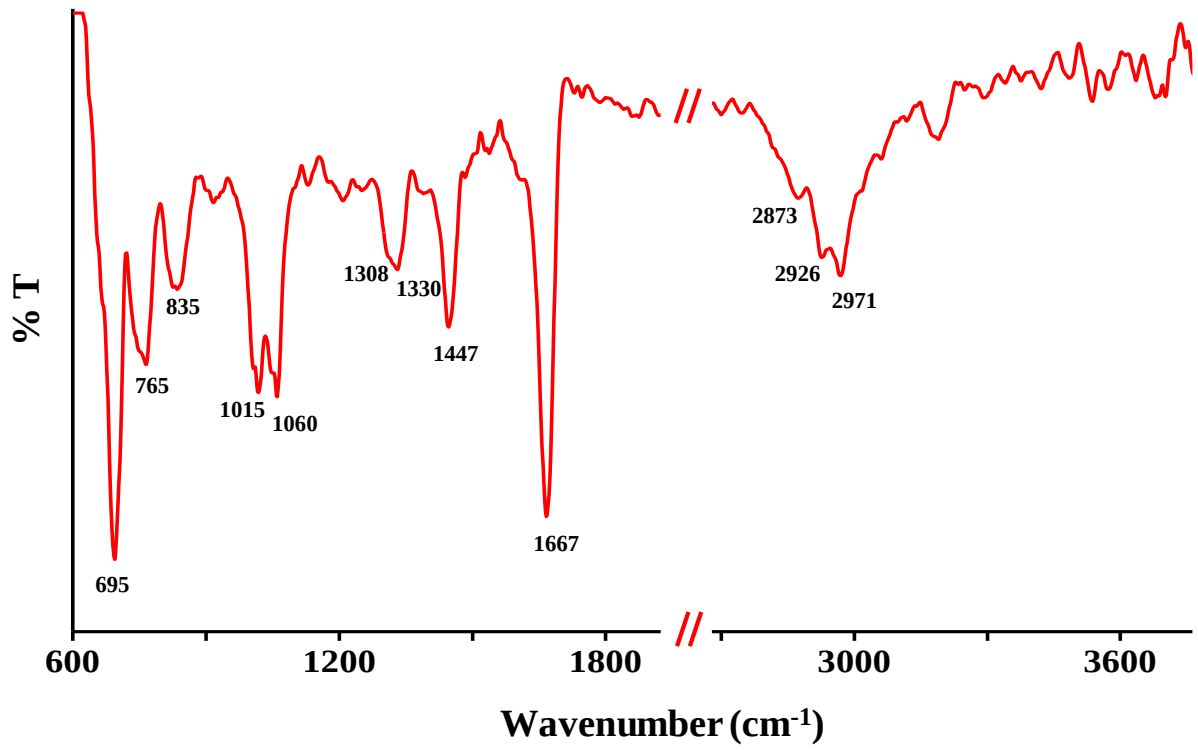

Figure S17. *FTIR spectra of cyclic dipeptide P5 in solid state.*

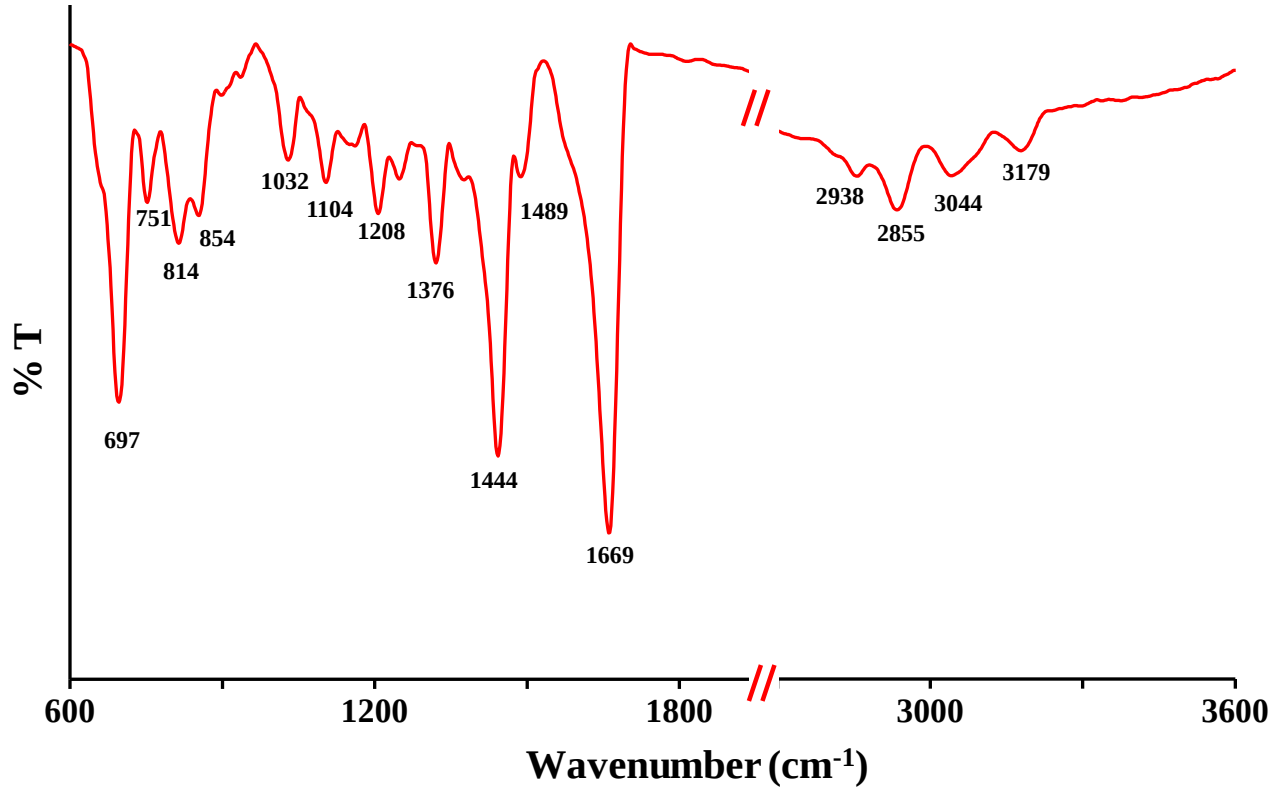

Figure S18. *FTIR spectra of cyclic dipeptide P6 in solid state.*

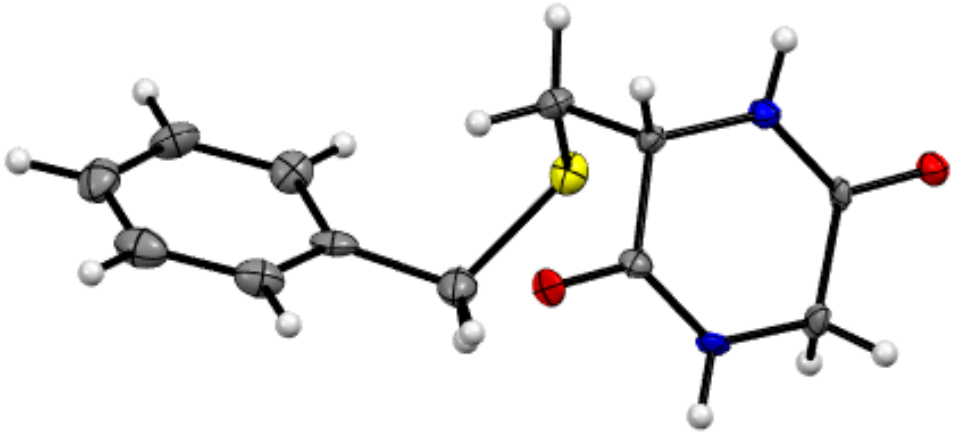

Figure S19. *ORTEP diagram of cyclic dipeptide P1. Thermal ellipsoids are shown in 50 % probability level.*

Table S1*: Important crystal data of* ***P1***

CCDC no	2233567
Empirical formula	$C_{12}H_{14}N_2O_2S$
Formula weight	250.323
Temperature/K	102.00
Crystal system	triclinic
Space group	P1
a/Å	6.0465(4)
b/Å	7.5828(5)
c/Å	13.285(1)
α/°	78.921(4)
β/°	89.875(4)
γ/°	89.981(4)
Volume/Å^3	597.76(7)
Z	2
ρ_{calc}g/cm^3	1.391
μ/mm^{-1}	2.346
F(000)	265.5
Crystal size/mm^3	0.21 × 0.18 × 0.15
Radiation	Cu Kα (λ = 1.54178)
2Θ range for data collection/°	6.78 to 144.6
Index ranges	$-6 \leq h \leq 7$, $-9 \leq k \leq 9$, $-16 \leq l \leq 16$
Reflections collected	11292
Independent reflections	4071 [R_{int} = 0.0468, R_{sigma} = 0.0550]

Data/restraints/parameters	4071/3/307
Goodness-of-fit on F^2	1.010
Final R indexes [I>=2σ (I)]	R_1 = 0.0646, wR_2 = 0.1719
Final R indexes [all data]	R_1 = 0.0653, wR_2 = 0.1723
Largest diff. peak/hole / e $Å^{-3}$	0.89/-0.51
Flack parameter	0.067(12)

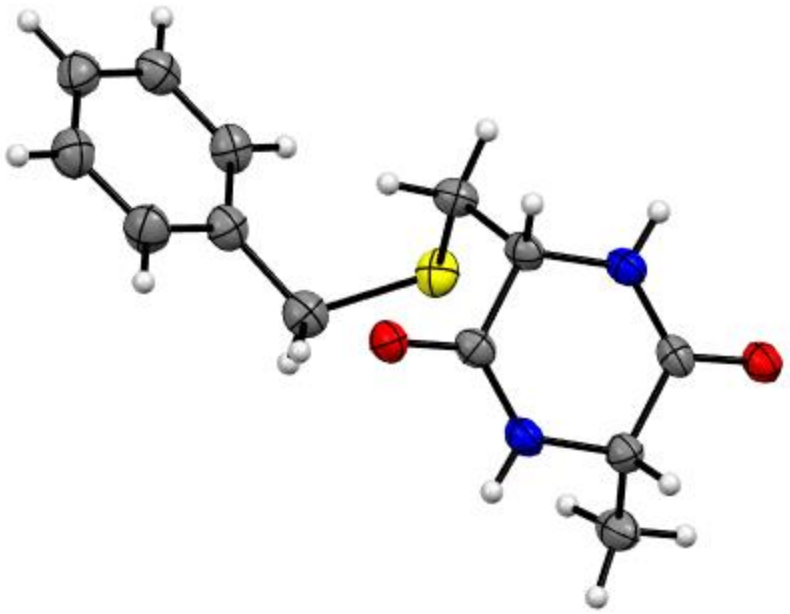

Figure S20. *ORTEP diagram of cyclic dipeptide P2. Thermal ellipsoids are shown in 50 % probability level.*

Table S2*: Important crystal data of* ***P2***

CCDC no	2233450
Empirical formula	$C_{13}H_{16}N_2O_2S$
Formula weight	264.34
Temperature/K	100.0
Crystal system	orthorhombic
Space group	$P2_12_12_1$
a/Å	6.0542(11)
b/Å	9.0593(15)
c/Å	23.816(4)
α/°	90

β/°	90
γ/°	90
Volume/Å^3	1306.2(4)
Z	4
ρ_{calc}g/cm^3	1.344
μ/mm^{-1}	2.175
F(000)	560.0
Crystal size/mm^3	0.25 × 0.015 × 0.01
Radiation	Cu Kα (λ = 1.54178)
2Θ range for data collection/°	7.424 to 133.756
Index ranges	-5 ≤ h ≤ 7, -10 ≤ k ≤ 10, -28 ≤ l ≤ 28
Reflections collected	19124
Independent reflections	2306 [R_{int} = 0.1426, R_{sigma} = 0.0709]
Data/restraints/parameters	2306/0/165
Goodness-of-fit on F^2	1.014
Final R indexes [I>=2σ (I)]	R_1 = 0.0552, wR_2 = 0.1300
Final R indexes [all data]	R_1 = 0.0615, wR_2 = 0.1344
Largest diff. peak/hole / e Å^{-3}	0.29/-0.29
Flack parameter	0.023(16)

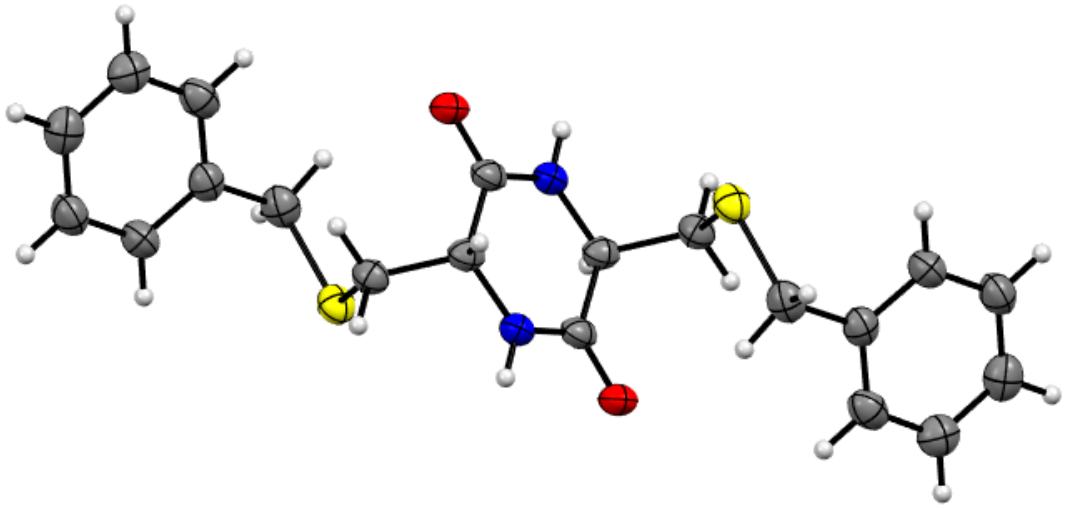

Figure S21. *ORTEP diagram of cyclic dipeptide P1. Thermal ellipsoids are shown in 50 % probability level.*

Table S3**: Important crystal data of **P6

CCDC no	2233563
Empirical formula	$C_{10}H_{11}NOS$
Formula weight	193.26
Temperature/K	104.0
Crystal system	triclinic
Space group	P-1
a/Å	5.9873(5)
b/Å	8.0025(7)
c/Å	10.2725(9)
α/°	84.253(6)
β/°	75.829(5)
γ/°	89.220(5)
Volume/Å^3	474.78(7)
Z	2
ρ_{calc}g/cm^3	1.352
μ/mm^{-1}	2.676
F(000)	204.0
Crystal size/mm^3	0.25 × 0.02 × 0.01
Radiation	Cu Kα (λ = 1.54178)
2Θ range for data collection/°	8.922 to 122.53
Index ranges	$-6 \leq h \leq 6$, $-9 \leq k \leq 9$, $-11 \leq l \leq 11$
Reflections collected	8746
Independent reflections	1446 [R_{int} = 0.0734, R_{sigma} = 0.0479]
Data/restraints/parameters	1446/0/119
Goodness-of-fit on F^2	1.169
Final R indexes [I>=2σ (I)]	R_1 = 0.0976, wR_2 = 0.2616
Final R indexes [all data]	R_1 = 0.1026, wR_2 = 0.2677
Largest diff. peak/hole / e Å^{-3}	1.43/-0.45

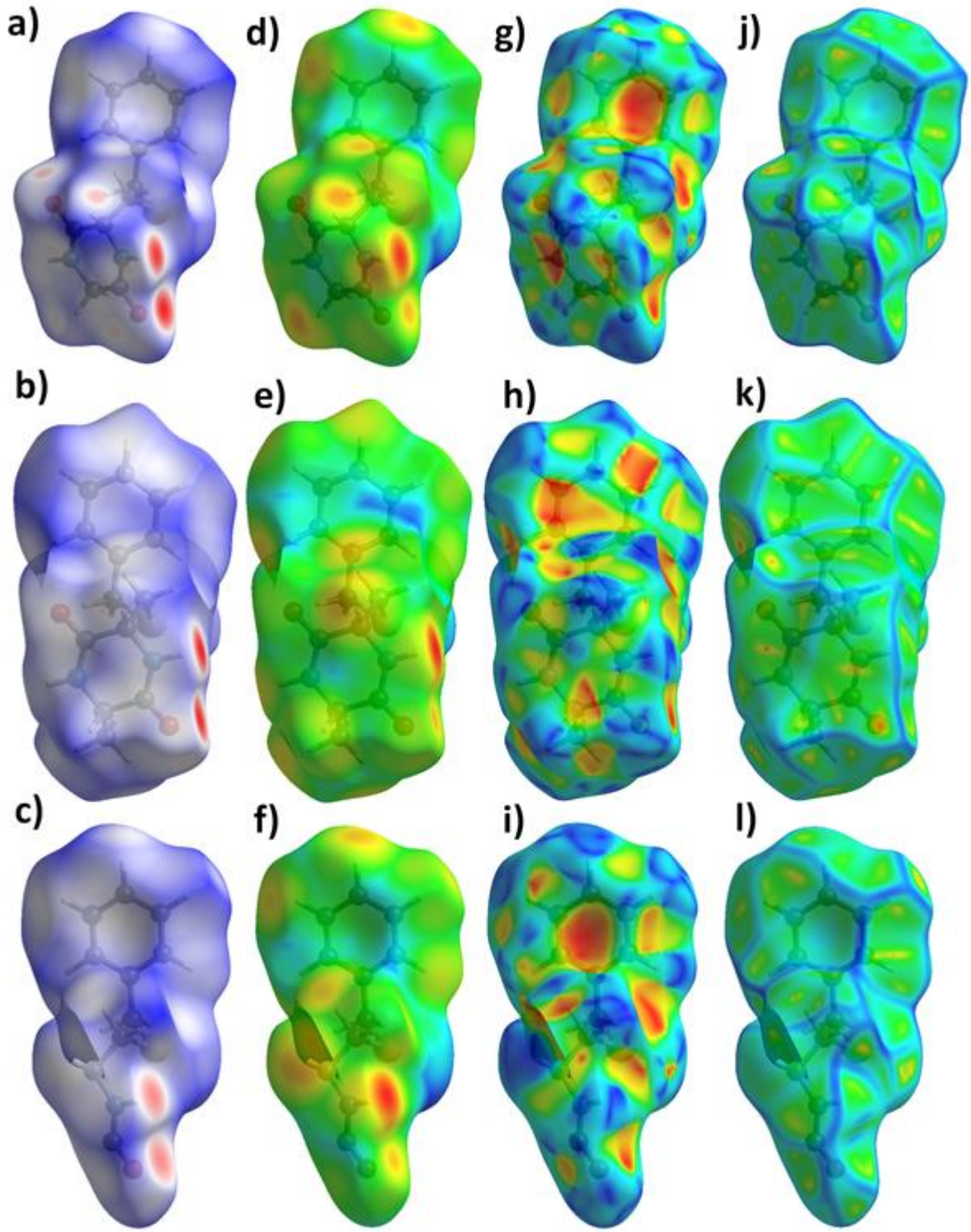

Figure S22. *Hisrhfield Surface of d_{norm} of (a) P1, (b) P2, (c) P6; d_i of (d) P1, (e) P2, (f) P6; shape index of (g) P1, (h) P2, (i) P6; curvedness of (j) P1, (k) P2, (l) P6.*

CHAPTER-4

Controlling Self-Assembly of Small Peptides into Different Nanostructures by Quinazolinone Capping

4.1 AIM OF THE PRESENT WORK

Self-assembly of short synthetic peptides is a rapidly expanding area of research due to their wide range of applications from biotechnology to nano-chemistry. The hydrogels produced as a result of self-assembly of these short peptides are of special interest due to their low cost synthesis and biocompatibility. However, the mechanism underlying this process and their underlying design principles were still poorly understood. Longer peptides have complementary connections between molecules that are strong enough for these peptides to create supramolecular gel networks. However shorter peptides often require an additional capping group to drive self-assembly into gel network. Thus in this chapter, efforts were made to synthesize four short peptides namely **QP1**, **QP2**, **QP3**, and **QP4** having quinazolinone as heterocyclic capping group. The main focus of this work was to examine the change in the self-assembling pattern and hydrogelation ability of these hybrid peptides by employing slight twists in their molecular structures. A small change in the linker and position of the terminal functional group of the peptide residues caused significant differences in the morphological pattern of the aggregates produced in 1% DMSO-PBS solvent system. This small variation was responsible for the formation of aggregates of two distinct morphologies: **QP1** and **QP2** produced elongated nano-fibrillar networks whereas **QP3** and **QP4** produced spherical assembly. Later on after prolonged incubation **QP3** produced nano-belt type of morphology. The influence of the quinazolinone capping and slight modifications in the molecular structures of these peptides were also reflected in their gelation behavior in 1% DMSO-PBS solvent system. Various microscopic and spectroscopic techniques like AFM, FESEM, NMR, FTIR, etc. along with crystallographic studies were performed for a better understanding of the self-assembling pattern, morphology of the nano-structures, and the noncovalent interactions that were involved in self-assembly process of these peptides.

Cytotoxic effect of the peptides was also examined by MTT assay in cervical cancer cell line (HeLa).

4.2 INTRODUCTION

Self-assembly is a phenomenon that occurs everywhere in nature. It is responsible for most of the fundamental biological functions, including the complementarity of DNA base pairs, the transport of ions across membranes, and the folding of proteins into functional tertiary structures.[243–246] The self-assembly of proteins and peptides is of particular interest, as the structure of the protein is intricately linked with its function.[247,248] Self-assembling short peptides have attracted widespread interest due to their resemblance with native proteins, tuneability, biocompatibility and they have potential applications in energy materials, tissue engineering, sensing, drug delivery, and various other fields.[249–253] The hierarchical self-assembly of these short peptides is often largely dependent on the choice of capping group, which is frequently used at the N-terminus of the peptide to induce self-assembly in addition to the selection of amino acid sequence. Self-assembled short peptide based hydrogels are currently receiving more attention than longer peptide based hydrogels since they are easier to synthesize and cost effective. These hydrogels can serve as extracellular matrix mimics, which encourage cell adhesion, differentiation, growth, and proliferation.[22,254,255] Moreover, Short peptide-based hydrogels have the advantage of being reversible in nature due to the non-covalent interactions that make up the gel network, in contrast to polymer hydrogels, which are typically formed by the incorporation of water-soluble groups on a synthetic polymer backbone through covalent interaction.[256,257] Despite the fact that the amino acid sequence utilized greatly influences the physical and chemical properties of these hydrogels, short peptide hydrogelators frequently require an aromatic capping group at their N-terminus to cause gelation.[258,259112,113,118,260] In these systems, the hydrophobic interaction offered by the capping group in

conjunction with hydrogen bonding interaction of the peptide backbone triggers the self-assembly. One of the most extensively researched capping groups for producing short peptide-based hydrogelators is fluorenylmethyloxycarbonyl (Fmoc), a protecting group that is frequently utilized in solid phase synthesis (SPPS).[112,113,118,260] In addition to Fmoc, naphthalene, anthracene, perylene, pyrene, indole, benzimidazole, or carbazole have also reportedly been used as capping groups to produce hydrogelators.[261–264] Diphenylalanine sequence (-FF), the core motif for the β-amyloid self-assembling sequence, is perhaps the most well-studied among the dipeptides and is frequently incorporated as a backbone to produce short peptide based hydrogelators owing to their ability to engage in extensive π-π stacking interactions driven by the two phenyl groups present on the amino acids. It is well known that the diphenylalanine sequence by itself (i.e., NH_2-Phe-Phe-OH) does not tend to form hydrogels but rather forms crystalline nanotubes, which have proven to be highly effective in a variety of applications.[88,212] Thus self-assembling, diphenylalanine-containing peptide hydrogels are frequently "capped" at the N-terminus by an aromatic group. Gazit first reported that the addition of the fluorenylmethyloxycarbonyl (Fmoc) group to the N-terminus of the diphenylalanine sequence (Fmoc-FF) led to the development of a self-supporting hydrogel via the dilution of Fmoc-FF dissolved in hexafluoroisopropanol with water.[265] The Adams group had used naphthalene-based capping group to generate hydrogels by incorporating FF and other peptide sequences.[264,266,267]

Among aromatic compounds, heterocycles in particular are prevalent in nature and serve as an excellent point to begin with when trying to increase the chemical variety of the N-terminal capping group in short peptides. For instance, it is evident that 84% of entire FDA-approved drugs have at least one heterocyclic moiety in their structures, and more than 75% of the FDA-

approved drugs that are currently available in the market have heterocyclic moieties that contain nitrogen.[268] The capping of an Ala-Gly-Ala-Gly-Ala

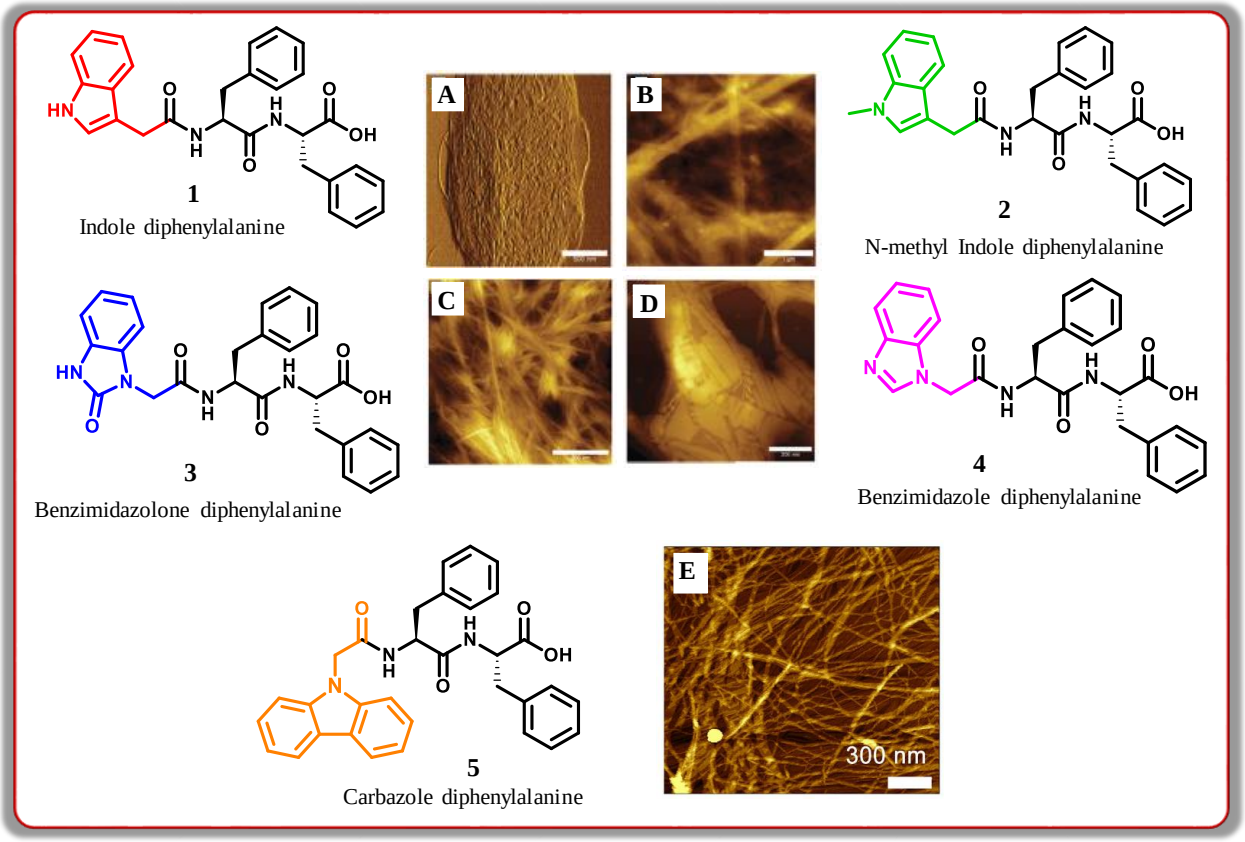

Figure 1. *Examples of few previously reported heterocyclic capped peptides: Related AFM images of gel network obtained from (A) indole diphenylalanine, (B) N-methyl indole diphenylalanine, (C) benzimidazolone dipehenylalanine, and (D) benzimidazole diphenylalanine at a concentration of 0.1% (w/v). Scale bars denote 500 nm for A, 1 µm for B, and 300 nm for C &D. Copyright 2016, Royal Society of Chemistry. (E) AFM image of carbazole-diphenylalanine sol at 0.01% (w/v). Scale bars represent 300 nm. Copyright 2017, Nature portfolio*

(AGAGA) pentapeptide sequence with an ex-tetrathiofulvalene (exTTF) sequence was first documented in 2012 which yielded the formation of helical nanofibers.[269] In 2014, Ulijn et al. reported gelation in multiple organic solvents, including chloroform, ethyl acetate, DMSO, and tetrahydrofuran by a TTF group capped diphenylalanine peptide bearing an amine at its C-terminus (TTF-FF -NH_2).[270] Naphthalene diimides have been utilized by Lin et al. to produce

multifunctional chemicals that can be used for cell imaging or, at higher concentrations, self-assemble into hydrogels, as well as by Ulijn et al. to produce charge-transfer supramolecular nanofibers.[271,272] In 2014, Martin et al. reported indole-3-acetic acid capping at the N-terminus of diphenylalanine, resulting in indole-diphenyl alanine (Ind-FF), which had a very high storage modulus and was one of the stiffest peptide hydrogels yet described.[263] In 2015, as a follow-up to their research on the indole capping group, Martin group reported the generation of biocompatible scaffolds by adding a carbazole group to the N-terminus of either the dipeptide Phe-Phe (FF) or tripeptide Gly-Phe-Phe (GFF).[261] Adams synthesized carbazole-capped alanine to avail use of the electropolymerizing properties of carbazole (Carb-Ala).[273] Diphenylalanine with a benzimidazole cap was found to form hydrogels and single crystals.[274]

Quinazolinone is a nitrogen-based fused heterocyclic molecule. About 150 naturally occurring alkaloids, identified from a range of kingdom Plantae, kingdom Animalia, and other sources, have 4-quinazolinone as their central building block.[275] Due to its numerous pharmacological properties, quinazolinone is a crucial pharmacophore with a wide range of pharmacological effects, including anticancer, anticonvulsant, antimalarial, antifungal, antibacterial, antiinflammatory, MMP inhibitors, antidiabetic, antileishmanial, and hypolipidemic characteristics.[276,277] Numerous medications based on quinazolinone have completed various phases of clinical trials. Additionally, certain medications based on quinazolinone have been commercialized as effective medicines. Self-assembly process can be triggered by the aromaticity and propensity for hydrogen bonding of the quinazolinone moiety. Despite quinazolinone's extensive use in chemistry, no examples of supramolecular hydrogels using quinazolinone as a capping group has been found. Herein, synthesis of four new S-benzyl-L-cysteine based peptides **QP1, QP2**, **QP3**, and **QP4** capped with quinazolinone group were reported in this chapter that was

able to form various distinct nanostructures at same physical and chemical conditions. Amongst these **QP1** and **QP3** were able to form hydrogel in 1% DMSO-PBS solvent at physiological conditions. A variety of microscopic and spectroscopic techniques were employed to track the self-assembly as well as gelation procedure of these four hybrid peptides.

4.3 RESULTS AND DISCUSSION

This study looked closely at the self-assembling ability of four hybrid peptides containing quinazolinone moiety and benzyl protected cysteine as common structural building blocks (**Figure 3**). For this, two sets of de novo peptides were designed by applying reversal of end terminal strategy and synthesized by three to four simple chemical reaction steps. A general designing strategy for the design and synthesis of four hybrid peptides was depicted below (**Figure 2**).

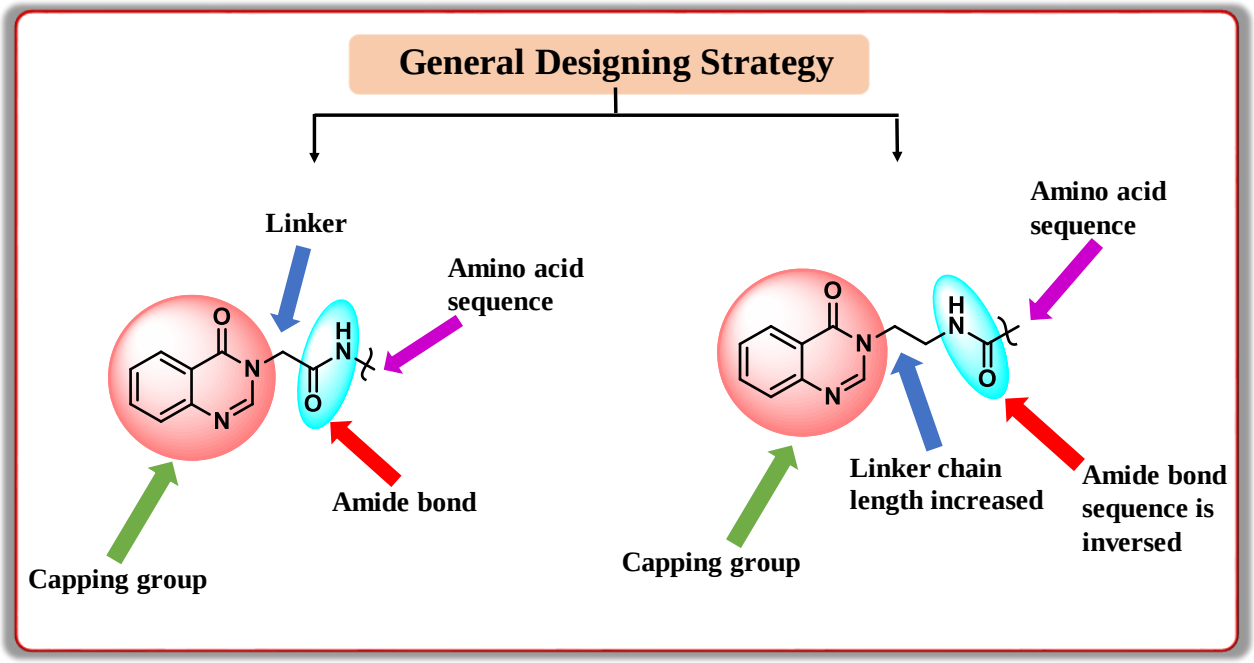

Figure 2. *General designing strategy for the synthesis of quinazolinone capped short peptides*

A quinazolinone group was added to the N-terminus of the first pair of hybrid peptides, **QP1** and **QP2**, which comprise a dipeptide constituting glycine and

the S-benzyl-L-cysteine (gly-cys). In another way, it can be said that the glycine backbone is acting as a linker between the capping group quinazolinone and the common amino acid component i.e. S-benzyl-L-cysteine, in both molecules. In **QP1**, the terminal acid group of S-benzyl-L-cysteine is methyl protected whereas, in **QP2**, the terminal acid group is free. To examine whether the reversal of the terminal of the cysteine moiety has any role in producing different self-assembled morphology another set of hybrid peptides containing **QP3** and **QP4** were synthesized where ethylenediamine was used as linker between quinazolinone and S-benzyl-L-cysteine moiety. In **QP3** the terminal –NH_2 group is BOC protected and in **QP4** the terminal –NH_2 group is free. In this chapter, investigations were made on how the self-assembly pattern of these four hybrid peptides composed of same heterocyclic capping and with a common constituting amino acid differ from each other due to having slight twists in their molecular structure. These small changes in the peptide structures caused significant differences in morphological pattern of the aggregates produced in aqueous solutions which are thoroughly discussed in this chapter.

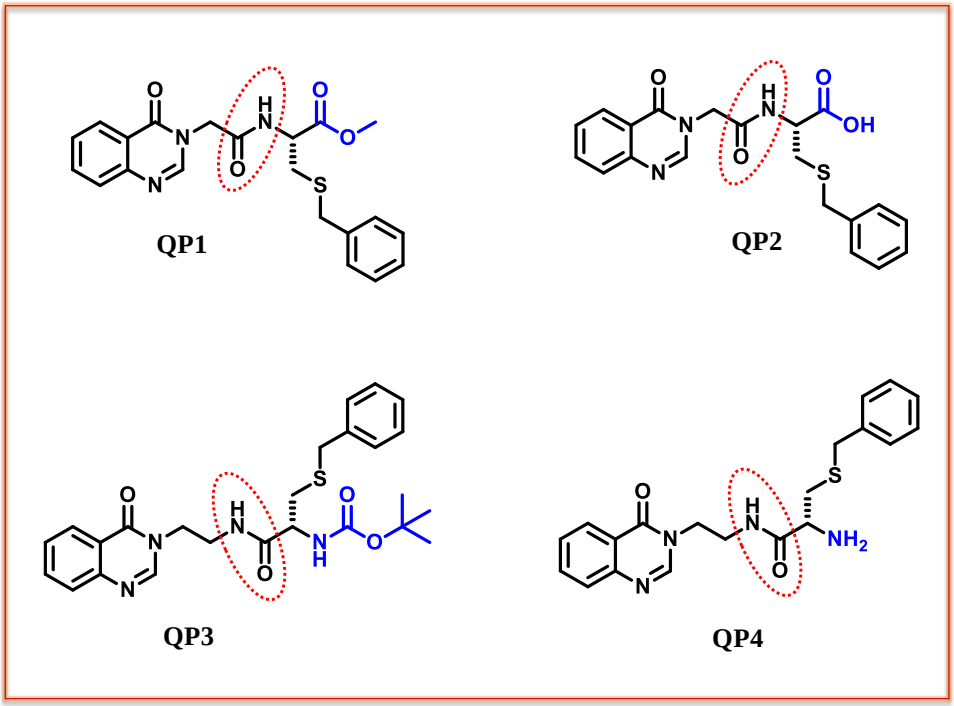

***Figure 3**. Structure of four synthesized heterocyclic capped peptides.*

4.3.1 Synthesis of Quinazolinone Capped Hybrid Peptides (QP1, QP2, QP3, and QP4)

All chemicals were purchased from Sigma Aldrich and used without further purification unless otherwise stated. All the solvents used in this study were purchased from Thermo Fischer Scientific and were freshly distilled by standard procedures before use. Column chromatography was performed on silica gel (100-200 mesh; Merck) with the required eluent. Mass spectrometric data were acquired through the electron spray ionization (ESI) technique on a Jeol MS station 700 and all ^{1}H and ^{13}C-NMR spectra were recorded on Bruker 600 MHz spectrometer for characterization of the compounds. Bruker Kappa Apex II X-ray crystallography machine was used to get the single crystal structures. The step-wise synthetic procedures of the above mentioned hybrid peptides (**QP1-QP4**) and their characterization were discussed elaborately in the experimental procedures and spectral data section.

(A)

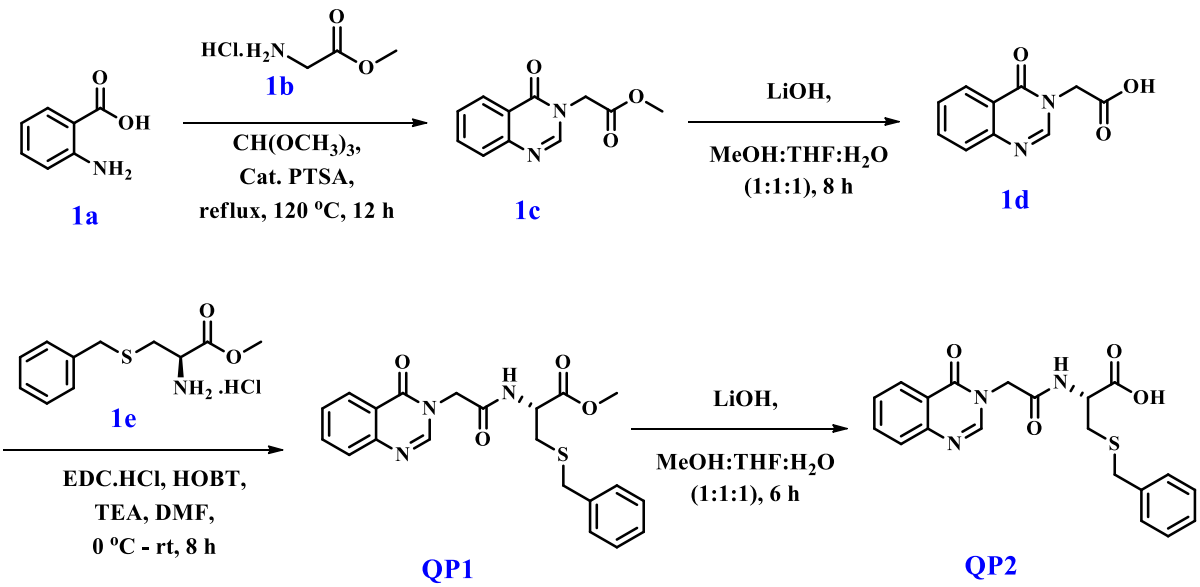

(B)

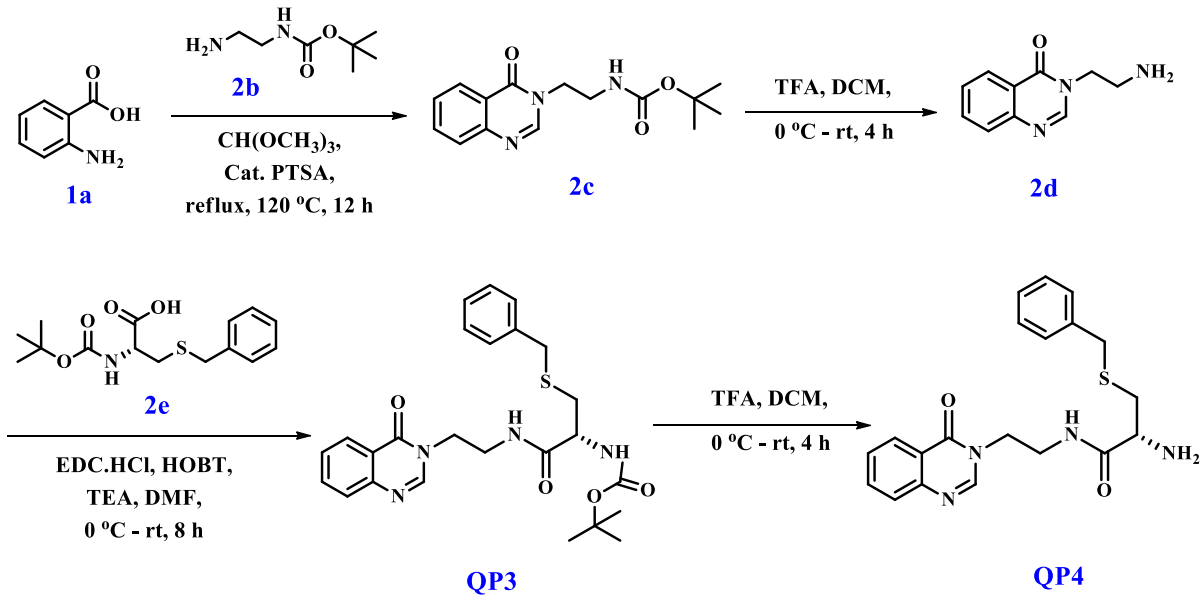

Scheme 1. *Schematic route to the synthesis of (A) QP1, QP2, and (B) QP3, QP4.*

4.3.2 Self-assembly study of quinazolinone capped peptides (QP1-QP4)

The self-assembly property of these hybrid small peptides was visualized by utilizing atomic force microscopy and field emission scanning electron microscopy experiments. AFM is a reliable technique for the visualization of surface morphology and nano-structures produced by self-assembling materials. AFM images were obtained on Pico Plus 5500 AFM (Agilent Technologies, Inc., Santa Clara, CA, USA) with the piezo scanner range of 9 μm. The images (256 × 256 pixels) were captured with a scan size between 0.5 and 5 μm at the scan speed rate of 0.5 rpm. The images were processed through flattening via Pico view software (Molecular Imaging Inc., Ann Arbor, MI, USA). Samples were prepared by drop casting the dilute solutions (50 μM in 1% DMSO-PBS) of each peptide individually onto freshly cleaved mica sheets after different times of incubation and then letting them dry at room temperature. After drying the sample under air,

images of the samples were obtained by placing the mica sheets under AFM laser beam.

AFM images revealed very interesting results where it was observed that two peptides **QP1** and **QP2** in which the N-terminal of cysteine is attached with quinazolinone formed fibrillar assembly whereas the other two peptides **QP3** and **QP4** in which the C-terminal of cysteine is attached with quinazolinone produced spherical assembly after 24 h of incubation in 1% DMSO-PBS buffer solution. The time taken for the formation of these fibrils was then examined by drop casting freshly prepared solutions of **QP1** and **QP2** just after 5 mins of incubation and AFM images were acquired after drying the samples. Surprisingly, it was observed that both **QP1** and **QP2** formed nano-fibrils only after 5mins of incubation which implied that the rate of fibrillization was very fast for both the hybrid peptides. **QP1** produced a highly cross-linked fibrillar network where some of the fibrils were seen to have helically twisted morphology (**Figure 4A**). The nano-fibers thus produced by **QP1** had an average diameter of 25-60 nm and after 24 h of incubation, the fiber morphologies were diversified, showing dense cross-linked fibrillar network structure, having width in the range of 35-75 nm. Similarly, for **QP2**, the fibrillar network became more cross-lined after 24 h of incubation (**Figure 4F**), and average diameter of fibrils produced after 5 mins of incubation increased from 20-50 nm to 25-65 nm after 24 h (**Figure 4E-4F**). The fibrils produced by both **QP1** and **QP2** had lengths of several microns. These results were further supported by FESEM images. It was found from FESEM image of **QP1** (**Figure 4D**) that it produced a highly dense inter woven web like architecture of numerous long nanofibers. The average width of the fibers was 70-120 nm and the length was several microns, indicating porous nanostructures with high surface area. Similarly, FESEM images reconfirmed the construction of unique nanofibrillar self-assembled architecture formed by xerogel of **QP2** (**Figure 4H**).

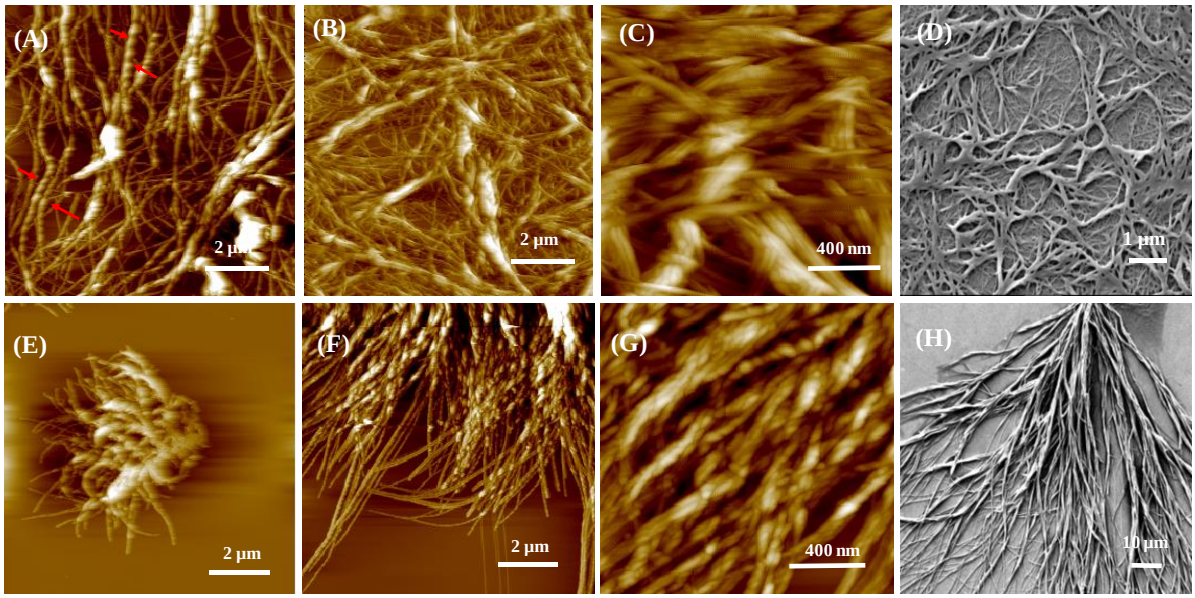

Figure 4. Upper panel: *Atomic Force microscopy images of QP1 obtained from 1% DMSO-PBS solvent system showing formation of fibrillar network (A) after 5 mins of incubation where red arrows indicted the helically twisted fibrils, (B) after 24 h of incubation, (C) higher magnification view of B showing dense highly cross-linked fibrillar network, and (D) FESEM image of fibrillar aggregates obtained from QP1 after 48 h of incubation.* ***Lower panel:*** *AFM images showing formation of fibrillar aggregates by QP2 in 1 % DMSO-PBS buffer (E) after 5 mins of incubation, (F) after 24 h of incubation, (G) higher magnification view of F. (H) FESEM image of nano-fibrillar network produced by QP2 after 48 h of incubation.*

On the other hand, AFM study of the dilute solutions of **QP3** and **QP4** showed that in 1% DMSO-PBS buffer solvent system both produced nano-sphere like assemblies having average diameters of 60-110 (**Figure 5A, 5B**) nm and 80-130 (**Figure 6A, 6B**) nm respectively after 24 h of incubation. Since, formation of fibrillar nanostructures is often initialized by formation of spheroidal assemblies, the solution of **QP3** and **QP4** were further incubated for another 24 h and AFM experiment was performed. After a total of 48 h of incubation, it was observed that **QP3** produced nano-belt like self-assembled structures along with some spherical assemblies (**Figure 5C**). These nano-belts were mostly straight and wide in nature having average width of 120-190 nm and lengths of several microns. Some of them were seen to stack with other nano-belts to give even wider nanostructures. FESEM images of **QP3** xerogel (**Figure 5F**) reconfirmed the production of highly

dense network of numerous numbers of nano-belts having average diameter of 150-210 nm. **QP4** even after 48 hours of incubation maintained its spherical morphology although the size (120-190 nm) of the nano-spheres thus produced by **QP4** was increased to some extent after 48 h of incubation (**Figure 6C, 6D**). The inability of **QP4** to form fibrillar or any other higher order morphology may be associated with higher solubility of **QP4** in water and PBS buffer.

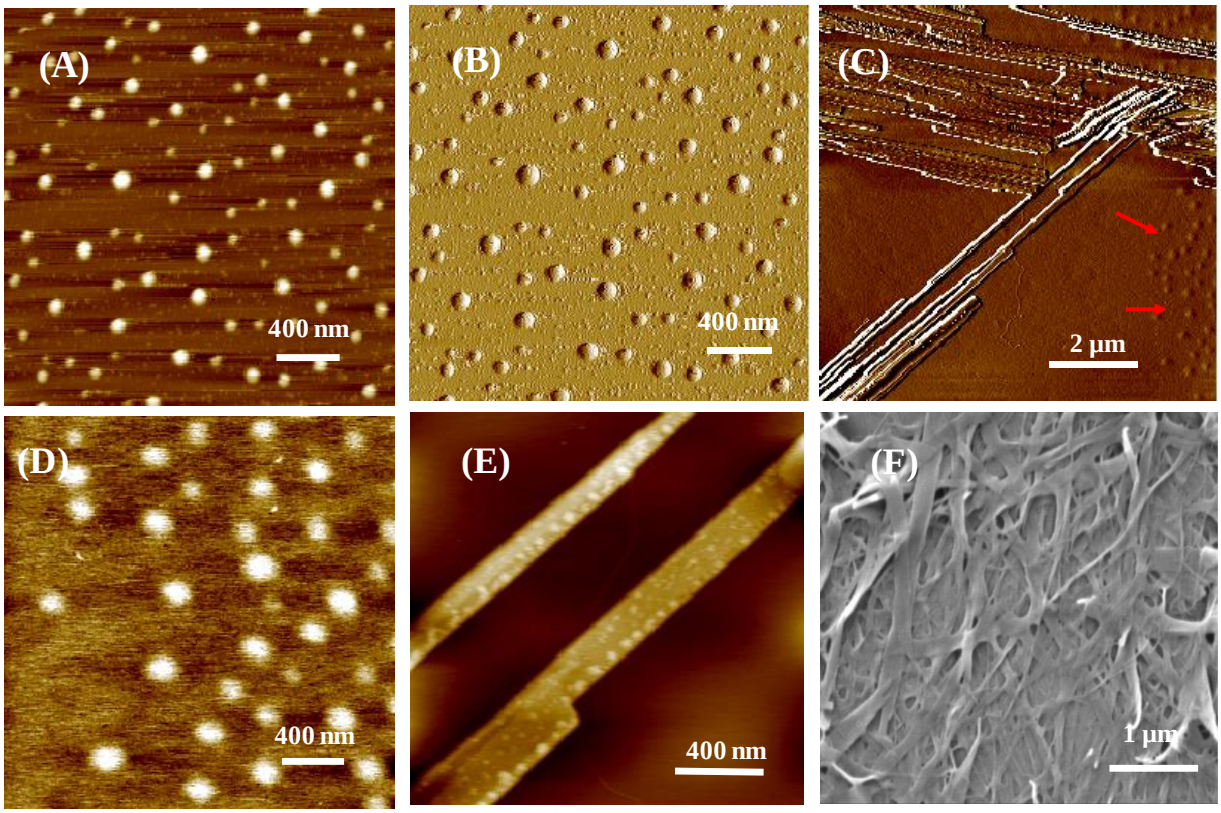

Figure 5. *(A) Atomic force microscopy (AFM) images of spherical aggregates produced by QP3 in 1% DMSO-PBS after incubation for 24h at RT (25^{0}C), (B) amplitude image of A. (C) Formation of nano-belt along with nanospheres as indicated by red arrows after 48 h of incubation of QP3. (D) Higher magnification view of spherical assemblies obtained from image C and (E) Higher magnification view of nano-belts as obtained from image C. (F) FESEM image of the dense network of numerous nano-belts produced by QP3.*

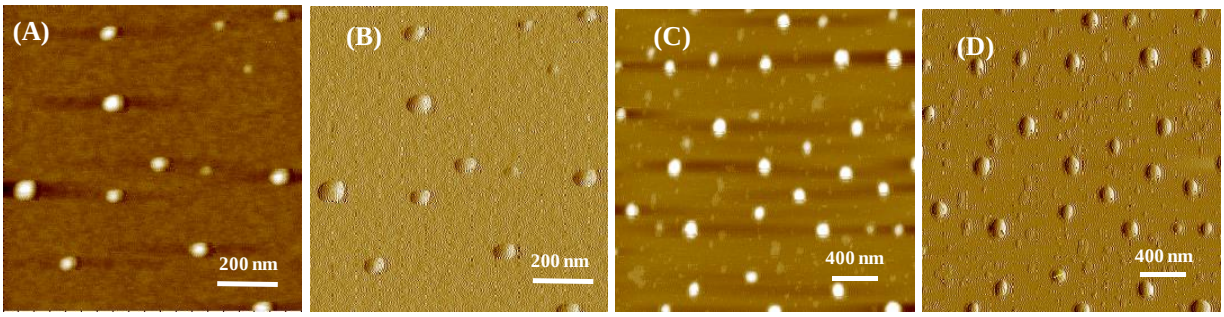

Figure 6. *Atomic Force microscopy images of spherical assemblies produced by QP4 in 1% DMSO-PBS solvent system (A) after 24 h of incubation, (B) amplitude image of A. (C) Bigger size spherical aggregates produced by QP4 after 48 h of incubation, (D) amplitude image of C.*

4.3.3 Gelation study of quinazolinone capped peptides

The aromatic capping group of small peptides often contributes to increase the self-assembling propensity of those peptides which in turn induces gelation property. Thus gelation behaviour was also examined for these quinazolinone capped small peptides in various aqueous solvent systems. None of the peptides produced hydrogel from pure water or pure buffer at physiological conditions; **QP1** and **QP3** were insoluble in water, **QP2** was partially soluble and **QP4** which is solid at low temperature but liquid at room temperature (gum like consistency) was completely soluble in water. Thus to initiate gelation first the peptides (5-10 mg) were weighed in small glass vials, solubilized in 10 µl of DMSO by strong heating, and then diluted with PBS buffer (Ph = 7.4). It was observed that for both **QP1** and **QP3** a white suspension was formed which then turned into stable translucent hydrogels 4-8 mins after addition of PBS buffer (**Figure 7**). The formation of gel was confirmed by the 'vial inversion test' where both the gels did not show any gravimetric flow after inversion of the tubes. On the other hand, **QP2** and **QP4** were unable to form hydrogel even after 24 h. **QP2** remained as white sol whereas **QP4** produced completely clear solutions. These results suggested that the free terminal –COOH group in **QP2** and $–NH_2$ group in **QP4** might increase the solubility of these peptides in water

due to which these peptides were unable to form hydrogels. Likewise, in **QP1** and **QP3** the terminal –COOH group was methyl protected and $–NH_2$ group was BOC protected respectively which helped **QP1** and **QP3** to maintain a balance between overall hydrophobicity and hydrophilicity of these peptides which in turn resulted in hydrogels. It is notable here that **QP2** after 3 days formed

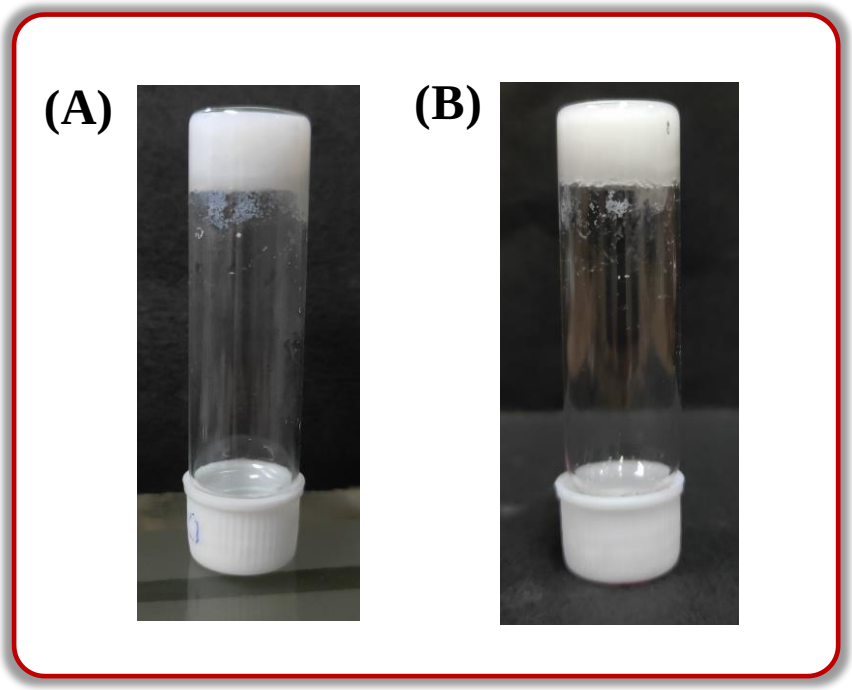

Figure 7. *Images of vial inversion test of hydrogels obtained from (A) QP1 and (B) QP3 in 1% DMSO-PBS solvent system.*

opaque hydrogel which was confirmed by tube inversion test but unfortunately it failed to survive under mechanical pressure during rheological tests later on. While kept undisturbed **QP2** hydrogel was also unable to maintain its gel structure for long and resulted in loose gel formation by releasing solvent from its gel network. The minimum gelation concentration (MGC) of **QP1** and **QP3** was found to be 0.70 % (w/v) and 0.59 % (w/v) respectively and both the hydrogels are thermoreversible in nature. The sol-to-gel transition temperature

or T_{gel} for **QP1** was calculated as 75 ^{o}C and that of **QP3** was found to be 78 ^{o}C. Both the hydrogels were seen to exhibit an intriguing viscoelastic property, thixotropy which was later confirmed by rheological experiments.

4.3.4 Rheological study

To measure the strength and other viscoelastic properties of the hydrogels obtained from **QP1** and **QP3** in 1% DMSO-PBS buffer solvent system rheological experiments were performed using an Antor Paar Compact Modular Rheometer (MCR 102). PP25 was used as the measuring system and a well-controlled system inside the instrument assured a constant temperature of 25℃ during all the rheological experiments.

The fundamental mechanical properties of a gel can be expressed through two main rheological experiments such as – amplitude/strain sweep, and frequency sweep experiments. These experiments represent the flow behaviour and viscoelastic properties of a gel. The hydrogels obtained **QP1** and **QP2** in 1% DMSO-PBS solvent system were investigated using strain sweep and frequency sweep experiments. The result obtained from the strain sweep test (**Figure 8A, 8B**) of both the peptides demonstrated the linear viscoelastic range (LVE) and the dependence of G′ and G″ on strain amplitude. G′ was linear with G″ up to a critical strain of 6.63 % and 11.91 % for **QP1** and **QP3** respectively, beyond this critical strain value G′ declined. Next, with these hydrogels frequency sweep experiments were performed at a constant strain of 0.5 % to monitor the storage modulus (G′) and the loss modulus (G″) as a function of applied angular frequency. It is evident from **Figures 8C** and **8D** that G′ was higher than G″ and no cross-over point was noticed within the experimental frequency regions (0.1-100 rad/s) for both the gels. For **QP1** hydrogel, G′ was an order of magnitude (~20 times) greater than G″, and for **QP3** G′ was almost 13 times greater than G″ at a constant shear strain of

0.5%. These results suggested the presence of soft 'solid-like' gel phase material and also these were mechanically quite stable.

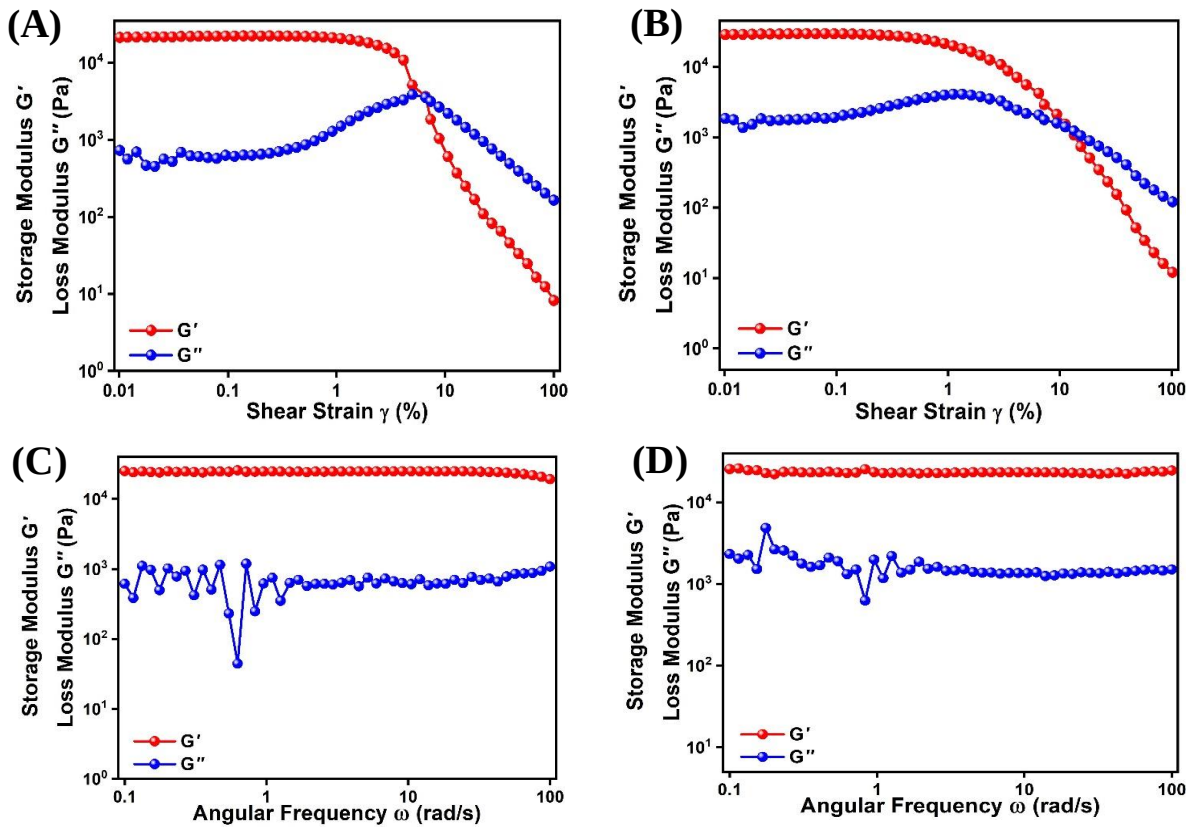

Figure 8. *Strain sweep test of hydrogel obtained from (A) QP1, (B) QP3; and frequency sweep test of hydrogels obtained from (C) QP1, (D) QP3.*

The gel obtained from **QP2** was also subjected to rheological experiments. It was observed during the strain sweep experiment that the gel could not bare the applied strain even in the lower range and started to rupture leaving behind the solvent from the gel network. Thus **QP2** could not be considered a true gel although it qualified for the 'tube inversion test'.

The thixotropic property of these hydrogels was further investigated by time sweep rheological experiments i.e. sequential application of low and high strains, separated by enough time to ensure the complete gel-to-sol (G′ > G″) and sol-to-gel (G″ > G′) conversions (**Figure 9**). This sol-gel interconversion

was performed repeatedly for seven consecutive steps. Thixotropy is a property of some of the non-Newtonian pseudoplastic fluids (e.g; gels) which refers to an isothermal gel-to-sol and sol-to-gel reversible transition in which the gel state is transformed into the sol state upon the application of specific external stimuli such mechanical shaking, agitation, etc. and returns to the gel state upon resting.

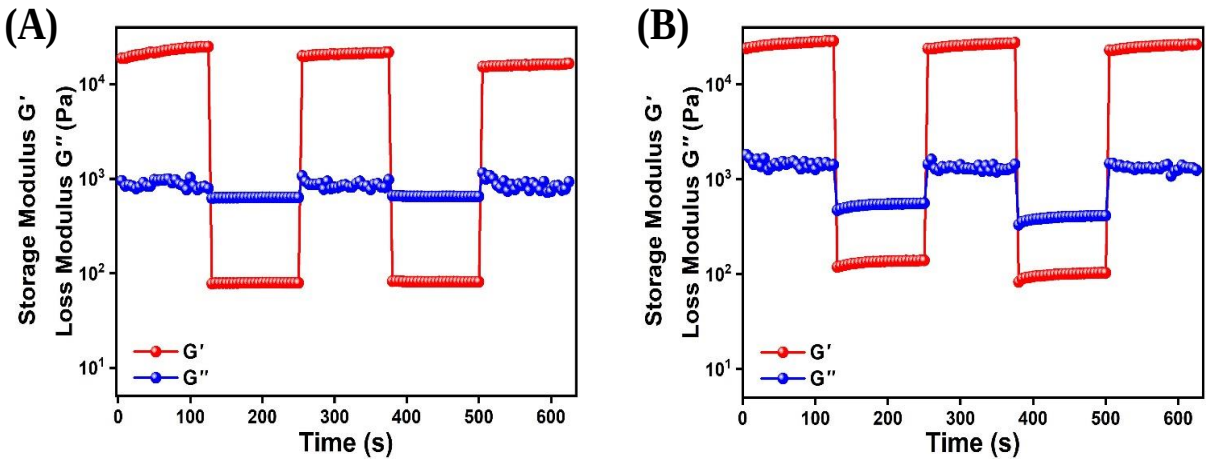

Figure 9. *Time sweep test of hydrogels obtained from (A) QP1 and (B) QP3 at a constant angular frequency of 10 rad/s.*

Low shear strain was used to begin the time sweep experiment in its initial phase. By applying significant strain in the second step, the gel was entirely broken and changed into a quasi-liquid condition (sol), as shown by the modulus values (G′, G″). The recovery of the gel was observed in the third stage using a time sweep experiment with the same strain value as in step 1 and modulus values that support the reformation of the gel (G′ > G″). The gel was once more ruptured with high strain at step four, then it was repaired with mild strain at step five. At one specific location, trials for each gel system were carried out. These observations collectively demonstrate the thixotropic and self-healing character of gel materials.

4.3.5 FT-IR analysis

To gain information about structural arrangement of the synthesized peptide molecules in their respective self-assembled network as well as the forces involved in the process of self-assembly is very crucial. Hydrogen bonding is one of the weak forces that have the biggest impact on how molecules self-assemble. Because of this, different hydrogen-bonding patterns are very important in regulating the secondary structure of peptide self-assembly. Since the amide backbone present in these peptides mostly determines the secondary structure adopted by these molecules after self-assembly, FT-IR spectroscopy can be used to determine the contribution of the amide groups to the self-assembly process effectively.

The Fourier transform infrared (FT-IR) spectra of the samples in solid and gel states were recorded on a Bruker TENSOR 27 spectrometer using the attenuated total reflection (ATR) technique. The spectra were scanned from 600 to 4000 cm^{-1}. Bruker software was used for data processing and experimental data obtained were analyzed using Origin Pro 8.0 SRO software (Origin Lab Corporation).

Fourier Transform Infrared spectroscopy was used to characterize the secondary conformation acquired by the hybrid peptides in solid state as well as in gel state. From solid state FT-IR spectrum of all four peptides, a wide range of vibrational bands were observed due to the presence of different functional groups for example -CONH, -$COOCH_3$, -NH_2, -NHBOC, aromatic groups, and aliphatic groups (-CH_3, -CH_2), etc. Important band positions obtained from the solid state FTIR spectrum of the peptides were marked in their respective spectrum (Figure S). Generally, in FT-IR spectrum, characteristic amide I, amide II, and amide III bands mainly originating from backbone vibrations appeared at 1600-1690 cm^{-1}, 1480-1580 cm^{-1}, and 1230-1300 cm^{-1} respectively. The origin of amide I mode of vibration is due to >C=O stretching vibration and the amide II and amide III bands

correspond to the coupling of C-N stretching and N-H in-plane bending. For **QP1** (**Figure 10A**). characteristic amide bands appeared at 1665 cm^{-1} and 1608 cm^{-1} along with a hump at 1687 cm^{-1}. The band that appeared at 1734 cm^{-1} corresponds to the carbonyl of terminal ester group. Moreover, there are many reports where it was mentioned that peptides having inclination towards antiparallel β-sheet conformation, give two characteristic bands around 1645-1665 cm^{-1} and the other one is between 1680-1700 cm^{-1} in the FT-IR region. The appearance of two amides I bands at 1665 and 1687 cm^{-1} indicated the presence of an antiparallel β-sheet secondary structure in the solid state of **QP1**. In gel state of **QP1,** the amide carbonyl band shifted to a lower frequency and appeared at 1658 cm^{-1} along with two other peaks at 1612 cm^{-1} and 1687 cm^{-1}. The shifting of amide I band from 1665 cm^{-1} in solid state to 1658 cm^{-1} in gel state indicated weakening of amide carbonyl bond due to involvement of the carbonyl bond in extensive intermolecular hydrogen bonding with the solvent and other peptide molecules. Reappearance of amide I band at 1687 cm^{-1} indicated the formation of antiparallel β-sheet secondary structure in the gel state of **QP1** (**Figure 10A**). Although **QP2** formed only loose gel after long incubation, FTIR spectra were also acquired with that loose gel obtained from **QP2** in 1% DMSO-PBS. For **QP2**, the shifting of amide carbonyl stretching frequency from 1665 and 1614 cm^{-1} in solid state to 1654 cm^{-1} and 1611 cm^{-1} in loose gel state indicated presence of greater extent of intermolecular hydrogen bonding in the gel state (**Figure 10B**). . Presence of another weaker transition at 1686 cm^{-1} both in solid and gel state of **QP2** suggested that the peptide molecules were arranged in antiparallel β-sheet fashion in their extended structures. Therefore, from the FTIR study, it can be said that the fibrillar network formed by **QP1** and **QP2** in 1% DMSO-PBS resulted from the β-sheet arrangements of the respective molecules in aqueous solution. In case of **QP3**, the characteristic amide I bands appeared at 1659 and 1606 cm^{-1} in its solid state and the band appeared at 1520 cm^{-1} corresponds to the amide II band. No significant shifting of the characteristics amide bands were observed and the band in the

region 1680-1690 cm^{-1} (**Figure 10C**) which corresponds to antiparallel nature β-sheet structure was also not distinct. This fact suggested that **QP3** may acquired a parallel β-sheet structure which resulted in sheet like nano-belt morphology. Moreover, the amide –NH band for all four peptides appeared in range between 3298-3329 cm^{-1} and none of them appeared above the region of 3400 cm^{-1} indicating the involvement of all these peptides in extensive intermolecular hydrogen bonding.

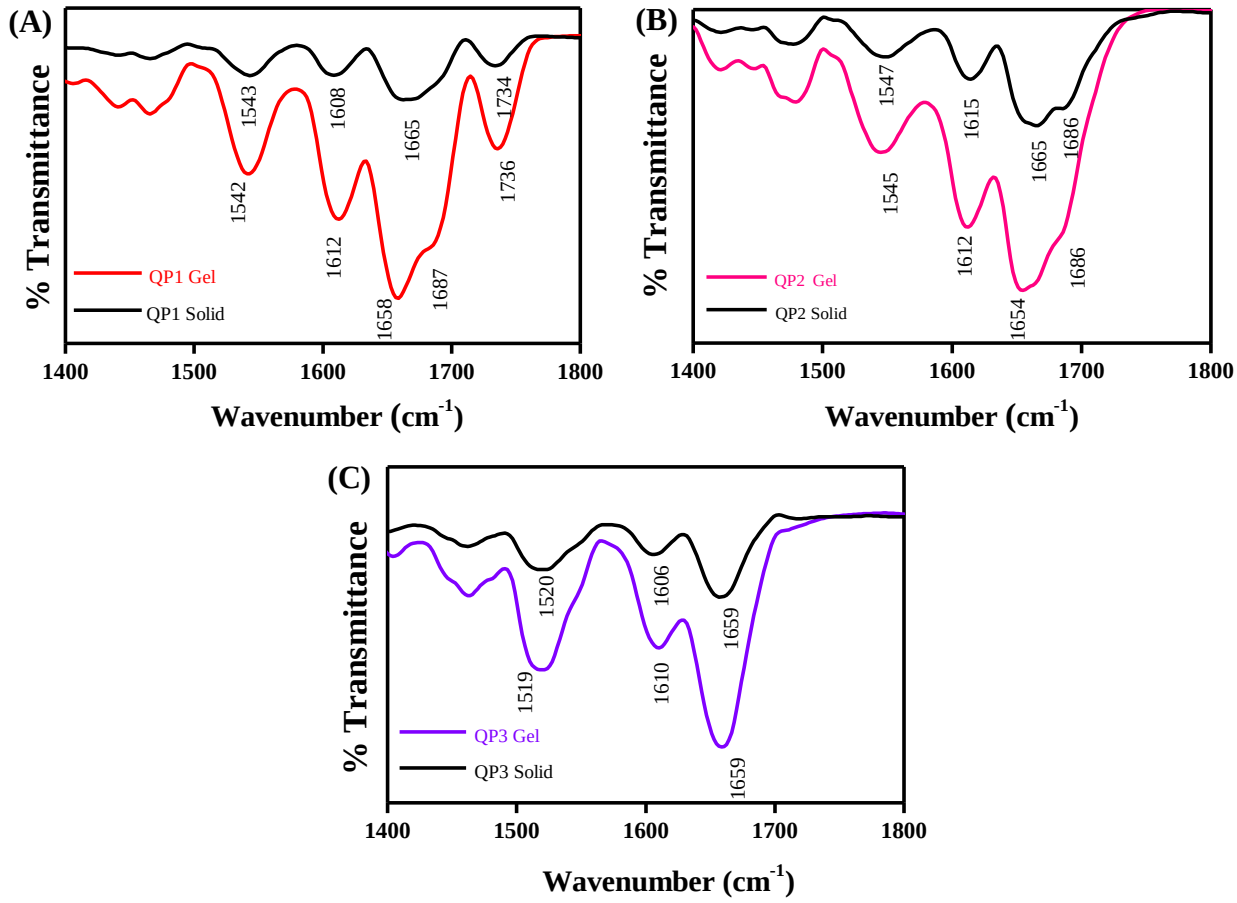

Figure 10. *FTIR spectra of (A) QP1, (B) QP2, and (C) QP3 in solid and gel states.*

4.3.6 Crystallographic Study

The structure of the molecules and their self-assembly process can be understood using crystallographic study. The compounds **QP1** and **QP3** were crystallized in quality crystals which were characterized with the help of single

crystal X-ray crystallography. It is interesting to note that both the compounds were crystallized with monoclinic unit cell and P1 21 1 space group. Compound **QP1-QP4** contains two different sets of structures having quinazolinone moiety. Therefore, this crystallographic similarities of the representative molecules of each set indicated the similarity of the interactions in their solid state. In the case of **QP1**, the amide –NH of one peptide molecule formed hydrogen bond with amide C=O of another adjacent peptide molecule which produced a long one-dimensional β-sheet like structure (**Figure 11**). Such formation was stabilized through π-π stacking, π…alky, and CH…O=C interactions. Here, one β-sheet like structure interacted with another one through facing ester groups with each other by CH…O=C interaction.

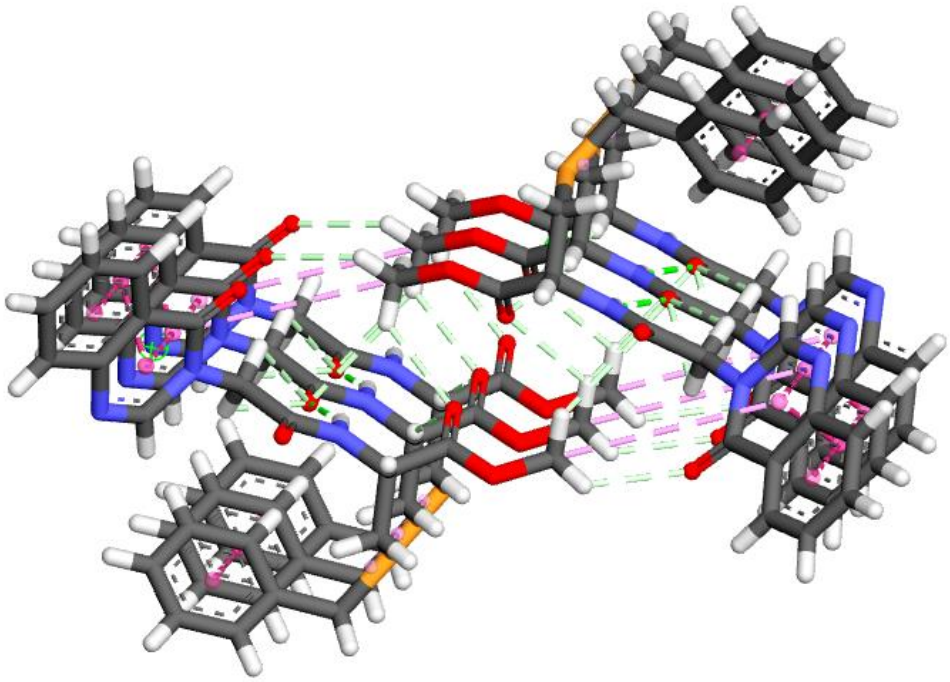

Figure 11. *Network of noncovalent interactions in the β-sheet structure QP1.*

In case of **QP3**, BOC amide, and peptide amide are involved in hydrogen bonding with the same functionality of adjacent molecules (**Figure 12A**). Moreover, π-π stacking, π…alkyl, S…π, and CH…O=C are the key interactions

to construct β-sheet like structure in the solid state self-assembly. Such two infinitely large β-sheet like structures can further assemble to build complex assembly (**Figure 12B**). Here, aforesaid assembly was formed through CH…O=C interactions. Therefore, the remaining two molecules can also utilize same mechanism to produce their self-assembled structures.

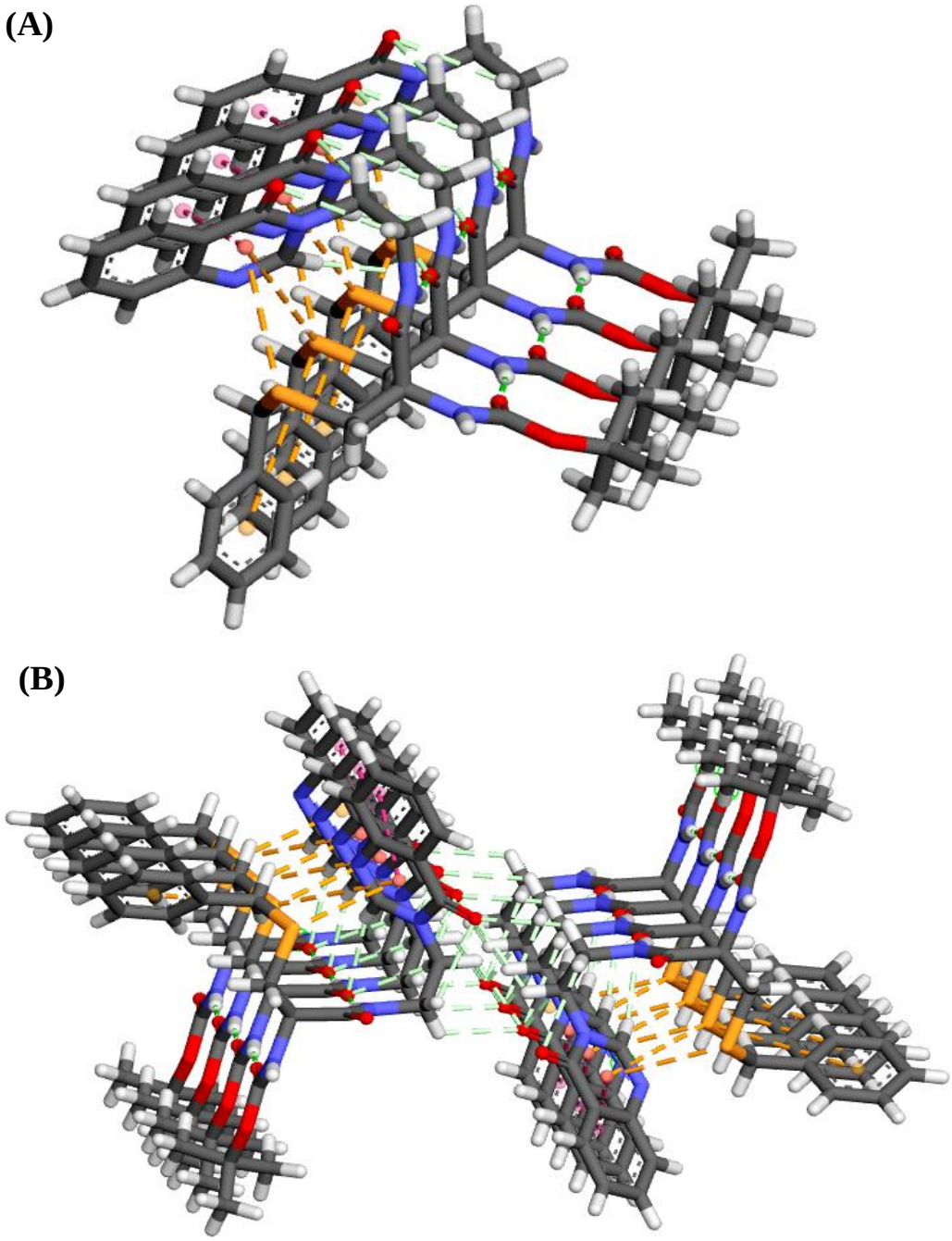

Figure 12. *(A) Network of noncovalent interactions in the extended structure of QP3 and (B) interactions between two adjacent extended units of QP3.*

4.3.7 Cytotoxicity Study

To check biocompatibility and practical applicability of the quinazolinone capped peptides (**QP1-QP4**), cytotoxicity was checked via MTT assay on human cervical cancer cell line (HeLa). Cells were acquired from the National Centre for Cell Science, Pune, India, and was used in the study. Cells were cultured in Iscove's modified Dulbecco's medium (IMDM), supplemented with 10% fetal calf serum and 1% antibiotic, antimycotic solution and maintained at 37 °C under 5% CO2 and 95% air. For the assay, HeLa cells (1×10^4 cells/well) were seeded in 96-well plates. The synthesized peptides (**QP1-QP4**) were added to the wells to various final concentrations (10, 25, 50 and 100 μM). Cells were incubated in presence of these molecules for 24 h at 37 °C. Following treatment, 3-(4,5-dimethylthiazol-2-yl)-2,5-diphenyl tetrazolium bromide (MTT) solution (100 μg/well, dissolved in medium) was added to each well of the 96-well plate, and further incubated at 37 °C for 3 h for formazan crystal formation. Medium was carefully removed from the wells, 200 μl of DMSO was added to dissolve the crystals and intensity of developing colour was measured by a plate reader at 550 nm. Experiments were performed in triplicate and the relative cell viability (%) was expressed as a percentage relative to the untreated control cells.

Treatment of the HeLa cancer cells with quinazolinone capped peptides having varying concentrations of 0, 10, 25, 50, and 100 μM for 24 h revealed no significant cancer cell death, even upto concentration of 50 μM. For each peptide the percentage of cell survivability ranged between 65% to 80% at 50 μM concentration (**Figure 13**) and at a higher concentration, i.e., after 60 μM showed a negligible rise of cell death in Hela cell line (**Figure 13**). **QP1**, **QP2**, and **QP4** reached their IC_{50} when half of the total cell death occurred at conecentrations of almost 82 μM, 93 μM, and 87 μM respectively. **QP3** could not attaine its IC_{50} value even after treatment with 100 μM concentration of

QP3. Thus such high IC_{50} values of all peptides suggested that **QP1-QP4** do not induce any acute cytotoxic effects in the cells, which provides new opportunities for the safe application in biomedical field.

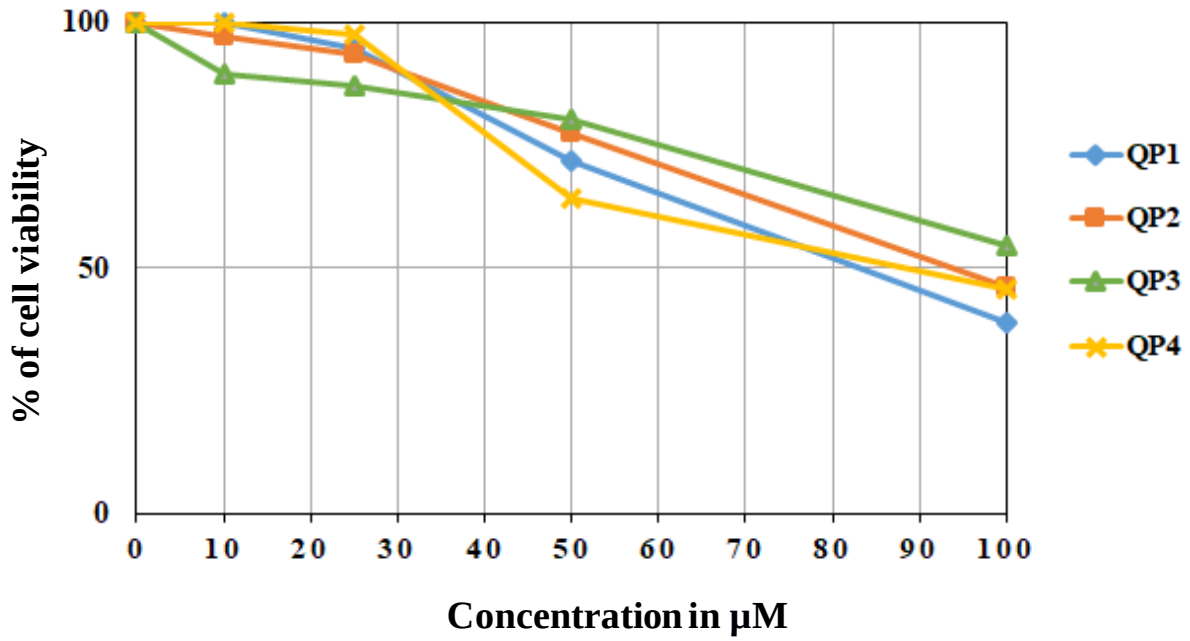

Figure 13. *Growth inhibitory effect of quinazolinone capped peptides (QP1-QP4) on HeLa cells, at concentrations ranging between (0-100) µM.*

4.4 CONCLUSION

In conclusion, two sets of quinazolinone capped S-benzyl-L-cysteine based hybrid peptides were designed and synthesized in three to four simple chemical reaction steps. These peptides exhibited distinct morphological patterns in their self-assembled nanostructures. Small twists in the molecular structure of these peptides brought about the differences in their morphology. Compounds of the first set i.e. **QP1** and **QP2** formed highly cross-linked nanofibrillar assemblies whereas compounds of another set (**QP3** and **QP4**) formed nanospherical self-assembly in 1% DMSO-PBS solvent system. **QP1** and **QP3** formed hydrogels in 1% DMSO-PBS solvent with MGC 0.70% (w/v) and 0.59 % (w/v)

respectively. These gels were thermoreversible in nature, mechanically stable for weeks, and showed thixotropic properties. The solid state crystallographic analysis of the crystals obtained from **QP1** and **QP3** suggested that **QP1** exhibited β-sheet structure in the crystalline state which is stabilized through π-π stacking, π…alky, and CH…O=C interactions which may be responsible for fibril formation. Along with π-π stacking, π…alkyl and CH…O=C interactions one more key interaction which is responsible for construction of β-sheet like structure in the solid state self-assembly of **QP3** was S…π interaction. FT-IR analysis also revealed presence of intermolecular hydrogen bonded b-sheet secondary structure in these peptides which corroborated well with single crystal X-ray crystallographic results. Thus the overall study on quinazolinone capped cysteine based peptides gave a glimpse of different secondary structures adopted by these small peptides. The improvisation of tuning factors like use of quinazolinone as capping group, and reversal of amide bond sequence help to adopt two completely different nano-architectures which is rare in the literature. Moreover, biocompatibility of peptide self-assembled nano-architectures and nanomaterials makes them valuable for applications in biomedical and biotechnological fields.

4.5 FUTURE SCOPE

Heterocyclic capping groups were often used by many researchers in order to improve gelation propensity of short peptide molecules. Choosing correct capping moiety to get a desired nano morphology for a particular application is very crucial. There are lots of examples where researchers have used carbazole, imidazole, benzimidazole, indole, etc. as capping groups of short peptide sequences which formed a variety of nanostructures and served different applications. In this work, quinazolinone was used as capping group which is the first such example so far thus there are lot of scopes to further explore the effect of this capping group in self-assembly as well as in gelation process.

Many of the heterocyclic capped short peptides reportedly showed antibacterial or antimicrobial properties. Since quinazolinone moiety itself have some antibacterial properties, there may be chances for these peptides to exhibit antibacterial activities. Again these peptides have no significant cytotoxicity upto concentrations as high as 100 μM against HeLa cells which makes these peptides even more suitable for cellular application. Short peptide based nanostructures were often seen to inhibit amyloid fibril formation which is the main factor behind many neurodegenerative diseases like Alzheimer, Perkinson's disease, etc. Thus use of these peptides in a-synuclein aggregation inhibition is also included in future plans.

4.6 EXPERIMENTAL PROCEDURES AND SPECTRAL DATA

4.6.1 Procedure for Synthesis of Intermediate 1c:

To a solution of 2-aminobenzoic acids (**1a**; 10.0 mmol, 1.0 equiv.) in trimethylorthoformate (TMOF; 15.0 mmol, 1.5 equiv.), glycine methylester hydrochloride (**1b**; 12.0 mmol, 1.2 equiv.), and *p*-toluene sulfonic acid (PTSA; 5 mol %) were added and stirred under reflux for 6 h in an oil bath maintaining 120 ^{o}C temperature. After completion of the reaction as indicated by TLC, the reaction contents were condensed under reduced pressure and the organic part was extracted from water using ethyl acetate (25 ml x 3 times). The organic part was then dried over anhydrous sodium sulfate and after removing the solvent at reduced pressure the crude product was purified in column chromatography using 100-200 mesh silica gel and 40% ethyl acetate in hexane eluent. The product was obtained as white solid, yield = 81%.

4.6.2 Procedure for Synthesis of Intermediate 1d

To a well-stirred solution of **1c** (10 mmol, 1 equiv) dissolved in methanol, THF, and water in 1:1:1 ratio, was added lithium hydroxide (5 equiv) and the reaction mixture was stirred for 6 hrs. After completion of the reaction as confirmed by TLC, the crude mixture was concentrated by removing the organic solvents under reduced pressure. Then the crude was dissolved in water and neutralized by 1N citric acid solution. The product was then collected from water by ethyl acetate (3 x 20 ml) and dried over anhydrous Na_2SO4. After evaporation of the solvent, the crude product obtained was purified by column chromatography using 100-200 mesh silica gel and methanol-dichloromethane as eluent. The product was obtained as a white solid (yield = 72%).

4.6.3 Procedure for Synthesis of QP1

To a well-stirred solution of **1d** (600 mg, 2.16 mmol) dissolved in *N*,*N*-dimethylformamide (10 ml), was added anhydrous hydroxybenzotriazole (HOBT; 350 mg, 2.59 mmol) slowly followed by 1-ethyl-3,3-(dimethylamino) propyl carbodiimide hydrochloride (EDC·HCl; 622 g, 3.24 mmol) at 0 ^{o}C under nitrogen atmosphere. Then stirring was continued for 10 mins at ice-cooled condition and after that to this mixture, triethylamine (TEA; 1.5 ml, 10.8 mmol) was added followed by S-benzyl-L-cysteine methyl ester hydrochloride (**1e**; 679 mg, 2.59 mmol). The reaction was further continued for 8 h at room temperature (monitoring via TLC). The reaction mixture was then concentrated under reduced pressure and extracted with ethyl acetate (3 × 20 ml). Evaporation of solvent left a crude residue, which was purified by column chromatography over 60-120 mesh silica gel (hexane/ethyl acetate 70:30) to afford the compound '**QP1**' as white solid (yield = 74%).

^{1}H NMR of QP1 (600 MHz, DMSO-d_6): δ (in ppm) 8.98 (d, *J* = 7.8 Hz, 1H), 8.30 (s, 1H), 8.14 (d, *J* = 6.9 Hz, 1H), 7.85 (t, *J* = 7.7 Hz, 1H), 7.70 (d, *J* = 8.0

Hz, 1H), 7.56 (t, *J* = 7.6 Hz, 1H), 7.32 (d, *J* = 4.3 Hz, 4H), 7.24 (dt, *J* = 8.6, 4.4 Hz, 1H), 4.75 (s, 2H), 4.59 – 4.53 (m, 1H), 3.78 (s, 2H), 3.65 (s, 3H), 2.80 (dd, *J* = 13.8, 5.7 Hz, 1H), 2.72 (dd, *J* = 13.8, 7.7 Hz, 1H).

^{13}C NMR of QP1 (150 MHz, DMSO-d_6) δ (in ppm) 166.94, 148.58, 138.05, 134.48, 128.97, 128.42, 127.24, 126.96, 126.05, 52.22, 47.66, 35.37, 32.20.

HRMS (**ESI-MS):** m/z calculated for $C_{21}H_{21}N_3O_4S$ $[M+H]^+$ = 412.1331; found m/z = 412.1328.

4.6.4 Procedure for Synthesis of QP2

To a well-stirred solution of **QP1** (4 mmol, 1 equiv) dissolved in methanol, THF, and water in 1:1:1 ratio, was added lithium hydroxide (5 equiv) and the reaction mixture was stirred for 6 hrs. After completion of the reaction as confirmed by TLC, the crude mixture was concentrated by removing the organic solvents under reduced pressure. Then the crude was dissolved in water and neutralized by 1N citric acid solution. The product was then collected from water by ethyl acetate (3 x 20 ml) and dried over anhydrous Na_2SO_4. After evaporation of the solvent, the crude product obtained was purified by column chromatography using 100-200 mesh silica gel and methanol/dichloromethane (2:98) as eluent. The product was obtained as white solid, yield = 68%.

^{1}H NMR of QP2 (600 MHz, DMSO-d_6): δ (in ppm) 8.83 (d, *J* = 8.0 Hz, 1H), 8.29 (s, 1H), 8.14 (d, *J* = 7.9 Hz, 1H), 7.85 (t, *J* = 8.1 Hz, 1H), 7.70 (d, *J* = 8.1 Hz, 1H), 7.56 (t, *J* = 7.5 Hz, 1H), 7.31 (d, *J* = 6.8 Hz, 4H), 7.24 (t, *J* = 6.5 Hz, 1H), 4.76 (s, 2H), 4.50 (t, *J* = 7.6 Hz, 1H), 3.79 (s, 2H), 2.81 (dd, *J* = 13.7, 5.2 Hz, 1H), 2.71 (dd, *J* = 13.7, 7.7 Hz, 1H).

^{13}C NMR (150 MHz, DMSO-d_6): δ (in ppm) 171.73, 166.80, 160.13, 148.61, 148.06, 138.21, 134.45, 128.96, 128.38, 127.22, 127.07, 126.89, 126.05, 121.48, 52.22, 47.68, 35.49, 32.53.

HRMS (**ESI-MS):** m/z calculated for $C_{20}H_{19}N_3O_4S$ $[M+H]^+$ = 398.1175; found m/z = 398.1172.

4.6.5 Procedure for Synthesis of Intermediate 2c

To a solution of 2-aminobenzoic acids (1a; 30.0 mmol, 1.0 equiv.) in trimethylorthoformate (TMOF; 45.0 mmol, 1.5 equiv.), N-Boc-1,2-diaminoethane (**2b**; 36.0 mmol, 1.2 equiv.), and *p*-toluenesulfonic acid (PTSA; 5 mol %) were added and stirred under reflux for 6 h in an oil bath maintaining 120 ^oC temperature. After completion of the reaction as indicated by TLC, the reaction contents were condensed under reduced pressure and the organic part was extracted from water using ethyl acetate (20 ml x 3 times). The organic part was then dried over anhydrous sodium sulphate and after removing the solvent at reduced pressure the crude product was purified in column chromatography using 100-200 mesh silica gel a 40% ethyl acetate in hexane eluent. The product was obtained as white solids (yield = 75%).

4.6.6 Procedure for Synthesis of Intermediate 2d

In the next step, intermediate '**2c**' (700 mg, 1.59 mmol) was treated with trifluoroacetic acid (TFA; 732 µl, 9.58 mmol) in dichloromethane solvent (12 ml) at 0 ^oC. The reaction mixture was slowly brought to room temperature and stirring continued. After 6 h, the completion of the reaction was confirmed via TLC and the reaction mixture was then concentrated under reduced pressure. After evaporation of the solvent, the crude was washed with diethyl ether and dried under reduced pressure to obtain the product as a white solid (yield=60%) and was directly used for the next step.

4.6.7 Procedure for Synthesis of QP3

To a well-stirred solution of **2d** (500 mg, 2.16 mmol) dissolved in *N*,*N*-dimethylformamide (10 ml), was added anhydrous hydroxybenzotriazole

(HOBT; 350 mg, 2.59 mmol) slowly followed by 1-ethyl-3,3-(dimethylamino) propyl carbodiimide hydrochloride (EDC·HCl; 622 g, 3.24 mmol) at 0 °C under nitrogen atmosphere. Then stirring was continued for 10 mins at ice-cooled condition and after that to this mixture, triethylamine (TEA; 1.5 ml, 10.8 mmol) was added followed by N-Boc-S-benzyl-L-cysteine (**2e**; 679 mg, 2.59 mmol). The reaction was further continued for 8 h at room temperature (monitoring via TLC). The reaction mixture was then concentrated under reduced pressure and extracted with ethyl acetate (3 × 20 ml). Evaporation of solvent left a crude residue, which was purified by column chromatography over 60-120 mesh silica gel (hexane/ethyl acetate 70:30) to afford the compound '**QP3**' as white solid (yield = 68%).

^{1}H NMR of QP3 (600 MHz, DMSO-d_6): δ (in ppm) 8.23 (t, *J* = 5.8 Hz, 1H), 8.19 – 8.13 (m, 2H), 7.82 (t, *J* = 7.6 Hz, 1H), 7.66 (d, *J* = 8.1 Hz, 1H), 7.54 (t, *J* = 7.8 Hz, 1H), 7.28 (d, *J* = 2.7 Hz, 4H), 7.25 – 7.19 (m, 1H), 6.95 (d, *J* = 8.3 Hz, 1H), 4.10 – 4.03 (m, 1H), 4.03 – 3.98 (m, 2H), 3.69 (s, 2H), 3.49 (dq, *J* = 11.1, 5.7 Hz, 1H), 3.43 (d, *J* = 5.6 Hz, 1H), 2.66 (dd, *J* = 13.6, 5.4 Hz, 1H), 2.46 (dd, *J* = 13.6, 9.0 Hz, 1H), 1.38 (s, 9H).

^{13}C NMR of QP3 (150 MHz, DMSO-d_6): δ (in ppm) 167.73, 160.50, 148.07, 134.35, 128.91, 128.50, 127.19, 127.09, 127.02, 126.02, 121.61, 51.69, 45.91, 37.50, 35.33, 32.08.

HRMS (**ESI-MS):** m/z calculated for $C_{25}H_{30}N_4O_4S$ $[M+H]^+$ = 483.2066; found m/z = 483.2063.

4.6.8 Procedure for Synthesis of QP4

To a solution of QP3 (700 mg, 1.59 mmol) in dichloromethane solvent (12 ml), trifluoroacetic acid (TFA; 732 µl, 9.58 mmol) was added dropwise at 0 °C. The reaction mixture was slowly brought to room temperature and stirring continued. After 6 h, the completion of the reaction was confirmed by

monitoring TLC and the reaction mixture was then concentrated under reduced pressure. The crude mixture was then neutralized by treating it with 1 (N) sodium bicarbonate solution and extracted with dichloromethane (3 x 20 ml) from the aqueous layer and the product was purified by column chromatography over 60-120 silica gel using dichloromethane/methanol 95:5 as eluent to afford the final product '**QP4**' (yield = 50%) as white solid.

^{1}H NMR of QP4 (600 MHz, DMSO-*d*$_6$): δ (in ppm) 8.76 (t, *J* = 5.9 Hz, 1H), 8.31 (s, 2H), 8.27 (s, 1H), 8.16 (d, *J* = 8.0 Hz, 1H), 7.83 (t, *J* = 7.6 Hz, 1H), 7.68 (d, *J* = 8.1 Hz, 1H), 7.55 (t, *J* = 7.5 Hz, 1H), 7.32 (d, *J* = 6.6 Hz, 4H), 7.28 – 7.23 (m, 1H), 4.16 – 4.08 (m, 1H), 4.06 – 3.99 (m, 1H), 3.89 (t, *J* = 6.7 Hz, 1H), 3.74 (q, *J* = 12.9 Hz, 2H), 3.70 – 3.63 (m, 1H), 3.46 (d, *J* = 9.3 Hz, 1H), 2.83 (dd, *J* = 14.1, 6.0 Hz, 1H), 2.65 (dd, *J* = 14.1, 7.6 Hz, 1H).

^{13}C NMR of QP4 (150 MHz, DMSO-*d*$_6$): δ (in ppm) 167.73, 160.50, 148.07, 134.35, 128.91, 128.50, 127.19, 127.09, 127.02, 126.02, 121.61, 51.69, 45.91, 37.50, 35.33, 32.08.

HRMS (**ESI-MS):** m/z calculated for $C_{20}H_{22}N_4O_2S$ $[M+H]^+$ = 383.1542; found m/z = 383.1539.

^{1}H NMR of QP4 (600 MHz in D$_2$O): δ (in ppm) 8.10 (s, 1H), 7.99 – 7.95 (m, 1H), 7.77 – 7.72 (m, 1H), 7.52 (d, *J* = 8.2 Hz, 1H), 7.47 (t, *J* = 7.6 Hz, 1H), 7.21 – 7.12 (m, 3H), 7.12 – 7.07 (m, 2H), 4.13 – 4.02 (m, 2H), 3.84 – 3.74 (m, 2H), 3.49 (d, *J* = 1.9 Hz, 2H), 3.40 (dt, *J* = 14.6, 5.1 Hz, 1H), 2.62 (qd, *J* = 14.3, 6.7 Hz, 2H).

^{13}C NMR of QP4 (150 MHz, D$_2$O): δ (in ppm) 168.05 , 147.24 , 136.75, 135.02, 128.34, 128.26, 127.73, 127.10, 125.66, 125.60, 120.27, 45.51, 37.44, 34.91, 30.76.

^{1}H and ^{13}C NMR Spectra of Synthesized Peptides

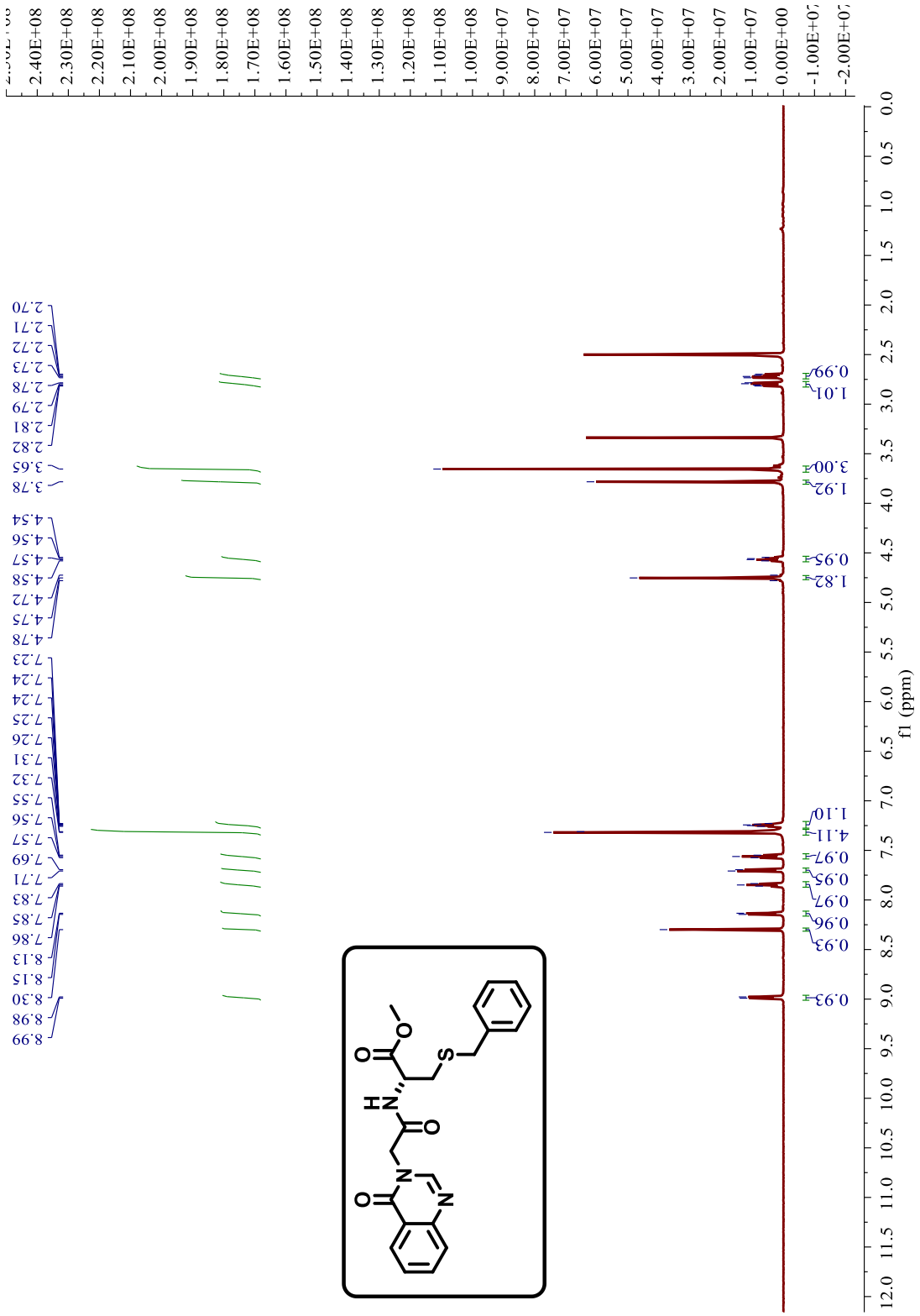

Figure S1. *^{1}H-NMR spectra of QP1 dissolved in DMSO-d_6 solvent.*

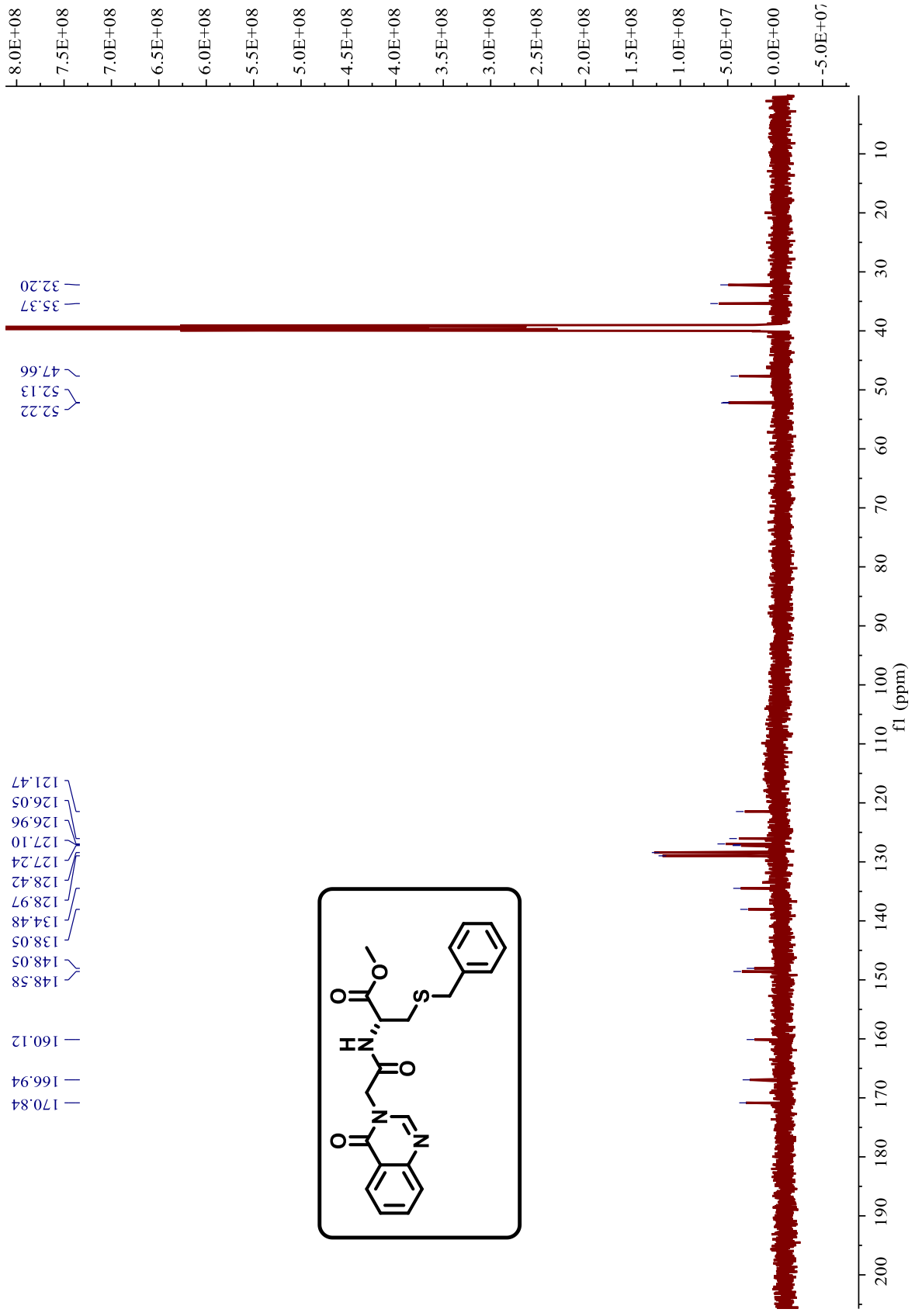

Figure S2. *^{13}C-NMR spectra of QP1 dissolved in DMSO-d_6 solvent.*

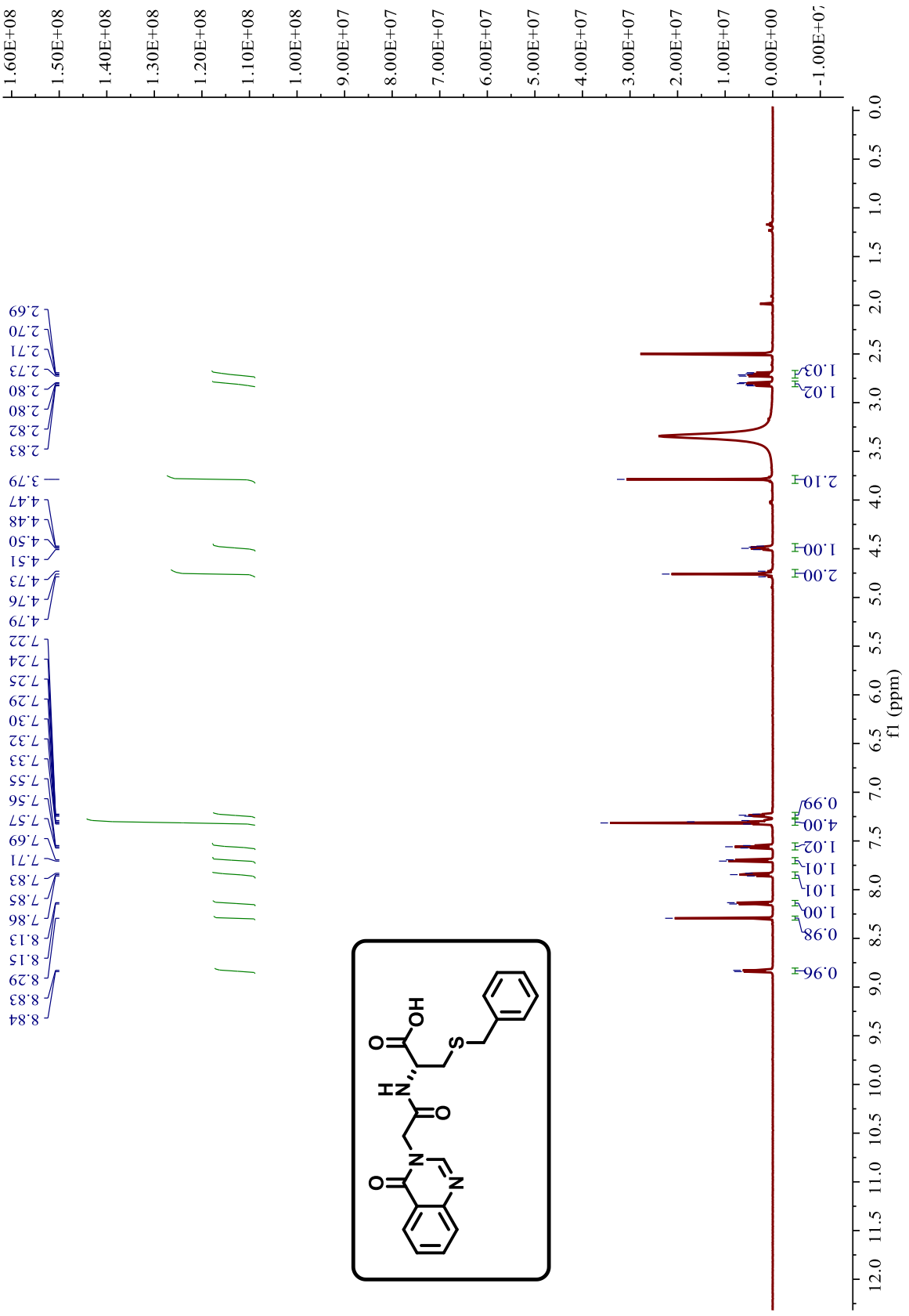

Figure S3. *^{1}H-NMR spectra of QP2 dissolved in DMSO-d_6 solvent.*

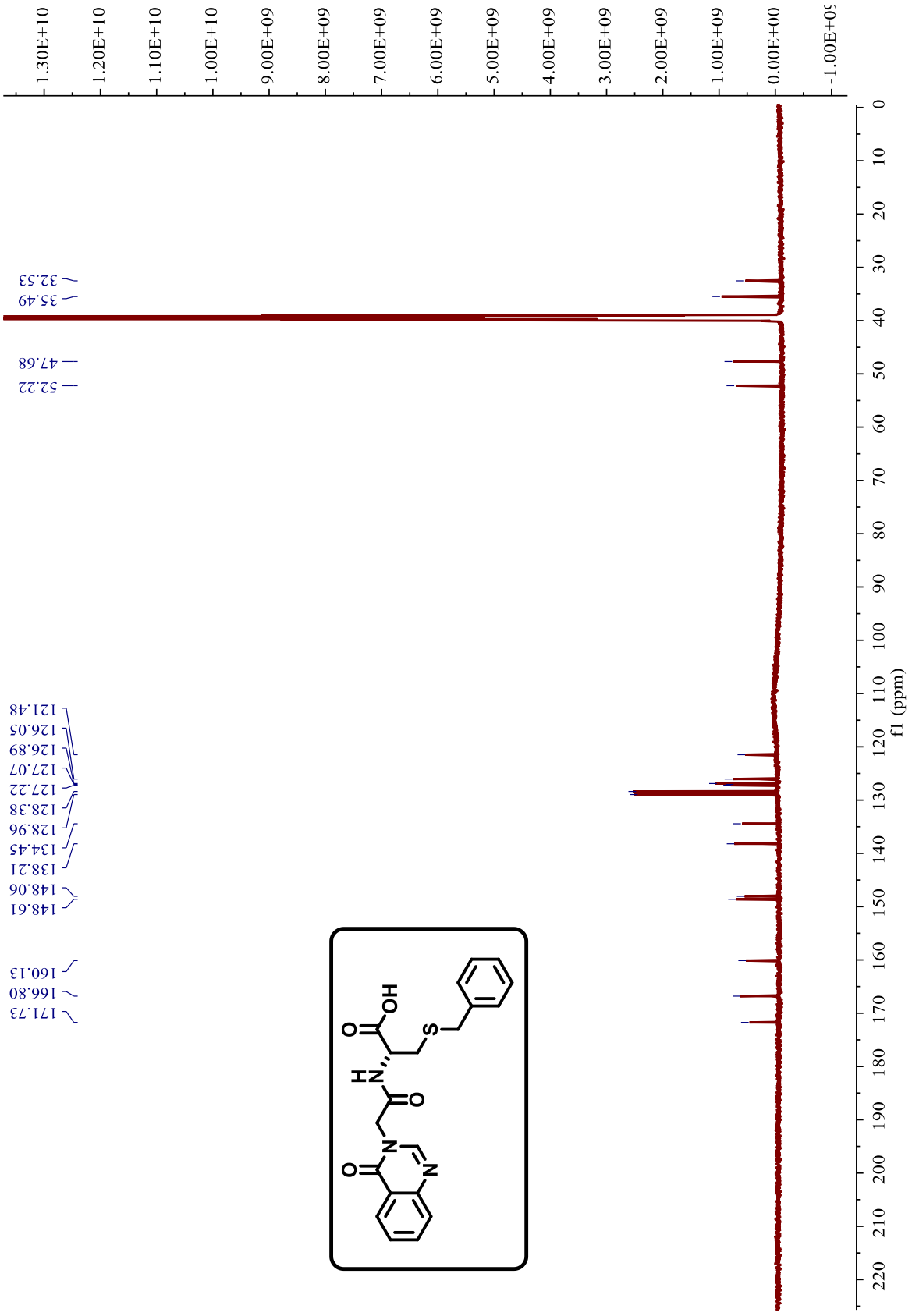

Figure S4. *^{13}C-NMR spectra of QP2 dissolved in DMSO-d_6 solvent.*

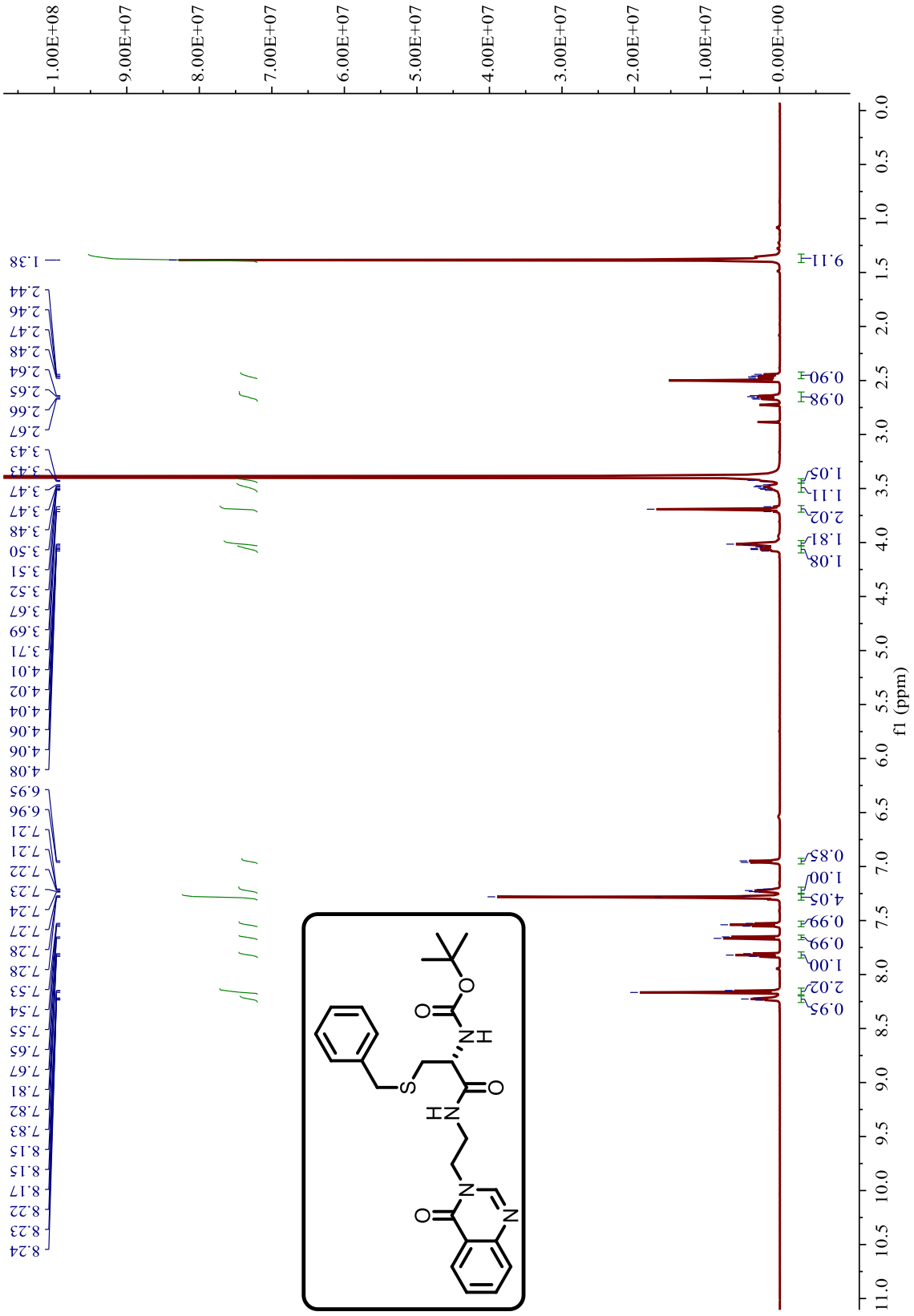

Figure S5. *^{1}H-NMR spectra of QP3 dissolved in DMSO-d_6 solvent.*

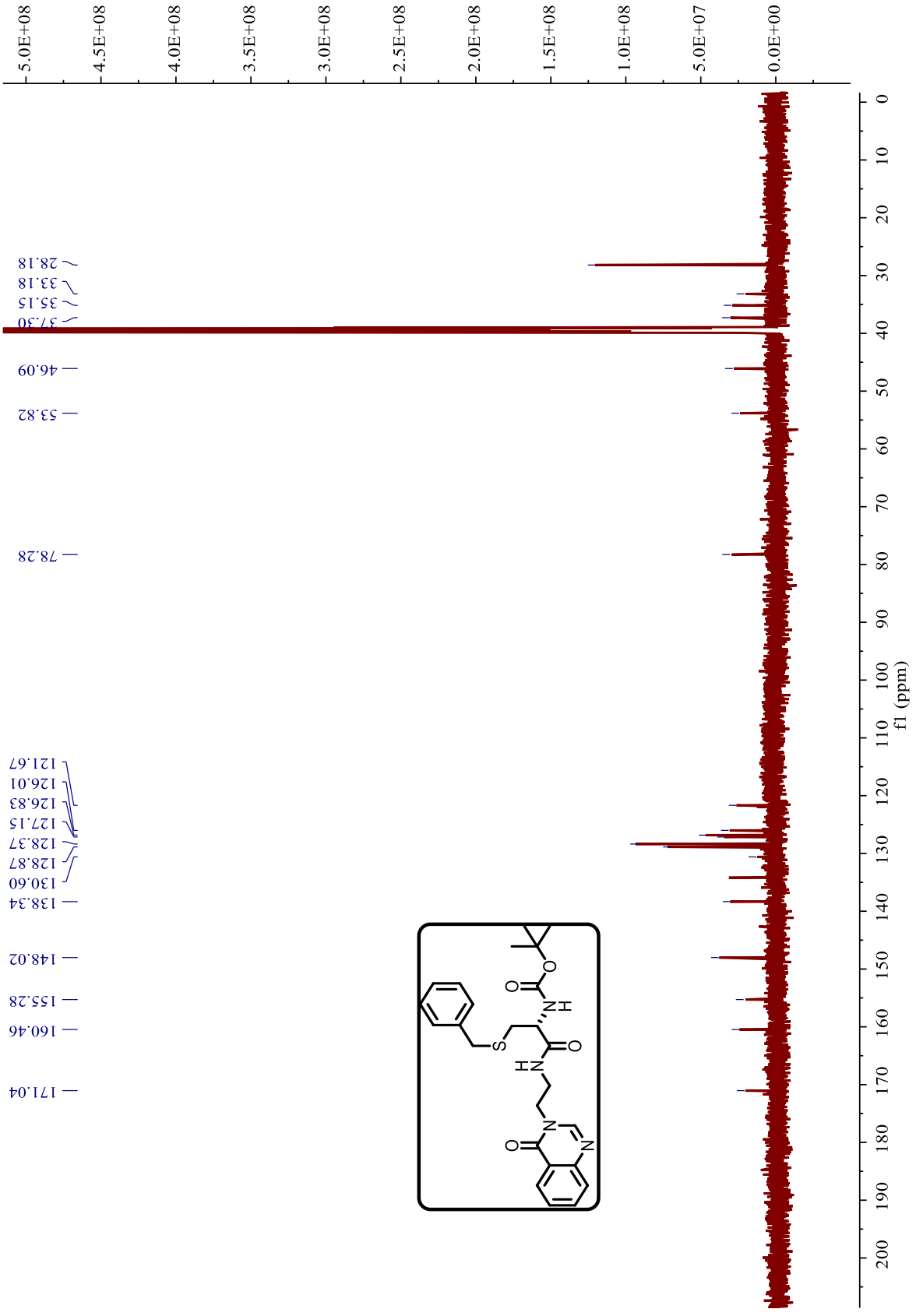

Figure S6. *^{13}C-NMR spectra of QP3 dissolved in DMSO-d_6 solvent.*

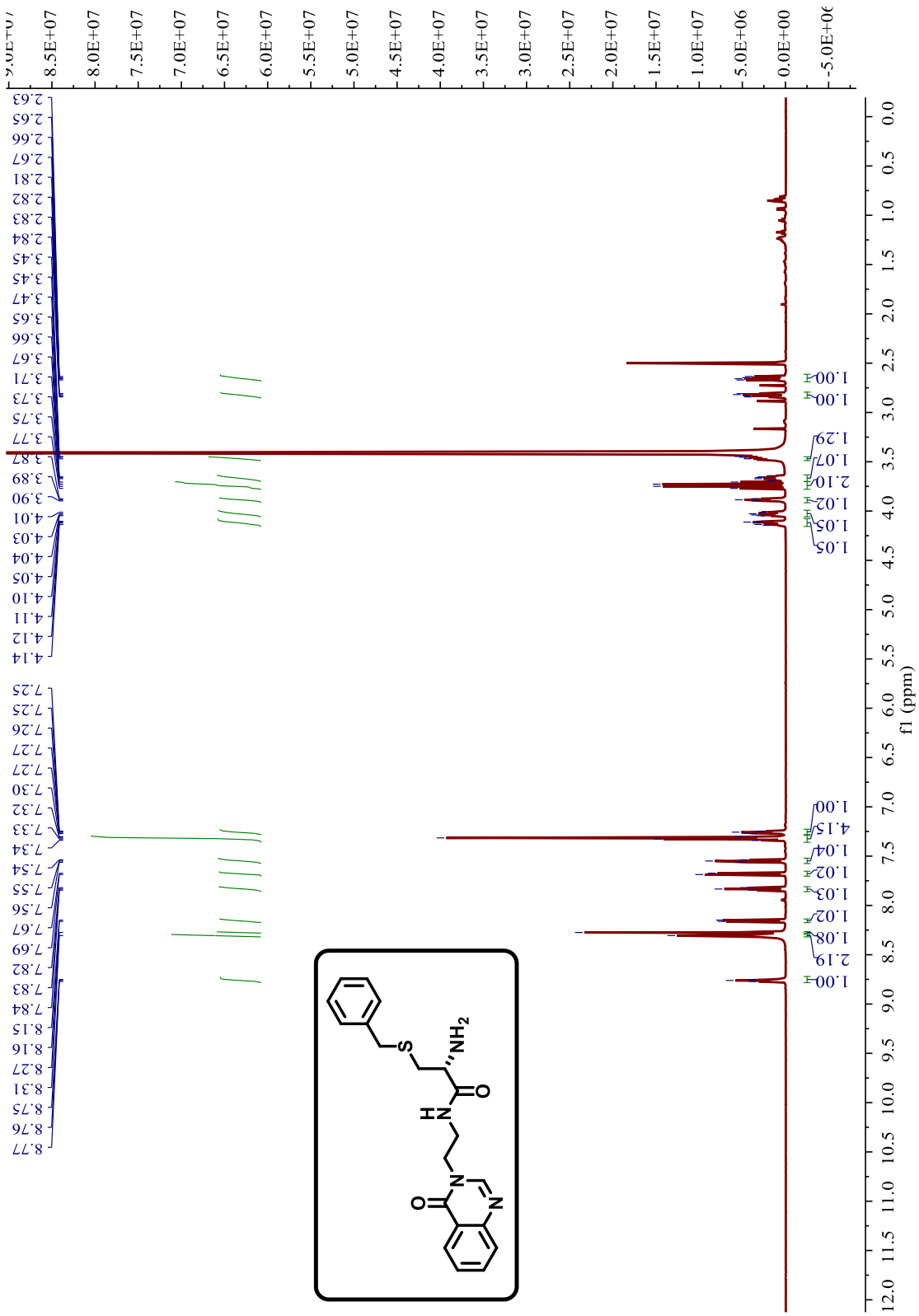

Figure S7. *^{1}H-NMR spectra of QP4 dissolved in DMSO-d_6 solvent.*

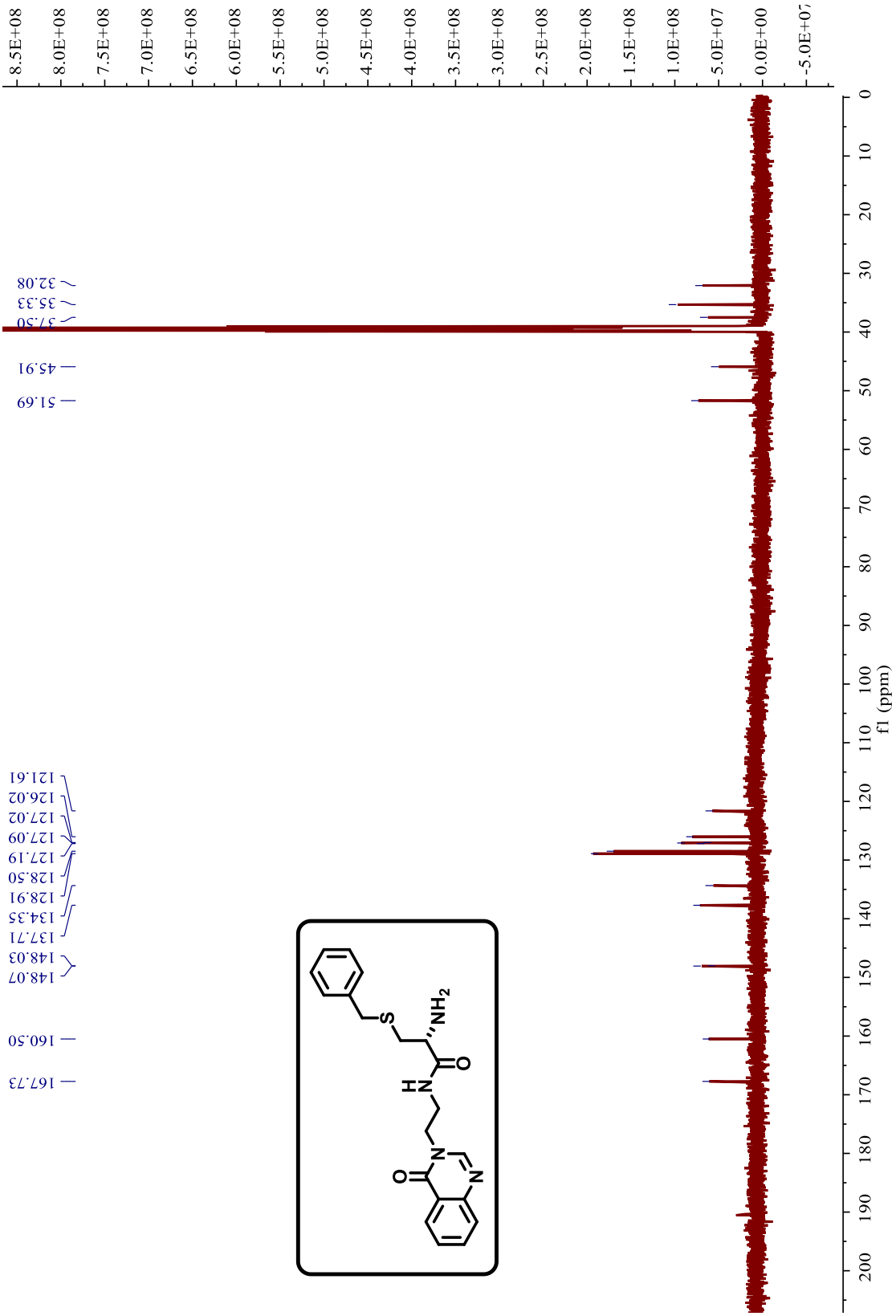

Figure S8. *^{13}C-NMR spectra of QP4 dissolved in DMSO-d_6 solvent.*

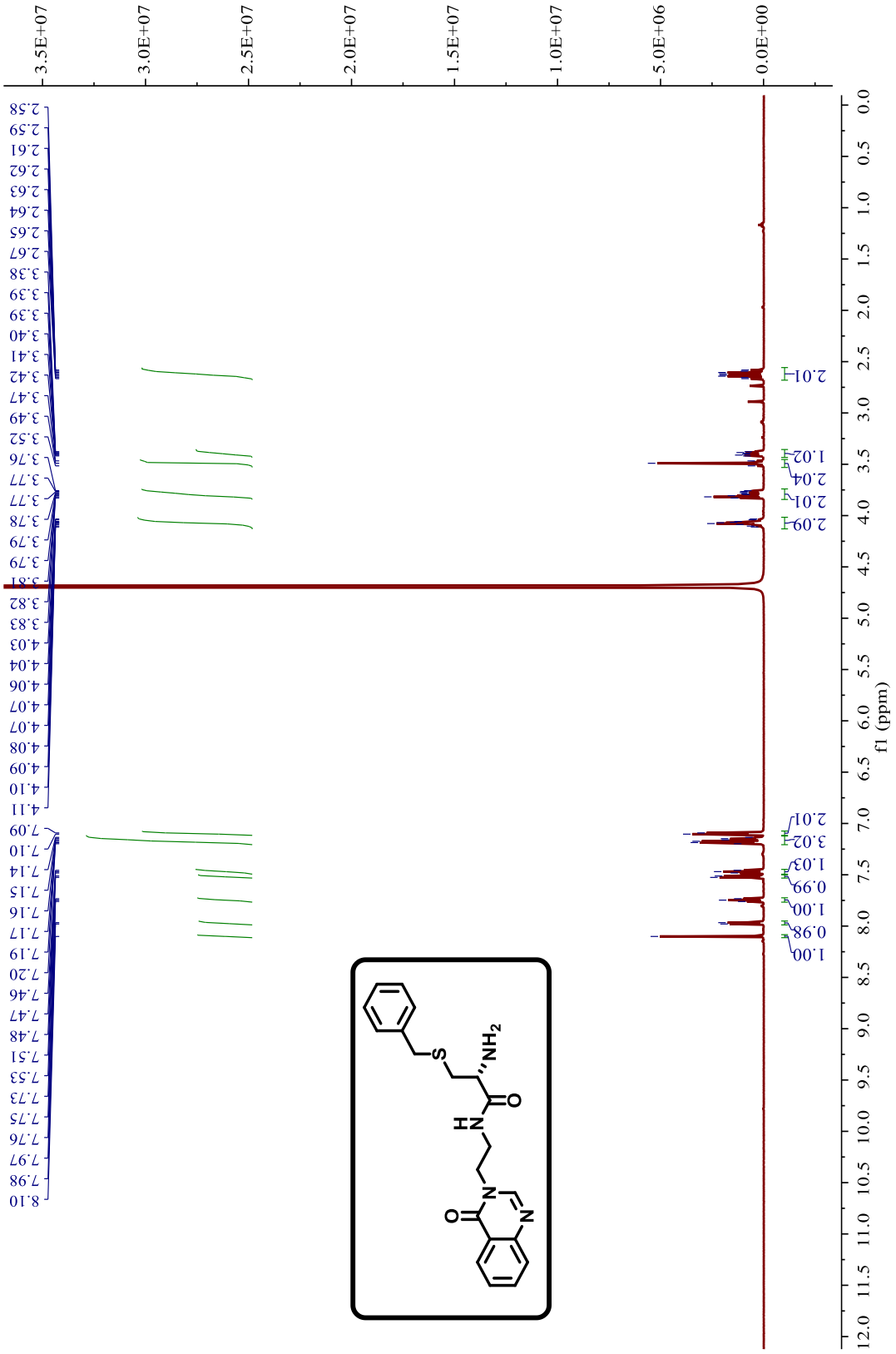

Figure S9. *^{1}H-NMR spectra of QP4 dissolved in D_2O solvent.*

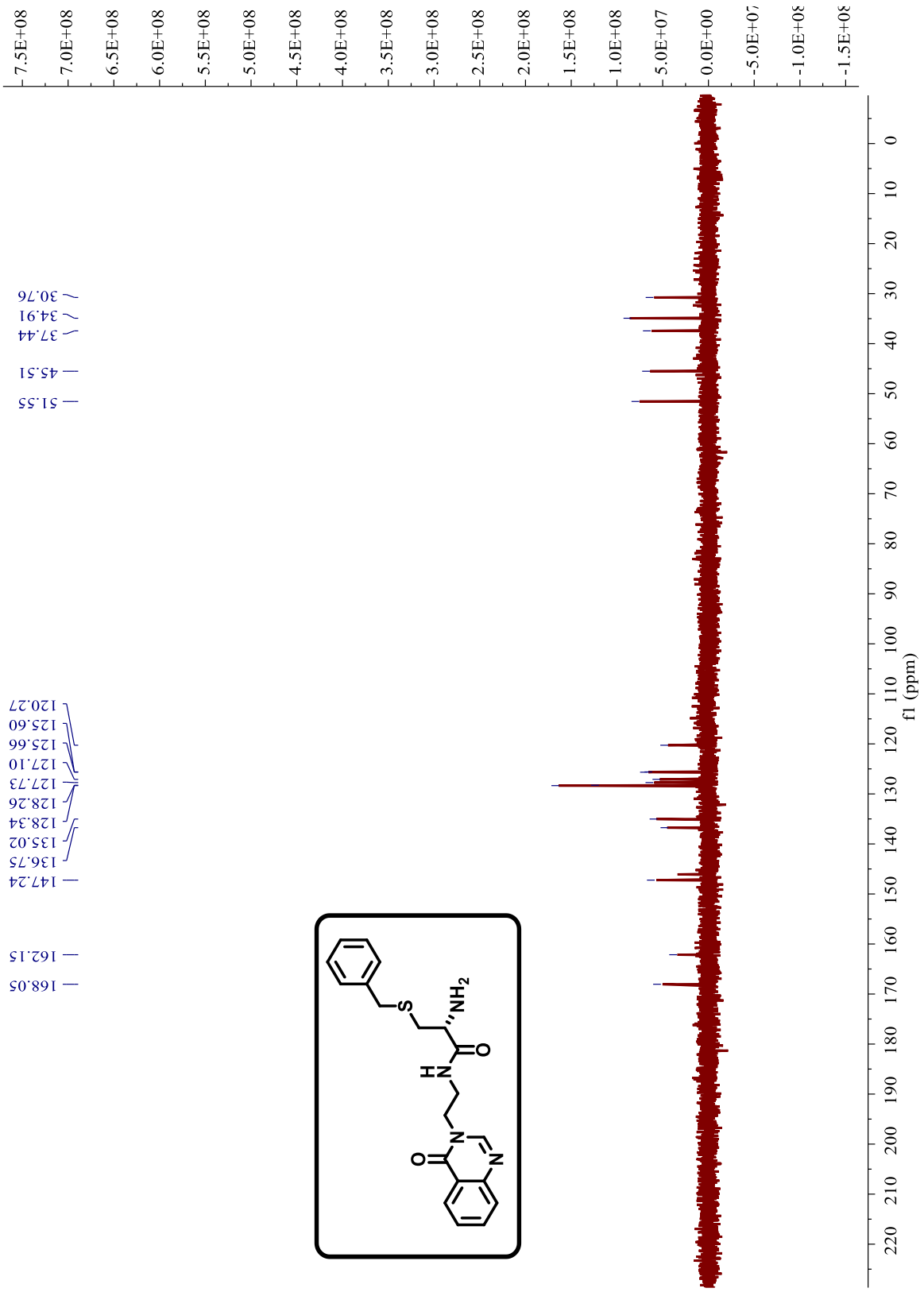

Figure S10. *^{13}C-NMR spectra of QP4 dissolved in D_2O solvent.*

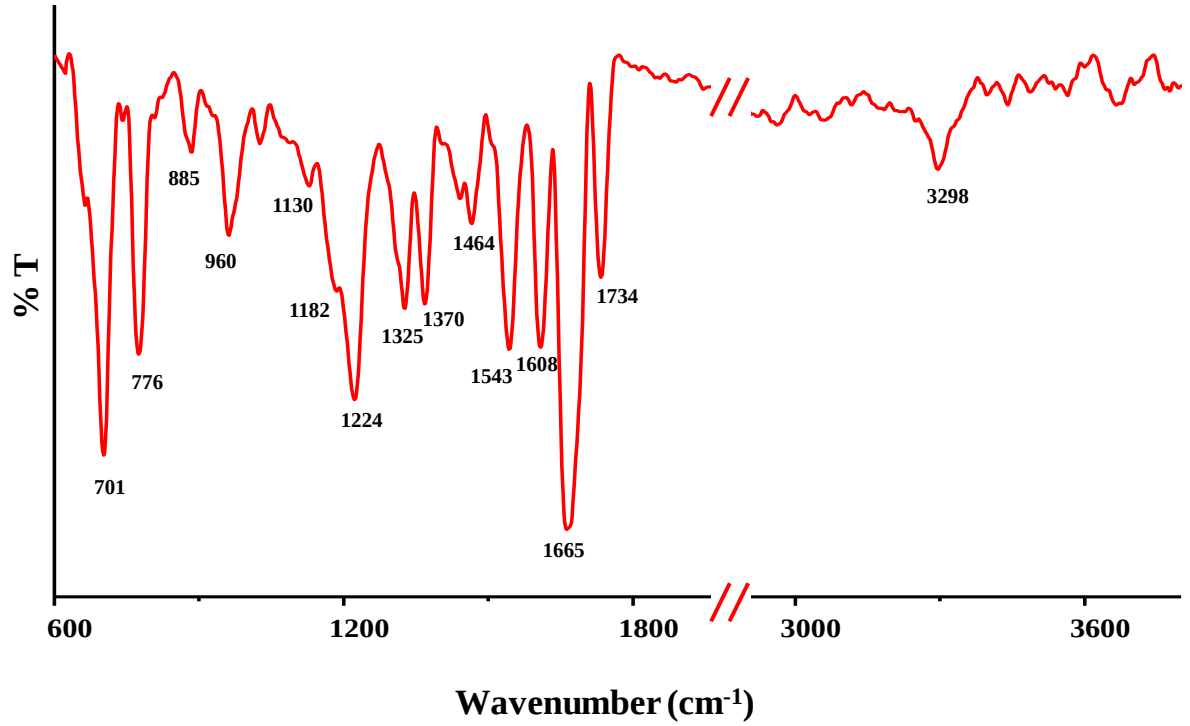

Figure S11. *FTIR spectra of peptide QP1 in solid state.*

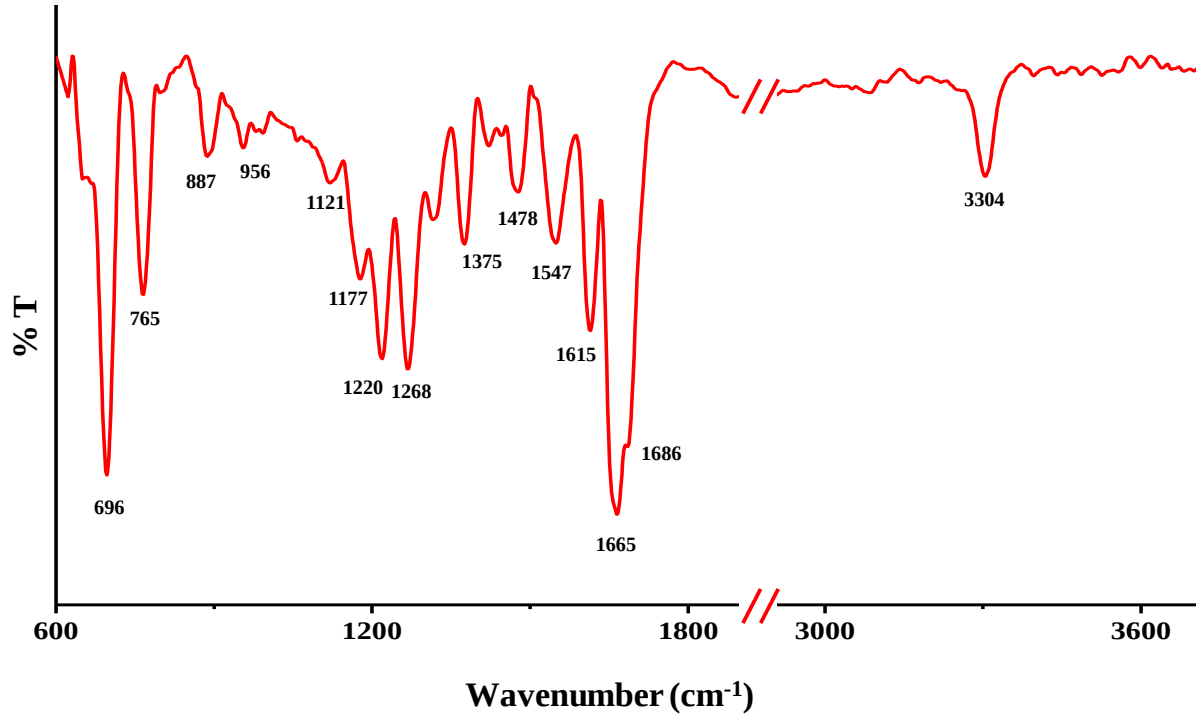

Figure S12. *FTIR spectra of peptide QP2 in solid state.*

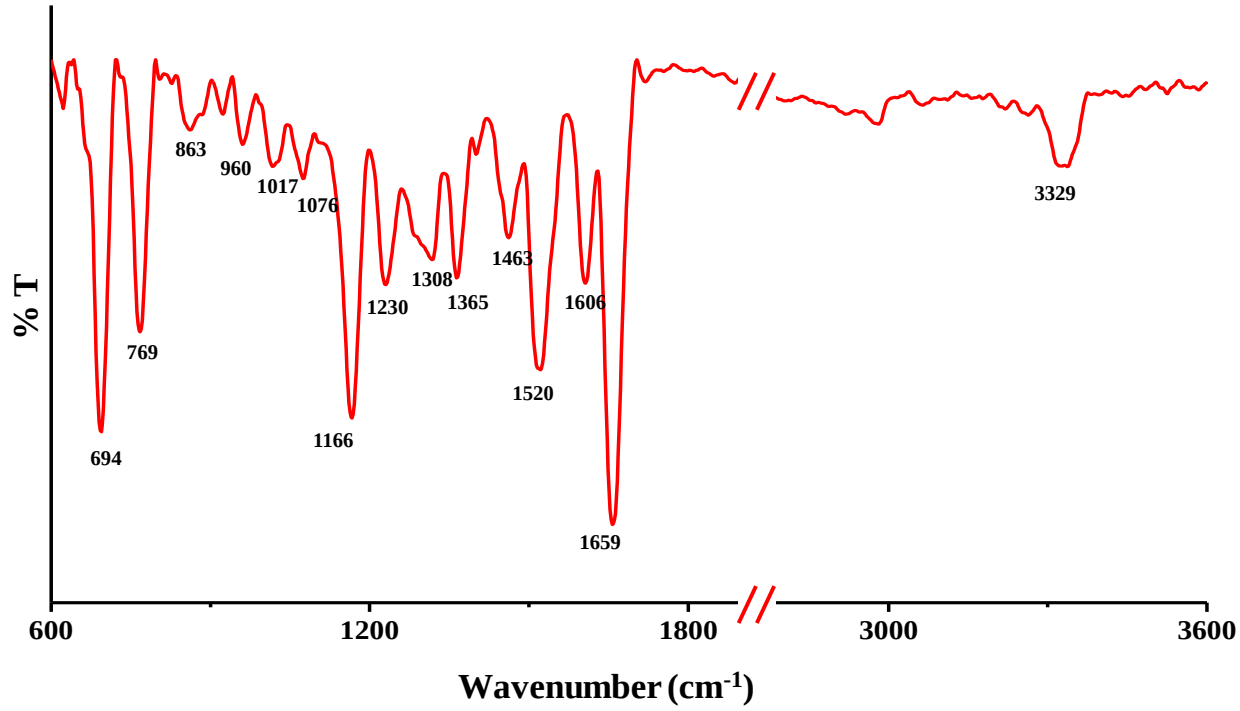

Figure S13. *FTIR spectra of peptide QP3 in solid state.*

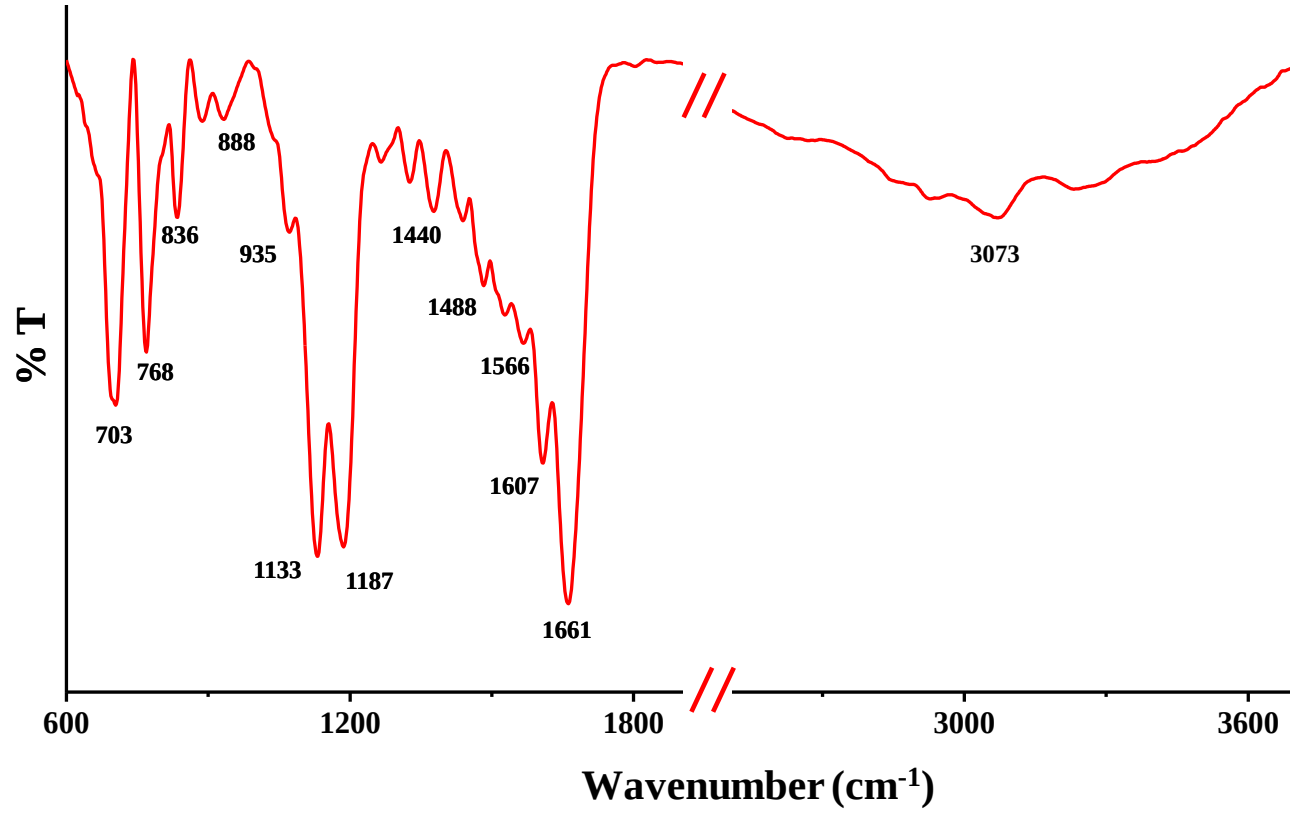

Figure S14. *FTIR spectra of peptide QP4 in solid state.*

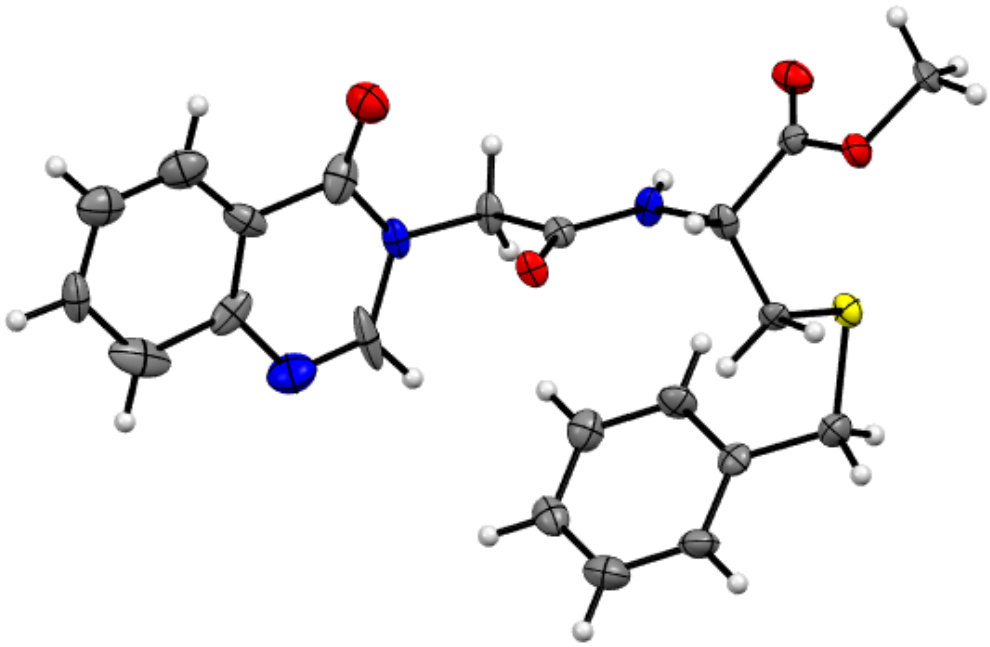

Figure S15. *ORTEP diagram of peptide QP1. Thermal ellipsoids are shown at 50 % probability level.*

Table S1*: Important crystal data of QP1*

CCDC no	2233454
Empirical formula	$C_{21}H_{21}N_3O_4S$
Formula weight	411.47
Temperature/K	117.0
Crystal system	monoclinic
Space group	$P2_1$
a/Å	10.7777(7)
b/Å	4.9011(3)
c/Å	19.0941(11)
α/°	90
β/°	104.915(4)
γ/°	90
Volume/Å^3	974.62(11)
Z	2
ρ_{calc}g/cm^3	1.402
μ/mm^{-1}	1.766
F(000)	432.0

Crystal size/mm^3	0.2 × 0.02 × 0.01
Radiation	CuKα (λ = 1.54178)
2Θ range for data collection/°	4.79 to 133.13
Index ranges	-12 ≤ h ≤ 12, -5 ≤ k ≤ 5, -22 ≤ l ≤ 22
Reflections collected	16790
Independent reflections	3396 [R_{int} = 0.0817, R_{sigma} = 0.0666]
Data/restraints/parameters	3396/7/264
Goodness-of-fit on F^2	1.083
Final R indexes [I>=2σ (I)]	R_1 = 0.0654, wR_2 = 0.1508
Final R indexes [all data]	R_1 = 0.0720, wR_2 = 0.1549
Largest diff. peak/hole / e Å^{-3}	1.12/-0.43
Flack parameter	0.051(17)

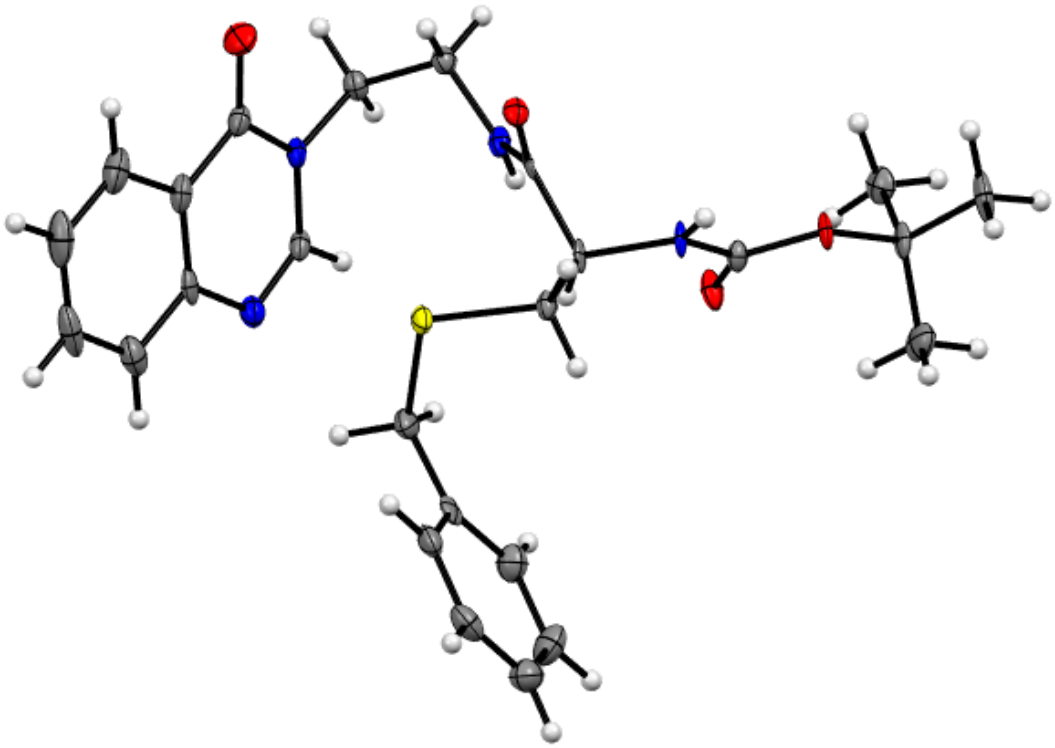

Figure S16. *ORTEP diagram of peptide QP3. Thermal ellipsoids are shown at 50 % probability level.*

***Table S2**: Important crystal data of QP3*

CCDC no	2233446
Empirical formula	$C_{25}H_{30}N_4O_4S$
Formula weight	482.59
Temperature/K	100.0
Crystal system	monoclinic
Space group	$P2_1$
a/Å	14.3258(5)
b/Å	5.1860(2)
c/Å	16.1792(6)
α/°	90
β/°	93.848(2)
γ/°	90
Volume/Å^3	1199.30(8)
Z	2
ρ_{calc}g/cm^3	1.336
μ/mm^{-1}	1.525
F(000)	512.0
Crystal size/mm^3	0.35 × 0.02 × 0.01
Radiation	CuKα (λ = 1.54178)
2Θ range for data collection/°	5.474 to 132.516
Index ranges	$-16 \leq h \leq 16$, $-6 \leq k \leq 5$, $-19 \leq l \leq 19$
Reflections collected	19421
Independent reflections	4083 [R_{int} = 0.0824, R_{sigma} = 0.0646]
Data/restraints/parameters	4083/1/310
Goodness-of-fit on F^2	1.053
Final R indexes [I>=2σ (I)]	R_1 = 0.0463, wR_2 = 0.1091
Final R indexes [all data]	R_1 = 0.0507, wR_2 = 0.1114
Largest diff. peak/hole / e Å^{-3}	0.41/-0.44
Flack parameter	0.063(17)

REFERENCES

(1) Mansoori, G. A.; Soelaiman, T. A. F. Nanotechnology - An Introduction for the Standards Community. *J. ASTM Int.* **2005**, *2* (6), 17–38. https://doi.org/10.1520/JAI13110.

(2) Sahoo, S. K.; Labhasetwar, V. Nanotech Approaches to Drug Delivery and Imaging. *Drug Discov. Today* **2003**, *8* (24), 1112–1120. https://doi.org/10.1016/S1359-6446(03)02903-9.

(3) Roco, M. C. National Nanotechnology Initiative. *Hawley's Condens. Chem. Dict.* **2007**, 1–40. https://doi.org/10.1002/9780470114735.hawley11400.

(4) Kroto, H. W.; Heath, J. R.; O'Brien, S. C.; Curl, R. F.; Smalley, R. E. C60 : Buckminsterfullerene. *Nature* **1985**, *318*, 162–163.

(5) Watson, J. D. Molecular Structure of Nucleic Acids. *Jama* **1993**, *269* (15), 1966. https://doi.org/10.1001/jama.1993.03500150078030.

(6) Kahlenberg, L. "Colloids and the Ultramicroscope, A Manual of Colloid Chemistry and Ultramicroscopy. *Science (80-.).* **1909**, *30* (762), 184–184. https://doi.org/10.1126/science.30.762.184.

(7) Feynman, R. P. There's Plenty of Room at the Bottom. *Engineering and Science*. 1960, pp 22–36. https://doi.org/10.1201/9780429500459.

(8) Shew, A. Nanotech's History. *Bull. Sci. Technol. Soc.* **2008**, *28* (5), 390–399. https://doi.org/10.1177/0270467608322535.

(9) Hulla, J. E.; Sahu, S. C.; Hayes, A. W. Nanotechnology: History and Future. *Hum. Exp. Toxicol.* **2015**, *34* (12), 1318–1321. https://doi.org/10.1177/0960327115603588.

(10) Sumio Iijima. Helical Microtubules of Graphitic Carbon. *Nature* **1991**, *354*, 56–58.

(11) Iqbal, P.; Preece, J. A.; Mendes, P. M. Nanotechnology: The "Top-Down" and "Bottom-Up" Approaches. *Supramol. Chem.* **2012**. https://doi.org/10.1002/9780470661345.smc195.

(12) Sanchez, F.; Sobolev, K. Nanotechnology in Concrete - A Review. *Constr. Build. Mater.* **2010**, *24* (11), 2060–2071. https://doi.org/10.1016/j.conbuildmat.2010.03.014.

(13) Weiss, J.; Takhistov, P.; McClements, D. J. Functional Materials in Food Nanotechnology. *J. Food Sci.* **2006**, *71* (9). https://doi.org/10.1111/j.1750-

3841.2006.00195.x.

(14) Jin, T.; Sun, D.; Su, J. Y.; Zhang, H.; Sue, H. J. Antimicrobial Efficacy of Zinc Oxide Quantum Dots against Listeria Monocytogenes, Salmonella Enteritidis, and Escherichia Coli O157:H7. *J. Food Sci.* **2009**, *74* (1). https://doi.org/10.1111/j.1750-3841.2008.01013.x.

(15) Nie, S.; Xing, Y.; Kim, G. J.; Simons, J. W. Nanotechnology Applications in Cancer. *Annu. Rev. Biomed. Eng.* **2007**, *9*, 257–288. https://doi.org/10.1146/annurev.bioeng.9.060906.152025.

(16) Chen, X.; Schluesener, H. J. Nanosilver: A Nanoproduct in Medical Application. *Toxicol. Lett.* **2008**, *176* (1), 1–12. https://doi.org/10.1016/j.toxlet.2007.10.004.

(17) Gu, Z.; Aimetti, A. A.; Wang, Q.; Dang, T. T.; Zhang, Y.; Veiseh, O. Injectable Nano-Network for Glucose-Mediated Insulin Delivery. **2013**, No. 5, 4194–4201.

(18) Egusquiaguirre, S. P.; Igartua, M.; Hernández, R. M.; Pedraz, J. L. Nanoparticle Delivery Systems for Cancer Therapy: Advances in Clinical and Preclinical Research. *Clin. Transl. Oncol.* **2012**, *14* (2), 83–93. https://doi.org/10.1007/s12094-012-0766-6.

(19) Kagan, V. E.; Bayir, H.; Shvedova, A. A. Nanomedicine and Nanotoxicology: Two Sides of the Same Coin. *Nanomedicine Nanotechnology, Biol. Med.* **2005**, *1* (4), 313–316. https://doi.org/10.1016/j.nano.2005.10.003.

(20) Zhu, S.; Oberdörster, E.; Haasch, M. L. Toxicity of an Engineered Nanoparticle (Fullerene, C60) in Two Aquatic Species, Daphnia and Fathead Minnow. *Mar. Environ. Res.* **2006**, *62* (SUPPL. 1), S5. https://doi.org/10.1016/j.marenvres.2006.04.059.

(21) Dehsorkhi, A.; Gouveia, R. M.; Smith, A. M.; Hamley, I. W.; Castelletto, V.; Connon, C. J.; Reza, M.; Ruokolainen, J. Self-Assembly of a Dual Functional Bioactive Peptide Amphiphile Incorporating Both Matrix Metalloprotease Substrate and Cell Adhesion Motifs. *Soft Matter* **2015**, *11* (16), 3115–3124. https://doi.org/10.1039/c5sm00459d.

(22) Lee, K. Y.; Mooney, D. J. Hydrogels for Tissue Engineering. *Chem. Rev.* **2001**, *101* (7), 1869–1879. https://doi.org/10.1021/cr000108x.

(23) Decandio, C. C.; Silva, E. R.; Hamley, I. W.; Castelletto, V.; Liberato, M. S.; Oliveira, V. X.; Oliveira, C. L. P.; Alves, W. A. Self-Assembly of a Designed Alternating Arginine/Phenylalanine Oligopeptide. *Langmuir* **2015**, *31* (15), 4513–4523. https://doi.org/10.1021/acs.langmuir.5b00253.

(24) Adler-Abramovich, L.; Gazit, E. The Physical Properties of Supramolecular Peptide Assemblies: From Building Block Association to Technological Applications. *Chem. Soc. Rev.* **2014**, *43* (20), 6881–6893. https://doi.org/10.1039/c4cs00164h.

(25) Singh, N.; Conte, M. P.; Ulijn, R. V.; Miravet, J. F.; Escuder, B. Insight into the Esterase like Activity Demonstrated by an Imidazole Appended Self-Assembling Hydrogelator. *Chem. Commun.* **2015**, *51* (67), 13213–13216. https://doi.org/10.1039/c5cc04281j.

(26) Ghobril, C.; Charoen, K.; Rodriguez, E. K.; Nazarian, A.; Grinstaff, M. W. A Dendritic Thioester Hydrogel Based on Thiol-Thioester Exchange as a Dissolvable Sealant System for Wound Closure. *Angew. Chemie - Int. Ed.* **2013**, *52* (52), 14070–14074. https://doi.org/10.1002/anie.201308007.

(27) Basu, K.; Baral, A.; Basak, S.; Dehsorkhi, A.; Nanda, J.; Bhunia, D.; Ghosh, S.; Castelletto, V.; Hamley, I. W.; Banerjee, A. Peptide Based Hydrogels for Cancer Drug Release: Modulation of Stiffness, Drug Release and Proteolytic Stability of Hydrogels by Incorporating d-Amino Acid Residue(S). *Chem. Commun.* **2016**, *52* (28), 5045–5048. https://doi.org/10.1039/c6cc01744d.

(28) Bhattacharya, S.; Krishnan-Ghosh, Y. First Report of Phase Selective Gelation of Oil from Oil/Water Mixtures. Possible Implications toward Containing Oil Spills. *Chem. Commun.* **2001**, No. 2, 185–186. https://doi.org/10.1039/b007848o.

(29) Marchesan, S.; Vargiu, A. V.; Styan, K. E. The Phe-Phe Motif for Peptide Self-Assembly in Nanomedicine. *Molecules* **2015**, *20* (11), 19775–19788. https://doi.org/10.3390/molecules201119658.

(30) Zhou, M.; Smith, A. M.; Das, A. K.; Hodson, N. W.; Collins, R. F.; Ulijn, R. V.; Gough, J. E. Self-Assembled Peptide-Based Hydrogels as Scaffolds for Anchorage-Dependent Cells. *Biomaterials* **2009**, *30* (13), 2523–2530. https://doi.org/10.1016/j.biomaterials.2009.01.010.

(31) Kim, S. H.; Kaplan, J. A.; Sun, Y.; Shieh, A.; Sun, H. L.; Croce, C. M.; Grinstaff, M. W.; Parquette, J. R. The Self-Assembly of Anticancer Camptothecin-Dipeptide Nanotubes: A Minimalistic and High Drug Loading Approach to Increased Efficacy. *Chem. - A Eur. J.* **2015**, *21* (1), 101–105. https://doi.org/10.1002/chem.201404520.

(32) Singh, M.; Kundu, S.; Reddy M, A.; Sreekanth, V.; Motiani, R. K.; Sengupta, S.; Srivastava, A.; Bajaj, A. Injectable Small Molecule Hydrogel as a Potential Nanocarrier for Localized and Sustained in Vivo Delivery of Doxorubicin. *Nanoscale* **2014**, *6* (21), 12849–12855.

https://doi.org/10.1039/c4nr04064c.

(33) Altunbas, A.; Lee, S. J.; Rajasekaran, S. A.; Schneider, J. P.; Pochan, D. J. Encapsulation of Curcumin in Self-Assembling Peptide Hydrogels as Injectable Drug Delivery Vehicles. *Biomaterials* **2011**, *32* (25), 5906–5914. https://doi.org/10.1016/j.biomaterials.2011.04.069.

(34) Baral, A.; Roy, S.; Dehsorkhi, A.; Hamley, I. W.; Mohapatra, S.; Ghosh, S.; Banerjee, A. Assembly of an Injectable Noncytotoxic Peptide-Based Hydrogelator for Sustained Release of Drugs. *Langmuir* **2014**, *30* (3), 929–936. https://doi.org/10.1021/la4043638.

(35) Bowerman, C. J.; Nilsson, B. L. Self-Assembly of Amphipathic β-Sheet Peptides: Insights and Applications. *Biopolymers* **2012**, *98* (3), 169–184. https://doi.org/10.1002/bip.22058.

(36) Rebek, J. Introduction to the Molecular Recognition and Self-Assembly Special Feature. *Proc. Natl. Acad. Sci. U. S. A.* **2009**, *106* (26), 10423–10424. https://doi.org/10.1073/pnas.0905341106.

(37) He, Q.; Duan, L.; Qi, W.; Wang, K.; Cui, Y.; Yan, X.; Li, J. Microcapsules Containing a Biomolecular Motor for ATP Biosynthesis. *Adv. Mater.* **2008**, *20* (15), 2933–2937. https://doi.org/10.1002/adma.200800622.

(38) Ajayaghosh, A.; Praveen, V. K.; Vijayakumar, C. Organogels as Scaffolds for Excitation Energy Transfer and Light Harvesting. *Chem. Soc. Rev.* **2008**, *37* (1), 109–122. https://doi.org/10.1039/b704456a.

(39) Nie, Z.; Kumacheva, E. Nmat2109.Pdf. *Materials (Basel).* **2008**, *7*, 277–290.

(40) Ariga, K.; Hill, J. P.; Lee, M. V.; Vinu, A.; Charvet, R.; Acharya, S. Challenges and Breakthroughs in Recent Research on Self-Assembly. *Sci. Technol. Adv. Mater.* **2008**, *9* (1). https://doi.org/10.1088/1468-6996/9/1/014109.

(41) Palmer, L. C.; Newcomb, C. J.; Kaltz, S. R.; Spoerke, E. D.; Stupp, S. I. Biomimetic Systems for Hydroxyapatite Mineralization Inspired by Bone and Enamel. *Chem. Rev.* **2008**, *108* (11), 4754–4783. https://doi.org/10.1021/cr8004422.

(42) Das, S.; Ahn, B. K.; Martinez-Rodriguez, N. R. Biomimicry and Bioinspiration as Tools for the Design of Innovative Materials and Systems. *Appl. Bionics Biomech.* **2018**, *2018*, 277–288. https://doi.org/10.1155/2018/6103537.

(43) Aizenberg, J.; Fratzl, P. Biological and Biomimetic Materials. *Adv. Mater.* **2009**, *21* (4), 387–388. https://doi.org/10.1002/adma.200803699.

(44) Lehn, J. M. Towards Complex Matter: Supramolecular Chemistry and Self-Organization. *Eur. Rev.* **2009**, *17* (2), 263–280. https://doi.org/10.1017/S1062798709000805.

(45) Whitesides, G. M.; Grzybowski, B. Self-Assembly at All Scales. *Science (80-.).* **2002**, *295* (5564), 2418–2421. https://doi.org/10.1126/science.1070821.

(46) Wang, J.; Liu, K.; Xing, R.; Yan, X. Peptide Self-Assembly: Thermodynamics and Kinetics. *Chem. Soc. Rev.* **2016**, *45* (20), 5589–5604. https://doi.org/10.1039/c6cs00176a.

(47) Whitesides, G. M.; Mathias, J. P.; Seto, C. T. Molecular Self-Assembly and Nanochemistry: A Chemical Strategy for the Synthesis of Nanostructures. *Science (80-.).* **1991**, *254* (5036), 1312–1319. https://doi.org/10.1126/science.1962191.

(48) Wilson, A. J. Supramolecular Chemistry. *Annu. Reports Prog. Chem. - Sect. B* **2008**, *104*, 164–183. https://doi.org/10.1039/b716600c.

(49) Stupp, S. I. Self-Assembly and Biomaterials. *Nano Lett.* **2010**, *10* (12), 4783–4786. https://doi.org/10.1021/nl103567y.

(50) Zhang, S. Fabrication of Novel Biomaterials through Molecular Self-Assembly. *Nat. Biotechnol.* **2003**, *21* (10), 1171–1178. https://doi.org/10.1038/nbt874.

(51) Rotello, V. M. *Core Concepts in Supramolecular Chemistry and Nanochemistry By Jonathan W. Steed (Durham University, U.K.), David R. Turner (Monash University, Australia), and Karl J. Wallace (University of Southern Mississippi). John Wiley & Sons, Ltd: Chichester. 2007.*; 2007; Vol. 129. https://doi.org/10.1021/ja0769853.

(52) Jones, M. R.; Seeman, N. C.; Mirkin, C. A. Programmable Materials and the Nature of the DNA Bond. *Science (80-.).* **2015**, *347* (6224). https://doi.org/10.1126/science.1260901.

(53) Van Anders, G.; Ahmed, N. K.; Smith, R.; Engel, M.; Glotzer, S. C. Entropically Patchy Particles: Engineering Valence through Shape Entropy. *ACS Nano* **2014**, *8* (1), 931–940. https://doi.org/10.1021/nn4057353.

(54) Glotzer, S. C.; Solomon, M. J. Anisotropy of Building Blocks and Their Assembly into Complex Structures. *Nat. Mater.* **2007**, *6* (8), 557–562.

https://doi.org/10.1038/nmat1949.

(55) Harper, E. S.; van Anders, G.; Glotzer, S. C. The Entropic Bond in Colloidal Crystals. *Proc. Natl. Acad. Sci. U. S. A.* **2019**, *116* (34), 16703–16710. https://doi.org/10.1073/pnas.1822092116.

(56) Van Anders, G.; Klotsa, D.; Ahmed, N. K.; Engel, M.; Glotzer, S. C. Understanding Shape Entropy through Local Dense Packing. *Proc. Natl. Acad. Sci. U. S. A.* **2014**, *111* (45), E4812–E4821. https://doi.org/10.1073/pnas.1418159111.

(57) De Santis, E.; Ryadnov, M. G. Peptide Self-Assembly for Nanomaterials: The Old New Kid on the Block. *Chem. Soc. Rev.* **2015**, *44* (22), 8288–8300. https://doi.org/10.1039/c5cs00470e.

(58) Tao, K.; Levin, A.; Adler-Abramovich, L.; Gazit, E. Fmoc-Modified Amino Acids and Short Peptides: Simple Bio-Inspired Building Blocks for the Fabrication of Functional Materials. *Chem. Soc. Rev.* **2016**, *45* (14), 3935–3953. https://doi.org/10.1039/c5cs00889a.

(59) Gazit, E. Self-Assembled Peptide Nanostructures: The Design of Molecular Building Blocks and Their Technological Utilization. *Chem. Soc. Rev.* **2007**, *36* (8), 1263–1269. https://doi.org/10.1039/b605536m.

(60) Tao, K.; Wang, J.; Zhou, P.; Wang, C.; Xu, H.; Zhao, X.; Lu, J. R. Self-Assembly of Short Aβ(16-22) Peptides: Effect of Terminal Capping and the Role of Electrostatic Interaction. *Langmuir* **2011**, *27* (6), 2723–2730. https://doi.org/10.1021/la1034273.

(61) Tian, F.; Cziferszky, M.; Jiao, D.; Wahlström, K.; Geng, J.; Scherman, O. A. Peptide Separation through a CB[8]-Mediated Supramolecular Trap-and-Release Process. *Langmuir* **2011**, *27* (4), 1387–1390. https://doi.org/10.1021/la104346k.

(62) Maity, S.; Jana, P.; Maity, S. K.; Haldar, D. Fabrication of Hollow Self-Assembled Peptide Microvesicles and Transition from Sphere-to-Rod Structure. *Langmuir* **2011**, *27* (7), 3835–3841. https://doi.org/10.1021/la104461m.

(63) M. Reza Ghadiri, Juan R. Granja, Ronald A. Milligan, D. E. M. & N. K. Self-Assembling Organic Nanotubes Based on a Cyclic Peptide Architecture. *Nature* **1993**, *366* (C), 324–327. https://doi.org/doi.org/10.1038/366324a0.

(64) Mandal, D.; Nasrolahi Shirazi, A.; Parang, K. Self-Assembly of Peptides to Nanostructures. *Org. Biomol. Chem.* **2014**, *12* (22), 3544–3561. https://doi.org/10.1039/c4ob00447g.

(65) Khazanovich, N.; Granja, J. R.; McRee, D. E.; Milligan, R. A.; Ghadiri, M. R. Nanoscale Tubular Ensembles with Specified Internal Diameters. Design of a Self-Assembled Nanotube with a 13-Å Pore. *J. Am. Chem. Soc.* **1994**, *116* (13), 6011–6012. https://doi.org/10.1021/ja00092a079.

(66) Steve Santoso, Wonmuk Hwang, Hyman Hartman, and S. Z. Self-Assembly of Surfactant-like Peptides with Variable Glycine Tails to Form Nanotubes and Nanovesicles. *NANO Lett.* **2002**, *2* (7), 687–691. https://doi.org/10.1073/pnas.072089599.

(67) Ranganathan, D.; Samant, M. P.; Karle, I. L. Self-Assembling, Cystine-Derived, Fused Nanotubes Based on Spirane Architecture: Design, Synthesis, and Crystal Structure of Cystinospiranes. *J. Am. Chem. Soc.* **2001**, *123* (24), 5619–5624. https://doi.org/10.1021/ja0101734.

(68) Scanlon, S.; Aggeli, A. Self-Assembling Peptide Nanotubes. *Nano Today* **2008**, *3* (3–4), 22–30. https://doi.org/10.1016/S1748-0132(08)70041-0.

(69) Lakshmanan, A.; Zhang, S.; Hauser, C. A. E. Short Self-Assembling Peptides as Building Blocks for Modern Nanodevices. *Trends Biotechnol.* **2012**, *30* (3), 155–165. https://doi.org/10.1016/j.tibtech.2011.11.001.

(70) Rajagopal, K.; Schneider, J. P. Self-Assembling Peptides and Proteins for Nanotechnological Applications. *Curr. Opin. Struct. Biol.* **2004**, *14* (4), 480–486. https://doi.org/10.1016/j.sbi.2004.06.006.

(71) Vauthey, S.; Santoso, S.; Gong, H.; Watson, N.; Zhang, S. Molecular Self-Assembly of Surfactant-like Peptides to Form Nanotubes and Nanovesicles. *Proc. Natl. Acad. Sci. U. S. A.* **2002**, *99* (8), 5355–5360. https://doi.org/10.1073/pnas.072089599.

(72) Tu, R. S.; Tirrell, M. Bottom-up Design of Biomimetic Assemblies. *Adv. Drug Deliv. Rev.* **2004**, *56* (11), 1537–1563. https://doi.org/10.1016/j.addr.2003.10.047.

(73) Schneider, J.; Berndt, P.; Haverstick, K.; Kumar, S.; Chiruvolu, S.; Tirrell, M. Force and Adhesion Measurements between Hydrogen-Bonded Layers of Glycine-Functionalized Amphiphiles. *J. Am. Chem. Soc.* **1998**, *120* (14), 3508–3509. https://doi.org/10.1021/ja972779r.

(74) Bitton, R.; Schmidt, J.; Biesalski, M.; Tu, R.; Tirrell, M.; Bianco-Peled, H. Self-Assembly of Model DNA-Binding Peptide Amphiphiles. *Langmuir* **2005**, *21* (25), 11888–11895. https://doi.org/10.1021/la051811p.

(75) Marini, D. M.; Hwang, W.; Lauffenburger, D. A.; Zhang, S.; Kamm, R. D. Left-Handed Helical Ribbon Intermediates in the Self-Assembly of a ß-Sheet Peptide. *Nano Lett.* **2002**, *2* (4), 295–299.

https://doi.org/10.1021/nl015697g.

(76) Holmes, T. C.; De Lacalle, S.; Su, X.; Liu, G.; Rich, A.; Zhang, S. Extensive Neurite Outgrowth and Active Synapse Formation on Self-Assembling Peptide Scaffolds. *Proc. Natl. Acad. Sci. U. S. A.* **2000**, *97* (12), 6728–6733. https://doi.org/10.1073/pnas.97.12.6728.

(77) Trim, D.-B.; Ammonium, E.; Fuoss, B. Y. R. M.; Ed, D.; Son, E. L. Bola Trim Ethyl Ammonium. **1951**, *7* (6).

(78) Qiu, F.; Chen, Y.; Tang, C.; Zhou, Q.; Wang, C.; Shi, Y. K.; Zhao, X. De Novo Design of a Bolaamphiphilic Peptide with Only Natural Amino Acids. *Macromol. Biosci.* **2008**, *8* (11), 1053–1059. https://doi.org/10.1002/mabi.200800180.

(79) Menzenski, M. Z.; Banerjee, I. A. Self-Assembly of Supramolecular Nanostructures from Phenylalanine Derived Bolaamphiphiles. *New J. Chem.* **2007**, *31* (9), 1674–1680. https://doi.org/10.1039/b702586f.

(80) Kogiso, M.; Okada, Y.; Hanada, T.; Yase, K.; Shimizu, T. Self-Assembled Peptide Fibers from Valylvaline Bola-Amphiphiles by a Parallel β-Sheet Network. *Biochim. Biophys. Acta - Gen. Subj.* **2000**, *1475* (3), 346–352. https://doi.org/10.1016/S0304-4165(00)00088-X.

(81) Claussen, R. C.; Rabatic, B. M.; Stupp, S. I. Aqueous Self-Assembly of Unsymmetric Peptide Bolaamphiphiles into Nanofibers with Hydrophilic Cores and Surfaces. *J. Am. Chem. Soc.* **2003**, *125* (42), 12680–12681. https://doi.org/10.1021/ja035882r.

(82) Tenidis, K.; Waldner, M.; Bernhagen, J.; Fischle, W.; Bergmann, M.; Weber, M.; Merkle, M. L.; Voelter, W.; Brunner, H.; Kapurniotu, A. Identification of a Penta- and Hexapeptide of Islet Amyloid Polypeptide (IAPP) with Amyloidogenic and Cytotoxic Properties. *J. Mol. Biol.* **2000**, *295* (4), 1055–1071. https://doi.org/10.1006/jmbi.1999.3422.

(83) Reches, M.; Gazit, E. Amyloidogenic Hexapeptide Fragment of Medin: Homology to Functional Islet Amyloid Polypeptide Fragments. *Amyloid* **2004**, *11* (2), 81–89. https://doi.org/10.1080/13506120412331272287.

(84) Westermark, P.; Engstrom, U.; Johnson, K. H.; Westermark, G. T.; Betsholtz, C. Islet Amyloid Polypeptide: Pinpointing Amino Acid Residues Linked to Amyloid Fibril Formation. *Proc. Natl. Acad. Sci. U. S. A.* **1990**, *87* (13), 5036–5040. https://doi.org/10.1073/pnas.87.13.5036.

(85) Tjernberg, L.; Hosia, W.; Bark, N.; Thyberg, J.; Johansson, J. Charge Attraction and β Propensity Are Necessary for Amyloid Fibril Formation from Tetrapeptides. *J. Biol. Chem.* **2002**, *277* (45), 43243–43246.

https://doi.org/10.1074/jbc.M205570200.

(86) Maji, S. K.; Haldar, D.; Drew, M. G. B.; Banerjee, A.; Das, A. K.; Banerjee, A. Self-Assembly of β-Turn Forming Synthetic Tripeptides into Supramolecular β-Sheets and Amyloid-like Fibrils in the Solid State. *Tetrahedron* **2004**, *60* (14), 3251–3259. https://doi.org/10.1016/j.tet.2004.02.019.

(87) Bose, P. P.; Das, A. K.; Hegde, R. P.; Shamala, N.; Banerjee, B. A. PH-Sensitive Nanostructural Transformation of a Synthetic Self-Assembling Water-Soluble Tripeptide: Nanotube to Nanovesicle. *Chem. Mater.* **2007**, *19* (25), 6150–6157. https://doi.org/10.1021/cm0716147.

(88) Reches, M.; Gazit, E. Casting Metal Nanowires within Discrete Self-Assembled Peptide Nanotubes. *Science (80-.).* **2003**, *300* (5619), 625–627. https://doi.org/10.1126/science.1082387.

(89) Adler-Abramovich, L.; Aronov, D.; Beker, P.; Yevnin, M.; Stempler, S.; Buzhansky, L.; Rosenman, G.; Gazit, E. Self-Assembled Arrays of Peptide Nanotubes by Vapour Deposition. *Nat. Nanotechnol.* **2009**, *4* (12), 849–854. https://doi.org/10.1038/nnano.2009.298.

(90) Wang, M.; Du, L.; Wu, X.; Xiong, S.; Chu, P. K. Charged Diphenylalanine Nanotubes and Controlled Hierarchical Self-Assembly. *ACS Nano* **2011**, *5* (6), 4448–4454. https://doi.org/10.1021/nn2016524.

(91) Zhu, P.; Yan, X.; Su, Y.; Yang, Y.; Li, J. Solvent-Induced Structural Transition of Self-Assembled Dipeptide: From Organogels to Microcrystals. *Chem. - A Eur. J.* **2010**, *16* (10), 3176–3183. https://doi.org/10.1002/chem.200902139.

(92) Ryu, J.; Park, C. B. High-Temperature Self-Assembly of Peptides into Vertically Well-Aligned Nanowires by Aniline Vapor. *Adv. Mater.* **2008**, *20* (19), 3754–3758. https://doi.org/10.1002/adma.200800364.

(93) Reches, M.; Gazit, E. Controlled Patterning of Aligned Self-Assembled Peptide Nanotubes. *Nat. Nanotechnol.* **2006**, *1* (3), 195–200. https://doi.org/10.1038/nnano.2006.139.

(94) Adler-Abramovich, L.; Reches, M.; Sedman, V. L.; Allen, S.; Tendler, S. J. B.; Gazit, E. Thermal and Chemical Stability of Diphenylalanine Peptide Nanotubes: Implications for Nanotechnological Applications. *Langmuir* **2006**, *22* (3), 1313–1320. https://doi.org/10.1021/la052409d.

(95) Kim, J.; Han, T. H.; Kim, Y. Il; Park, J. S.; Choi, J.; Churchill, D. G.; Kim, S. O.; Ihee, H. Role of Water in Directing Diphenylalanine Assembly into Nanotubes and Nanowires. *Adv. Mater.* **2010**, *22* (5), 583–

587. https://doi.org/10.1002/adma.200901973.

(96) Görbitz, C. H. Nanotubes from Hydrophobic Dipeptides: Pore Size Regulation through Side Chain Substitution. *New J. Chem.* **2003**, *27* (12), 1789–1793. https://doi.org/10.1039/b305984g.

(97) Görbitz, C. H. Nanotubes of L-Isoleucyl-L-Leucine 0.91-Hydrate. *Acta Crystallogr. Sect. E Struct. Reports Online* **2004**, *60* (4), 626–628. https://doi.org/10.1107/S1600536804006427.

(98) Görbitz, C. H. L-Phenylalanyl-L-Tryptophan 0.75-Hydrate. *Acta Crystallogr. Sect. C Cryst. Struct. Commun.* **2006**, *62* (6), 328–330. https://doi.org/10.1107/S0108270106014491.

(99) Görbitz, C. H. Nanotube Formation by Hydrophobic Dipeptides. *Chem. - A Eur. J.* **2001**, *7* (23), 5153–5159. https://doi.org/10.1002/1521-3765(20011203)7:23<5153::AID-CHEM5153>3.0.CO;2-N.

(100) Görbitz, C. H. An Exceptionally Stable Peptide Nanotube System with Flexible Pores. *Acta Crystallogr. Sect. B Struct. Sci.* **2002**, *58* (5), 849–854. https://doi.org/10.1107/S0108768102012314.

(101) Birkedal, H.; Schwarzenbach, D. Observation of Uniaxial Negative Thermal Expansion in an Organic Crystal. *Angew. Chemie - Int. Ed.* **2002**, *41* (5), 754–756. https://doi.org/10.1002/1521-3773(20020301)41:5<754::AID-ANIE754>3.0.CO;2-R.

(102) Pan, Y.; Birkedal, H.; Pattison, P.; Brown, D.; Chapuis, G. Molecular Dynamics Study of Tryptophylglycine: A Dipeptide Nanotube with Confined Water. *J. Phys. Chem. B* **2004**, *108* (20), 6458–6466. https://doi.org/10.1021/jp037219v.

(103) Görbitz, C. H.; Nilsen, M.; Szeto, K.; Tangen, L. W. Microporous Organic Crystals: An Unusual Case for L-Leucyl-L-Serine. *Chem. Commun.* **2005**, No. 34, 4288–4290. https://doi.org/10.1039/b504976h.

(104) Görbitz, C. H. Microporous Organic Materials from Hydrophobic Dipeptides. *Chem. - A Eur. J.* **2007**, *13* (4), 1022–1031. https://doi.org/10.1002/chem.200601427.

(105) Reches, M.; Gazit, E. Formation of Closed-Cage Nanostructures by Self-Assembly of Aromatic Dipeptides. *Nano Lett.* **2004**, *4* (4), 581–585. https://doi.org/10.1021/nl035159z.

(106) Reches, M.; Gazit, E. Designed Aromatic Homo-Dipeptides: Formation of Ordered Nanostructures and Potential Nanotechnological Applications. *Phys. Biol.* **2006**, *3* (1). https://doi.org/10.1088/1478-3975/3/1/S02.

(107) Carny, O.; Shalev, D. E.; Gazit, E. Fabrication of Coaxial Metal Nanocables Using a Self-Assembled Peptide Nanotube Scaffold. *Nano Lett.* **2006**, *6* (8), 1594–1597. https://doi.org/10.1021/nl060468l.

(108) Comotti, A.; Bracco, S.; Distefano, G.; Sozzani, P. Methane, Carbon Dioxide and Hydrogen Storage in Nanoporous Dipeptide-Based Materials. *Chem. Commun.* **2009**, No. 3, 284–286. https://doi.org/10.1039/b820200a.

(109) De Groot, N. S.; Parella, T.; Aviles, F. X.; Vendrell, J.; Ventura, S. Ile-Phe Dipeptide Self-Assembly: Clues to Amyloid Formation. *Biophys. J.* **2007**, *92* (5), 1732–1741. https://doi.org/10.1529/biophysj.106.096677.

(110) Guha, S.; Drew, M. G. B.; Banerjee, A. Dipeptide Nanotubes, with N-Terminally Located ω-Amino Acid Residues, That Are Stable Proteolytically, Thermally, and over a Wide Range of PH. *Chem. Mater.* **2008**, *20* (6), 2282–2290. https://doi.org/10.1021/cm703159b.

(111) Guha, S.; Chakraborty, T.; Banerjee, A. Water Soluble Synthetic Dieptide-Based Biodegradable Nanoporous Materials. *Green Chem.* **2009**, *11* (8), 1139–1145. https://doi.org/10.1039/b822607e.

(112) Mahler, A.; Reches, M.; Rechter, M.; Cohen, S.; Gazit, E. Rigid, Self-Assembled Hydrogel Composed of a Modified Aromatic Dipeptide. *Adv. Mater.* **2006**, *18* (11), 1365–1370. https://doi.org/10.1002/adma.200501765.

(113) Reches, M.; Gazit, E. Self-Assembly of Peptide Nanotubes and Amyloid-like Structures by Charged-Termini-Capped Diphenylalanine Peptide Analogues. *Isr. J. Chem.* **2005**, *45* (3), 363–371. https://doi.org/10.1560/5mc0-v3dx-ke0b-yf3j.

(114) Liang, G.; Yang, Z.; Zhang, R.; Li, L.; Fan, Y.; Kuang, Y.; Gao, Y.; Wang, T.; Lu, W. W.; Xu, B. Supramolecular Hydrogel of a D-Amino Acid Dipeptide for Controlled Drug Release in Vivo. *Langmuir* **2009**, *25* (15), 8419–8422. https://doi.org/10.1021/la804271d.

(115) Xing, B.; Yu, C. W.; Chow, K. H.; Ho, P. L.; Fu, D.; Xu, B. Hydrophobic Interaction and Hydrogen Bonding Cooperatively Confer a Vancomycin Hydrogel: A Potential Candidate for Biomaterials. *J. Am. Chem. Soc.* **2002**, *124* (50), 14846–14847. https://doi.org/10.1021/ja028539f.

(116) Yang, Z.; Gu, H.; Zhang, Y.; Wang, L.; Xu, B. Small Molecule Hydrogels Based on a Class of Antiinflammatory Agents. *Chem. Commun.* **2004**, *4* (2), 208–209. https://doi.org/10.1039/b310574a.

(117) Liebmann, T.; Rydholm, S.; Akpe, V.; Brismar, H. Self-Assembling Fmoc Dipeptide Hydrogel for in Situ 3D Cell Culturing. *BMC Biotechnol.*

2007, *7*, 1–11. https://doi.org/10.1186/1472-6750-7-88.

(118) Jayawarna, V.; Ali, M.; Jowitt, T. A.; Miller, A. F.; Saiani, A.; Gough, J. E.; Ulijn, R. V. Nanostructured Hydrogels for Three-Dimensional Cell Culture through Self-Assembly of Fluorenylmethoxycarbonyl-Dipeptides. *Adv. Mater.* **2006**, *18* (5), 611–614. https://doi.org/10.1002/adma.200501522.

(119) Jayawarna, V.; Smith, A.; Gough, J. E.; Ulijn, R. V. Bionanotechnology: From Self-Assembly to Cell Biology Three-Dimensional Cell Culture of Chondrocytes on Modified Di-Phenylalanine Scaffolds. *Biochem. Soc. Trans.* **2007**, *35* (3), 535–537.

(120) Yang, Z.; Liang, G.; Xu, B. Supramolecular Hydrogels Based on β-Amino Acid Derivatives. *Chem. Commun.* **2006**, No. 7, 738–740. https://doi.org/10.1039/b516133a.

(121) Naskar, J.; Banerjee, A. Concentration Dependent Transformation of Oligopeptide Based Nanovesicles to Nanotubes and an Application of Nanovesicles. *Chem. - An Asian J.* **2009**, *4* (12), 1817–1823. https://doi.org/10.1002/asia.200900274.

(122) Gupta, M.; Bagaria, A.; Mishra, A.; Mathur, P.; Basu, A.; Ramakumar, S.; Chauhan, V. S. Self-Assembly of a Dipeptide-Containing Conformationally Restricted Dehydrophenylalanine Residue to Form Ordered Nanotubes. *Adv. Mater.* **2007**, *19* (6), 858–861. https://doi.org/10.1002/adma.200601774.

(123) Mishra, A.; Panda, J. J.; Basu, A.; Chauhan, V. S. Nanovesicles Based on Self-Assembly of Conformationally Constrained Aromatic Residue Containing Amphiphilic Dipeptides. *Langmuir* **2008**, *24* (9), 4571–4576. https://doi.org/10.1021/la7034533.

(124) Ryan, D. M.; Doran, T. M.; Anderson, S. B.; Nilsson, B. L. Effect of C-Terminal Modification on the Self-Assembly and Hydrogelation of Fluorinated Fmoc-Phe Derivatives. *Langmuir* **2011**, *27* (7), 4029–4039. https://doi.org/10.1021/la1048375.

(125) Yang, Z.; Xu, B. A Simple Visual Assay Based on Small Molecule Hydrogels for Detecting Inhibitors of Enzymes. *Chem. Commun.* **2004**, *1* (21), 2424–2425. https://doi.org/10.1039/b408897b.

(126) Yang, Z.; Liang, G.; Xu, B. Enzymatic Hydrogelation of Small Molecules. *Acc. Chem. Res.* **2008**, *41* (2), 315–326. https://doi.org/10.1021/ar7001914.

(127) Yang, Z.; Gu, H.; Fu, D.; Gao, P.; Lam, J. K.; Xu, B. Enzymatic

Formation of Supramolecular Hydrogels. *Adv. Mater.* **2004**, *16* (16), 1440–1444. https://doi.org/10.1002/adma.200400340.

(128) Adler-Abramovich, L.; Vaks, L.; Carny, O.; Trudler, D.; Magno, A.; Caflisch, A.; Frenkel, D.; Gazit, E. Phenylalanine Assembly into Toxic Fibrils Suggests Amyloid Etiology in Phenylketonuria. *Nat. Chem. Biol.* **2012**, *8* (8), 701–706. https://doi.org/10.1038/nchembio.1002.

(129) Lee, J. S.; Yoon, I.; Kim, J.; Ihee, H.; Kim, B.; Park, C. B. Self-Assembly of Semiconducting Photoluminescent Peptide Nanowires in the Vapor Phase. *Angew. Chemie - Int. Ed.* **2011**, *50* (5), 1164–1167. https://doi.org/10.1002/anie.201003446.

(130) Govindaraju, T. Spontaneous Self-Assembly of Aromatic Cyclic Dipeptide into Fibre Bundles with High Thermal Stability and Propensity for Gelation. *Supramol. Chem.* **2011**, *23* (11), 759–767. https://doi.org/10.1080/10610278.2011.628393.

(131) Hanabusa, K.; Matsumoto, M.; Kimura, M.; Kakehi, A.; Shirai, H. Low Molecular Weight Gelators for Organic Fluids: Gelation Using a Family of Cyclo(Dipeptide)S. *J. Colloid Interface Sci.* **2000**, *224* (2), 231–244. https://doi.org/10.1006/jcis.1999.6672.

(132) Joshi, K. B.; Verma, S. Participation of Aromatic Side Chains in Diketopiperazine Ensembles. *Tetrahedron Lett.* **2008**, *49* (27), 4231–4234. https://doi.org/10.1016/j.tetlet.2008.04.156.

(133) Flory, B. Y. P. J. Introductory Lecture. *Lancet* **1855**, *66* (1675), 309–313. https://doi.org/10.1016/S0140-6736(02)53801-0.

(134) Tomasini, C.; Castellucci, N. Peptides and Peptidomimetics That Behave as Low Molecular Weight Gelators. *Chem. Soc. Rev.* **2013**, *42* (1), 156–172. https://doi.org/10.1039/c2cs35284b.

(135) Zhou, S. L.; Matsumoto, S.; Tian, H. D.; Yamane, H.; Ojida, A.; Kiyonaka, S.; Hamachi, I. PH-Responsive Shrinkage/Swelling of a Supramolecular Hydrogel Composed of Two Small Amphiphilic Molecules. *Chem. - A Eur. J.* **2005**, *11* (4), 1130–1136. https://doi.org/10.1002/chem.200400677.

(136) Harrison, R. S.; Sharpe, P. C.; Singh, Y.; Fairlie, D. P. Amyloid Peptides and Proteins in Review. *Rev. Physiol. Biochem. Pharmacol.* **2007**, *159* (February), 1–77. https://doi.org/10.1007/112_2007_0701.

(137) Sipe, J. D.; Cohen, A. S. Review: History of the Amyloid Fibril. *J. Struct. Biol.* **2000**, *130* (2–3), 88–98. https://doi.org/10.1006/jsbi.2000.4221.

(138) Rochet, J. C.; Conway, K. A.; Lansbury, P. T. Inhibition of Fibrillization and Accumulation of Prefibrillar Oligomers in Mixtures of Human and Mouse α-Synuclein. *Biochemistry* **2000**, *39* (35), 10619–10626. https://doi.org/10.1021/bi001315u.

(139) Serpell, L. C.; Berriman, J.; Jakes, R.; Goedert, M.; Crowther, R. A. Fiber Diffraction of Synthetic α-Synuclein Filaments Shows Amyloid-like Cross-β Conformation. *Proc. Natl. Acad. Sci. U. S. A.* **2000**, *97* (9), 4897–4902. https://doi.org/10.1073/pnas.97.9.4897.

(140) Pawar, A. P.; DuBay, K. F.; Zurdo, J.; Chiti, F.; Vendruscolo, M.; Dobson, C. M. Prediction of "Aggregation-Prone" and "Aggregation-Susceptible" Regions in Proteins Associated with Neurodegenerative Diseases. *J. Mol. Biol.* **2005**, *350* (2), 379–392. https://doi.org/10.1016/j.jmb.2005.04.016.

(141) Gazit, E. A Possible Role for Π-stacking in the Self-assembly of Amyloid Fibrils. *FASEB J.* **2002**, *16* (1), 77–83. https://doi.org/10.1096/fj.01-0442hyp.

(142) Sacchettini, J. C.; Kelly, J. W. Therapeutic Strategies for Human Amyloid Diseases. *Nat. Rev. Drug Discov.* **2002**, *1* (4), 267–275. https://doi.org/10.1038/nrd769.

(143) Kaytor, M. D.; Warren, S. T. Aberrant Protein Deposition and Neurological Disease. *J. Biol. Chem.* **1999**, *274* (53), 37507–37510. https://doi.org/10.1074/jbc.274.53.37507.

(144) Görbitz, C. H. The Structure of Nanotubes Formed by Diphenylalanine, the Core Recognition Motif of Alzheimer's β-Amyloid Polypeptide. *Chem. Commun.* **2006**, No. 22, 2332–2334. https://doi.org/10.1039/b603080g.

(145) Banerji, B.; Chatterjee, M.; Pal, U.; Maiti, N. C. Formation of Annular Protofibrillar Assembly by Cysteine Tripeptide: Unraveling the Interactions with NMR, FTIR, and Molecular Dynamics. *J. Phys. Chem. B* **2017**, *121* (26), 6367–6379. https://doi.org/10.1021/acs.jpcb.7b04373.

(146) Banerji, B.; Pramanik, S. K.; Pal, U.; Maiti, N. C. Potent Anticancer Activity of Cystine-Based Dipeptides and Their Interaction with Serum Albumins. *Chem. Cent. J.* **2013**, *7* (1), 1–10. https://doi.org/10.1186/1752-153X-7-91.

(147) Banerji, B.; Pramanik, S. K.; Pal, U.; Maiti, N. C. Dipeptide Derived from Benzylcystine Forms Unbranched Nanotubes in Aqueous Solution. *J. Nanostructure Chem.* **2013**, *3* (1), 1–6. https://doi.org/10.1186/2193-

8865-3-12.

(148) Banerji, B.; Chatterjee, M.; Prodhan, C.; Chaudhuri, K. Tripeptide Consisting of Benzyl Protected Di-Cysteine and Phenylalanine Forms Spherical Assembly and Induces Cytotoxicity in Cancer Cells via Apoptosis. *RSC Adv.* **2016**, *6* (113), 112667–112676. https://doi.org/10.1039/C6RA23911K.

(149) Li, J.; Xing, R.; Bai, S.; Yan, X. Recent Advances of Self-Assembling Peptide-Based Hydrogels for Biomedical Applications. *Soft Matter* **2019**, *15* (8), 1704–1715. https://doi.org/10.1039/C8SM02573H.

(150) Tesauro, D.; Accardo, A.; Diaferia, C.; Milano, V.; Guillon, J.; Ronga, L.; Rossi, F. Peptide-Based Drug-Delivery Systems in Biotechnological Applications: Recent Advances and Perspectives. *Molecules* **2019**, *24* (2), 1–27. https://doi.org/10.3390/molecules24020351.

(151) Ray, S.; Das, A. K.; Banerjee, A. PH-Responsive, Bolaamphiphile-Based Smart Metallo-Hydrogels as Potential Dye-Adsorbing Agents, Water Purifier, and Vitamin B12 Carrier. *Chem. Mater.* **2007**, *19* (7), 1633–1639. https://doi.org/10.1021/cm062672f.

(152) Liu, C.; Zhang, Q.; Zhu, S.; Liu, H.; Chen, J. Preparation and Applications of Peptide-Based Injectable Hydrogels. *RSC Adv.* **2019**, *9* (48), 28299–28311. https://doi.org/10.1039/c9ra05934b.

(153) Xing, R.; Liu, K.; Jiao, T.; Zhang, N.; Ma, K.; Zhang, R.; Zou, Q.; Ma, G.; Yan, X. An Injectable Self-Assembling Collagen-Gold Hybrid Hydrogel for Combinatorial Antitumor Photothermal/Photodynamic Therapy. *Adv. Mater.* **2016**, *28* (19), 3669–3676. https://doi.org/10.1002/adma.201600284.

(154) Raymond, D. M.; Abraham, B. L.; Fujita, T.; Watrous, M. J.; Toriki, E. S.; Takano, T.; Nilsson, B. L. Low-Molecular-Weight Supramolecular Hydrogels for Sustained and Localized in Vivo Drug Delivery. *ACS Appl. Bio Mater.* **2019**, *2* (5), 2116–2124. https://doi.org/10.1021/acsabm.9b00125.

(155) Sun, L.; Fan, Z.; Wang, Y.; Huang, Y.; Schmidt, M.; Zhang, M. Tunable Synthesis of Self-Assembled Cyclic Peptide Nanotubes and Nanoparticles. *Soft Matter* **2015**, *11* (19), 3822–3832. https://doi.org/10.1039/c5sm00533g.

(156) Abbas, M.; Zou, Q.; Li, S.; Yan, X. Self-Assembled Peptide- and Protein-Based Nanomaterials for Antitumor Photodynamic and Photothermal Therapy. *Adv. Mater.* **2017**, *29* (12).

https://doi.org/10.1002/adma.201605021.

(157) Wang, J.; Liu, K.; Xing, R.; Yan, X. Peptide Self-Assembly: Thermodynamics and Kinetics. *Chem. Soc. Rev.* **2016**, *45* (20), 5589–5604. https://doi.org/10.1039/c6cs00176a.

(158) Naskar, J.; Palui, G.; Banerjee, A. Tetrapeptide-Based Hydrogels: For Encapsulation and Slow Release of an Anticancer Drug at Physiological Ph. *J. Phys. Chem. B* **2009**, *113* (35), 11787–11792. https://doi.org/10.1021/jp904251j.

(159) Jonker, A. M.; Lo, D. W. P. M.; Hest, J. C. M. Van. Peptide- and Protein-Based Hydrogels. **2012**.

(160) Du, X.; Zhou, J.; Shi, J.; Xu, B. Supramolecular Hydrogelators and Hydrogels: From Soft Matter to Molecular Biomaterials. *Chem. Rev.* **2015**, *115* (24), 13165–13307. https://doi.org/10.1021/acs.chemrev.5b00299.

(161) Liu, X.; Fei, J.; Wang, A.; Cui, W.; Zhu, P.; Li, J. Transformation of Dipeptide-Based Organogels into Chiral Crystals by Cryogenic Treatment. *Angew. Chemie - Int. Ed.* **2017**, *56* (10), 2660–2663. https://doi.org/10.1002/anie.201612024.

(162) van Bommel, K. J. C.; van der Pol, C.; Muizebelt, I.; Friggeri, A.; Heeres, A.; Meetsma, A.; Feringa, B. L.; van Esch, J. Responsive Cyclohexane-Based Low-Molecular-Weight Hydrogelators with Modular Architecture. *Angew. Chemie* **2004**, *116* (13), 1695–1699. https://doi.org/10.1002/ange.200352396.

(163) Diaferia, C.; Rosa, E.; Balasco, N.; Sibillano, T.; Morelli, G.; Giannini, C.; Vitagliano, L.; Accardo, A. The Introduction of a Cysteine Residue Modulates The Mechanical Properties of Aromatic-Based Solid Aggregates and Self-Supporting Hydrogels. *Chem. - A Eur. J.* **2021**, *27* (60), 14886–14898. https://doi.org/10.1002/chem.202102007.

(164) Li, Y.; Wang, F.; Cui, H. Peptide-based Supramolecular Hydrogels for Delivery of Biologics. *Bioeng. Transl. Med.* **2016**, *1* (3), 306–322. https://doi.org/10.1002/btm2.10041.

(165) Manchineella S, G. T. Molecular Self-Assembly of Cyclic Dipeptide Derivatives and Their Applications. *Chempluschem* **2016**, *82* (1), 88–106.

(166) Montenegro, J.; Ghadiri, M. R.; Granja, J. R. Ion Channel Models Based on Self-Assembling Cyclic Peptide Nanotubes. *Acc. Chem. Res.* **2013**, *46* (12), 2955–2965. https://doi.org/10.1021/ar400061d.

(167) Eskandari, S.; Guerin, T.; Toth, I.; Stephenson, R. J. Recent Advances in Self-Assembled Peptides: Implications for Targeted Drug Delivery and Vaccine Engineering. *Adv. Drug Deliv. Rev.* **2017**, *110–111*, 169–187. https://doi.org/10.1016/j.addr.2016.06.013.

(168) Bellezza, I.; Peirce, M. J.; Minelli, A. Cyclic Dipeptides: From Bugs to Brain. *Trends Mol. Med.* **2014**, *20* (10), 551–558. https://doi.org/10.1016/j.molmed.2014.08.003.

(169) Pandurangan, K.; Roy, B.; Rajasekhar, K.; Suseela, Y. V.; Nagendra, P.; Chaturvedi, A.; Satwik, U. R.; Murugan, N. A.; Ramamurty, U.; Govindaraju, T. Molecular Architectonics of Cyclic Dipeptide Amphiphiles and Their Application in Drug Delivery. *ACS Appl. Bio Mater.* **2020**, *3* (5), 3413–3422. https://doi.org/10.1021/acsabm.0c00340.

(170) Balachandra, C.; Govindaraju, T. Cyclic Dipeptide-Guided Aggregation-Induced Emission of Naphthalimide and Its Application for the Detection of Phenolic Drugs. *J. Org. Chem.* **2020**, *85* (3), 1525–1536. https://doi.org/10.1021/acs.joc.9b02580.

(171) Balachandra, C.; Padhi, D.; Govindaraju, T. Cyclic Dipeptide: A Privileged Molecular Scaffold to Derive Structural Diversity and Functional Utility. *ChemMedChem* **2021**, *16* (17), 2558–2587. https://doi.org/10.1002/cmdc.202100149.

(172) You, Y.; Xing, R.; Zou, Q.; Shi, F.; Yan, X. High-Tolerance Crystalline Hydrogels Formed from Self-Assembling Cyclic Dipeptide. *Beilstein J. Nanotechnol.* **2019**, *10*, 1894–1901. https://doi.org/10.3762/bjnano.10.184.

(173) Brahmachari, G. Bioactive Natural Products. *Bioact. Nat. Prod.* **2011**. https://doi.org/10.1142/8033.

(174) Mollica, A.; Costante, R.; Fiorito, S.; Genovese, S.; Stefanucci, A.; Mathieu, V.; Kiss, R.; Epifano, F. Synthesis and Anti-Cancer Activity of Naturally Occurring 2,5-Diketopiperazines. *Fitoterapia* **2014**, *98*, 91–97. https://doi.org/10.1016/j.fitote.2014.07.010.

(175) Scarel, M.; Marchesan, S. Diketopiperazine Gels: New Horizons from the Self-Assembly of Cyclic Dipeptides. *Molecules* **2021**, *26* (11). https://doi.org/10.3390/molecules26113376.

(176) Hill, T. A.; Shepherd, N. E.; Diness, F.; Fairlie, D. P. Constraining Cyclic Peptides to Mimic Protein Structure Motifs. *Angew. Chemie - Int. Ed.* **2014**, *53* (48), 13020–13041. https://doi.org/10.1002/anie.201401058.

(177) Corey, R. B. The Crystal Structure of Diketopiperazine. *J. Am. Chem.*

Soc. **1938**, *7*, 1598–1604.

(178) Benedetti, E.; Corradini, P.; Pedone, C. The Crystal and Molecular Structure of Trans-3,6-Dimethyl-2,5-Piperazinedione (L-Alanyl-D-Alanyl-2,5-Diketopiperazine). *J. Phys. Chem.* **1969**, *73* (9), 2891–2895. https://doi.org/10.1021/j100843a018.

(179) Yang, M.; Xing, R.; Shen, G.; Yuan, C.; Yan, X. A Versatile Cyclic Dipeptide Hydrogelator: Self-Assembly and Rheology in Various Physiological Conditions. *Colloids Surfaces A Physicochem. Eng. Asp.* **2019**, *572* (April), 259–265. https://doi.org/10.1016/j.colsurfa.2019.04.020.

(180) Manchineella, S.; Murugan, N. A.; Govindaraju, T. Cyclic Dipeptide-Based Ambidextrous Supergelators: Minimalistic Rational Design, Structure-Gelation Studies, and in Situ Hydrogelation. *Biomacromolecules* **2017**, *18* (11), 3581–3590. https://doi.org/10.1021/acs.biomac.7b00924.

(181) Nanda, J.; Banerjee, A. β-Amino Acid Containing Proteolitically Stable Dipeptide Based Hydrogels: Encapsulation and Sustained Release of Some Important Biomolecules at Physiological PH and Temperature. *Soft Matter* **2012**, *8* (12), 3380–3386. https://doi.org/10.1039/c2sm07168a.

(182) Karcher, J.; Kirchner, S.; Leistner, A. L.; Hald, C.; Geng, P.; Bantle, T.; Gödtel, P.; Pfeifer, J.; Pianowski, Z. L. Selective Release of a Potent Anticancer Agent from a Supramolecular Hydrogel Using Green Light. *RSC Adv.* **2021**, *11* (15), 8546–8551. https://doi.org/10.1039/d0ra08893e.

(183) Majumder, L.; Chatterjee, M.; Bera, K.; Maiti, N. C.; Banerji, B. Solvent-Assisted Tyrosine-Based Dipeptide Forms Low-Molecular Weight Gel: Preparation and Its Potential Use in Dye Removal and Oil Spillage Separation from Water. *ACS Omega* **2019**, *4* (11), 14411–14419. https://doi.org/10.1021/acsomega.9b01301.

(184) Banerji, B.; Pramanik, S. K.; Pal, U.; Maiti, N. C. Dipeptide Derived from Benzylcystine Forms Unbranched Nanotubes in Aqueous Solution. *J. Nanostructure Chem.* **2013**, *3* (1), 1–6. https://doi.org/10.1186/2193-8865-3-12.

(185) Martin, A. D.; Robinson, A. B.; Thordarson, P. Biocompatible Small Peptide Super-Hydrogelators Bearing Carbazole Functionalities. *J. Mater. Chem. B* **2015**, *3* (11), 2277–2280. https://doi.org/10.1039/c5tb00067j.

(186) Longley, D. B.; Harkin, D. P.; Johnston, P. G. 5-Fluorouracil: Mechanisms of Action and Clinical Strategies. *Nat. Rev. Cancer* **2003**, *3* (5), 330–338. https://doi.org/10.1038/nrc1074.

(187) Zaremba, L. S.; Smoleński, W. H. Optimal Portfolio Choice under a Liability Constraint. *Ann. Oper. Res.* **2000**, *97* (1–4), 131–141.

(188) Krawtchenko, N.; Roewert-Huber, J.; Ulrich, M.; Mann, I.; Sterry, W.; Stockfleth, E. A Randomised Study of Topical 5% Imiquimod vs. Topical 5-Fluorouracil vs. Cryosurgery in Immunocompetent Patients with Actinic Keratoses: A Comparison of Clinical and Histological Outcomes Including 1-Year Follow-Up. *Br. J. Dermatol.* **2007**, *157* (SUPPL. 2), 34–40. https://doi.org/10.1111/j.1365-2133.2007.08271.x.

(189) Carethers, J. M.; Smith, E. J.; Behling, C. A.; Nguyen, L.; Tajima, A.; Doctolero, R. T.; Cabrera, B. L.; Goel, A.; Arnold, C. A.; Miyai, K.; Boland, C. R. Use of 5-Fluorouracil and Survival in Patients with Microsatellite-Unstable Colorectal Cancer. *Gastroenterology* **2004**, *126* (2), 394–401. https://doi.org/10.1053/j.gastro.2003.12.023.

(190) Cwikiel, M.; Albertsson, M.; Kinhult, S.; Eskilsson, J. 5-Fluorouracil-I Nduced Small Bowel Toxicity in Patients with Colorectal Carcinoma [3] (Multiple Letters). *Cancer* **2000**, *89* (3), 712–713. https://doi.org/10.1002/1097-0142(20000801)89:3<712::AID-CNCR34>3.0.CO;2-W.

(191) Daniel E Shumer, N. J. N. N. P. S. 乳鼠心肌提取 HHS Public Access. *Physiol. Behav.* **2017**, *176* (12), 139–148.

(192) Entezar-Almahdi, E.; Mohammadi-Samani, S.; Tayebi, L.; Farjadian, F. Recent Advances in Designing 5-Fluorouracil Delivery Systems: A Stepping Stone in the Safe Treatment of Colorectal Cancer. *Int. J. Nanomedicine* **2020**, *15*, 5445–5458. https://doi.org/10.2147/IJN.S257700.

(193) Rosas-Valdéz, M. E.; Escalante, J.; Bustos-Jaimes, I.; Regla, I.; Boto, A. Synthesis and Modification of the Amyloid Peptide Sequence 37-42 of Aβ42 (AβPP): Efficient Synthesis of N-Methylated Peptides, Expanding the Toolsfor Peptide Research. *J. Mex. Chem. Soc.* **2016**, *60* (3), 125–134. https://doi.org/10.29356/jmcs.v60i3.94.

(194) Zhang, Y. -Z; Roder, H.; Paterson, Y. Rapid Amide Proton Exchange Rates in Peptides and Proteins Measured by Solvent Quenching and Two-dimensional NMR. *Protein Sci.* **1995**, *4* (4), 804–814. https://doi.org/10.1002/pro.5560040420.

(195) Adochitei, A.; Drochioiu, G. Rapid Characterization of Peptide Secondary Structure by FT-IR Spectroscopy. *Rev. Roum. Chim.* **2011**, *56* (8), 783–791.

(196) Barth, A. Infrared Spectroscopy of Proteins. *Biochim. Biophys. Acta - Bioenerg.* **2007**, *1767* (9), 1073–1101. https://doi.org/10.1016/j.bbabio.2007.06.004.

(197) Aggeli, A.; Bell, M.; Carrick, L. M.; Fishwick, C. W. G.; Harding, R.; Mawer, P. J.; Radford, S. E.; Strong, A. E.; Boden, N. PH as a Trigger of Peptide β-Sheet Self-Assembly and Reversible Switching between Nematic and Isotropic Phases. *J. Am. Chem. Soc.* **2003**, *125* (32), 9619–9628. https://doi.org/10.1021/ja021047i.

(198) Choudhury, P.; Mandal, D.; Brahmachari, S.; Das, P. K. Hydrophobic End-Modulated Amino-Acid-Based Neutral Hydrogelators: Structure-Specific Inclusion of Carbon Nanomaterials. *Chem. - A Eur. J.* **2016**, *22* (15), 5160–5172. https://doi.org/10.1002/chem.201504888.

(199) Roy, K.; Pandit, G.; Chetia, M.; Sarkar, A. K.; Chowdhuri, S.; Bidkar, A. P.; Chatterjee, S. Peptide Hydrogels as Platforms for Sustained Release of Antimicrobial and Antitumor Drugs and Proteins. *ACS Appl. Bio Mater.* **2020**, *3* (9), 6251–6262. https://doi.org/10.1021/acsabm.0c00314.

(200) Lu, K.; Jacob, J.; Thiyagarajan, P.; Conticello, V. P.; Lynn, D. G. Exploiting Amyloid Fibril Lamination for Nanotube Self-Assembly. *J. Am. Chem. Soc.* **2003**, *125* (21), 6391–6393. https://doi.org/10.1021/ja0341642.

(201) Ashwanikumar, N.; Kumar, N. A.; Nair, S. A.; Vinod Kumar, G. S. Phenylalanine-Containing Self-Assembling Peptide Nanofibrous Hydrogel for the Controlled Release of 5-Fluorouracil and Leucovorin. *RSC Adv.* **2014**, *4* (55), 29157–29164. https://doi.org/10.1039/c4ra04393f.

(202) Sharma, P.; Kaur, H.; Roy, S. Inducing Differential Self-Assembling Behavior in Ultrashort Peptide Hydrogelators Using Simple Metal Salts. *Biomacromolecules* **2019**, *20* (7), 2610–2624. https://doi.org/10.1021/acs.biomac.9b00416.

(203) Cinar, G.; Orujalipoor, I.; Su, C. J.; Jeng, U. S.; Ide, S.; Guler, M. O. Supramolecular Nanostructure Formation of Coassembled Amyloid Inspired Peptides. *Langmuir* **2016**, *32* (25), 6506–6514. https://doi.org/10.1021/acs.langmuir.6b00704.

(204) Biancalana, M.; Koide, S. Molecular Mechanism of Thioflavin-T Binding to Amyloid Fibrils. *Biochim. Biophys. Acta - Proteins Proteomics* **2010**, *1804* (7), 1405–1412. https://doi.org/10.1016/j.bbapap.2010.04.001.

(205) Nanda, J.; Biswas, A.; Banerjee, A. Single Amino Acid Based Thixotropic Hydrogel Formation and PH-Dependent Morphological

Change of Gel Nanofibers. *Soft Matter* **2013**, *9* (16), 4198–4208. https://doi.org/10.1039/c3sm27050e.

(206) Kamath, K. R.; Park, K. Biodegradable Hydrogels in Drug Delivery. *Adv. Drug Deliv. Rev.* **1993**, *11* (1–2), 59–84. https://doi.org/10.1016/0169-409X(93)90027-2.

(207) Florento, L.; Matias, R.; Tuaño, E.; Santiago, K.; Cruz, F. Dela; Tuazon, A. Comparison of Cytotoxic Activity of Anticancer Drugs against Various Human Tumor Cell Lines Using in Vitro Cell-Based Approach. *Int. J. Biomed. Sci.* **2012**, *8* (1), 76–80.

(208) Silva, V. R.; Corrêa, R. S.; Santos, L. D. S.; Soares, M. B. P.; Batista, A. A.; Bezerra, D. P. A Ruthenium-Based 5-Fluorouracil Complex with Enhanced Cytotoxicity and Apoptosis Induction Action in HCT116 Cells. *Sci. Rep.* **2018**, *8* (1), 1–13. https://doi.org/10.1038/s41598-017-18639-6.

(209) Liu, K.; Liu, P. cheng; Liu, R.; Wu, X. Dual AO/EB Staining to Detect Apoptosis in Osteosarcoma Cells Compared with Flow Cytometry. *Med. Sci. Monit. Basic Res.* **2015**, *21*, 15–20. https://doi.org/10.12659/MSMBR.893327.

(210) Berrouet, C.; Dorilas, N.; Rejniak, K. A.; Tuncer, N. Comparison of Drug Inhibitory Effects (IC 50) in Monolayer and Spheroid Cultures. *Bull. Math. Biol.* **2020**, *82* (6). https://doi.org/10.1007/s11538-020-00746-7.

(211) Wigmore, P. M.; Mustafa, S.; El-Beltagy, M.; Lyons, L.; Umka, J.; Bennett, G. Effects of 5-FU. *Adv. Exp. Med. Biol.* **2010**, *678*, 157–164. https://doi.org/10.1007/978-1-4419-6306-2_20.

(212) Adler-Abramovich, L.; Gazit, E. The Physical Properties of Supramolecular Peptide Assemblies: From Building Block Association to Technological Applications. *Chem. Soc. Rev.* **2014**, *43* (20), 6881–6893. https://doi.org/10.1039/c4cs00164h.

(213) Ulijn, R. V.; Smith, A. M. Designing Peptide Based Nanomaterials. *Chem. Soc. Rev.* **2008**, *37* (4), 664–675. https://doi.org/10.1039/b609047h.

(214) Mendes, A. C.; Baran, E. T.; Reis, R. L.; Azevedo, H. S. Self-Assembly in Nature: Using the Principles of Nature to Create Complex Nanobiomaterials. *Wiley Interdiscip. Rev. Nanomedicine Nanobiotechnology* **2013**, *5* (6), 582–612. https://doi.org/10.1002/wnan.1238.

(215) Philp, D.; Fraser Stoddart, J. Self-Assembly in Natural and Unnatural Systems. *Angew. Chemie (International Ed. English)* **1996**, *35* (11), 1154–1196. https://doi.org/10.1002/anie.199611541.

(216) Krieg, E.; Bastings, M. M. C.; Besenius, P.; Rybtchinski, B. Supramolecular Polymers in Aqueous Media. *Chem. Rev.* **2016**, *116* (4), 2414–2477. https://doi.org/10.1021/acs.chemrev.5b00369.

(217) De Greef, T. F. A.; Smulders, M. M. J.; Wolffs, M.; Schenning, A. P. H. J.; Sijbesma, R. P.; Meijer, E. W. Supramolecular Polymerization. *Chem. Rev.* **2009**, *109* (11), 5687–5754. https://doi.org/10.1021/cr900181u.

(218) Desiraju, G. R. The Supramolecular Synthon in Crystal Engineering. *Stimul. Concepts Chem.* **2005**, 293–306. https://doi.org/10.1002/3527605746.ch19.

(219) Ma, M.; Zhong, J.; Li, W.; Zhou, J.; Yan, Z.; Ding, J.; He, D. Comparison of Four Synthetic Model Peptides to Understand the Role of Modular Motifs in the Self-Assembly of Silk Fibroin. *Soft Matter* **2013**, *9* (47), 11325–11333. https://doi.org/10.1039/c3sm51498f.

(220) Pashuck, E. T.; Stupp, S. I. Direct Observation of Morphological Tranformation from Twisted Ribbons into Helical Ribbons. *J. Am. Chem. Soc.* **2010**, *132* (26), 8819–8821. https://doi.org/10.1021/ja100613w.

(221) Jin, Y.; Xu, X. D.; Chen, C. S.; Cheng, S. X.; Zhang, X. Z.; Zhuo, R. X. Bioactive Amphiphilic Peptide Derivatives with PH Triggered Morphology and Structure. *Macromol. Rapid Commun.* **2008**, *29* (21), 1726–1731. https://doi.org/10.1002/marc.200800455.

(222) Zhang, L.; Zhong, J.; Huang, L.; Wang, L.; Hong, Y.; Sha, Y. Parallel-Oriented Fibrogenesis of a β-Sheet Forming Peptide on Supported Lipid Bilayers. *J. Phys. Chem. B* **2008**, *112* (30), 8950–8954. https://doi.org/10.1021/jp802424h.

(223) Kumaraswamy, P.; Lakshmanan, R.; Sethuraman, S.; Krishnan, U. M. Self-Assembly of Peptides: Influence of Substrate, PH and Medium on the Formation of Supramolecular Assemblies. *Soft Matter* **2011**, *7* (6), 2744–2754. https://doi.org/10.1039/c0sm00897d.

(224) Yamamoto, Y.; Fukushima, T.; Suna, Y.; Ishii, N.; Saeki, A.; Seki, S.; Tagawa, S.; Taniguchi, M.; Kawai, T.; Aida, T. Photoconductive Coaxial Nanotubes of Molecularly Connected Electron Donor and Acceptor Layers. *Science (80-.).* **2006**, *314* (5806), 1761–1764. https://doi.org/10.1126/science.1134441.

(225) Skilling, K. J.; Citossi, F.; Bradshaw, T. D.; Ashford, M.; Kellam, B.; Marlow, M. Insights into Low Molecular Mass Organic Gelators: A Focus on Drug Delivery and Tissue Engineering Applications. *Soft Matter* **2014**, *10* (2), 237–256. https://doi.org/10.1039/c3sm52244j.

(226) Steed, J. W. Supramolecular Gel Chemistry: Developments over the Last Decade. *Chem. Commun.* **2011**, *47* (5), 1379–1383. https://doi.org/10.1039/c0cc03293j.

(227) George, M.; Weiss, R. G. Molecular Organogels. Soft Matter Comprised of Low-Molecular-Mass Organic Gelators and Organic Liquids. *Acc. Chem. Res.* **2006**, *39* (8), 489–497. https://doi.org/10.1021/ar0500923.

(228) Worthington, P.; Pochan, D. J.; Langhans, S. A. Peptide Hydrogels - Versatile Matrices for 3D Cell Culture in Cancer Medicine. *Front. Oncol.* **2015**, *5* (APR), 1–10. https://doi.org/10.3389/fonc.2015.00092.

(229) Ikeda, M.; Tanida, T.; Yoshii, T.; Kurotani, K.; Onogi, S.; Urayama, K.; Hamachi, I. Installing Logic-Gate Responses to a Variety of Biological Substances in Supramolecular Hydrogel-Enzyme Hybrids. *Nat. Chem.* **2014**, *6* (6), 511–518. https://doi.org/10.1038/nchem.1937.

(230) Giano, M. C.; Ibrahim, Z.; Medina, S. H.; Sarhane, K. A.; Christensen, J. M.; Yamada, Y.; Brandacher, G.; Schneider, J. P. Injectable Bioadhesive Hydrogels with Innate Antibacterial Properties. *Nat. Commun.* **2014**, *5* (May), 1–9. https://doi.org/10.1038/ncomms5095.

(231) Yan, C.; Pochan, D. J. Rheological Properties of Peptide-Based Hydrogels for Biomedical and Other Applications. *Chem. Soc. Rev.* **2010**, *39* (9), 3528–3540. https://doi.org/10.1039/b919449p.

(232) Rad-Malekshahi, M.; Lempsink, L.; Amidi, M.; Hennink, W. E.; Mastrobattista, E. Biomedical Applications of Self-Assembling Peptides. *Bioconjug. Chem.* **2016**, *27* (1), 3–18. https://doi.org/10.1021/acs.bioconjchem.5b00487.

(233) Robertson, E. J.; Battigelli, A.; Proulx, C.; Mannige, R. V.; Haxton, T. K.; Yun, L.; Whitelam, S.; Zuckermann, R. N. Design, Synthesis, Assembly, and Engineering of Peptoid Nanosheets. *Acc. Chem. Res.* **2016**, *49* (3), 379–389. https://doi.org/10.1021/acs.accounts.5b00439.

(234) Bong, D. T.; Clark, T. D.; Granja, J. R.; Reza Ghadiri, M. Self-Assembling Organic Nanotubes. *Angew. Chemie - Int. Ed.* **2001**, *40* (6), 988–1011. https://doi.org/10.1002/1521-3773(20010316)40:6<988::AID-ANIE9880>3.0.CO;2-N.

(235) Xie, Z.; Zhang, A.; Ye, L.; Feng, Z. G. Organo- and Hydrogels Derived from Cyclo(L-Tyr-L-Lys) and Its ε-Amino Derivatives. *Soft Matter* **2009**, *5* (7), 1474–1482. https://doi.org/10.1039/b816664a.

(236) Hoshizawa, H.; Suzuki, M.; Hanabusa, K. Cyclo(L-Aspartyl-L-Phenylalanyl)-Containing Poly(Dimethylsiloxane)-Based Thixotropic

Organogels. *Chem. Lett.* **2011**, *40* (10), 1143–1145. https://doi.org/10.1246/cl.2011.1143.

(237) Hoshizawa, H.; Minemura, Y.; Yoshikawa, K.; Suzuki, M.; Hanabusa, K. Thixotropic Hydrogelators Based on a Cyclo(Dipeptide) Derivative. *Langmuir* **2013**, *29* (47), 14666–14673. https://doi.org/10.1021/la402333h.

(238) Hanabusa, K.; Fukui, H.; Suzuki, M.; Shirai, H. Specialist Gelator for Ionic Liquids. *Langmuir* **2005**, *21* (23), 10383–10390. https://doi.org/10.1021/la051323h.

(239) Geng, H.; Ye, L.; Zhang, A. Y.; Li, J.; Feng, Z. G. Low-Molecular-Weight Organo- and Hydrogelators Based on Cyclo(l-Lys-l-Glu). *Langmuir* **2016**, *32* (18), 4586–4594. https://doi.org/10.1021/acs.langmuir.6b01059.

(240) Borthwick, A. D.; Grove, T.; Nw, L. And Bioactive Natural Products. **2012**.

(241) Adhikary, A.; Das, K. S.; Saha, S.; Roy, M.; Mondal, R. A Free-Standing, Self-Healing Multi-Stimuli Responsive Gel Showing Cryogenic Magnetic Cooling. *Dalt. Trans.* **2020**, *49* (38), 13487–13495. https://doi.org/10.1039/d0dt02356f.

(242) Ghosh, G.; Barman, R.; Mukherjee, A.; Ghosh, U.; Ghosh, S.; Fernández, G. Control over Multiple Nano- and Secondary Structures in Peptide Self-Assembly. *Angew. Chemie - Int. Ed.* **2022**, *61* (5), 1–8. https://doi.org/10.1002/anie.202113403.

(243) Evans, N. H.; Beer, P. D. Advances in Anion Supramolecular Chemistry: From Recognition to Chemical Applications. *Angew. Chemie - Int. Ed.* **2014**, *53* (44), 11716–11754. https://doi.org/10.1002/anie.201309937.

(244) Gale, P. A.; Howe, E. N. W.; Wu, X. Anion Receptor Chemistry. *Chem* **2016**, *1* (3), 351–422. https://doi.org/10.1016/j.chempr.2016.08.004.

(245) McMillan, J. R.; Hayes, O. G.; Winegar, P. H.; Mirkin, C. A. Protein Materials Engineering with DNA. *Acc. Chem. Res.* **2019**, *52* (7), 1939–1948. https://doi.org/10.1021/acs.accounts.9b00165.

(246) Sivakova, S.; Rowan, S. J. Nucleobases as Supramolecular Motifs. *Chem. Soc. Rev.* **2005**, *34* (1), 9–21. https://doi.org/10.1039/b304608g.

(247) Eckert. Evidence of Mitochondrial Dysfunction in Post-Mortem AD Brain and Peripheral Cells. *Alzheimers. Res. Ther.* **2011**, *3*.

(248) Nisbet, R. M.; Polanco, J. C.; Ittner, L. M.; Götz, J. Tau Aggregation and Its Interplay with Amyloid-β. *Acta Neuropathol.* **2015**, *129* (2), 207–220. https://doi.org/10.1007/s00401-014-1371-2.

(249) Newcomb, C. J.; Sur, S.; Ortony, J. H.; Lee, O. S.; Matson, J. B.; Boekhoven, J.; Yu, J. M.; Schatz, G. C.; Stupp, S. I. Cell Death versus Cell Survival Instructed by Supramolecular Cohesion of Nanostructures. *Nat. Commun.* **2014**, *5*. https://doi.org/10.1038/ncomms4321.

(250) Yao, X.; Liu, Y.; Gao, J.; Yang, L.; Mao, D.; Stefanitsch, C.; Li, Y.; Zhang, J.; Ou, L.; Kong, D.; Zhao, Q.; Li, Z. Nitric Oxide Releasing Hydrogel Enhances the Therapeutic Efficacy of Mesenchymal Stem Cells for Myocardial Infarction. *Biomaterials* **2015**, *60*, 130–140. https://doi.org/10.1016/j.biomaterials.2015.04.046.

(251) Ikeda, M.; Tanida, T.; Yoshii, T.; Kurotani, K.; Onogi, S.; Urayama, K.; Hamachi, I. Installing Logic-Gate Responses to a Variety of Biological Substances in Supramolecular Hydrogel-Enzyme Hybrids. *Nat. Chem.* **2014**, *6* (6), 511–518. https://doi.org/10.1038/nchem.1937.

(252) King, P. J. S.; Giovanna Lizio, M.; Booth, A.; Collins, R. F.; Gough, J. E.; Miller, A. F.; Webb, S. J. A Modular Self-Assembly Approach to Functionalised β-Sheet Peptide Hydrogel Biomaterials. *Soft Matter* **2016**, *12* (6), 1915–1923. https://doi.org/10.1039/c5sm02039e.

(253) Weiss, R. G. The Past, Present, and Future of Molecular Gels. What Is the Status of the Field, and Where Is It Going? *J. Am. Chem. Soc.* **2014**, *136* (21), 7519–7530. https://doi.org/10.1021/ja503363v.

(254) Stevens, M. M.; George, J. H. Exploring and Engineering the Cell Surface Interface. *Science (80-.).* **2005**, *310* (5751), 1135–1138. https://doi.org/10.1126/science.1106587.

(255) Lutolf, M. P.; Hubbell, J. A. Synthetic Biomaterials as Instructive Extracellular Microenvironments for Morphogenesis in Tissue Engineering. *Nat. Biotechnol.* **2005**, *23* (1), 47–55. https://doi.org/10.1038/nbt1055.

(256) Aida, T.; Meijer, E. W.; Stupp, S. I. Functional Supramolecular Polymers. *Science (80-.).* **2012**, *335* (6070), 813–817. https://doi.org/10.1126/science.1205962.

(257) Chaterji, S.; Kwon, I. K.; Park, K. Smart Polymeric Gels: Redefining the Limits of Biomedical Devices. *Prog. Polym. Sci.* **2007**, *32* (8–9), 1083–1122. https://doi.org/10.1016/j.progpolymsci.2007.05.018.

(258) Hsu, S. M.; Lin, Y. C.; Chang, J. W.; Liu, Y. H.; Lin, H. C.

Intramolecular Interactions of a Phenyl/Perfluorophenyl Pair in the Formation of Supramolecular Nanofibers and Hydrogels. *Angew. Chemie - Int. Ed.* **2014**, *53* (7), 1921–1927. https://doi.org/10.1002/anie.201307500.

(259) Fichman, G.; Gazit, E. Self-Assembly of Short Peptides to Form Hydrogels: Design of Building Blocks, Physical Properties and Technological Applications. *Acta Biomater.* **2014**, *10* (4), 1671–1682. https://doi.org/10.1016/j.actbio.2013.08.013.

(260) Tang, C.; Smith, A. M.; Collins, R. F.; Ulijn, R. V.; Saiani, A. Fmoc-Diphenylalanine Self-ASsembly Mechanism Induces Apparent PK a Shifts. *Langmuir* **2009**, *25* (16), 9447–9453. https://doi.org/10.1021/la900653q.

(261) Adam D. Martin,*a Andrew B. Robinson, a P. T. Biocompatible Small Peptide Superhydrogelators Bearing Carbazole Functionalities. *J. Mater. Chem. B* **2019**, *2019-Novem*. https://doi.org/10.1039/x0xx00000x.

(262) Martin, A. D.; Wojciechowski, J. P.; Warren, H.; In Het Panhuis, M.; Thordarson, P. Effect of Heterocyclic Capping Groups on the Self-Assembly of a Dipeptide Hydrogel. *Soft Matter* **2016**, *12* (10), 2700–2707. https://doi.org/10.1039/c6sm00025h.

(263) Martin, A. D.; Robinson, A. B.; Mason, A. F.; Wojciechowski, J. P.; Thordarson, P. Exceptionally Strong Hydrogels through Self-Assembly of an Indole-Capped Dipeptide. *Chem. Commun.* **2014**, *50* (98), 15541–15544. https://doi.org/10.1039/c4cc07941h.

(264) Chen, L.; Morris, K.; Laybourn, A.; Elias, D.; Hicks, M. R.; Rodger, A.; Serpell, L.; Adams, D. J. Self-Assembly Mechanism for a Naphthalene-Dipeptide Leading to Hydrogelation. *Langmuir* **2010**, *26* (7), 5232–5242. https://doi.org/10.1021/la903694a.

(265) Reches, M.; Gazit, E. Self-Assembly of Peptide Nanotubes and Amyloid-like Structures by Charged-Termini-Capped Diphenylalanine Peptide Analogues. *Isr. J. Chem.* **2005**, *45* (3), 363–371. https://doi.org/10.1560/5MC0-V3DX-KE0B-YF3J.

(266) Draper, E. R.; Eden, E. G. B.; McDonald, T. O.; Adams, D. J. Spatially Resolved Multicomponent Gels. *Nat. Chem.* **2015**, *7* (10), 848–852. https://doi.org/10.1038/nchem.2347.

(267) McAulay, K.; Dietrich, B.; Su, H.; Scott, M. T.; Rogers, S.; Al-Hilaly, Y. K.; Cui, H.; Serpell, L. C.; Seddon, A. M.; Draper, E. R.; Adams, D. J. Using Chirality to Influence Supramolecular Gelation. *Chem. Sci.* **2019**,

10 (33), 7801–7806. https://doi.org/10.1039/c9sc02239b.

(268) Kerru, N.; Gummidi, L.; Maddila, S.; Gangu, K. K.; Jonnalagadda, S. B. A Review on Recent Advances in Nitrogen-Containing Molecules and Their Biological Applications. *Molecules* **2020**, *25* (8). https://doi.org/10.3390/molecules25081909.

(269) López, J. L.; Atienza, C.; Insuasty, A.; López-Andarias, J.; Romero-Nieto, C.; Guldi, D. M.; Martín, N. Concave versus Planar Geometries for the Hierarchical Organization of Mesoscopic 3D Helical Fibers. *Angew. Chemie* **2012**, *124* (16), 3923–3927. https://doi.org/10.1002/ange.201109162.

(270) Gupta, S.; Frederix, P. W. J. M.; Skabara, P. J.; Gleskova, H.; Ulijn, R. V. Conducting Nano Fi Bers and Organogels Derived from the Self-Assembly of Tetrathiafulvalene-Appended Dipeptides. **2014**.

(271) Liu, Y. H.; Hsu, S. M.; Wu, F. Y.; Cheng, H.; Yeh, M. Y.; Lin, H. C. Electroactive Organic Dye Incorporating Dipeptides in the Formation of Self-Assembled Nanofibrous Hydrogels. *Bioconjug. Chem.* **2014**, *25* (10), 1794–1800. https://doi.org/10.1021/bc500299c.

(272) Nalluri, S. K. M.; Berdugo, C.; Javid, N.; Frederix, P. W. J. M.; Ulijn, R. V. Biocatalytic Self-Assembly of Supramolecular Charge-Transfer Nanostructures Based on n-Type Semiconductor-Appended Peptides. *Angew. Chemie* **2014**, *126* (23), 5992–5997. https://doi.org/10.1002/ange.201311158.

(273) Kubiak, P. S.; Awhida, S.; Hotchen, C.; Deng, W.; Alston, B.; McDonald, T. O.; Adams, D. J.; Cameron, P. J. Polymerization of Low Molecular Weight Hydrogelators to Form Electrochromic Polymers. *Chem. Commun.* **2015**, *51* (52), 10427–10430. https://doi.org/10.1039/c5cc03053f.

(274) Martin, A. D.; Wojciechowski, J. P.; Bhadbhade, M. M.; Thordarson, P. A Capped Dipeptide Which Simultaneously Exhibits Gelation and Crystallization Behavior. *Langmuir* **2016**, *32* (9), 2245–2250. https://doi.org/10.1021/acs.langmuir.5b03963.

(275) Wahan, S. K.; Sharma, B.; Chawla, P. A. Medicinal Perspective of Quinazolinone Derivatives: Recent Developments and Structure–Activity Relationship Studies. *J. Heterocycl. Chem.* **2022**, *59* (2), 239–257. https://doi.org/10.1002/jhet.4382.

(276) Narasimhulu, M.; Mahesh, K. C.; Reddy, T. S.; Rajesh, K.; Venkateswarlu, Y. Lanthanum(III) Nitrate Hexahydrate or p-

Toluenesulfonic Acid Catalyzed One-Pot Synthesis of 4(3H)-Quinazolinones under Solvent-Free Conditions. *Tetrahedron Lett.* **2006**, *47* (26), 4381–4383. https://doi.org/10.1016/j.tetlet.2006.04.096.

(277) Larksarp, C.; Alper, H. Palladium-Catalyzed Cyclocarbonylation of o-Iodoanilines with Heterocumulenes: Regioselective Preparation of 4(3H)-Quinazolinone Derivatives. *J. Org. Chem.* **2000**, *65* (9), 2773–2777. https://doi.org/10.1021/jo991922r.

LIST OF PUBLICATIONS

1. **Ghosh, S.**, Nag, S., Saha, K.D. and Banerji, B., 2022. S-Benzyl Cysteine Based Cyclic Dipeptide Super Hydrogelator: Enhancing Efficacy of an Anticancer Drug via Sustainable Release. Journal of Peptide Science, p.e3403.

2. Srinath, R., Manna, A., Shee, S., Pathi, V.B., **Ghosh, S**., Khamaru, K., Maiti, N.C. and Banerji, B., 2021. Synthesis of N-Fused Triazole–Piperazine–Quinazolinones via One-Pot Tandem Click Reaction and Cross-Dehydrogenative Coupling. Organic Letters, 23(24), pp.9365-9370.

3. Banerji, B., Adhikary, S., Majumder, L. and **Ghosh, S**., 2019. A Green Synthetic Approach towards Polyarylated Oxazoles via Iodine-Catalyzed One-Pot sp3 C− H Functionalization in Water: From Natural Product Synthesis To Photophysical Studies. Asian Journal of Organic Chemistry, 8(4), pp.514-525.

4. Banerji, B., Chatterjee, S., Chandrasekhar, K., **Ghosh, S**., Mukherjee, K. and Mandal, C., 2018. Detection of Lysosome by a Fluorescent Heterocycle: Development of Fused Pyrido–Imidazo–Indole Framework via Cu-Catalyzed Tandem N-Arylation. The Journal of Organic Chemistry, 83(21), pp.13011-13018.

Received: 7 November 2021 | Revised: 23 December 2021 | Accepted: 30 December 2021

DOI: 10.1002/psc.3403

RESEARCH ARTICLE

Journal of PeptideScience WILEY

S-Benzyl cysteine based cyclic dipeptide super hydrogelator: Enhancing efficacy of an anticancer drug via sustainable release

Saswati Ghosh[1] | Sayoni Nag[3] | Krishna Das Saha[3] | Biswadip Banerji[1,2]

[1]Organic & Medicinal Chemistry Division, Indian Institute of Chemical Biology (CSIR-IICB), Kolkata, India

[2]Academy of Scientific and Innovative Research (AcSIR), Indian Institute of Chemical Biology (CSIR-IICB), Kolkata, India

[3]Cancer Biology & Inflammatory Disorder, Indian Institute of Chemical Biology (CSIR-IICB), Kolkata, India

Correspondence
Biswadip Banerji, Organic & Medicinal Chemistry Division, Indian Institute of Chemical Biology (CSIR-IICB), Kolkata, 700032, India.
Email: biswadip.banerji@gmail.com

Peptide-based low molecular weight supramolecular hydrogels hold promising aspects in various fields of application especially in biomaterial and biomedical sciences such as drug delivery, wound healing, tissue engineering, cell proliferation, and so on due to their extreme biocompatibility. Unlike linear peptides, cyclic peptides have more structural rigidity and tolerance to enzymatic degradation and high environmental stability which make them even better candidates for the above-said applications. Herein, a new small cyclic dipeptide (CDP) cyclo-(Leu-*S*-Bzl-Cys) (P1) consisting of L-leucine and *S*-benzyl protected L-cysteine was reported which formed a hydrogel at physiological conditions (at 37°C and pH = 7.46). The hydrogel formed from the cyclic dipeptide P1 showed very good tolerance towards environmental parameters such as pH and temperature and was seen to be stable for more than a year without any deformation. The hydrogel was thermoreversible and stable in the pH range 6–12. Mechanical strength of P1 hydrogel was measured by rheology experiments. Atomic force microscopy (AFM) and field emission scanning electron microscopy (FE-SEM) images revealed that, in aqueous solvents, P1 self-assembled into a highly cross-linked nanofibrillar network which immobilized water molecules inside the cages and formed the hydrogel. The self-assembled cyclic dipeptide acquired the antiparallel β-sheet secondary structure, which was evident from CD and Fourier transform infrared (FT-IR) studies. The β-sheet arrangement and formation of amyloid fibrils were further established by ThT binding assay. Furthermore, P1 was able to form a hydrogel in the presence of the anticancer drug 5-fluorouracil (5FU), and sustainable release of the drug from the hydrogel was measured in vitro. The hydrogelator P1 showed almost no cytotoxicity towards the human colorectal cancer cell line HCT116 up to a considerably high concentration and showed potential application in sustainable drug delivery. The co-assembly of 5FU and P1 hydrogel exhibited much better anticancer activity towards the HCT116 cancer cell line than 5FU alone and decreased the IC_{50} dose of 5FU to a much lower value.

KEYWORDS
5-fluorouracil, anticancer activity, cyclic dipeptide, drug delivery vehicle, nanofibrillar self-assembly, super hydrogelator, sustainable drug release

Abbreviations: 5FU, 5-fluorouracil; AFM, atomic force microscopy; Bzl, benzyl; CD, circular dichroism; CDP, cyclic dipeptide; Cys, cysteine; DMSO, dimethyl sulfoxide; ESI-MS, electrospray ionization mass spectrometry; FE-SEM, field emission scanning electron microscopy; FT-IR, Fourier transform infrared; Leu, leucine; MGC, minimum gelation concentration; NMR, nuclear magnetic resonance; PBS, phosphate-buffered saline.

OL Organic Letters

pubs.acs.org/OrgLett Letter

Synthesis of N-Fused Triazole−Piperazine−Quinazolinones via One-Pot Tandem Click Reaction and Cross-Dehydrogenative Coupling

Ravuri Srinath, Arindam Manna, Subhankar Shee, Vijay Babu Pathi, Saswati Ghosh, Krishnendu Khamaru, Nakul Chandra Maiti, and Biswadip Banerji*

Cite This: *Org. Lett.* 2021, 23, 9365−9370 Read Online

ACCESS | Metrics & More | Article Recommendations | Supporting Information

ABSTRACT: Herein, a one-pot protocol to synthesize tetracyclic triazole−piperazine−quinazolinone-fused N-heterocyclic scaffolds is reported. In this strategy, a tandem approach of two highly efficient synthetic reactions, click and cross-dehydrogentive coupling reactions, with high atom economy were employed to obtain the target N-fused scaffolds. Being highly functional group tolerable, this method has broad substrate scope. Interestingly, some of these derivatives showed strong white solid-state fluorescence.

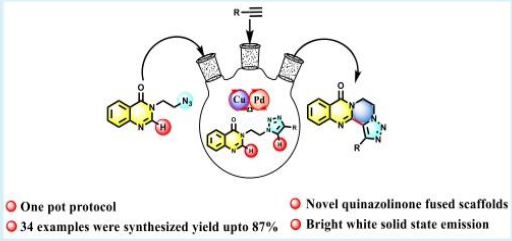

Nature is a tremendous source of many natural products, which contain many medicinally important N-fused heterocycles as their core moiety and are often responsible for their biological efficacies.[1] Synthesis of these fused heterocycles by various transition-metal-catalyzed approaches in the laboratory is always a challenging task for synthetic organic chemists worldwide. It is interesting to note that most of the time, these molecules possess potential therapeutic applications along with high luminescence properties due to high electronic conjugations because of their extended π-aromatic frameworks.[2a−c] In an ongoing project in our laboratory on the synthesis and efficacy studies of natural-product-inspired hybrid molecules, we were interested to synthesize a library of N-fused heterocyclic molecules, which may be useful as potential therapeutic agents. In the present design strategy, we incorporated quinazolinone, pyrazine, and triazole heterocyclic moieties, which individually have very good reported therapeutic efficacies (Figure 1). In recent times, transition-metal-catalyzed cross-dehydrogenative coupling (CDC) approaches have emerged as the most versatile and atom-economical procedures for C−C bond formations.[3] Furthermore, no use of prefunctionalized substrates and very clean conversions[4] are major advantages of the CDC reaction by various transition metals such as Ru,[5] Rh,[6] and Pd.[7] In addition to that, there are several synthetic methods which utilize palladium-catalyzed intermolecular C−H bond functionalization to synthesize fused quinazolinones.[8] On the other hand, Cu-catalyzed click chemistry is well-known for the synthesis of 1,2,3-triazoles through 1,3-dipolar cycloaddition. The triazole moiety has potential applications in many biochemical as well as drug discovery studies.[9] For the past few years, our group was engaged in developing simple protocols to access novel N-fused polyheterocycles by utilizing C−H activation strategies.[10]

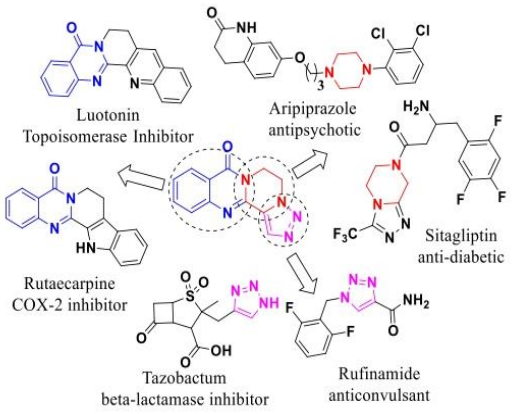

Figure 1. Some of the important drugs containing quinazolinone, piperazine, and triazole moieties.

In the present work, we report a one-pot protocol to synthesize a tetracyclic triazolodihydropyrazine-fused quinazolinone framework via the click reaction followed by palladium-catalyzed oxidative intramolecular cross-dehydrogenative coupling from 3-(2-azidoethyl)quinazolin-4(3*H*)-one (**1a**). Typi-

Received: October 11, 2021
Published: November 21, 2021

https://doi.org/10.1021/acs.orglett.1c03435
Org. Lett. 2021, 23, 9365−9370

ACES Asian Chemical Editorial Society

DOI: 10.1002/ajoc.201800742

ASIAN JOURNAL OF ORGANIC CHEMISTRY
Full Paper

A Green Synthetic Approach towards Polyarylated Oxazoles via Iodine-Catalyzed One-Pot sp^3 C–H Functionalization in Water: From Natural Product Synthesis To Photophysical Studies

Biswadip Banerji,*[a, b] Saswati Adhikary,[a] Leena Majumder,[a] and Saswati Ghosh[a]

Abstract: A 'green' methodology for the convenient synthesis of specific regioisomers of polysubstituted oxazoles through iodine catalyzed, water-mediated, aerobic oxidative C(sp^3)–H functionalization of primary amines has been developed. This mild and regioselective domino procedure does not require toxic peroxides, transition metals and organic solvents. The versatility of this methodology was demonstrated by preparing a natural product, texaline. It is also scalable and has a wide substrate scope. This methodology opens up a simple avenue for the synthesis of polyarylated oxazoles from various readily available amines as well as 1,2-diketones and acyloins (α-hydroxyl ketones) in moderate to excellent yields. Furthermore, these highly substituted oxazole molecules showed excellent fluorescence properties and thus have enormous potential to be a new type of fluorescent probe for use in medicinal applications and materials science.

Introduction

Recently, sp^3C–H bond functionalization has gained great interests. Organic reactions carried out under metal-free conditions have become popular due to the drawbacks of expensive, toxic, and air-sensitive metals or organometallics. Iodine serves as an alternative catalyst for transition metals in many reactions.[1] Studies show that molecular iodine has the capability to functionalize carbon-hydrogen bonds to form new carbon-carbon and carbon-hetero bonds as well.[2] Iodine is insensitive to air and moisture and can also be removed from the reaction mixture by simple washing with reducing agents. Till now, an enormous number of organic synthesis have been successfully carried out in aqueous medium.[3] Water is non-flammable, non-toxic, non-hazardous, inexpensive environmentally benign as well as readily obtainable solvent in nature.

In organic synthesis, cascade reaction is an efficient and atom-economical methodology as it offers several advantages like avoiding multiple steps, long time duration and purification of the intermediates. Oxazole framework belongs to one of the most widely occurring scaffolds found in many pharmaceutically active compounds, and natural products which exhibit attractive biological activities. For instance antimycobacterial naturalproduct texaline, non-steroidal anti-inflammatory drug oxaprozin[6] and aristoxazole,[7] anti-pancreatic cancer agent PC-046[8] contain oxazole in their framework[9] (Scheme 1). Oxazole scaffolds also have important application in fluorescence dyes,[10] polymers[11] and are also essential building blocks in synthetic organic chemistry.[12] Due to numerous importance of this scaffold, several synthetic methodologies were developed to construct fully functionalized oxazoles.[13]

Very recently easily accessible 1,2-diketone (benzil) were exploited for the synthesis of fully substituted oxazole[4d,14] (Scheme 2). Regardless of their applicability and broad substrate scope, these methods suffer from limitations of transition metal reagent and organic solvents. Therefore, environmentally benign chemical processes are still in high demand. From these points, the progress of synthetically more practical, and convergent domino protocol using an aqueous medium as a green solvent source is of key interest.In addition, a synthetic method, that affords single regioisomers exclusively instead of a mixture, is highly advantageous.

Results and Discussion

The investigation was conducted with benzil (**1a**) (1 equiv) and benzylamine (**2a**) (1 equiv) as model substrates, treating I_2 as a catalyst in water at room temperature under air for 8 hrs. The desired oxazole **3a** was achieved upto 48% yield (Table 1, entry **1**). We studied the temperature effect of the reaction and were found that 60 °C was the optimal temperature for this procedure (Table 1, entry **2–4**). To further improve the yield, different organic and inorganic bases were then investigated. In particular, K_2CO_3 efficiently improve the yield of the desired product up to 92% (Table 1, entry **5–11**). The effect of organic solvents was further examined (Table 1, entry **12–17**). None of these could improve the yield. In addition, other oxidants were also efficient for this transformation (Table 1, entry **18** and **19**).

[a] Dr. B. Banerji, S. Adhikary, L. Majumder, S. Ghosh
Organic and Medicinal Chemistry Division, Indian Institute of Chemical Biology (CSIR-IICB)
4 Raja S. C. Mullick Road
Kolkata, 700032, India
E-mail: biswadip.banerji@gmail.com
biswadip@iicb.res.in

[b] Dr. B. Banerji
Academy of Scientific and Innovative Research (AcSIR)
Indian Institute of Chemical Biology (CSIR-IICB)
4 Raja S. C. Mullick Road
Kolkata, 700032, India
Fax: +91 33 24735197
Fax: +91 33 24723967
Tel : +91 33 24995709

Supporting information for this article is available on the WWW under https://doi.org/10.1002/ajoc.201800742

JOC The Journal of Organic Chemistry Cite This: J. Org. Chem. 2018, 83, 13011−13018 Article pubs.acs.org/joc

Detection of Lysosome by a Fluorescent Heterocycle: Development of Fused Pyrido−Imidazo−Indole Framework via Cu-Catalyzed Tandem N-Arylation

Biswadip Banerji,*[,†,‡] Satadru Chatterjee,[†] Kadaiahgari Chandrasekhar,[†] Saswati Ghosh,[†] Kaustuv Mukherjee,[§] and Chitra Mandal[§]

[†]Organic and Medicinal Chemistry Division, [‡]Academy of Scientific and Innovative Research (AcSIR), [§]Cancer Biology and Inflammatory Disorder Division, Indian Institute of Chemical Biology (CSIR-IICB), 4 Raja S. C. Mullick Road, Kolkata 700032, India

Supporting Information

ABSTRACT: Fluorescent active small molecules for organelle-specific bioimaging are in great demand. We synthesized 20 different pyrido−imidazo−indole fused heterocycles (6−5−5−6 ring) via copper catalyzed tandem N-arylation reaction in moderate to good yields. Due to decent fluorescent property, lysosome-directing moieties were attached on two of these heterocycles. Delightfully, those molecules tracked lysosome with bright blue fluorescence and colocalized with a known lysosome marker (Lysotracker Red) in human/murine cells. Therefore, it may be considered as a rapid (10 min) lysosome staining probe.

INTRODUCTION

In living systems, cells are the most important core unit, inside which all the biochemical reactions take place continuously. These various chemical reactions simultaneously transduct into various important signals thoughout the body and are responsible for sustaining life.[1] Organelle-targetable fluorescent probes (OTFPs) are namely those (Figure 1) which can directly anchor to a specific organelle inside the cell and make the target organelle visible by the principle of fluorescence.[2] In recent times, nitrogen containing heterocycles have gained high importance due to their impactful and versatile applications in various fields.[3−10] Thus, researchers are interested in synthesis of these kinds of fused heterocycles. These fused heterocycles due to their extensive conjugations are also highly fluorescent and can be used in bioimaging.[11−13] Imidazo[1,2-*a*]pyridine, one of the most important examples of nitrogen bearing heterocycles, was found to be major constituent of different pharmaceuticals (Figure 2). Some of the reported anticancer,[14] antiparasitic,[15] anti-inflammatory,[16] antiviral,[17] and antibacterial[18] drugs consist of the imidazo[1,2-*a*]pyridine motif. As a result, efforts were made for the preparation and derivation of imidazo[1,2-*a*]pyridine for a long period of time. On the other hand, indole and its derivatives were prevalent in a wide class of natural products with enormous biomedical activities (Figure 2).[19−24] In an ongoing project in our laboratory, we were interested to build a new fused heterocycle consisting of a pyrido−imidazo−indole framework. Previously, our group reported the synthetic methodology of the fused pyrido−imidazo−phenthridine scaffold (Figure 3).[11] In the present study, we developed a new synthetic route to prepare imidazo[1,2-*a*]pyridine-indole fused heterocycles (**5**) using Ullmann-type tandem N-arylation reaction of various amines with the corresponding dihalo-biaryl substrates (**4**). Unlike previously reported methods (Figure 3),[25−28] this methodology avoids the uses of toxic chemicals such as isocyanide and is not dependent to any specific structural orientation, thus resulting a wide functional group tolerance with a variety of substrates. Due to the decent luminescence properties of the synthesized molecules, their photophysical characteristics were further explored and extended to live cell imaging. Two of these new heterocycles were preinstalled with lysosome directing groups at one end, precisely to examine their cellular localization behavior. Gratifyingly, we observed that those molecules can selectively go into lysosomes inside the cell and gave bright blue fluorescence. Being acidic in nature, lysosomes play a key role in cellular defense, antigen processing, apoptosis, and autophagic pathways and also in various other physiological processes.[29,30] Moreover, lysosomes are involved in receptor cycling and trafficking. Thus, by tracking lysosomes at the cellular level, these fused heterocycles can be used as new potent fluorescent probes.

RESULTS AND DISCUSSION

The synthesis started with a well-established C−H amination strategy by reacting compounds **1** and **2** to get compound **3**.[31] The dihalo-biaryl precursor **4** was synthesized from compound **3** using *N*-iodosuccinimide (NIS) in MeCN at room temperature. Compound **4** was then subjected to copper catalyzed (CuI)

Received: June 15, 2018
Published: October 2, 2018

DOI: 10.1021/acs.joc.8b01513
J. Org. Chem. 2018, 83, 13011−13018